Thèse en cotutelle

University of Science and Technology of China

Université de Lille 1 – Sciences et Technologies

The role of the Pacific subduction in the genesis of Cenozoic basalts in eastern China: New constraints from water content and oxygen isotope composition

by

Huan Chen

In partial fulfillment of the requirements for the degree of

Doctor of Philosophy at USTC

and

Docteur de l'Université Lille I

Supervisors : Qunke Xia and Jannick Ingrin

22 March, 2017

Université de Lille 1

UMR CNRS 8207 Unité Matériaux Et Transformations

THÈSE

Pour obtenir le grade de

Docteur de l'Université Lille 1

Par

Huan CHEN

The role of the Pacific subduction in the genesis of Cenozoic basalts in eastern China: New constraints from water content and oxygen isotope composition

Soutenue le 22 Mars 2017

Présentée devant la commission d'examen composée de:

Etienne DELOULE	Director of Research at the CNRS, CRPG, Nancy	President, Rapporteur
Yigang XU	Researcher, Guangzhou Institute of Geochemistry, CAS, China	Rapporteur
Qin WANG	Professor, Nanjing University, China	Examinatrice
István KOVÁCS	Researcher, Geological and Geophysical Institute of Hungary, Hungary	Examinateur
Jannick INGRIN	Director of Research at the CNRS, Universty Lille 1, Lille	Directeur de thèse
Qunke XIA	Professor, Zhejiang University, China	Directeur de thèse

Acknowledgement

When I started writing this section, I knew my thesis came to the end. I would like to express my sincerely gratitude to many persons who helped me a lot during my PhD study at Hefei and Lille.

Firstly, I am really grateful to my supervisors Dr. Qunke Xia and Dr. Jannick Ingrin. I became a team member of Dr. Xia`s group since I was an undergraduate student in 2010. He concerned me a lot, not only on my research but also on my life. He made the group a warm and sweet family. I thank greatly to Dr. Xia, who taught me how to do the research on natural science. He also provided me the opportunity to go to France as a jointed student. Dr. Jannick Ingrin offered great assistance to me during my stay in France. His careful and serious attitude on research impressed me deeply. He and his wife Claudia are very nice and easygoing, and I really admire the love between them.

Thanks to the professors, who have contributed greatly to my geological education at USTC: Dr. Shuguang Li, Dr. Yongfei Zheng, Dr. Fukun Chen, Dr. Fang Huang, Dr. Yilin Xiao, Dr. Yican Liu, Dr. Gentao Zhou, Dr. Xiaoyong Yang, Dr. Jun Tang, Dr. Min Feng, Dr. Zhi Xie, Dr. Ji'an Hong and Dr. Yingming Sheng, and at USTL: Dr. Patrick Cordier, Dr. Sébastien Merkel.

I thank Jiangling Xu for his help on EPMA, Christophe Depecker and Isabelle De Waele for their help in FTIR and Raman analysis. Thanks to Dr. Etienne Deloule, Andrey Gurenko and Nordine Bouden at CRPG, Nancy for their assistance on the measurements of SIMS. Thanks also go to Xiaoyan Gu and Yanan Zhang for their careful help in daily life when I was conducting the ion microprobe measurement at Nancy.

I am grateful to my colleagues in Lille: Alexandra Goryaeva, Christopher Langrand, Srinivasan Mahendran, Billy Clitton Nzogang, Riccardo Reali, Pierre-Marie Zanetta and Xiaoyu Sun. They offered me a lot of help and I had a happy time with them. I also thank my Chinese friends in France, Yufei Hao, Dandan Niu, Yabin Jin, Zhijun Wu, Fan Gao, Haifeng Yuan, Shuo Li, Xiaoping Hou, Chao Meng, who accompanied with me when I was abroad.

Acknowledgement

Much gratitude should go to the members of our group in China: Bo Zhao, Jiangling, Xu, Yantao Hao, Yan Yang, Pei Li, Peipei Zhang, Yaping Zhang, Guicai Yang, Bin Wang, Jia Liu, Ling Liu, Qichao Zhao, Shaochen Liu, Zubing Jia, Zizhen Wang, Zhenzhen Tian, Yao Bi and Hui Cheng. I really enjoy the work and life with them, we are a big family! I also want to thank my friends and classmates Junjie Shen, Haihao Guo, Haibing Ruan and Guoqiang Wang, who offered me lots of help and advice.

I can’t forgot to thank the China Scholarship Council for supporting my study in France.

Last but not least, I would like to appreciate my devoted family. My parents Qilong Chen and Yun Hu raised and educated me, and devoted all their love to me. Without their support and understanding, I could not finish my doctoral thesis. I owe a special thanks to my fiancée Jiuxing Xia for the encouragement and love.

Résumé

Cette étude met en évidence le rôle de la subduction Pacifique dans la genèse des basaltes est- chinois à l'aide de la mesure de leur teneur en eau par infrarouge en transformé de Fourier (IRTF) et de leur composition isotopique en oxygène analysée par sonde ionique (SIMS).

Les valeurs en $\delta^{18}O$ des phénocristaux de clinopyroxènes (cpx) des basaltes de Shuangliao, varient entre 4.10‰ et 6.73‰. Elles suggèrent la présence d'une croûte océanique recyclée (ROC) dans la source magmatique. La forte valeur de la concentration en H_2O et du rapport H_2O/Ce de la source magmatique (0.90-3.06 pds.%, 158-737), suggère également la contribution de sédiments riches en eau à la source. Par contre, les basaltes de Wulanhada ont une teneur en eau nettement plus faible (0.21-0.69 pds.%). Leur $\delta^{18}O$ élevé (5.49-7.38 ‰) et la corrélation du rapport H_2O/Ce avec $^{87}Sr/^{86}Sr$, Ba/Th, Nb/La, Nb/U et Ce/Pb indiquent clairement une contribution de sédiments déshydratés dans la source, en plus de la croûte (ROC). Dans les basaltes de Chaihe-aershan, le $\delta^{18}O$ des cpx ainsi que la teneur en H_2O initiale du magma varient sur une large gamme (4.27-8.57‰, 0.23-2.70 pds.%). À partir de la comparaison entre le $\delta^{18}O$ des phénocristaux de cpx, H_2O/Ce, Ba/Th et l'anomalie en Eu en roche totale, nous avons clairement identifié trois composantes distinctes dans la source magmatique : une croûte océanique supérieure avec des sédiments marins, une croûte océanique inférieure gabbroïque altérée et le manteau au voisinage de la source. Les mesures faites sur les basaltes ultra potassiques de Xiaogulihe révèlent des teneurs en H_2O et des rapport H_2O/Ce faibles (0.36-0.50 pds.%, ~15). Les valeurs en $\delta^{18}O$ des phénocristaux d'olivine de ces basaltes, couplées à des valeurs basses en $^{206}Pb/^{204}Pb$ et relativement hautes en $^{87}Sr/^{86}Sr$ de la roche, suggèrent que l'origine de ces basaltes est très probablement liée à la présence de sédiments anciens fortement déshydratés, riches en potassium.

Notre estimation de la concentration en eau de ces basaltes varie de 150 à 4500 ppm (essentiellement > 500 ppm). Ceci est nettement supérieur aux valeurs du manteau

lithosphérique de la région, ce qui supporte l'idée que la source des basaltes continentaux Cénozoïques de l'est de la Chine a une origine profonde, probablement dans la zone de transition. Les contributions des différentes composantes de la croûte océanique recyclée changent de façon importante sur une courte période (par exemple pour Chaihe-aershan et Shuangliao). L'évolution avec le temps de la source est très probablement dictée par l'apport continuel de matériau recyclé par la plaque Pacifique. Notre étude privilégie une source profonde, probablement dans la zone de transition, en accord avec les observations Géophysiques qui montrent la présence de reliques de la plaque Pacifique dans la zone de transition à l'aplomb de la région étudiée.

La concentration en H_2O et le rapport H_2O/Ce des basaltes est chinois varient sur une large gamme de valeurs (0.19 to 3.89 pds.%, 12 to 737) et sont significativement plus élevés que ceux des OIBs. Il est à noter que ces valeurs décroisent d'est en ouest dans le sens de la subduction, excepté pour Chaihe-aershan. Ce comportement pourrait être expliqué par une déshydratation progressive de la plaque Pacifique. Plus généralement, il est clair que les contributions à la source de matériaux recyclés varient sur l'ensemble de la zone étudiée, indiquant des degrés d'altération et de déshydratation variables avant ou pendant la subduction de la partie de la plaque Pacifique incriminée.

Abstract

This work is focused on the role of the Pacific subduction in the genesis of the Cenozoic continental basalts in eastern China, based on the approaches of the water contents (analyzed by Fourier transform infrared spectroscopy (FTIR)) and oxygen isotope compositions (analyzed by Secondary ion mass spectrometry (SIMS)).

The $\delta^{18}O$ values of cpx phenocrysts in the Shuangliao basalts range from 4.10‰ to 6.73‰, which provides a strong evidence for the contribution of recycled oceanic crust (ROC) in the mantle source. Combined with the high H_2O content and H_2O/Ce ratios of the "primary" magma (0.90-3.06 wt.%, 158-737), the contribution of water-rich sediment component has also been suggested. Unlike the Shuangliao basalts, the Wulanhada basalts have lower H_2O contents (0.21-0.69 wt.%). The high oxygen isotope compositions (5.49-7.38 ‰) and the correlations of H_2O/Ce with $^{87}Sr/^{86}Sr$, Ba/Th, Nb/La, Nb/U and Ce/Pb ratios indicate that the contributions of a significantly dehydrated sediments and ROC to the mantle source. In Chaihe-aershan basalts, the $\delta^{18}O$ values of cpx phenocrysts and the H_2O contents of "primary" magmas vary widely (4.27-8.57‰, 0.23-2.70 wt.%).Three components (altered upper oceanic crust and marine sediments, altered lower gabbroic oceanic crust, ambient mantle) have been identified in the mantle source based on the relations between $\delta^{18}O$ values of the cpx phenocrysts, H_2O/Ce and Ba/Th ratios and the Eu anomaly of bulk rock. For the Xiaogulihe ultrapotassic volcanic rocks, the estimated H_2O contents and H_2O/Ce ratios are low (0.36-0.50 wt%, ~15). Combined with the high $\delta^{18}O$ values of olivine phenocrysts, the low $^{206}Pb/^{204}Pb$ ratios and moderately high $^{87}Sr/^{86}Sr$ ratios of the bulk rock, we concluded that highly dehydrated ancient sediments could be a most likely candidate for the K-rich component in the mantle source.

The conservatively estimated water contents of mantle source are 150-4500 ppm (mostly high than 500 ppm), significantly higher than those of lithospheric mantle from the same region, which provides clear evidences that the Cenozoic continental basalts in eastern China originated from the hydrous MTZ. The contributions of the different recycled oceanic components to the mantle source of the basalts changed significantly

within a limited time (e.g., Chaihe-aershan, Shuangliao). This temporal heterogeneity of the source components is most likely triggered by the ongoing Pacific slab subduction, which continuously transports recycled materials to the mantle. In other words, the Pacific slab located in the MTZ may be a primary source for the enriched components.

The H_2O contents and H_2O/Ce ratios of basalts from eastern China vary widely (0.19 to 3.89 wt.%, 12 to 737), and are relatively higher than those of typical OIBs. Interestingly, the H_2O contents and H_2O/Ce ratios of basalts in eastern China decrease from the east to the west, along the subducting direction of the Pacific slab, except for the Chaihe-aershan basalts. This situation might be associated with the dehydration process of the subducted Pacific plate. The contributions of recycled components to the mantle source of basalts from different areas of eastern China vary widely, which could be caused by varying degrees of alterations and dehydration before and during the subduction of the Pacific plate.

Key Words: Continental basalt, water content, oxygen isotope, source heterogeneity, mantle transition zone, Pacific slab, eastern China

摘 要

为了研究太平洋板块俯冲与中国东部板内玄武岩起源之间的联系，本文从玄武岩水含量、斑晶氧同位素组成以及地幔源区时间和空间上的不均一性的角度，选取位于中国东北地区的双辽、乌兰哈达、柴河-阿尔山和小古里河新生代玄武质火山群作为研究对象，详细地分析了全岩的主、微量元素，单斜辉石斑晶的主量元素、水含量和氧同位素的组成，通过最早结晶的单斜辉石斑晶的水含量结合水在单斜辉石斑晶（镁值 Mg#>75）和熔体之间的分配系数计算得到“原始”岩浆的水含量。

对于双辽玄武岩，单斜辉石斑晶的氧同位素($\delta^{18}O$)从 4.10‰变化到 6.73‰，类似于经典的蚀变洋壳氧同位素的变化特征。另外，氧同位素与全岩的 Eu 和 Sr 的异常存在相关性。这些都指示其地幔源区存在再循环洋壳组分。 经过计算，双辽玄武岩“原始”水含量为 0.90-3.06wt.%，明显高于 MORBs(大洋中脊玄武岩)和 OIBs(洋岛玄武岩)的水含量。结合双辽玄武岩显著的 K 正异常以及全岩 H_2O/Ce 与 Ba/Th, Ce/Pb 比值之间的相关性，推测其源区还存在富水沉积物组分。

不同于双辽玄武岩，位于太平洋板块俯冲最前缘的乌兰哈达玄武岩具有相对低的水含量(0.21-0.69 wt.%)，介于 MORBs 和 OIBs 之间。单斜辉石斑晶具有较高的氧同位素组成（5.49-7.38‰），显著高于典型 MORB 和地幔橄榄岩中单斜辉石的氧同位素组成。另外，乌兰哈达玄武岩全岩的 H_2O/Ce 比值与全岩的 $^{87}Sr/^{86}Sr$, Ba/Th, Nb/La, Nb/U 和 Ce/Pb 比值之间存在相关性。这些说明了其源区中存在脱水的沉积物和再循环洋壳组分。

柴河-阿尔山火山群由超过 35 座第四纪（<2Ma）玄武质火山组成。不同样品之间单斜辉石斑晶的氧同位素组成和“原始”熔体水含量变化范围很大(4.27-8.57‰, 0.23-2.70 wt.%)，指示其地幔源区化学组成的高度不均一性。另外，单个样品内部单斜辉石斑晶氧同位素组成和水含量同样具有很大的变化范围，表明在火山喷发前发生了快速的岩浆混合作用。其斑晶的氧同位素组成，全岩的 H_2O/Ce 和 Ba/Th 比值，Eu 异常之间的关系说明柴河-阿尔山玄武岩地幔源区中存在三个组分(再循环蚀变上部洋壳和沉积物，蚀变的下部辉长质洋壳和周围地幔)。

对于小古里河超钾质火山岩，计算得到的水含量和 H_2O/Ce 比值很低（0.36-0.50 wt%，~15），显著低于中国东部钠质碱性玄武岩。这意味着其源区中富 K 组分是相对“干”的。结合其高的橄榄石斑晶氧同位素比值，低的全岩 $^{206}Pb/^{204}Pb$ 比值和较高的全岩 $^{87}Sr/^{86}Sr$ 比值，推

测脱水的古老沉积物组分很可能是小古里河超钾质玄武岩源区中富钾组分的来源。

由于地幔不同圈层之间的含水性差异很大，因此水含量可以成为示踪大陆玄武岩来源的有力证据。根据玄武岩“原始”熔体的水含量，源区的部分熔融程度和水的分配系数，我们计算了中国东部新生代玄武岩源区的水含量。其中，最保守估计的水含量是 150-4000 ppm (大部分超过 500 ppm)，仍然显著的高于相应地区地幔橄榄岩的水含量。并且中国东部新生代玄武岩源区的水含量与橄榄岩包体的水含量呈现不同的空间变化特征，这更加清晰地表明岩石圈地幔并不是这些玄武岩的源区。另外，除了海南岛，地球物理的观测并没有发现中国东部存在深部地幔柱的痕迹，而且位于地幔过渡带的太平洋板块也会阻挡深部地幔柱的上涌。因此，具有高水含量特征的中国东部新生代板内玄武岩只可能来源于富水的地幔过渡带。对单个火山群中研究发现，不同的再循环洋壳组分（沉积物，上部洋壳，下部洋壳）对地幔源区的贡献随时间有强烈变化(例如，柴河-阿尔山玄武岩，双辽玄武岩)。由于太平洋板块正不断地向中国东部俯冲，持续地向地幔输送再循环物质，因此这种地幔源区时间上的不均一性很可能是由持续俯冲地太平洋板块俯冲引起的。换句话说，位于地幔过渡带的太平洋板块很可能是中国东部新生代玄武岩源区富集组分的主要来源。

统计发现，中国东部新生代玄武岩的水含量和 H_2O/Ce 比值变化很大(0.19-3.89 wt.%, 12-737)，大部分高于典型的 OIBs 的水含量。值得注意的是，靠近太平洋海沟的玄武岩的水含量和 H_2O/Ce 比值（双辽，山东和浙江）要高于远离太平洋海沟的玄武岩的水含量和 H_2O/Ce 比值（乌兰哈达，小古里河和太行山），除了柴河-阿尔山玄武岩。这可能与太平洋板块的脱水过程有关。另外，在双辽，乌兰哈达，柴河-阿尔山，小古里河，山东，太行山和浙江玄武岩源区之间，源区再循环组分贡献的差异变化很大。太平洋板块在循环过程中会经历不同程度的蚀变和脱水，可能导致不同地区再循环组分的比例和组成发生变化，进而引起中国东部板内玄武岩地幔源区空间上的不均一性。

关键词：大陆玄武岩，水含量，氧同位素，源区不均一性，地幔过渡带，太平洋板块，中国东部

Table of Contents

Table of Contents

List of Illustrations

<Chapter1>

<Chapter 3>

<Chapter 4>

List of Tables

<Chapter 3 >

<Chapter 4 >

Chapter 1. Introduction

1.1 The continental intraplate basalts

The Cenozoic continental intraplate basalts are one of the most common rocks and widely spread in continents (e.g., eastern Asia, Western Africa, western North America, western/central Europe, southeastern Australia) (Farmer, 2014) (Fig. 1-1). Unlike the magmatism taking place at the active plate margins, these basalts formed in the interior of the plate, and their genesis has been hotly debated over the last 30 years. They are mainly subdivided into sodic alkaline basalts ($Na_2O/K_2O>1$), potassic alkaline basalts ($Na_2O/K_2O<1$) and tholeiitic basalt. Based on trace element patterns and Sr-Nd-Pb isotopic compositions, these basalts have characteristics of typical OIBs (ocean island basalts) (Farmer, 2014; Hoffman, 1997). It indicates the presence of an enriched component in the mantle sources. Studying the continental basalts is helpful to understand the influence of recycled materials on mantle geochemical heterogeneities and its evolution.

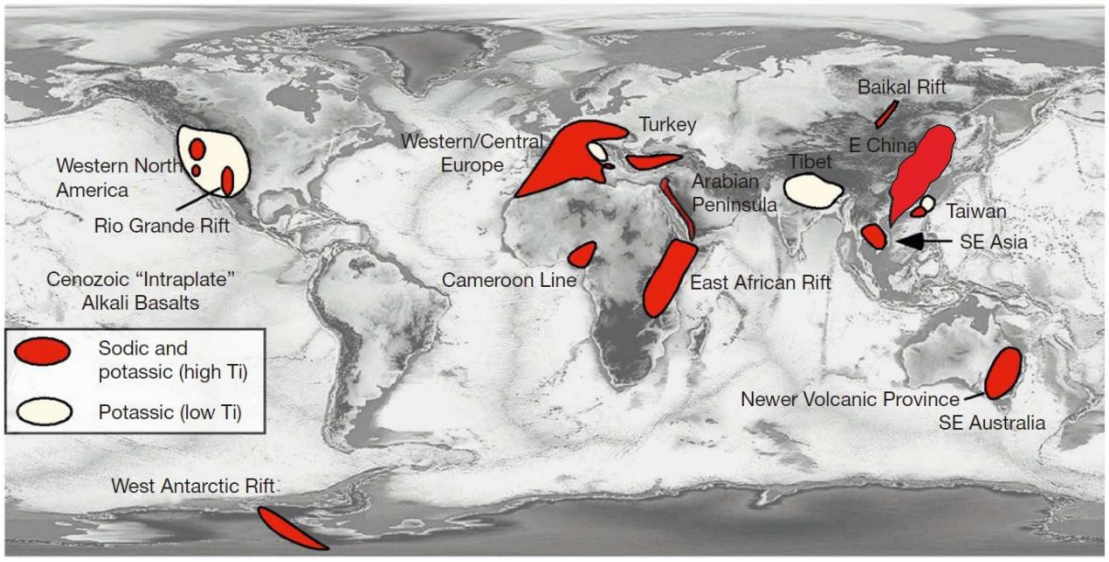

Figure 1-1. Location of the Cenozoic sodic and potassic 'intraplate' alkali basalt volcanic fields worldwide (modified after Farmer (2014)).

1.1.1 Research status of continental basalts from eastern China

There are widespread Cenozoic continental basalts in eastern China, extending from the northernmost to the southernmost, along the continental margin (Lei et al., 2013) (Fig. 1-2). They form an important part of the volcano belt of the western circum-Pacific rim, and provide a noteworthy opportunity to study the continental intraplate magmatism.

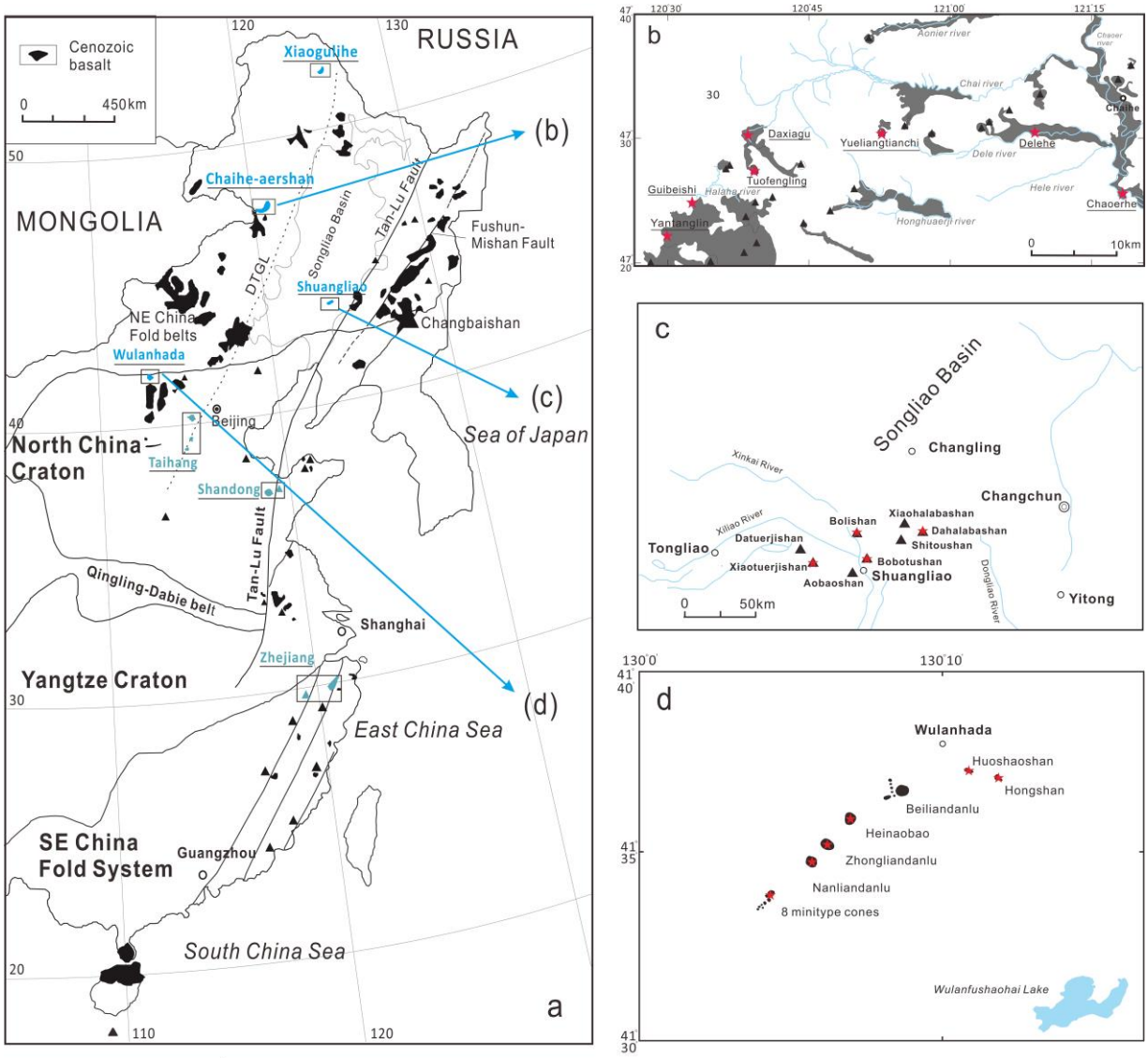

Figure 1-2. Simplified tectonic units and distribution of Cenozoic basalts in eastern China as well as the location of the Chaihe-aershan, Shuangliao, Wulanhada and Xiaogulihe volcanic field (modified according to Fan et al., 2011; 2014; Xu et al., 2012).

A great deal of work has been conducted over the last 30 years to study the genesis of this intraplate volcanism (e.g., Chen et al., 2007; Chen et al., 2009; Choi et al., 2005; Fan and Hooper, 1991; Ho et al., 2003, 2008; Kuritani et al., 2009, 2011, 2013; Niu, 2005; Sakuyama et al., 2013; Tang et al., 2006; Xu, 2014; Xu et al., 2012; Wang et al., 2011; Zhi et al., 1990; Zhou and Armstrong, 1982; Zhang et al., 1995; Zhang et al., 2009; Zou et al., 2000, 2003, 2008). The associated challenges are primarily concentrated on source of the enriched components and the region where the basalts was formed.

Similar to continental intraplate basalts worldwide, these basalts display OIB (ocean island basalt)-like trace element patterns and variable Sr-Nd-Pb isotopic compositions (e.g., Zhou and Armstrong, 1982; Zhi et al., 1990; Fan and Hooper, 1991; Zou et al., 2000; Chen et al., 2007). There are controversial opinions on the source of the associated enriched components: (1) recycled lower continental crust (e.g., Chen et al., 2009; Zeng et al., 2011; Chu et al., 2013); (2) asthenospheric mantle or lithospheric mantle metasomatized by melts rich in water, which were produced by dehydration of subducted oceanic lithosphere (e.g., Niu, 2005; Zhang et al., 2009; Wang et al., 2011); (3) direct partial melt of the subducted oceanic crust (e.g., Sakuyama et al., 2013; Xu et al., 2012); and (4) recycled ancient and/or recent marine sediments (e.g., Kuritani et al., 2011, 2013). Accordingly, different regions in which the basalts were produced have been proposed, including the lithospheric mantle (e.g., Chu et al., 2013; Wang et al., 2011; Zhang et al., 2009), the asthenospheric mantle (e.g., Choi et al., 2005; Niu, 2005; Zou et al., 2000) and the MTZ (mantle transition zone) (e.g., Sakuyama et al., 2013; Xu et al., 2012; Kuritani et al., 2011; 2013).

In the last ten years, seismic imaging has identified the remnants of the subducted Pacific slab in the MTZ of eastern China (Fig. 1-3) (e.g., Fukao et al., 1992; Huang and Zhao, 2006; Wei et al., 2012; Liu et al., 2017b). New geochemical approaches have been developed to trace different components that are involved in the mantle source, such as the H_2O content of magma (Liu et al., 2015a, b), O isotopic compositions of the phenocrysts (Liu et al., 2015a, b; Wang et al., 2015), Mg isotopic compositions of bulk

rock (Huang et al., 2015; Wang et al., 2017), and composition of melt inclusions (Li et al., 2016). The signal of the recycled oceanic crust has been identified in the mantle source of these basalts. Considering the presence of the Pacific slab in the MTZ, they linked the recycled oceanic components with the subducted Pacific slab. However, eastern China underwent several subduction events (e.g., Paleo-Tethyan, Paleo-Asian and Izanagi plate subduction) (Müller et al. 2008; Windley et al. 2010), and the recycled oceanic materials could also be derived from these ancient subduction events. Currently, there is no direct evidence for whether the enriched component is derived from the subducted Pacific plate and whether the mantle source of these basalts is in the MTZ.

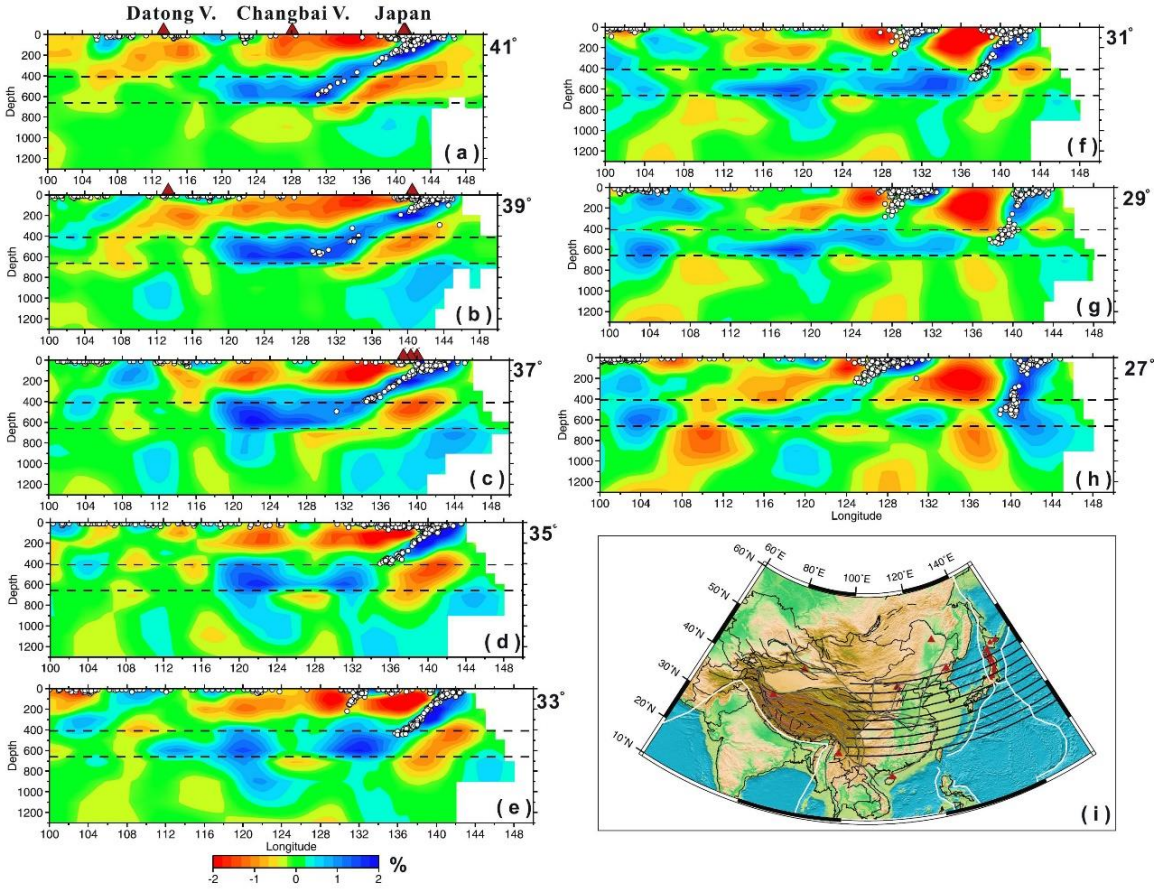

Figure 1-3. (a–h) East-west vertical cross sections of P wave velocity perturbations along the profiles in eatern China shown in (i) the map (modified from Huang and Zhao, 2006). The velocity perturbation scale is shown at the bottom.

The recycled oceanic crust is a mixture of sediments, upper oceanic crust and lower gabbro oceanic crust. The slab underwent various forms of alterations and dehydration during the recycling process (e.g., Pietruszka et al., 2013). Understanding the temporal and spatial influences of these different components in the mantle source is essential to identify the contribution of the subducted oceanic slab on mantle heterogeneity and its contribution to the genesis of intraplate basalts.

This work is focused on the role of the Pacific subduction in the genesis of the Cenozoic continental basalts in eastern China, including: the source of the enriched components in the mantle source of continental basalts, the region where the continental basalts is produced and the temporal and spatial heterogeneity of the source components.

1.1.2 Continental basalts studied in this work

Throughout eastern China, the basalts in Northeast China (NE China) are the most widely distributed (Fig. 1-2). There are hundreds of Cenozoic volcanoes in NE China with a total area of about 50,000 km^2. Among them, the Shuangliao volcanic field is located in the east part (southeast of the Songliao Basin), Chaihe-aershan and Wulahada volcanic field are distributed in the west part (near the Daxing'anling-Taihang Gravity Lineament (DTGL), above the front edge of the subducted Pacific slab) (Fan et al., 2014; Ho et al., 2013; Huang and Zhao, 2006; Liu et al., 2017b; Wei et al., 2012; Xu et al., 2012; Zhao and Fan, 2012). These areas are appropriate places to explore the possible effects of the spatial extent of the Pacific slab. Furthermore, the volcanoes in each volcanic fields erupted within a limited time period, especially those in Chaihe-aershan, more than 35 small-volume Quaternary basaltic volcanoes have erupted in the last 2 Myr. The large number of volcanic eruptions over a short period in a single volcanic field provides an opportunity to study the evolution of mantle source in detail and explores the possible factors that trigger the variation of the components in the mantle source.

Previous studies showed that the OIB-like trace elements and Sr-Nd isotopic

compositions of basalts in these areas were similar to those of other basalts in eastern China. Xu et al. (2012) conducted a detailed geochemical study including major and trace elements analysis and Sr-Nd-Pb isotopes for the basalts of Shuangliao, NE China. Due to the low $^{206}Pb/^{204}Pb$ ratios (18.13-18.34) compared with typical HIMU OIBs, Xu et al. (2012) proposed the presence of young subducted oceanic crust in the mantle source of the Shuangliao basalts, with the high contribution of the upper oceanic crust to the source of earlier (51-48 Ma) basalts and the high contribution of the lower oceanic crust for the later (41-43 Ma) basalts. Several studies have been carried out on the Chaihe-aershan and Wulanhada basalts (Fan et al., 2014; Ho et al., 2013; Zhao and Fan, 2012). They suggested that these basalts originated from the partial melting of garnet lherzolites in the asthenosphere, but there was no further discussion on the source of the enriched components.

It is worth noting that, there are a small amount of ultrapotassic/potassic basalts distributed in the northernmost China, including Xiaogulihe volcano, together with the Wudalianchi, Erkeshan and Keluo (WEK) volcanoes (Fig. 1-2). Unlike the sodic alkaline basalts, the mantle-derived ultrapotassic/potassic volcanic rocks are characterized by high K_2O content and K_2O/Na_2O ratios and low CaO and Al_2O_3 contents, high Mg# (=Mg/(Mg+Fe), in mole ratio) and extreme enrichment of incompatible elements (Foley et al., 1987). The origin of these ultrapotassic volcanic rocks, particularly, the source of potassium-rich component is highly discussed and lots of works have addressed this question (Kuritani et al., 2013; Murphy et al., 2002; Sun et al., 2014; 2015; Zhang et al., 1995). There are still controversial opinions on the origin of the potassium-rich component. One possibility is phlogopite-bearing garnet-peridotites in metasomatic sub-continental lithospheric mantle (SCLM) (Zhang et al., 1995; Sun et al., 2014; 2015). Another view was proposed recently, suggesting that the potassium-rich component came from subducted potassium-rich continental-derived sediments located in the mantle transition zone (Murphy et al., 2002; Kuritani et al., 2013). In this work, two samples from Xiaogulihe have been studied to investigate the possible source of the potassium-rich component and to compare it with other sodic

alkaline basalts.

1.2 New research approaches

Combined with the traditional approaches (major and trace element compositions of bulk rock and major element concentrations of phenocrysts), we have developed a new approach which is based on the analysis of water content of the magma and sources and oxygen isotope composition to identify the source of these basalts.

1.2.1 Water content of magma and source

The water contents in different layers of mantle vary greatly. The H_2O content of the upper mantle is estimated to be 50-250 ppm wt. H_2O (e.g., Bodnar et al., 2013; Hirschmann et al., 2005; Ohtani et al., 2015) and the H_2O content of the lower mantle might be similar or lower (e.g., Bodnar et al., 2013; Panero et al., 2015), however, the H_2O content in MTZ can be as high as 1% (e.g., Bodnar et al., 2013; Pearson et al., 2014). Thus, the water content in the source of continental basalts can be a diagnostic index to recognize if the enriched components in the source of basalts came from the MTZ or not. Due to the impact of multi-stage metasomatism, hydrous minerals (amphibole, phlogopite) were formed in some continental lithosphere, which may be rich in water (Menzies et al., 1987; Hawkesworth et al., 1987). Many studies on H_2O content of the lithosphere in eastern China have been conducted (Hao et al., 2014, 2016; Xia et al., 2010, 2013a; Yang et al., 2008; Yu et al., 2011). They provide relevant references for water content of the source for continental basalts.

On the other hand, H_2O and Ce are expected to have similar partition coefficients between mantle minerals and melt, and their ratios remain unchanged through partial melting and crystal fractionation. Thus, H_2O/Ce ratios of melts can be used to reflect information on the mantle sources of basalts (Dixon et al., 2002; Michael et al., 1995; Shaw et al., 2012). Recycled components have distinct H_2O/Ce ratios from that of

normal mantle. For instance, the H_2O/Ce ratio of GLOSS (global subducting sediment) is about 1280, higher than DMM (depleted MORB mantle, ~200), EM (enriched mantle, <100) and dehydrated ROC (recycled oceanic crust) which has low H_2O/Ce (~100) (Dixon et al., 2002; Plank and Langmuir, 1998). Therefore, H_2O/Ce ratios of basalts is a potential index for identifying different components in the basalts source.

Generally, three approaches are uesed to estimate the water content of magma, including the volcanic glass (e.g., Michael, 1995; Dixon et al., 1997; Dixon and Clague, 2001), the melt inclusions in olivine phenocrysts (e.g., Sobolev and Chaussidon, 1996; Wallace, 2005) and calculation through the water content of clinopyroxene (cpx) phenocryst and H partition coefficient based on the phenocryst-melt equilibrium (e.g., Wade et al., 2008; Xia et al., 2013b). For continental basalts, volcanic glass is rare, and without the water pressure of the deep ocean to prevent H degassing, the water content of glass is not considered to be representative of the true water content of continental basalts. The melt inclusion approach is complex to operate, and experimental studies have demonstrated that the water of melt inclusions in olivine can re-equilibrate rapidly, if the cooling speed is not fast enough (Portnyagin et al., 2008; Gaetani et al., 2012). In contrast, the measurement of H_2O in cpx phenocryst is more convenient and H diffusion coefficient is relatively low (Ingrin and Blanchard, 2006).

Cpx phenocrysts in basalts are commonly small, thus it is extremely difficult to polish them to get two oriented sections from one single grain for polarized measurement by Fourier transform infrared spectrometry (FTIR) (Libowitzky and Rossman, 1996). Recent studies have indicated that when polarized absorbance is low (<0.3) and the mineral is less anisotropic, the water content of the mineral can be estimated by a single measurement using unpolarized light by FTIR (30% error is considered) (Kovacs et al., 2008; Liu et al., 2015b; Sambrige et al., 2008; Withers 2013; Xia et al., 2013b). Besides, O'Leary et al. (2010) conducted experimental study on the relationship of H partition coefficient between cpx and melt ($D^{cpx/melt}$) with varying Al_2O_3 contents of cpx (0.2 % to 19 %). They have shown that $D^{cpx/melt}$ is mainly a function of the Al^{3+} concentration in tetrahedral site in cpx. The H_2O partition

coefficients of cpx can be calculated from Equation 10 in O'Leary et al. (2010), which is expressed as: D = exp (-4.2+6.5*X (^{iv}Al)-X (Ca)), where X (^{iv}Al) and X (Ca) are the concentrations of Al^{3+} in a tetrahedral site in cpx and total Ca^{2+} in cpx, respectively. Thus, the water content of a magma can be estimated from the H_2O content in cpx phenocrysts measured by FTIR and the $D^{cpx/melt}$ calculated from major element composition of cpx phenocrysts. With this method, Xia et al. (2013b) confirmed the H_2O content (3.4±0.7 wt.%) for the primitive "arc-type" basaltic melts from Feixian area in the North China Craton (NCC), which is in agreement with the average H_2O content (3.9±0.4 wt.%) of global mafic arc magmas (Plank et al., 2013).

1.2.2 Oxygen isotope composition

The variations in the oxygen isotopic composition in silicate rocks are primarily due to water-rock interactions on the Earth's surface and crust; thus, these variations are a powerful tool for tracing crustal components in the mantle (Eiler, 2001; Eiler et al., 1997). The oceanic crust undergoes hydrothermal alteration during its formation in mid-ocean ridges, which leads to the exchange of oxygen isotope compositions between oceanic crust and seawater (Muehlenbach and Clayton, 1976). Because the temperature of hydrothermal alteration is gradually decreasing from the lower to the upper part of the oceanic crust, the oxygen isotopic composition of the oceanic crust in different layers will change with the nature and depth in the oceanic crust (Taylor, 1974). The altered oceanic crust will form a unique oxygen isotope composition profile throughout the section of oceanic crust, which exhibits in a way that the $\delta^{18}O$ values of the upper altered oceanic crust are generally higher than that of the normal mantle, but the $\delta^{18}O$ values of the lower altered oceanic crust are more or less lower than that of the normal mantle (Fig. 1-4) (Eiler, 2001; Gao et al., 2006; Gregory and Taylor, 1981; Hoffman SE et al., 1986). Therefore, oxygen isotope can be a powerful tool to trace the component of oceanic crust in the mantle source (Eiler et al., 2000; Kokfelt et al., 2006; Putlitz et al., 2000; Wang et al., 2015; Woodhead et al., 1993).

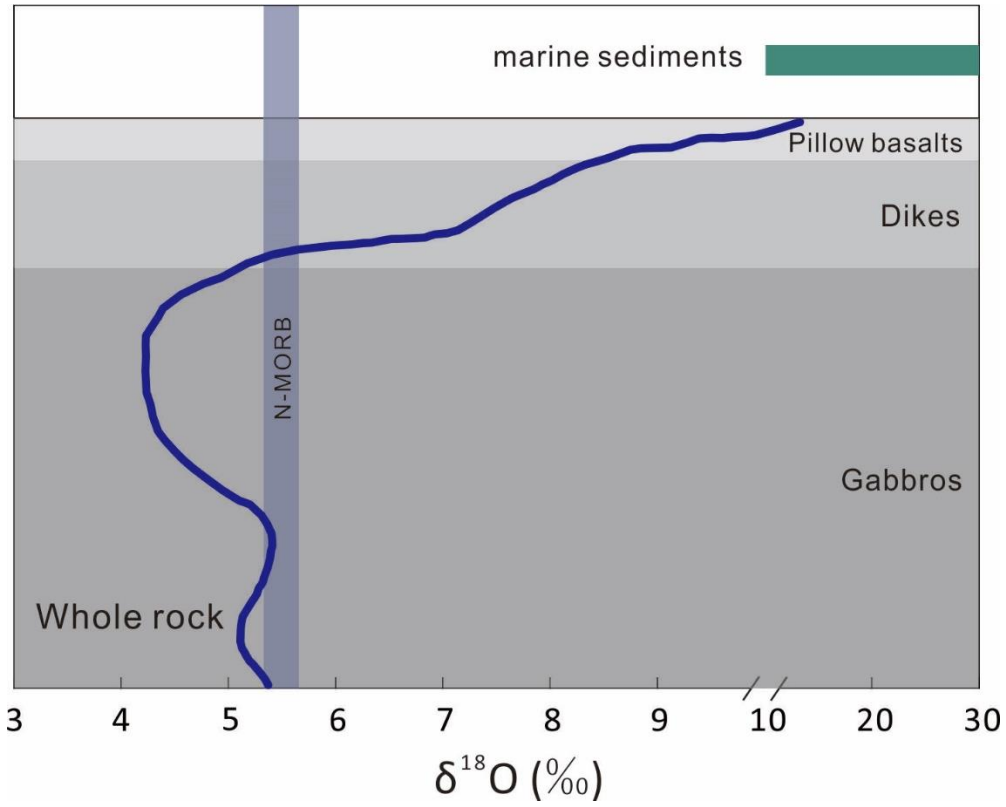

Figure 1-4. Typical oxygen isotope profile of altered sediment-covered oceanic crust. The data for oceanic crust are based on the Samail Ophiolite (Gregory and Taylor, 1981), the $\delta^{18}O$ values of marine sediments are from Eiler, (2001).

The mineral oxygen isotope composition can be estimated by laser fluorination method or in-situ secondary ion mass spectrometry (SIMS) method, typically (e.g., Clayton and Mayeda, 1963; Fitzsimons et al., 2000; Valley and Graham, 1991; Valley et al., 1995). The continental basalts generally contain abundant xenoliths and xenocrysts that it is not easy to exclude xenocrysts when phenocrysts are separated from the basalts for laser fluorination measurements. Therefore SIMS is a more appropriate method. The matrix effect is the main problem for SIMS analysis. A group of cpx megacrysts (NSH2, NSH5, NSH8, NSH9, NSH10, NSH14) from Nushan, eastern China have been extensively studied by Xia et al. (2004). It turned out that the major element concentration and oxygen isotope ratio of these cpx megacrysts were homogeneous. Given that the chemical compositions of cpx phenocrysts in this work

are nearly the same as the compositions of cpx megacrysts mentioned above, these cpx megacrysts were used as standards for correction of matrix effect in this study.

1.3 Aims of this work

In this work, major and trace element compositions of bulk rocks and O isotope compositions, water contents and major element compositions of cpx phenocrysts have been analyzed for the Shuangliao basalts, Wulanhada basalts, Chaihe-aershan basalts, Xiaogulihe ultrapotassic basalts form NE China.

The H_2O contents and oxygen isotope compositions were combined with the trace element ratios (e.g., Ba/Th, Nb/La) to trace the possible contributions of recycled components and investigate the geochemical heterogeneity in the mantle sources of Shuangliao basalts, Wulanhada basalts and Chahe-aershan basalts. The H_2O content of Xiaogulihe ultrapotassic volcanic rocks has been determined to constrain the H_2O content of K-rich component in the mantle source.

Estimating the water content in the mantle source of the basalts in eastern China through water content of the magma, partition coefficient of H_2O and partial melting degree to provide direct evidence for the mantle source of these basalts and find out if they can be connected to the MTZ.

We studied the temporal variation of the source components to investigate the evolution of the mantle source and the possible factors that trigger these variations.

Then combined the basalts studied in this work with the results of previous studies on other basalts (Shandong, Taihang, Zhejiang) in eastern China (Liu et al., 2015a, b; Liu et al., 2016), we investigated the potential influence of the recycled oceanic slab on the spatial heterogeneity of the mantle source for intraplate basalts in eastern China.

Chapter 2. Geological background

2.1 Northeast China

Northeast China (NE China) lies in the Xing'an-Mongolia Orogenic Belt (XMOB), which belongs to the east part of the Paleozoic Central Asian Orogenic Belt (Fig. 1-2a). It is composed of several minor blocks (e.g., Erguna, Xing'an, Songliao, Jiamusi) amalgamated during subduction and collision among the Siberian craton, the North China Craton (NCC) and the Pacific plate (Li, 2006; Sengör and Natalin, 1996; Sengör et al., 1993). The tectonic evolutions of NE China mainly include closure of the Paleo-Asian Ocean, amalgamation of several minor blocks and subduction of the Pacific plate since late Mesozoic (Maruyama et al., 1997; Sengör and Natalin, 1996; Sengör et al., 1993).

Cenozoic basalts are more extensively exposed in NE China compared to the South China Block (SCB) and the NCC. There are hundreds of Cenozoic volcanoes in NE China with a total area of 50,000 km^2. They are mostly distributed in and around the Songliao Basin along the Yilan-Yitong and Fushun-Mishan faults (Fig.1-2a). Among them, the majority are sodic alkaline basalts. A small amount of potassic basalts are distributed at the north margin of Songliao Basin.

2.2 The Cenozoic basalts studied in this work

2.2.1 Shuangliao basalts

The Shuangliao volcanic field is located in the southeast of the Songliao Basin, it consists of eight volcanoes: Aobaoshan (ABS), Bobotushan (BBT), Bolishan (BLS), Shitoushan (STS), Dahalabashan (DHLB), Xiaohalabashan (XHLB), Datuerjishan (DTEJ) and Xiaotuerjishan (XTEJ) (Fig 1-2c). Seismic tomography has shown the presence of a stagnant subducted Pacific slab in the mantle transition zone beneath Shuangliao volcanic field (Huang and Zhao, 2006; Liu et al., 2017b; Wei et al., 2012). The rocks of Shuangliao basalts vary from basanite, alkaline olivine basalt, and

transitional basalts to dolerites (Xu et al., 2012). During the eruption of these volcanoes, abundant peridotite xenoliths were carried out by the basalts, especially by the ones with high alkalinity (Yu et al., 2009). Ar-Ar dating results have shown that all volcanoes erupted between 51.0 Ma and 41.6 Ma. Volcanic cones with high alkalinity erupted between 51 Ma and 48.5 Ma, while transitional or subalkaline cones erupted between 43.0 Ma and 41.6 Ma, indicating that the alkalinity of the Shuangliao volcanic rocks decreased with time (Xu et al., 2012).

Our samples were collected from BBT, BLS, DHLB and XTEJ (red stars in Fig. 1-2c). These rocks can be classified into three types based on their petrography and major element compositions: basanite (BBT and BLS), alkali olivine basalt (DHLB) and transitional basalt (XTEJ) (Xu et al., 2012). The basanites from BBT and BLS contain 20% of olivine and clinopyroxene phenocrysts. The entrained mantle xenoliths are mainly spinel lherzolites with minor spinel harzburgites. In alkali olivine basalts and transitional basalts, phenocrysts are composed of olivine, clinopyroxene and plagioclase. The Ar-Ar plateau ages of BBT, BLS, DHLB and XTEJ basalt are 50.1±0.8, 49.7±0.2, 51.0±0.5 and 43.0±0.4 Ma, respectively (Xu et al., 2012).

2.2.2 Wulanhada basalts

The Wulanhada volcanic field is located between the Central Asian Orogenic Belt (NE China) and North China Craton, near Hannuoba Cenozoic basalts and in the west of Shuangliao volcanic field (Fig 1-2) (Bai et al., 2008; Fan et al., 2014). Seismic imaging showed that the Wulanhada volcanic field was above the front edge of the subducted Pacific slab (Huang and Zhao, 2006; Liu et al., 2017b; Wei et al., 2012). More than 30 volcanoes, including scoria cones and lava, are distributed in this volcanic field along the northeast to southwest direction (Fig. 1-2d). The stage of volcanic activity is mainly concentrated in late Pleistocene and Holocene. Interestingly, the volcanisms at northeast part, including Hongshan and Huoshanshan are relatively older, then the Beiliandanlu volcano, Zhongliandanlu volcano, Nanliandanlu volcano and the

8 mini scoria cones at northeast part are relatively younger (Fan et al., 2014).

The samples were collected from Hongshan (11NW01), Huoshanshan (11NW02), Heinaobao (11NW04), Zhongliandanlu (11NW05), Nanliandanlu (11NW06), and the 8 mini scoria cones (11NW08, 11NW09), which have been studied by Fan et al. (2014). All these basalts are characterized by typical vitrophyric texture and contain 10-20% phenocrysts, which are primarily clinopyroxene and olivine. The matrix are primarily glass and a small amount of plagioclase microcrystals, which suggest a rapid cooling process during the magma ascent.

2.2.3 Chaihe-aershan basalts

The Chaihe-aershan volcanic field includes more than 35 small-volume Quaternary basaltic volcanoes (< 2 Ma) and is located near the Daxing'anling-Taihang Gravity Lineament (DTGL, Fig. 1-2a) and above the front edge of the subducted Pacific slab (Ho et al., 2013; Huang and Zhao, 2006; Liu et al., 2017b; Wei et al., 2012; Zhao and Fan, 2012). The majority of the volcanoes are small cinder cones, and the lava flows are distributed along rivers, such as the Halaha, Chaoer, and Dele Rivers, extending over an area of 400 km^2. K-Ar dating have shown that the volcanoes erupted over a short period, 2.3 to 0.16 Ma (Fan et al., 2011; Ho et al., 2013). The basalts are primarily alkaline olivine basalts with OIB-like trace element patterns, and depleted $^{87}Sr/^{86}Sr$ (0.703485-0.704172) and $^{143}Nd/^{144}Nd$ (0.512812-0.512975) (Ho et al., 2013; Zhao and Fan, 2012).

The samples were collected from Chaoerhe (CEH), Delehe (DLH), Tuofengling (TFL), Guibeshi (GBS), Yantanglin (YTL), Daxiagu (DXG) and Yueliangtianchi (YLTC) (Fig. 1-2b). All of these eruptive rocks carried abundant mantle xenoliths and xenocrysts, suggesting a rapid magma ascent. The entrained mantle xenoliths are primarily spinel lherzolites with minor garnet lherzolites in TFL and DLH basalts. No crustal xenoliths were present in our samples. These basalts have a typical porphyritic texture and contain 10%-20% phenocrysts, which are primarily olivine and

clinopyroxene. The diameter of the phenocrysts can go up to 500 μm. The matrix primarily comprises olivine, clinopyroxene and plagioclase. Among these eruptive rocks, the K-Ar ages of the CEH, DLH, and TFL basalts are 0.27, 1.37 and 0.25 Ma, respectively (Fan et al., 2011).

2.2.4 Xiaogulihe ultrapotassic basalts

The Xiaogulihe volcano, together with the Wudalianchi, Erkeshan and Keluo (WEK) volcanos, are typical ultrapotassic/potassic volcanic rocks in NE China. They are located at the north margin of the Songliao Basin, near the Daxing'anling-Taihang Gravity Lineament, also located above the front edge of the subducted Pacific slab (Fig. 1-2a). The Xiaogulihe ultrapotassic rocks are characterized by extremely high K_2O contents (>7 wt.%) and K_2O/NaO ratios (>3). These basalt are characterized by porphyritic texture and contain ~20% phenocrysts, including olivine, clinopyroxene, and leucite phenocrysts. The matrix is primarily made up of the microcrystal of olivine, clinopyroxene, leucite, plagioclase, nepheline, sodalite and the Fe–Ti oxide (Sun et al., 2014). The K-Ar ages of these rock are 0.19-0.30Ma (Zhang, 1992). Two samples (named GLH12-02 and GLH12-16) have been collected from the Ma'anshan in the Xiaogulihe volcanic field, which have been studied by Sun et al. (2014) and Sun et al. (2015).

Chapter 3. Analytical methods

3.1 Major and trace element concentrations of bulk rock

After the weathered surfaces were removed, the samples were crushed into small fragments (<0.5 cm in diameter) to avoid xenoliths and xenocrysts. Then, the samples were cleaned with deionized water and ground to 200 mesh powder.

For the Shuangliao basalts, the major element compositions of bulk rock were determined in the Public Experiment Center of the University of Science and Technology of China (USTC), using an X-ray fluorescence spectrometer (XRF) on fused glass disks. Loss-on-ignition (LOI) was determined before XRF analysis. Analytical uncertainties of major elements were less than 5%, estimated from repeated analyses of the basalt standard GSR-3. 50 mg of sample powders used for trace element analysis were dissolved in concentrated HF: HNO_3 (1:1) mixture in Teflon bombs for 48 hours at ~190°C, after drying down on the hot plate, the residues were dried in concentrated HNO_3 and then diluted to 80g for analysis. The sample solutions were analyzed on the Agilent 7700 ICP-Ms at the CAS Key laboratory of Crust-Mantle Materials and Environments (CAS-CMME), USTC, following analytical method described in Hou and Wang, (2007). The precision of trace element concentrations is better than 5% from repeatedly analyzed USGS standards, BHVO-2 and AGV-2.

Major and trace element concentrations of Chaihe-aershan and Allegre basalts were analyzed at ALS Chemex (Guangzhou, China) Co., Ltd. Major element compositions were measured by X-ray fluorescence spectrometer (XRF) on a fused glass disk. Loss-on-ignition (LOI) was determined before XRF analysis. The precision for element concentrations >1 wt.% was 1%–3% and approximately 10% for element concentrations <1 wt.%. For trace elements, two methods were employed to check the accuracy of the results against each other. For the first method, the sample powder was mixed with lithium metaborate flux, fused at 1000°C and dissolved in 100 ml 4% nitric acid; the solution was then analyzed based on PerkinElmer inductively coupled plasma-mass spectrometry (ICP-MS). For the second method, the sample powder was dissolved

in concentrated HNO_3-HF-$HClO_4$ mixture in a Teflon bomb, diluted by dilute nitric acid after being dried on a hot plate, and then analyzed by ICP-MS. The precision is generally better than 5% for most trace elements. The differences between the concentrations of some trace elements measured by the two methods are less than 5% for most cases.

3.2 Water content of clinopyroxene phenocrysts and corresponding melt

3.2.1 Fourier transform infrared spectroscopy (FTIR) measurement

The water content of clinopyroxene phenocrysts was measured at CAS-CMME, USTC by a Nicolet 5700 Fourier transform infrared spectroscopy (FTIR) coupled with a Continuμm microscope, using a KBr beam splitter and a liquid-nitrogen cooled MCT-A detector (Fig. 3-1a) and at University Lille 1, France by a Bruker Vertex 70 spectrometer coupled with a Bruker Hyperion 3000 FTIR-microscope (Fig. 3-1b), following the unpolarized method described in Xia et al. (2013b). Double-polished thin sections with thicknesses between 40 and 120 μm (depending on the size of cpx phenocrysts) were prepared. Before the measurement, the thin sections were cleaned by acetone and alcohol, and dried in the oven to remove the absorbed water on the surface. Clean crack- and inclusion-free areas of cpx phenocrysts were chosen by microscope for measurement. Each measurement, a total of 128 or 256 scans with a resolution of 4 cm^{-1}, was conducted at wavelengths from 1000 to 4500 cm^{-1}. The aperture size was set from 20×20 to 50×50μm. For the calculation of water content, the modified Beer-Lambert law was used,

$$C = \mathrm{A}/(\mathrm{I} * \mathrm{t}) \qquad (3\text{-}1)$$

in which c is the content of water (ppm wt. H_2O), A is the total integral absorption of OH bands (cm^{-1}), I is the integral specific absorption coefficient, and t is the sample thickness (cm). The total integral absorption of OH bands is 3 times the integral area of unpolarized absorption (Kovács et al., 2008; Sambridge et al., 2008), and the chosen integral specific absorption coefficient for cpx was 7.09 ppm^{-1} cm^{-2} (Bell et al., 1995).

Baseline correction of each spectrum was conducted by hand along with the baseline trends (polynomial), and integral absorption of OH bands were calculated by OMNIC software.

Figure 3-1. a) A photo of the Nicolet 5700 FTIR coupled with a Continuμm microscope at CAS-CMME, USTC; b) The Bruker Vertex 70 spectrometer coupled with a Bruker Hyperion 3000 FTIR-microscope at University Lille 1, France.

3.2.2 Estimate the water content of corresponding melt

Based on the phenocryst-melt equilibration, the water content of melts from which the cpx phenocrysts crystallized has been estimated from the water content of cpx phenocrysts and the H_2O partition coefficients ($D^{cpx/melt}$) between cpx phenocrysts and melt. The experimental studies indicated that the $D^{cpx/melt}$ in cpx are linearly correlated with the Al_2O_3 contents of cpx in a wide range (Al_2O_3: 0.2%-19%) (O'Leary et al., 2010). The $D^{cpx/melt}$ can be calculated from equation:

$$D = \exp(-4.2 + 6.5 * X(^{iv}Al) - X(Ca) \quad (3\text{-}2)$$

where X (^{iv}Al) and X (Ca) are the concentrations of Al^{3+} in a tetrahedral site in cpx and Ca^{2+} in cpx (O'Leary et al., 2010).

3.2.3 Errors on water content

The uncertainty of H_2O content of melt mainly comes from the FTIR measurement of H_2O in cpx phenocryst and the uncertainties of $D^{cpx/melt}$, calculated by the regression line. The uncertainty of H_2O content for a single cpx phenocryst is less than 30% (Xia et al., 2013b). Considering the error of $D^{cpx/melt}$ (~10%, O'Leary et al., 2010), the total uncertainty of water content in melts is less than 40% (Xia et al., 2013b).

3.3 Major element contents of phenocrysts

The major element concentration of cpx and olivine phenocrysts was analyzed at CAS-CMME, USTC, using a Shimadzu Electron Probe Microanalyzer (EPMA 1600). The analytical points were performed within the FTIR analyzed regions for cpx phenocrysts and in the core for ol phenocrysts. Natural minerals and synthetic oxides were used as standards, and the operating conditions were as follows: 15 kV accelerating voltage, 20 nA beam current and <5 µm beam diameter. A program based on the ZAF procedure was used for data correction.

3.4 In-situ oxygen isotopic compositions of clinopyroxene phenocrysts

3.4.1 Analytical conditions and standards

In-situ cpx oxygen isotope measurements were conducted using a Cameca IMS-1270 at Centre de recherches rétrographiques et réochimiques - Centre national de la recherche scientifique (CRPG-CNRS), Nancy (Fig. 3-2). During the experiment, a Cs^+ primary beam was used in focused mode at ~5.3 nA and 10 kV with a spot size of approximately 20 μm in diameter. An electron gun was used to compensate for any sample charging. Secondary negative ions were accelerated at 10 kV, and the mass resolution power was established at 3000 to distinguish ^{17}OH and ^{18}O. Oxygen isotopes were measured in multi-collection mode with two off-axis Faraday cups (L'2 for ^{16}O, H1 for ^{18}O). The internal precision of individual measurements was generally less than 0.1‰ (2σ).

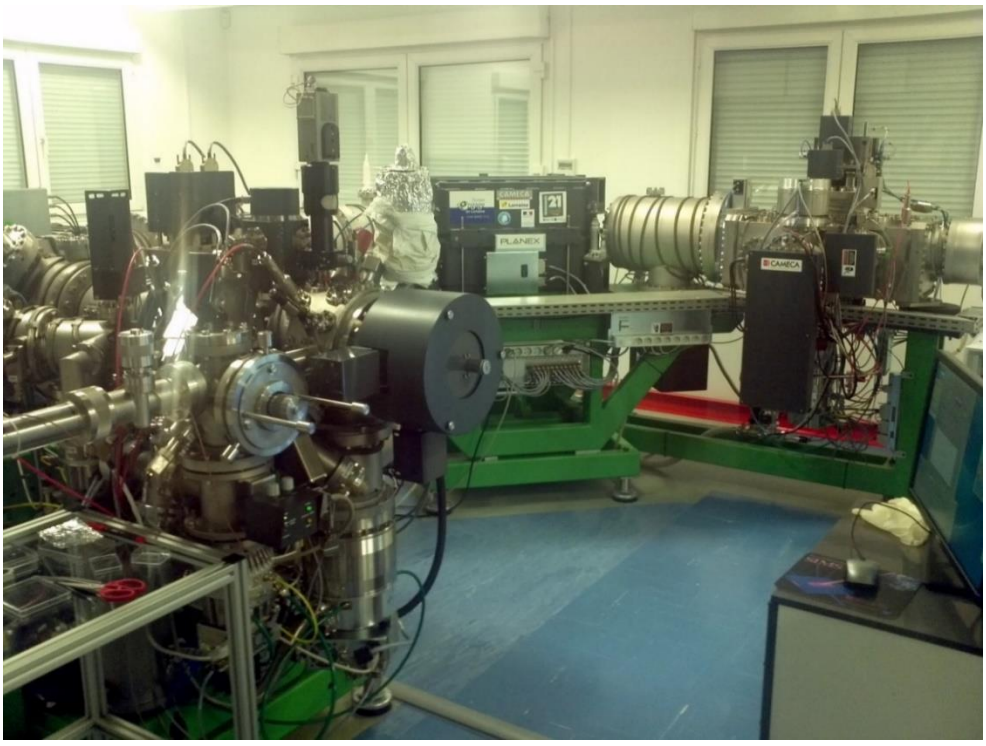

Figure 3-2. Photo of the IMS 1270 at CRPG, Nancy.

The matrix effect for measurement of oxygen isotopes in cpx was discussed by Gurenko et al. (2001). The effect was evaluated using the correlation between instrumental mass fractionation (IMF) and the Mg# of cpx. A group of standards, cpx megacrysts (NSH2, NSH5, NSH8, NSH9, NSH10, NSH14) from Nushan, eastern China, were used to correct matrix effect. As shown in Xia et al. (2004), the major element concentration and oxygen isotope ratio of the standard cpx megacrysts are homogeneous, and the chemical compositions of the standard cpx megacrysts are nearly the same as those of cpx phenocrysts in this study, thus they are appropriate standards. We also inlaid a standard (NSH9) in the center of each sample mount surrounded by cpx grains from this study to trace the instrumental drift during the measurement. The oxygen isotope compositions are displayed by $\delta^{18}O$ notation relative to reference standard (Vienna Mean Standard Ocean Water, VSMOW).

3.4.2 Instrumental Mass Fractionation corrections

The deviation between the measured and true values is generally called Instrumental Mass Fractionation (IMF) and it occurs during the SIMS measurement, including the production, transport and detection of secondary ions. Because these factors can be evaluated separately, we divided the factors into two sections. The later two processes (transport and detection of secondary ions) are primarily controlled by the state of the instrument, which may easily be corrected by periodically measuring the standard (NSH9). A large proportion of mass fractionation occurs during the process of secondary ions production, which depends on type and composition of the mineral (commonly referred as the “matrix effect”). For this part, the deviation could be corrected by a group of standards (NSH2, NSH5, NSH8, NSH9, NSH14; Table 3-1), with chemical compositions bracketing the unknown samples (Eiler et al., 1997; Hartley et al., 2012; Kita et al., 2009, 2010; Page et al., 2010; Valley and Kita, 2009).

Table 3-1. The chemical and oxygen isotopic compositions of standards (from Xia et al., 2004)

	NSH2	NSH14	NSH5	NSH8	NSH9	NSH10
SiO_2	48.84	49.04	50.69	49.42	50.22	51.37
Al_2O_3	9.68	9.82	8.2	8.98	8.5	7.99
TiO_2	1.52	1.47	0.82	1.04	0.89	0.52
Cr_2O_3	0.02	0.01	b.l.d.	b.l.d.	b.l.d.	0.13
FeO	7.84	8.02	6.54	6.97	6.55	6.27
NiO	b.l.d.	b.l.d.	0.02	0.02	b.l.d.	b.l.d.
MnO	0.13	0.13	0.08	0.11	0.18	0.15
MgO	11.8	11.35	14.99	13.68	14.74	16.54
CaO	17.63	17.42	16.51	16.53	16.43	14.65
Na_2O	1.94	2.11	1.56	1.81	1.42	1.34
K_2O	0.01	0.01	0.01	0.02	b.l.d.	0.01
Total	99.41	99.38	99.42	98.58	98.93	98.97
Mg#	72.9	71.6	80.3	77.8	80	82.5
$\delta^{18}O$ (‰)	5.46±0.07	5.07±0.15	5.88±0.02	5.99±0.12	5.33±0.21	5.77±0.05

Note: b.l.d., below the limit of detection.

For the first source of deviation caused by processes such as transportation and/or detection, we used the bracketing analysis of standard NSH9, which was mounted in every sample block. The fractionation factor ($\alpha^{18}O_{SIMS}$) could be calculated from the measured value of NSH9 ($\delta^{18}O_{raw}$) and the "true" value ($\delta^{18}O_{true}$) on the VSMOW scale based on the following equation (Equation 2.1 in Kita et al., 2009):

$$\alpha^{18}O_{SIMS} = \frac{1+(\delta^{18}O_{raw}+1)}{1+(\delta^{18}O_{true}+1)} \quad (3\text{-}3)$$

This factor can also be defined as the instrumental bias in the permil deviation of $\alpha^{18}O_{SIMS}$ from the unity equation (Equation 2.2 in Kita et al., 2009):

$$\alpha^{18}O_{SIMS} = 1 + bias_{(1)}/100 \quad (3\text{-}3)$$

Because the instrumental biases $\delta^{18}O_{true}$ and $\delta^{18}O_{true}$ of our standards and unknown samples are all smaller than ±10‰, the combination of Equations 3-3 and 3-4 can lead to an approximated formula (Equation 2.4 in Kita et al., 2009):

$$(bias_{(1)}) \approx \delta^{18}O_{raw} - \delta^{18}O_{true} \quad (3\text{-}5)$$

The raw data for unknown samples were then corrected by Equation 3-5 as follows:

$$\delta^{18}O^{*} = \alpha^{18}O_{raw}^{sample} - bias_{(1)}$$

$$= \alpha^{18}O_{raw}^{sample} - (\delta^{18}O_{raw}^{NSH9} - \delta^{18}O_{true}^{NSH9}) \quad (3\text{-}6)$$

With Equation 3-6, the instrumental bias generated by transport and detection is corrected. For sessions with a linearly time-dependent bias drift, a linear correlation between this bias and time is used to correct the drift.

For the deviation caused by the mineral type and composition (matrix effect), the correlation between the relative instrumental mass fractionations (IMF) and the Mg# of a group of cpx standards was estimated (Figs. 3-3, 3-4), as suggested by Gurenko et al. (2001). First, a linear function correlation between IMF and cpx's Mg# for each session was obtained:

$$IMF = f(Mg\#) \quad (3\text{-}7)$$

Then, the bias caused by the matrix effect was corrected based on the following equation:

$$bias_{(2)} = IMF - IMF_{(NSH9)} = f(Mg\#) - IMF_{(NSH9)} \quad (3\text{-}8)$$

The corrected "true" value ($\delta^{18}O_{corrected}^{sample}$) for unknown samples was calculated using the following equation:

$$\delta^{18}O_{corrected}^{sample} = \alpha^{18}O_{raw}^{sample} - bias_{(1)} - bias_{(2)}$$

$$= \alpha^{18}O_{raw}^{sample} - (\delta^{18}O_{raw}^{NSH9} - \delta^{18}O_{true}^{NSH9}) - (f(Mg\#) - IMF_{(NSH9)}) \quad (3\text{-}9)$$

The analysis of the standards and their IMF are listed in Tables 3-2 and 3-3.

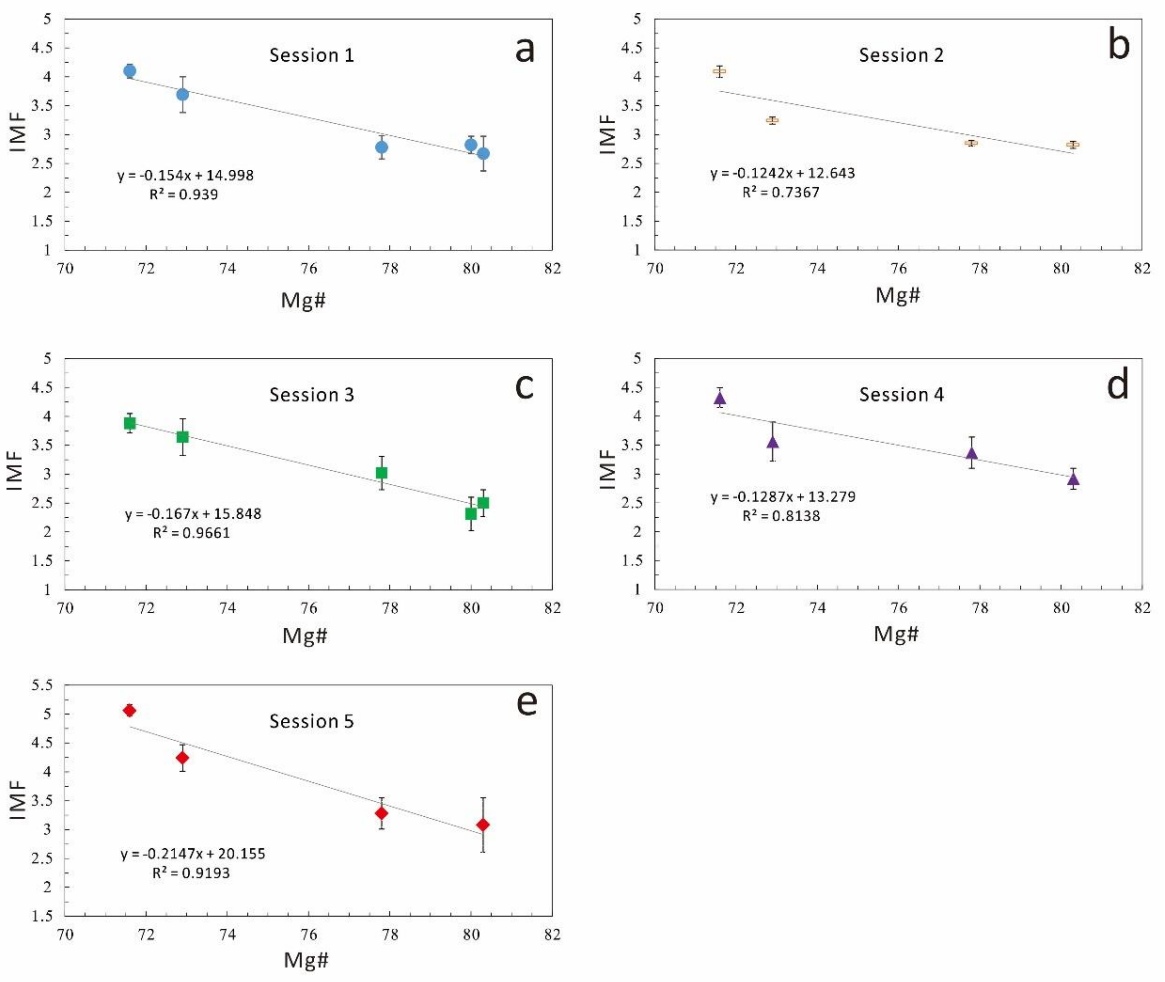

Figure 3-3. The correlation between Mg# and IMF of standards in each session (measured at September 2015)

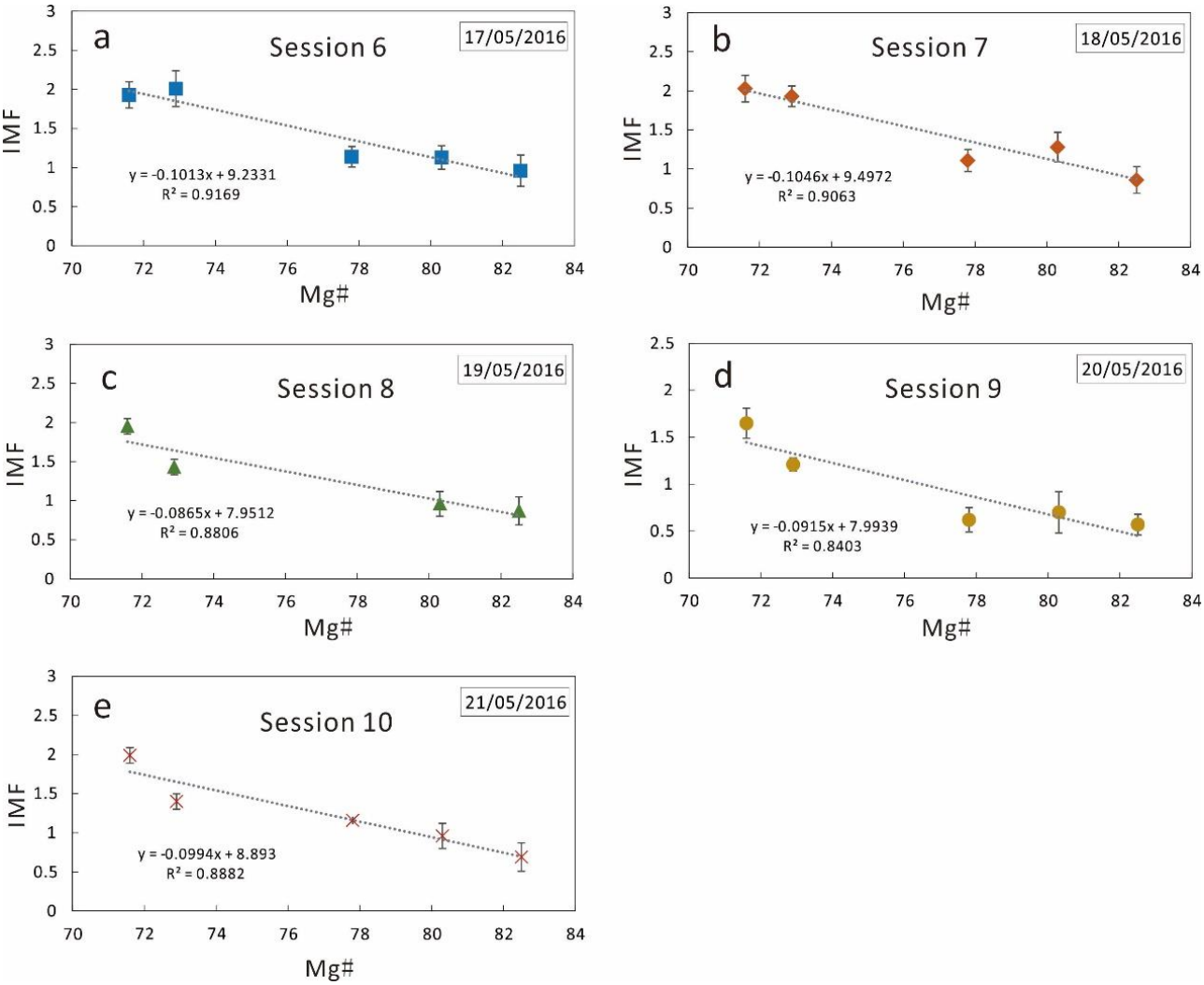

Figure 3-4. The correlation between Mg# and IMF of standards in each session (measured at May 2016).

Table 3-2. The SIMS analysis result of standards for matrix effect correction (Sessions 1-5)

		Mg#[a]	$\delta^{18}O_{true}$[a]	$\delta^{18}O_{measured}$	IMF	SE
session 1	NSH2	72.9	5.46	9.15	3.69	0.31
	NSH8	77.8	5.99	8.77	2.78	0.20
	NSH9	80.0	5.33	8.15	2.82	0.15
	NSH14	71.6	5.07	9.17	4.10	0.12
	NSH5	80.3	5.88	8.55	2.67	0.30
session 2	NSH2	72.9	5.46	8.70	3.24	0.06
	NSH8	77.8	5.99	8.84	2.85	0.05
	NSH14	71.6	5.07	9.16	4.09	0.10
	NSH5	80.3	5.88	8.70	2.82	0.06
session 3	NSH2	72.9	5.46	9.10	3.64	0.32
	NSH8	77.8	5.99	9.01	3.02	0.29
	NSH9	80.0	5.33	7.64	2.31	0.29
	NSH14	71.6	5.07	8.95	3.88	0.17
	NSH5	80.3	5.88	8.38	2.50	0.23
session 4	NSH2	72.9	5.46	9.02	3.56	0.34
	NSH8	77.8	5.99	9.36	3.37	0.27
	NSH14	71.6	5.07	9.39	4.32	0.17
	NSH5	80.3	5.88	8.80	2.92	0.18
session 5	NSH2	72.9	5.46	9.70	4.24	0.23
	NSH8	77.8	5.99	9.27	3.28	0.27
	NSH14	71.6	5.07	10.13	5.06	0.10
	NSH5	80.3	5.88	8.96	3.08	0.47

Note: a, data from Xia et al. (2004).

Table 3-3. The SIMS analysis result of standards for matrix effect correction (Sessions 6-10)

		Mg#[a]	$\delta^{18}O_{true}$[a]	$\delta^{18}O_{measured}$	IMF	SE
session 6	NSH2	72.9	5.46	7.47	2.01	0.23
	NSH5	80.3	5.88	7.01	1.13	0.15
	NSH8	77.8	5.99	7.13	1.14	0.13
	NSH10	82.5	5.77	6.73	0.96	0.20
	NSH14	71.6	5.07	7	1.93	0.17
session 7	NSH2	72.9	5.46	7.39	1.93	0.13
	NSH5	80.3	5.88	7.16	1.28	0.19
	NSH8	77.8	5.99	7.1	1.11	0.14
	NSH10	82.5	5.77	6.63	0.86	0.17
	NSH14	71.6	5.07	7.1	2.03	0.17
session 8	NSH2	72.9	5.46	6.89	1.43	0.10
	NSH5	80.3	5.88	6.84	0.96	0.16
	NSH10	82.5	5.77	6.64	0.87	0.18
	NSH14	71.6	5.07	7.02	1.95	0.10
session 9	NSH2	72.9	5.46	6.67	1.21	0.07
	NSH5	80.3	5.88	6.58	0.7	0.22
	NSH8	77.8	5.99	6.61	0.62	0.13
	NSH10	82.5	5.77	6.34	0.57	0.11
	NSH14	71.6	5.07	6.72	1.65	0.16
session 10	NSH2	72.9	5.46	6.86	1.4	0.09
	NSH5	80.3	5.88	6.84	0.96	0.08
	NSH8	77.8	5.99	7.15	1.16	0.00
	NSH10	82.5	5.77	6.46	0.69	0.09
	NSH14	71.6	5.07	7.06	1.99	0.14

Note: a, data from Xia et al. (2004).

3.4.3 Precision and accuracy

The error of an unknown measured data comprises three parts: the internal precision of the instrument, the reproducibility or repeatability during measurement and additional error caused by IMF corrections.

For the Cameca IMS 1270 at CRPG-Nancy, the internal precision of the instrument is typically in the range of ±0.08‰~0.14‰ (in most cases <0.1‰) (2SE). The reproducibility or repeatability of the measurement, generally called external precision, can be calculated from the standard deviation of N measurements on a homogeneous standard (Fitzsimons et al., 2000; Kita et al., 2007, 2009; Valley and Kita, 2009). In this

work, the external precision presented by the standards of each session is typically within ±0.3‰ (SE). For each unknown cpx grain, the internal precision for one spot analysis was typically better than 0.1‰, several spots analyses are conducted (typically 3 measurements), and the standard error (SE) is typically less than ±0.3‰. The additional error, caused by IMF corrections, derives from: 1) the uncertainty regarding the standards' oxygen isotopic composition, 2) the uncertainty regarding the chemical composition of cpx, and 3) the uncertainty regarding the linear least-square calibration "matrix effect" line (Equation 5). First, the uncertainty of all standards is less than ±0.2‰ (2SD, Xia et al., 2004). Second, the error of Mg# obtained by EPMA analysis is only about 1 unit, which introduces an uncertainty of oxygen isotopes within ±0.1‰ (calculated based on Equation 3-7). The uncertainty caused by the "matrix effect" least-square regression line can be calculated based on the following equation:

$$SE_{\delta\ pred} = SE_{\delta\ std}\sqrt{\frac{1}{n} + \frac{(Mg\#^{*} - \overline{Mg\#})^2}{\sum_{i=1}^{n}(Mg\#_i - \overline{Mg\#})^2}} \quad (3\text{-}10)$$

where n is the number of data points (standards) involved in the regression line, $Mg\#^{*}$ is the Mg number of cpx to be interpolated, $\overline{Mg\#}$ is the average Mg# of all the data points, $Mg\#_i$ is the Mg# of the i-th data point, and the $SE_{\delta\ std}$ is the standard deviation of the data points regarding the regression line, which is calculated as follows:

$$SE_{\delta\ std} = \sqrt{\sum_{i=1}^{n}\frac{(y_i - Ax_i - B)^2}{n-2}} \quad (3\text{-}11)$$

where A and B are the parameters in the linear regression (Equation 5, IMF=A*Mg#+B). The calculated inaccuracy is less than ±0.1‰ for Sessions 1, 3, 6, 7, 9 and 10 and less than ±0.2‰ for Sessions 2, 4, 5 and 8 (Fig. 3-5). Overall, the total errors are typically within ±0.5‰.

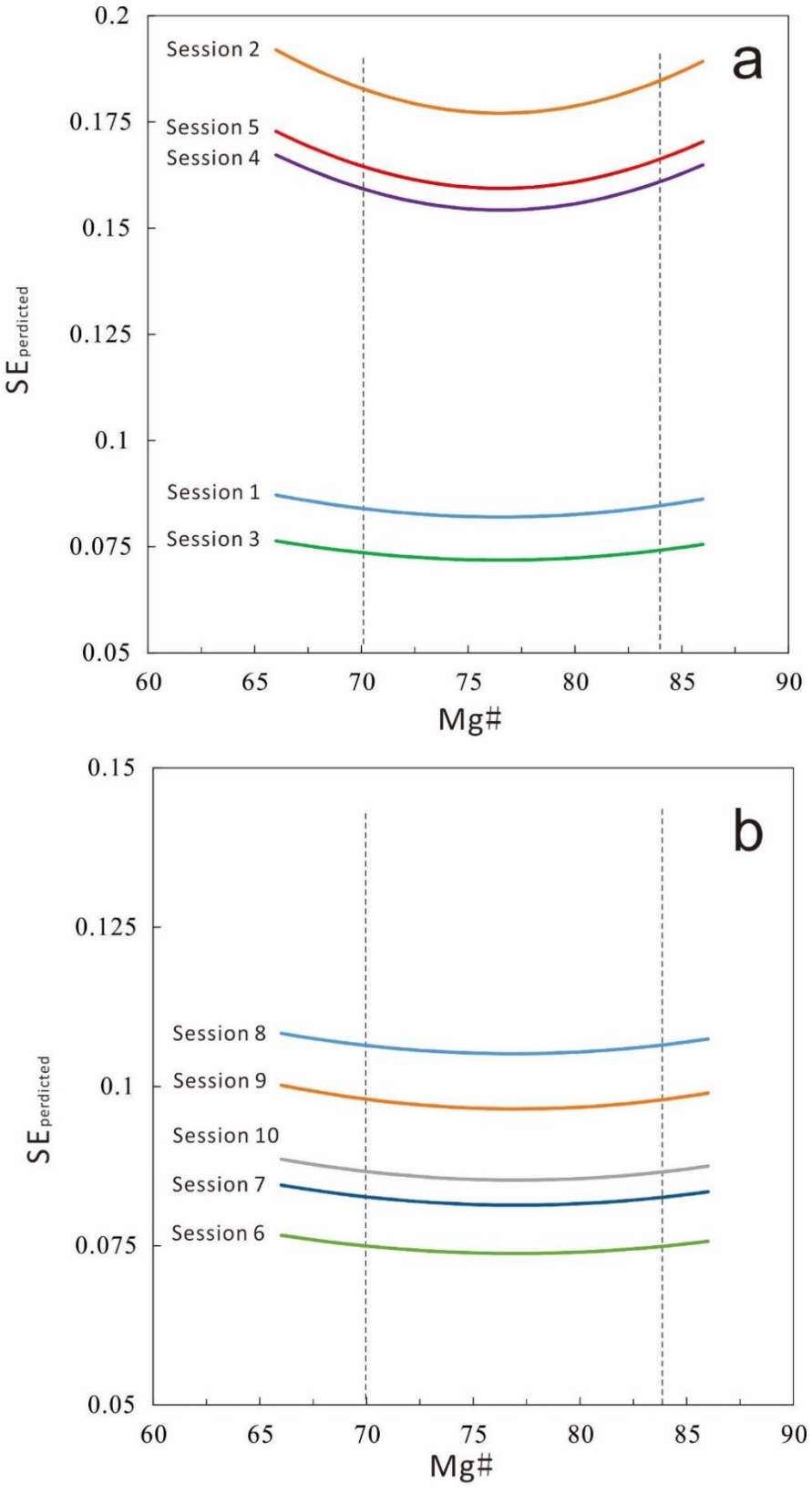

Figure 3-5. The relationship between the errors caused by matrix effect regression line and the Mg# of cpx, calculated by Equations 3-10 and 3-11.

Chapter 4. Results and discussion

4.1 Shuangliao basalts

4.1.1 Results

4.1.1.1 Major and Trace element concentrations of bulk rock

Bulk rock major and trace element concentrations are reported in Table 4-1. The basalts can be classified into three types based on petrography and major element composition: basanite (BBT and BLS), alkali olivine basalt (DHLB) and transitional basalt (XTEJ), in agreement with the analyses of Xu et al. (2012) (Fig. 4-1).

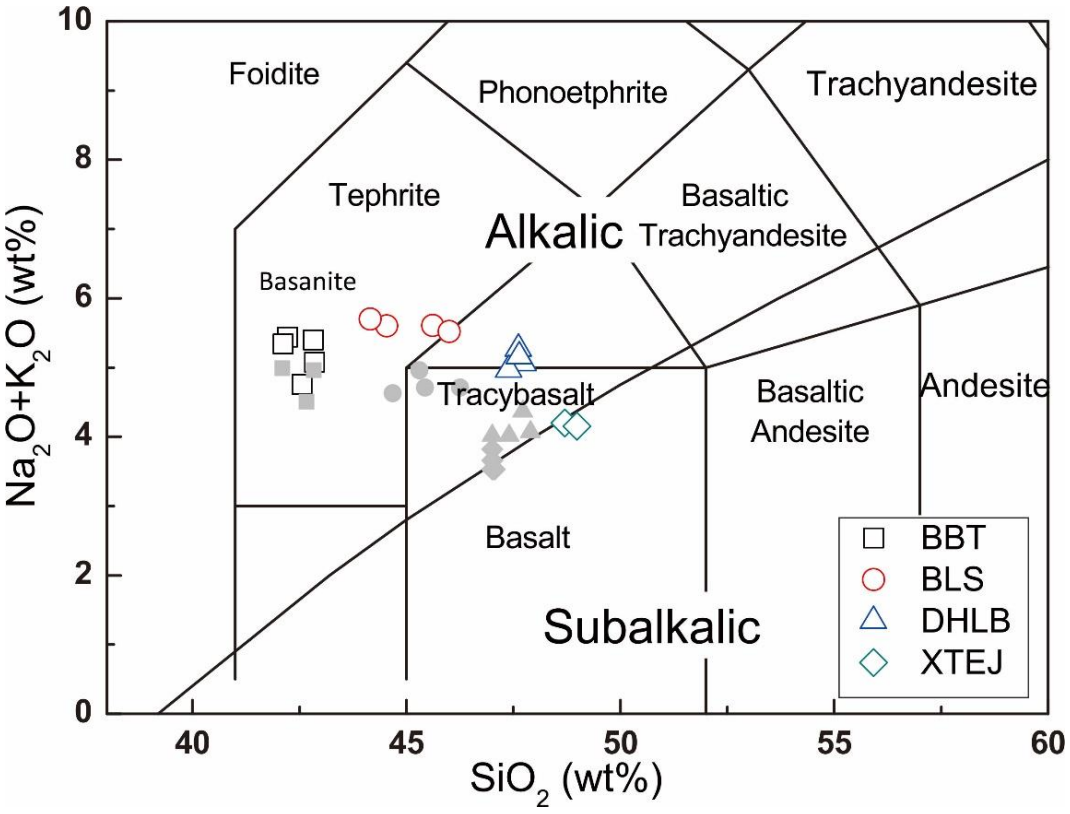

Figure 4-1. Total alkali vs. SiO_2 plots for the Shuangliao basalts. The classification of rock types is after Le Bas et al. (1986). The light gray dots are from Xu et al. (2012) which were collected from the same locations as our samples.

Table 4-1. Major and Trace element compositions of the Shuangliao basalts and calculated water contents of basaltic melt

	Bobotushan					Bolishan				Dahalabashan				Xiaotuerjishan	
Sample	BBT-1	BBT-2	BBT-3	BBT-5	BBT-8	BLS-4	BLS-6	BLS-7	BLS-8	DHLB-4	DHLB-5	DHLB-9	DHLB-10	XTEJ-2	XTEJ-4
Rock type	BAS	BAS	BAS	BAS	BAS	BAS	BAS	BAS	BAS	AOB	AOB	AOB	AOB	TB	TB
SiO_2	42.82	42.22	42.85	42.56	42.12	44.54	45.61	44.15	46.00	47.62	47.73	47.39	47.64	48.70	48.99
TiO_2	2.78	2.91	2.89	2.49	2.82	2.23	2.21	2.28	2.13	2.06	2.05	1.92	2.04	1.84	1.78
Al_2O_3	11.66	11.81	11.75	10.77	11.48	11.93	11.91	11.89	12.35	14.01	13.71	13.50	13.82	14.38	14.45
Fe_2O_3T	12.78	13.13	12.90	12.72	13.42	13.55	13.47	13.75	13.13	12.61	12.80	13.30	12.93	12.63	12.84
MnO	0.17	0.18	0.17	0.17	0.17	0.17	0.17	0.17	0.17	0.17	0.17	0.18	0.18	0.16	0.16
MgO	11.41	11.18	11.60	15.47	12.19	11.98	11.11	11.92	10.51	7.71	8.12	8.79	8.28	8.11	8.49
CaO	10.06	9.80	9.83	8.71	9.33	7.98	8.03	8.14	8.12	9.13	9.26	9.22	9.06	9.30	9.37
Na_2O	3.97	4.11	3.54	3.23	4.30	3.51	3.69	3.62	3.58	3.85	3.64	3.72	3.77	3.37	3.33
K_2O	1.43	1.33	1.54	1.53	1.04	2.09	1.92	2.08	1.94	1.42	1.42	1.25	1.39	0.73	0.72
P_2O_5	0.65	0.72	0.56	0.54	0.70	0.76	0.69	0.73	0.73	0.44	0.38	0.40	0.40	0.18	0.18
LOI*	3.20	3.24	2.79	2.71	2.16	1.01	0.50	0.56	0.41	-0.01	-0.18	-0.05	-0.09	-0.13	-0.09
Total	100.93	100.62	100.42	100.89	99.72	99.75	99.31	99.29	99.06	99.01	99.10	99.62	99.43	99.27	100.23
Mg#	67.54	66.49	67.70	73.92	67.92	67.33	65.78	66.89	65.10	58.76	59.65	60.64	59.88	59.95	60.65
H_2O cpx with highest Mg#	1.22	1.33	2.66	2.64	1.18	3.75	2.70	2.91	2.44	2.28	2.19	2.22	2.03	1.22	0.72
H_2O (cpx Mg#>75)	1.22	1.32	2.35	1.71	1.44	3.06	2.29	2.41	2.57	2.02	2.01	1.86	2.21	1.22	0.90
H_2O (cpx Mg#>70)	1.00	1.24	1.87	1.64	1.15	2.84	2.78	2.40	2.67	1.95	1.99	1.74	2.10	1.21	0.90
V	266.0	254.8	252.2	240.4	254.8	170.0	174.7	182.5	171.9	205.6	209.9	200.7	199.5	205.9	197.1
Cr	358.0	368.7	372.9	601.7	425.1	544.8	468.6	525.6	447.5	271.3	279.3	286.2	267.3	261.3	252.7
Co	58.3	62.0	61.6	68.5	62.4	57.7	56.6	58.3	53.8	47.5	49.6	53.6	48.7	54.3	54.9

Table 4-1 (continued)

	Bobotushan					Bolishan				Dahalabashan				Xiaotuerjishan	
Sample	BBT-1	BBT-2	BBT-3	BBT-5	BBT-8	BLS-4	BLS-6	BLS-7	BLS-8	DHLB-4	DHLB-5	DHLB-9	DHLB-10	XTEJ-2	XTEJ-4
Rock type	BAS	BAS	BAS	BAS	BAS	BAS	BAS	BAS	BAS	AOB	AOB	AOB	AOB	TB	TB
Ni	284	269	283	527	346	396	343	373	311	161	168	196	168	201	209
Sc	20.7	21.2	22.6	20.0	20.2	16.5	15.9	17.1	16.5	22.6	22.2	22.4	21.6	23.4	21.9
Ga	18.8	21.0	19.7	18.2	20.2	21.2	21.1	21.7	21.0	19.9	19.2	19.1	18.8	18.8	18.1
Rb	19.1	19.1	22.4	23.5	21.9	33.2	30.9	30.7	29.3	23.4	22.7	21.1	23.0	9.99	9.40
Sr	864	946	891	766	928	1003	1017	1009	984	739	738	714	714	363	351
Y	19.4	21.5	20.4	18.9	20.8	19.7	18.9	19.3	19.5	20.1	18.4	18.1	18.6	15.4	14.8
Zr	243	268	254	225	257	275	272	272	245	184	181	165	176	116	111
Nb	59.8	65.3	63.4	55.6	64.7	63.0	61.4	62.6	55.4	35.4	35.0	32.2	33.9	14.8	14.0
Ba	357	373	365	340	379	369	386	367	350	270	273	241	262	123	113
La	37.2	42.3	34.9	32.9	41.6	47.4	44.7	44.6	45.0	27.4	23.8	24.3	24.5	7.83	7.48
Ce	74.3	83.7	68.9	64.7	82.5	92.7	87.5	88.3	87.3	53.0	46.3	47.5	47.4	16.6	15.9
Pr	8.83	9.79	8.44	7.77	9.78	10.66	10.12	10.16	10.12	6.54	5.74	5.78	5.85	2.26	2.23
Nd	36.0	40.2	34.1	31.5	39.0	42.8	40.1	41.2	40.0	26.9	23.8	23.8	24.1	10.6	9.98
Sm	7.18	8.03	6.97	6.50	7.55	8.29	8.02	8.12	7.92	5.76	5.15	5.17	5.06	3.10	2.83
Eu	2.17	2.40	2.26	2.02	2.38	2.52	2.41	2.49	2.38	1.96	1.91	1.86	1.86	1.16	1.09
Gd	6.79	7.56	6.59	5.96	7.34	7.65	7.35	7.50	7.27	5.62	5.11	5.01	5.09	3.17	2.98
Tb	0.82	0.95	0.82	0.74	0.90	0.93	0.88	0.94	0.89	0.75	0.67	0.65	0.68	0.46	0.43
Dy	4.46	5.05	4.43	4.02	4.70	4.39	4.43	4.40	4.53	4.22	3.69	3.62	3.66	2.85	2.74
Ho	0.75	0.86	0.82	0.75	0.82	0.77	0.75	0.77	0.79	0.79	0.74	0.71	0.70	0.58	0.57
Er	1.83	2.07	1.93	1.79	1.93	1.80	1.77	1.81	1.86	1.89	1.82	1.74	1.78	1.46	1.38
Tm	0.24	0.25	0.24	0.23	0.24	0.20	0.22	0.21	0.24	0.27	0.26	0.25	0.24	0.23	0.20

Table 4-1 (continued)

	Bobotushan					Bolishan				Dahalabashan				Xiaotuerjishan	
Sample	BBT-1	BBT-2	BBT-3	BBT-5	BBT-8	BLS-4	BLS-6	BLS-7	BLS-8	DHLB-4	DHLB-5	DHLB-9	DHLB-10	XTEJ-2	XTEJ-4
Rock type	BAS	BAS	BAS	BAS	BAS	BAS	BAS	BAS	BAS	AOB	AOB	AOB	AOB	TB	TB
Yb	1.19	1.45	1.37	1.28	1.31	1.15	1.17	1.15	1.22	1.53	1.35	1.41	1.42	1.19	1.15
Lu	0.19	0.22	0.19	0.18	0.18	0.18	0.17	0.18	0.18	0.24	0.22	0.21	0.21	0.19	0.17
Hf	5.97	6.63	6.24	5.46	6.39	6.66	6.56	6.67	6.03	4.71	4.58	4.16	4.38	3.16	2.94
Ta	3.54	3.80	3.73	3.26	3.79	3.53	3.47	3.60	3.15	2.01	1.87	1.72	1.87	0.86	0.83
Pb	3.06	3.24	2.92	2.78	2.64	3.71	4.33	3.54	4.03	2.95	2.55	2.56	2.69	2.61	1.23
Th	4.57	5.17	4.57	4.22	5.11	5.55	5.45	5.25	5.24	3.05	2.89	2.60	2.85	1.17	1.08
U	1.51	1.67	1.49	1.38	1.66	1.69	1.69	1.63	1.60	0.92	0.89	0.86	0.84	0.36	0.36

Note： BAS=Basanite; AOB=Alkali olivine basalt; TB=Transitional basalt.

* Ferrous iron could be converted to ferric iron by the oxygen in the air that the LOI might be negative.

The Shuangliao basanites are characterized by high Mg# (65.1-67.9, Mg#=100*Mg/(Mg+Fe) mole%) except one sample BBT-5 with Mg# of 73.9 which might have been contaminated, high Co (53.8-62.5 ppm) and Ni (269-372 ppm) contents, high $Fe_2O_3^T$(≥12.78 wt.%) and TiO_2 (2.13-2.91 wt.%) and low Al_2O_3 (<12.5wt.%), indicating weak effect of fractional crystallization. Alkali olivine basalts and transitional basalts have relatively low Mg# (58.8-60.6) and Ni (161-209 ppm) content. It is worth noting that the compositions of basanites vary in different trends from those of alkali olivine basalts and transitional basalts on plots of major element oxides vs. MgO (Fig. 4-2), suggesting that these variations cannot be caused by different degrees of fractional crystallization from a single primary magma.

The chondrite normalized rare earth element and primitive-mantle normalized trace element patterns of the Shuangliao basalts show similar characteristics, but the concentrations vary with rock types and decrease with the alkalinity of the rocks (Fig. 4-3). The trace element concentrations of basanites are the highest of all samples, and they are enriched in light rare earth elements (LREEs) relative to heavy rare earth elements (HREEs) ($(La/Yb)_N$=18.3–29.5, N means chondrite normalization), and enriched in Nb and Ta, depleted in highly incompatible elements (Rb, Ba, Th, U), and have negative K anomaly and weak positive Eu and Sr anomalies. With the decrease of alkalinity of the Shuangliao samples, the fractionation between LREEs and HREEs decreases, the depletion of highly incompatible elements is reduced, the K anomaly turns from negative to positive, and the positive Eu and Sr anomalies are enhanced.

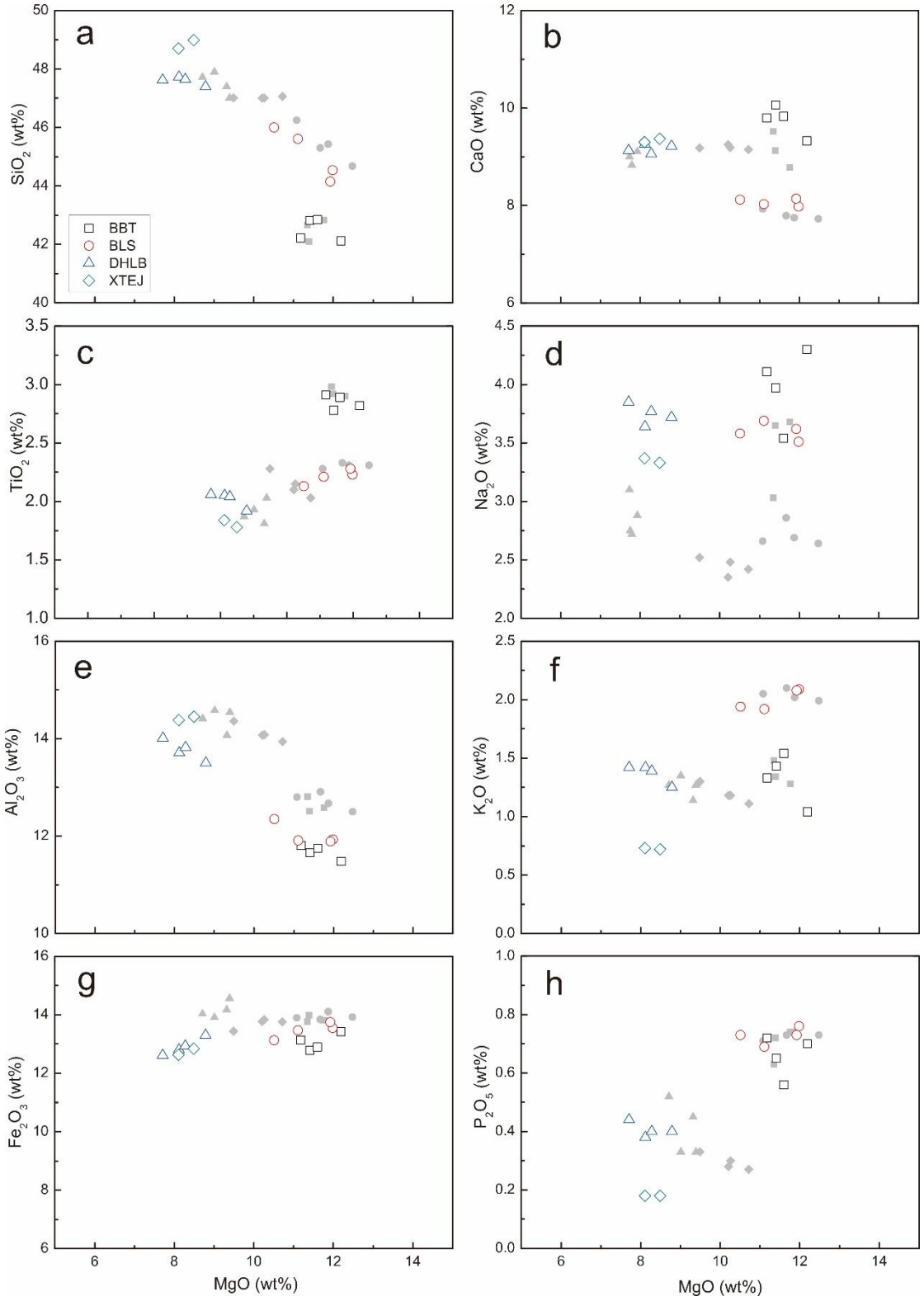

Figure 4-2. Major element oxides vs. MgO for the Shuangliao basalts. Data in gray dots are from Xu et al. (2012).

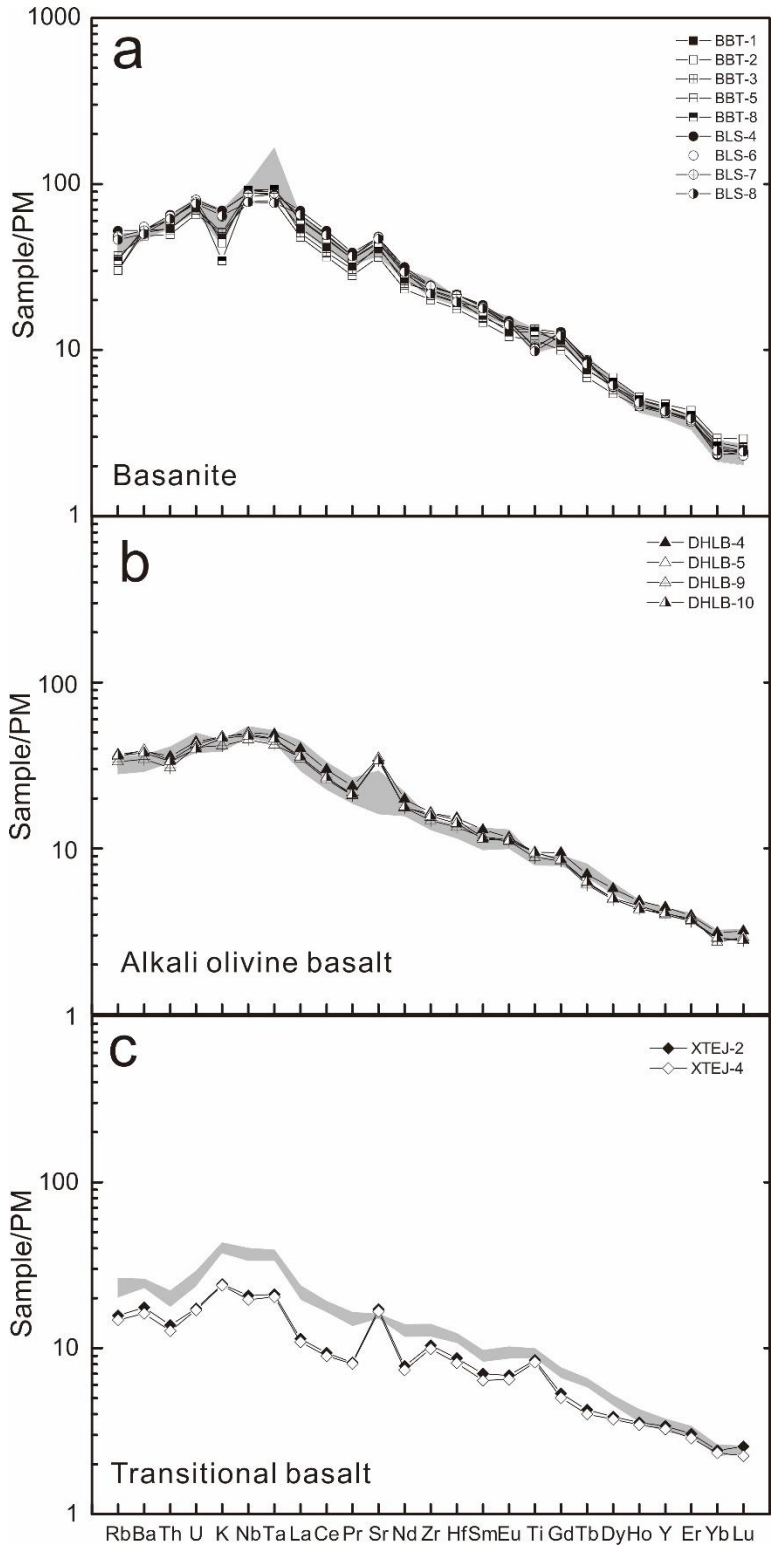

Figure 4-3. Primitive mantle-normalized trace elements concentration diagram for the Shuangliao basalts. Normalization values are after McDonough and Sun (1995). The data from Xu et al. (2012) are shown in the gray zone.

Major and trace element concentrations of Shuangliao basalts are consistent with the previous reported data of Shuangliao basalts (Xu et al., 2012) (Figs. 4-2, 4-3). Overall, the Shuangliao basalts are characterized by high Fe content and HIMU-like trace element pattern. In addition, it is highly impossible that alkaline olivine basalts and transitional basalts evolved from basanites via crystal fractionation, as they show different trends from basanites on both major and trace element diagrams.

4.1.1.2 Chemical compositions of phenocrysts

The major element contents of clinopyroxene (cpx) and olivine (ol) phenocrysts are listed in Tables 4-2 and 4-3. The BSE (Back-scattered Electron) images demonstrate that most of the cpx and ol phenocrysts are euhedral and homogeneous (Fig. 4-4), and only a few of them have different core composition which might be attributed to crystallisation around pre-exciting xenocrysts and were disregarded. The cpx phenocrysts are augitic to diopsidic, have relatively low Mg# (61.0-82.2) and Cr_2O_3 (<0.8 wt.%) and high TiO_2 (0.7-4 wt.%) compared to cpx in peridotite xenolith carried by the Shuangliao basalts (91.5-92.8 Mg#, 0.72-1.42 wt.% Cr_2O_3, 0.16-0.32 wt.% TiO_2) (Table 4-2; Hao et al., 2016). All measured olivines have CaO content above 0.1 wt%, indicating that they are igneous phenocrysts (Thompson and Gibson, 2000). The Mg# values of ol phenocrysts range from 62.4 to 84.9 (Table 4-3). Except for BBT, the highest Mg# values of cpx phenocrysts are similar to those of coexisting ol phenocrysts.

Table 4-2. Major element compositions and calculated water contents of cpx phenocrysts and corresponding melt of Shuangliao basalts

	Sample	SiO_2	Al_2O_3	TiO_2	Cr_2O_3	FeO	NiO	MnO	MgO	CaO	Na_2O	K_2O	Mg#	A (cm^{-2})	t (mm)	H_2O in cpx (wt. ppm)	$D^{cpx/melt}$	H_2O in melt (wt. %)
	1-01a	47.34	6.78	2.66	0.21	6.84	0.06	0.13	12.55	22.46	0.53	0.02	76.60	3.54	0.044	340.81	0.026	1.29
	1-01b	44.79	8.38	3.50	b.l.d.	8.24	0.06	0.06	11.39	22.86	0.50	b.l.d.	71.13	1.72	0.044	165.69	0.043	0.38
	1-02b	47.33	6.10	2.80	b.l.d.	8.06	b.l.d.	0.11	12.02	22.73	0.60	0.01	72.67	3.65	0.040	386.42	0.025	1.56
	1-04a	46.36	7.58	2.96	0.06	7.01	b.l.d.	0.08	11.59	22.95	0.60	b.l.d.	74.67	3.36	0.049	289.80	0.030	0.96
	1-08a	46.11	7.68	3.28	0.01	7.37	0.07	0.10	11.28	22.67	0.48	0.01	73.19	3.31	0.041	341.91	0.032	1.08
	1-09a	42.59	10.28	4.90	0.01	8.22	0.02	0.10	10.01	23.10	0.53	b.l.d.	68.48	2.20	0.031	300.70	0.070	0.43
	1-10a	47.46	6.93	2.83	b.l.d.	7.37	0.15	0.11	11.51	23.53	0.49	0.01	73.58	1.54	0.028	232.42	0.026	0.91
	1-11a	50.37	6.58	1.02	0.23	8.08	b.l.d.	0.10	15.26	17.46	0.93	b.l.d.	77.10	1.53	0.029	223.24	0.020	1.11
	1-12a	46.08	6.38	3.09	b.l.d.	8.29	b.l.d.	0.08	11.87	23.03	0.49	0.02	71.86	2.31	0.032	305.32	0.030	1.03
	1-13a	45.38	8.30	3.41	0.02	8.41	0.06	0.12	10.56	22.61	0.60	b.l.d.	69.12	2.21	0.048	195.17	0.037	0.53
BBT1	1-15a	47.22	5.61	2.70	0.01	7.29	0.01	0.09	12.72	23.14	0.24	b.l.d.	75.68	1.71	0.046	157.11	0.023	0.67
	1-16a	48.30	5.99	1.73	1.09	6.00	b.l.d.	0.07	13.12	22.86	0.52	0.01	79.58	1.76	0.029	256.36	0.022	1.19
	1-18a	44.85	8.24	3.93	0.01	8.10	0.02	0.15	11.07	23.20	0.44	b.l.d.	70.90	1.53	0.026	249.16	0.043	0.58
	1-18b	41.85	10.55	4.74	b.l.d.	8.21	b.l.d.	0.07	10.18	22.98	0.49	b.l.d.	68.87	1.92	0.026	312.14	0.077	0.40
	1-18c	49.36	7.92	1.90	0.08	6.57	b.l.d.	0.10	12.26	20.56	0.77	0.18	76.90	1.60	0.026	261.04	0.021	1.25
	1-18d	45.28	7.61	3.51	0.06	8.00	0.03	0.09	11.31	22.99	0.50	b.l.d.	71.58	2.11	0.026	343.06	0.037	0.93
	1-19a	43.15	9.43	4.75	0.04	7.92	0.02	0.07	10.80	22.64	0.51	b.l.d.	70.85	1.75	0.043	172.01	0.061	0.28
	1-20a	46.07	7.46	3.00	0.05	7.06	b.l.d.	0.11	11.51	23.15	0.54	b.l.d.	74.41	3.38	0.046	310.45	0.031	1.01
	1-22a	46.94	7.44	2.60	0.16	7.05	0.03	0.07	11.94	23.02	0.52	0.05	75.13	5.28	0.053	421.22	0.028	1.48
	1-23a	50.55	6.95	0.95	0.17	5.50	0.03	0.10	13.30	21.01	0.95	b.l.d.	81.17	2.73	0.057	202.95	0.016	1.26
	1-23b	44.69	8.85	4.00	0.96	6.74	0.27	0.15	10.99	22.95	0.59	b.l.d.	74.41	3.41	0.057	252.91	0.048	0.53

Table 4-2 (continued)

	Sample	SiO_2	Al_2O_3	TiO_2	Cr_2O_3	FeO	NiO	MnO	MgO	CaO	Na_2O	K_2O	Mg#	A (cm^{-2})	t (mm)	H_2O in cpx (wt. ppm)	$D^{cpx/melt}$	H_2O in melt (wt. %)
BBT1	1-24a	45.99	6.52	3.41	0.03	7.90	b.l.d.	0.08	12.07	23.29	0.47	0.01	73.15	1.78	0.053	141.87	0.032	0.44
	1-25a	47.63	5.95	2.68	0.01	7.65	0.03	0.16	12.02	22.90	0.52	0.01	73.68	2.80	0.055	215.41	0.023	0.94
	1-27a	45.57	6.76	3.65	b.l.d.	8.28	b.l.d.	0.09	12.02	23.01	0.42	0.01	72.13	4.31	0.047	388.29	0.035	1.10
BBT2	2-05a	50.93	6.05	0.86	0.64	7.68	0.06	0.11	14.37	17.96	0.92	b.l.d.	76.93	1.39	0.049	119.86	0.016	0.74
	2-07a	46.78	7.85	3.07	0.08	7.07	b.l.d.	0.10	11.49	22.95	0.46	0.02	74.35	5.30	0.059	380.32	0.030	1.26
	2-09a	50.82	4.60	1.58	0.54	5.30	0.01	0.09	13.68	21.91	0.97	0.01	82.15	2.36	0.046	217.45	0.014	1.59
	2-12a	47.88	6.47	2.30	0.41	6.37	0.06	0.13	12.54	22.51	0.56	0.04	77.83	5.56	0.066	356.65	0.023	1.55
	2-14a	45.36	8.20	3.36	b.l.d.	7.86	0.04	0.09	11.00	22.83	0.52	b.l.d.	71.40	3.52	0.060	248.52	0.037	0.67
	2-15a	43.20	9.79	4.36	0.01	8.24	0.01	0.12	10.08	22.47	0.70	0.01	68.54	4.34	0.060	306.14	0.058	0.53
	2-20a	46.21	6.71	3.51	b.l.d.	7.66	0.07	0.11	11.83	22.90	0.38	b.l.d.	73.35	3.22	0.047	289.80	0.031	0.95
	2-21a	48.04	6.06	2.59	0.03	7.66	b.l.d.	0.10	12.03	23.03	0.47	b.l.d.	73.69	4.23	0.054	331.22	0.022	1.50
	2-21b	45.71	7.53	3.42	b.l.d.	7.77	0.04	0.10	11.47	22.61	0.59	0.01	72.46	4.00	0.054	313.51	0.034	0.91
	2-22a	46.01	6.93	3.46	0.03	7.78	b.l.d.	0.10	11.68	22.77	0.42	0.01	72.79	3.18	0.040	336.18	0.031	1.07
	2-24a	46.95	7.29	3.01	0.03	7.27	b.l.d.	0.10	11.72	23.13	0.57	0.01	74.19	4.30	0.038	478.46	0.029	1.66
	2-25b	46.91	7.21	2.84	0.01	7.14	0.02	0.08	11.53	22.91	0.58	b.l.d.	74.22	3.27	0.038	363.89	0.027	1.36
	2-26a	45.58	8.14	3.30	0.03	7.26	b.l.d.	0.08	11.24	23.23	0.49	b.l.d.	73.40	2.67	0.038	297.75	0.036	0.84
	2-30a	46.90	7.08	2.78	0.02	7.03	b.l.d.	0.13	12.07	22.78	0.54	0.02	75.38	3.02	0.068	188.04	0.028	0.68
	2-34a	46.04	7.50	3.41	0.02	7.83	0.01	0.10	11.43	23.00	0.46	b.l.d.	72.25	5.32	0.060	374.82	0.033	1.13
	2-37a	47.69	6.79	2.55	0.16	7.17	b.l.d.	0.08	12.03	22.05	0.64	b.l.d.	74.95	3.76	0.037	429.99	0.024	1.81
BBT3	3-02a	47.44	9.00	2.25	0.16	6.72	0.08	0.08	12.10	20.88	0.93	b.l.d.	76.25	7.27	0.055	559.46	0.030	1.84
	3-03a	46.34	7.96	3.34	0.07	7.02	0.02	0.09	11.42	23.11	0.49	0.01	74.36	6.91	0.051	572.89	0.033	1.75
	3-04a	48.22	5.64	2.57	0.09	7.38	b.l.d.	0.14	12.89	22.89	0.43	0.01	75.70	6.10	0.048	538.08	0.022	2.43

Table 4-2 (continued)

	Sample	SiO_2	Al_2O_3	TiO_2	Cr_2O_3	FeO	NiO	MnO	MgO	CaO	Na_2O	K_2O	Mg#	A (cm^{-2})	t (mm)	H_2O in cpx (wt. ppm)	$D^{cpx/melt}$	H_2O in melt (wt. %)
BBT3	3-05a	45.54	8.15	3.56	0.06	6.86	0.03	0.09	11.51	22.90	0.53	b.l.d.	74.95	4.51	0.043	443.80	0.037	1.20
	3-05b	45.80	8.27	3.67	0.04	7.20	0.05	0.11	11.13	22.67	0.51	b.l.d.	73.39	4.41	0.043	434.15	0.036	1.21
	3-06a	44.71	8.69	3.94	0.05	7.67	b.l.d.	0.06	11.12	23.25	0.42	b.l.d.	72.11	4.75	0.040	502.79	0.045	1.11
	3-06b	48.39	5.16	2.51	0.02	6.98	b.l.d.	0.10	12.90	22.89	0.41	b.l.d.	76.71	3.15	0.040	333.00	0.020	1.70
	3-09a	43.11	10.27	4.03	0.05	7.99	b.l.d.	0.09	10.46	22.58	0.58	b.l.d.	70.01	5.39	0.041	556.06	0.062	0.90
	3-12a	50.02	4.92	1.80	0.36	6.48	0.02	0.05	13.51	22.62	0.50	b.l.d.	78.81	7.52	0.055	578.81	0.016	3.58
	3-13a	45.54	8.40	3.05	0.23	6.90	0.07	0.12	11.66	23.10	0.46	0.01	75.09	6.03	0.042	607.29	0.038	1.62
	3-14a	42.93	10.72	4.15	0.33	7.75	b.l.d.	0.06	10.64	22.31	0.60	0.01	70.99	7.42	0.043	729.66	0.068	1.07
	3-14b	42.92	10.67	4.55	0.11	8.24	0.07	0.08	10.31	22.19	0.63	0.01	69.04	7.25	0.043	713.12	0.070	1.02
	3-14c	48.33	5.63	2.11	0.01	7.35	0.04	0.09	12.81	22.34	0.52	b.l.d.	75.67	5.61	0.043	551.84	0.020	2.76
	3-21a	45.00	8.89	3.66	0.07	7.29	b.l.d.	0.06	10.79	23.06	0.50	0.01	72.52	4.57	0.048	402.50	0.041	0.98
	3-22b	47.59	5.85	2.35	0.08	7.54	0.02	0.07	12.54	22.55	0.43	b.l.d.	74.79	5.78	0.047	520.09	0.022	2.33
	3-22c	48.88	6.05	1.68	0.05	6.41	0.03	0.11	13.10	23.06	0.49	b.l.d.	78.45	6.88	0.047	619.78	0.019	3.20
	3-24a	48.94	5.78	2.00	b.l.d.	6.98	0.08	0.14	13.02	22.12	0.61	b.l.d.	76.89	5.10	0.045	479.27	0.019	2.49
	3-28a	43.29	9.84	4.36	0.18	8.05	b.l.d.	0.05	10.28	22.32	0.68	b.l.d.	69.48	8.55	0.037	977.32	0.059	1.67
	3-29a	47.67	5.72	2.55	0.02	7.48	0.03	0.13	12.55	22.56	0.47	b.l.d.	74.94	7.31	0.048	644.48	0.022	2.88
	3-30a	45.69	7.90	3.55	0.11	6.84	b.l.d.	0.07	11.57	22.78	0.54	b.l.d.	75.10	5.14	0.059	368.91	0.035	1.05
	3-32a	46.58	7.50	3.05	0.15	6.51	0.03	0.09	11.90	22.74	0.43	b.l.d.	76.53	4.37	0.049	377.45	0.029	1.28
	3-33a	48.75	6.59	1.78	0.09	6.03	0.02	0.10	13.33	22.69	0.52	b.l.d.	79.77	5.30	0.048	466.77	0.021	2.21
	3-33c	45.98	7.53	3.48	0.04	7.39	0.04	0.07	11.41	22.84	0.51	b.l.d.	73.36	4.43	0.048	390.60	0.033	1.19
	3-35a	45.61	7.74	3.48	0.08	7.12	0.01	0.06	11.72	23.05	0.41	b.l.d.	74.58	5.43	0.050	459.61	0.036	1.29
	3-36a	49.81	4.49	1.92	0.22	6.28	b.l.d.	0.08	13.71	23.26	0.40	b.l.d.	79.57	5.12	0.046	471.15	0.016	2.93

Table 4-2 (continued)

	Sample	SiO_2	Al_2O_3	TiO_2	Cr_2O_3	FeO	NiO	MnO	MgO	CaO	Na_2O	K_2O	Mg#	A (cm^{-2})	t (mm)	H_2O in cpx (wt. ppm)	$D^{cpx/melt}$	H2O in melt (wt. %)
BBT3	3-37a	43.84	9.94	4.02	0.41	7.48	b.l.d.	0.06	10.96	22.44	0.63	b.l.d.	72.33	7.76	0.045	729.67	0.058	1.27
	3-38a	45.04	9.02	3.49	0.21	7.52	0.055	0.07	11.00	22.75	0.63	b.l.d.	72.27	5.49	0.044	528.24	0.043	1.23
	3-41a	44.58	9.49	4.27	b.l.d.	7.24	0.046	0.09	10.88	22.92	0.55	b.l.d.	72.81	5.24	0.044	503.72	0.050	1.01
BBT5	5-01a	45.15	8.36	3.83	0.15	6.63	b.l.d.	0.08	11.45	23.12	0.42	0.01	75.48	6.08	0.062	414.87	0.040	1.04
	5-02a	48.81	5.33	2.44	0.13	6.38	b.l.d.	0.07	13.04	22.97	0.34	b.l.d.	78.45	8.56	0.061	593.77	0.019	3.15
	5-04a	46.83	7.53	3.43	0.09	7.06	0.05	0.05	11.73	23.02	0.43	b.l.d.	74.76	5.60	0.060	395.13	0.031	1.28
	5-06a	45.55	7.83	3.78	0.13	6.66	b.l.d.	0.04	11.85	23.16	0.43	0.01	76.03	7.76	0.064	512.91	0.037	1.37
	5-07a	52.48	3.80	0.32	0.03	7.97	0.01	0.18	12.82	21.49	0.70	b.l.d.	74.15	3.94	0.065	256.68	0.009	2.82
	5-07b	44.79	9.01	4.01	0.15	6.86	0.07	0.09	11.14	23.17	0.49	b.l.d.	74.35	6.22	0.065	404.71	0.046	0.89
	5-08a	48.42	5.75	2.63	0.12	7.03	b.l.d.	0.13	12.73	23.01	0.38	b.l.d.	76.36	6.16	0.061	426.95	0.021	1.99
	5-09a	45.75	8.30	3.59	0.18	6.93	0.04	0.09	11.63	23.19	0.52	0.01	74.94	5.98	0.065	389.09	0.039	1.01
	5-14a	45.11	8.80	4.13	0.13	6.61	0.05	0.07	11.15	22.86	0.51	0.01	75.06	5.78	0.055	444.90	0.042	1.05
	5-15a	46.33	7.65	3.16	0.72	6.37	0.01	0.07	12.26	23.11	0.44	b.l.d.	77.42	6.86	0.051	568.99	0.034	1.66
	5-17a	48.02	5.89	2.44	0.16	6.35	0.05	0.10	12.65	23.09	0.25	0.01	78.02	3.84	0.040	405.68	0.021	1.94
	5-18a	45.56	8.22	3.54	0.15	6.90	0.03	0.10	11.75	23.02	0.54	b.l.d.	75.22	4.98	0.035	602.06	0.039	1.55
	5-18b	45.02	8.50	3.64	0.10	7.06	0.07	0.13	11.66	23.06	0.42	b.l.d.	74.64	4.90	0.035	591.78	0.043	1.39
	5-19a	44.79	8.91	4.12	0.37	7.29	b.l.d.	0.07	11.24	22.76	0.50	b.l.d.	73.33	7.13	0.046	656.22	0.047	1.39
	5-20a	46.46	8.08	3.50	0.13	6.68	0.05	0.12	11.69	23.12	0.50	b.l.d.	75.71	4.46	0.034	554.43	0.034	1.62
	5-21a	45.56	8.32	3.54	0.04	7.18	0.04	0.09	10.89	23.14	0.43	0.01	73.00	4.10	0.030	578.70	0.036	1.62
	5-21b	46.29	7.92	3.59	0.16	6.75	0.04	0.08	11.42	23.18	0.44	b.l.d.	75.12	4.02	0.030	566.29	0.033	1.69
	5-21c	45.79	8.55	4.02	0.16	6.69	0.03	0.04	11.53	22.96	0.47	0.01	75.45	4.18	0.030	589.99	0.040	1.48

Table 4-2 (continued)

	Sample	SiO_2	Al_2O_3	TiO_2	Cr_2O_3	FeO	NiO	MnO	MgO	CaO	Na_2O	K_2O	Mg#	A (cm^{-2})	t (mm)	H_2O in cpx (wt. ppm)	$D^{cpx/melt}$	H_2O in melt (wt. %)
BBT5	5-22a	45.85	8.25	3.68	0.08	6.19	b.l.d.	0.09	11.72	23.08	0.53	0.01	77.15	3.50	0.036	411.61	0.036	1.13
	5-22b	45.47	8.45	3.82	0.15	6.22	b.l.d.	0.09	11.53	23.05	0.50	b.l.d.	76.76	3.63	0.036	426.66	0.039	1.10
	5-23b	44.29	9.35	4.08	0.17	6.85	0.01	0.06	11.01	22.78	0.42	b.l.d.	74.13	4.18	0.037	478.02	0.049	0.99
	5-24a	47.60	5.75	2.86	0.06	7.02	b.l.d.	0.09	12.63	22.92	0.33	b.l.d.	76.22	6.71	0.046	617.50	0.023	2.69
	5-26a	46.43	7.14	3.16	0.04	7.53	b.l.d.	0.09	11.96	22.87	0.49	0.02	73.90	5.09	0.045	478.89	0.031	1.55
	5-26b	50.24	5.16	1.25	0.48	5.69	b.l.d.	0.07	14.13	22.27	0.56	0.01	81.57	4.31	0.045	404.80	0.016	2.57
	5-28a	45.51	8.17	3.65	0.13	6.73	b.l.d.	0.08	11.49	22.90	0.49	b.l.d.	75.27	7.54	0.057	559.35	0.037	1.51
	5-29b	45.58	8.28	3.67	0.08	6.82	0.07	0.08	11.59	22.79	0.42	b.l.d.	75.20	4.74	0.046	436.29	0.038	1.16
	5-31a	46.12	7.84	3.50	0.14	6.54	0.07	0.07	11.74	22.93	0.51	0.01	76.20	4.64	0.052	377.73	0.034	1.12
	5-32a	44.13	9.55	4.21	0.13	6.98	b.l.d.	0.06	10.64	23.03	0.51	b.l.d.	73.10	5.33	0.044	512.28	0.050	1.02
	5-34a	45.58	7.97	3.71	0.18	6.43	0.04	0.10	11.85	23.04	0.46	b.l.d.	76.65	3.46	0.034	430.85	0.037	1.15
	5-34b	51.04	4.92	0.72	0.06	9.18	b.l.d.	0.14	11.75	20.45	0.78	0.005	69.52	1.94	0.034	241.18	0.011	2.11
	5-34c	46.16	7.76	3.36	0.13	6.84	b.l.d.	0.10	11.43	23.05	0.50	b.l.d.	74.88	4.65	0.034	578.20	0.032	1.79
	5-37a	47.33	6.83	2.59	0.12	6.72	b.l.d.	0.03	12.54	22.96	0.37	0.01	76.89	4.99	0.050	422.03	0.026	1.63
BBT8	8-03a	47.78	5.91	2.86	0.01	7.44	b.l.d.	0.12	12.44	23.02	0.41	b.l.d.	74.89	3.14	0.045	294.78	0.023	1.26
	8-04a	48.58	6.25	2.86	0.09	6.54	b.l.d.	0.12	12.33	22.34	0.53	0.08	77.08	2.23	0.044	214.64	0.021	1.02
	8-05a	46.43	6.71	3.09	b.l.d.	7.54	0.02	0.08	12.07	23.09	0.45	0.01	74.05	3.79	0.043	372.65	0.029	1.27
	8-06a	49.40	6.19	1.60	0.21	6.57	b.l.d.	0.11	13.14	22.20	0.66	0.02	78.10	3.99	0.047	359.40	0.019	1.91
	8-07a	47.77	5.58	2.55	0.05	6.73	0.04	0.07	12.88	22.99	0.48	b.l.d.	77.34	3.63	0.041	374.83	0.022	1.71
	8-08a	47.83	6.10	2.38	0.36	6.42	0.05	0.09	12.93	22.72	0.46	0.01	78.21	2.60	0.039	281.70	0.023	1.22
	8-14a	45.18	8.82	3.67	0.01	7.43	0.04	0.08	10.90	22.78	0.55	0.01	72.33	3.17	0.049	273.83	0.041	0.68
	8-16a	46.99	6.82	3.09	0.19	6.77	0.01	0.09	12.40	22.94	0.49	b.l.d.	76.56	3.72	0.052	302.78	0.028	1.07

Table 4-2 (continued)

	Sample	SiO_2	Al_2O_3	TiO_2	Cr_2O_3	FeO	NiO	MnO	MgO	CaO	Na_2O	K_2O	Mg#	A (cm^{-2})	t (mm)	H_2O in cpx (wt. ppm)	$D^{cpx/melt}$	H_2O in melt (wt. %)
	8-17a	43.91	9.43	4.24	0.02	7.39	0.04	0.13	10.43	23.01	0.61	b.l.d.	71.56	2.94	0.048	259.08	0.051	0.51
	8-18a	46.11	7.43	3.12	0.10	6.89	b.l.d.	0.09	11.83	23.15	0.56	0.01	75.38	3.68	0.045	345.56	0.032	1.08
	8-21a	47.15	5.66	3.14	b.l.d.	7.83	0.03	0.13	12.37	22.91	0.50	b.l.d.	73.81	2.48	0.035	299.70	0.025	1.19
	8-22a	46.34	7.78	3.17	0.01	6.84	0.02	0.07	11.69	23.07	0.57	b.l.d.	75.28	2.58	0.022	497.03	0.032	1.56
	8-22b	47.83	6.32	2.86	0.02	7.11	b.l.d.	0.06	12.45	22.97	0.55	0.01	75.73	1.99	0.022	383.32	0.024	1.57
	8-23a	48.88	4.73	2.48	b.l.d.	7.38	0.02	0.13	12.77	23.05	0.55	b.l.d.	75.52	2.05	0.026	332.97	0.018	1.83
	8-24a	42.03	10.01	5.23	b.l.d.	8.32	0.03	0.05	10.37	22.79	0.54	0.01	68.98	2.44	0.036	286.91	0.076	0.38
	8-25a	44.43	8.07	3.87	b.l.d.	8.40	0.04	0.08	11.00	22.61	0.59	b.l.d.	70.02	2.76	0.035	334.03	0.043	0.77
	8-26a	44.29	8.91	3.92	0.04	7.93	0.03	0.04	10.85	22.94	0.53	0.02	70.93	2.36	0.026	383.91	0.047	0.81
BBT8	8-27a	46.67	7.08	3.41	b.l.d.	7.20	b.l.d.	0.13	11.79	22.76	0.64	b.l.d.	74.50	0.98	0.023	180.47	0.030	0.61
	8-28a	44.70	8.27	3.65	0.02	7.63	0.02	0.09	11.27	22.99	0.51	b.l.d.	72.49	2.13	0.032	281.12	0.042	0.67
	8-29a	45.64	7.37	3.35	0.01	7.91	b.l.d.	0.11	11.29	22.96	0.44	0.01	71.78	2.41	0.036	282.79	0.033	0.85
	8-30a	46.58	6.72	3.28	0.02	7.49	b.l.d.	0.06	11.92	23.28	0.54	b.l.d.	73.94	2.15	0.034	267.94	0.029	0.91
	8-31a	45.96	7.36	3.36	0.02	7.94	0.01	0.12	11.44	22.72	0.40	b.l.d.	71.97	1.85	0.034	229.98	0.032	0.71
	8-31b	46.71	6.54	3.17	0.03	7.49	b.l.d.	0.08	11.74	23.22	0.34	b.l.d.	73.63	1.77	0.034	219.65	0.027	0.81
	8-32a	48.39	8.09	2.12	0.07	6.75	0.09	0.10	13.90	20.03	0.63	0.02	78.60	2.04	0.028	308.13	0.028	1.09
	8-32b	48.33	7.90	1.88	0.10	6.27	0.10	0.12	14.22	20.19	0.65	b.l.d.	80.16	1.92	0.028	290.45	0.027	1.07
	8-33a	42.83	9.72	4.54	b.l.d.	8.48	0.02	0.08	10.10	22.78	0.57	b.l.d.	67.97	2.66	0.038	295.97	0.062	0.48
	8-34c	47.28	5.95	3.07	0.02	7.45	b.l.d.	0.10	12.29	22.95	0.42	b.l.d.	74.64	1.68	0.023	309.62	0.025	1.25
	4-02a	52.09	2.41	1.53	0.03	6.43	b.l.d.	0.08	14.03	22.80	0.60	b.l.d.	79.55	3.33	0.042	335.48	0.010	3.45
BLS4	4-03a	49.43	4.54	2.48	0.10	6.97	0.03	0.12	12.07	22.72	0.65	b.l.d.	75.55	4.71	0.048	414.93	0.015	2.74
	4-04a	50.81	3.12	1.80	0.18	6.58	0.02	0.11	13.69	22.44	0.63	b.l.d.	78.78	4.70	0.032	620.81	0.012	5.19

Table 4-2 (continued)

	Sample	SiO_2	Al_2O_3	TiO_2	Cr_2O_3	FeO	NiO	MnO	MgO	CaO	Na_2O	K_2O	Mg#	A (cm^{-2})	t (mm)	H_2O in cpx (wt. ppm)	$D^{cpx/melt}$	H_2O in melt (wt. %)
BLS4	4-04b	50.78	3.54	1.85	0.06	7.02	b.l.d.	0.11	13.55	22.79	0.60	b.l.d.	77.49	4.62	0.032	610.90	0.013	4.70
	4-05a	48.57	5.65	2.55	0.05	7.08	0.04	0.13	12.04	22.85	0.61	0.02	75.21	4.69	0.040	496.54	0.019	2.58
	4-06a	48.06	5.85	2.74	0.10	6.94	b.l.d.	0.08	12.32	22.97	0.58	b.l.d.	76.00	3.85	0.048	339.65	0.022	1.56
	4-09a	49.34	5.08	2.16	0.09	7.19	0.02	0.09	12.78	22.27	0.58	b.l.d.	76.02	6.10	0.060	430.18	0.017	2.53
	4-10a	50.43	4.02	1.46	0.14	7.41	0.02	0.14	13.39	22.25	0.46	0.02	76.32	3.02	0.048	266.57	0.013	1.99
	4-11a	47.00	6.34	2.58	0.04	8.32	0.05	0.11	11.95	22.12	0.68	b.l.d.	71.91	4.38	0.045	412.13	0.025	1.62
	4-12a	46.66	7.20	3.05	0.01	8.16	0.02	0.08	11.32	22.73	0.67	0.02	71.21	4.28	0.042	431.49	0.029	1.47
	4-13a	48.70	6.70	1.67	0.42	7.03	0.02	0.10	12.31	21.96	0.72	b.l.d.	75.75	4.72	0.034	587.55	0.020	2.87
	4-17a	47.45	6.32	2.82	0.09	7.25	0.01	0.12	11.76	22.49	0.69	0.01	74.31	4.90	0.039	532.06	0.023	2.28
	4-20a	50.24	2.73	1.85	b.l.d.	10.52	b.l.d.	0.16	11.83	21.56	0.39	b.l.d.	66.72	1.06	0.039	114.66	0.011	1.00
	4-25a	48.40	5.55	2.46	0.05	7.03	0.05	0.11	12.24	22.74	0.63	0.01	75.64	4.58	0.034	569.53	0.019	2.94
	4-29a	50.51	4.70	1.06	0.53	5.72	b.l.d.	0.09	13.64	22.82	0.57	b.l.d.	80.97	5.52	0.042	556.52	0.014	4.04
	4-29b	51.00	2.41	1.39	0.03	9.25	b.l.d.	0.18	12.66	21.97	0.40	b.l.d.	70.94	3.36	0.042	338.81	0.010	3.34
	4-34a	49.77	4.36	1.71	0.43	7.47	b.l.d.	0.07	13.03	22.54	0.41	b.l.d.	75.67	3.18	0.041	328.08	0.015	2.16
BLS6	6-03a	51.41	2.19	1.25	0.03	8.96	0.04	0.12	14.03	21.98	0.37	0.01	73.62	5.76	0.054	451.42	0.011	4.17
	6-04a	49.81	4.46	1.43	0.52	6.90	0.05	0.11	13.29	22.19	0.43	0.01	77.44	2.89	0.050	244.23	0.015	1.66
	6-06a	51.22	3.99	1.10	0.44	7.04	b.l.d.	0.08	13.95	21.85	0.79	b.l.d.	77.94	4.18	0.048	368.65	0.013	2.85
	6-06a	50.27	3.77	1.93	0.17	7.20	0.06	0.13	13.34	22.59	0.74	b.l.d.	76.77	4.18	0.048	368.65	0.014	2.60
	6-07a	51.76	2.54	0.84	0.01	9.10	0.01	0.24	13.24	22.22	0.46	b.l.d.	72.18	2.65	0.050	224.43	0.010	2.27
	6-08a	51.74	2.51	0.96	0.35	6.74	0.05	0.12	14.49	22.35	0.34	b.l.d.	79.32	3.72	0.052	302.87	0.010	2.99
	6-09a	48.26	4.44	2.78	0.05	9.43	b.l.d.	0.07	12.19	20.95	1.06	0.10	69.74	3.95	0.059	283.14	0.019	1.46
	6-10a	51.03	3.46	1.28	0.55	6.84	0.04	0.10	14.13	22.31	0.47	b.l.d.	78.65	3.53	0.052	287.16	0.013	2.27

Table 4-2 (continued)

	Sample	SiO_2	Al_2O_3	TiO_2	Cr_2O_3	FeO	NiO	MnO	MgO	CaO	Na_2O	K_2O	Mg#	A (cm^{-2})	t (mm)	H_2O in cpx (wt. ppm)	$D^{cpx/melt}$	H_2O in melt (wt. %)
	6-12a	50.64	3.97	1.71	0.01	8.45	0.01	0.11	12.94	22.32	0.47	0.01	73.20	2.63	0.036	308.73	0.014	2.28
	6-13a	46.14	6.10	4.01	b.l.d.	10.98	0.06	0.15	10.04	21.06	1.00	0.10	62.00	2.46	0.042	247.73	0.030	0.84
	6-15a	50.31	3.36	1.74	0.01	8.57	b.l.d.	0.13	12.75	22.55	0.42	b.l.d.	72.63	2.95	0.048	260.14	0.013	2.05
BLS6	6-18a	51.85	1.42	1.04	0.01	9.85	0.02	0.20	13.31	20.85	0.87	0.08	70.67	3.48	0.030	490.38	0.009	5.59
	6-21a	50.49	3.56	1.72	0.03	7.88	b.l.d.	0.13	13.65	22.31	0.40	b.l.d.	75.54	2.82	0.052	229.55	0.014	1.70
	6-22a	48.16	4.56	2.94	b.l.d.	9.71	b.l.d.	0.15	11.35	21.81	0.67	0.03	67.57	2.22	0.054	173.88	0.019	0.93
	6-22b	49.58	3.09	2.72	b.l.d.	11.66	0.01	0.15	10.23	21.38	0.96	0.01	61.00	2.73	0.054	213.60	0.013	1.63
	7-06a	50.13	3.98	1.90	0.01	7.85	0.03	0.13	13.02	22.64	0.61	b.l.d.	74.74	4.99	0.061	346.41	0.014	2.40
	7-09a	48.80	5.84	1.93	0.38	7.06	0.01	0.08	12.67	22.32	0.61	b.l.d.	76.19	6.20	0.048	546.72	0.019	2.81
	7-11a	51.77	2.30	1.18	0.02	8.08	b.l.d.	0.12	13.73	21.96	0.41	b.l.d.	75.19	2.65	0.055	203.95	0.010	2.12
	7-14a	50.06	4.05	1.75	0.15	7.38	0.01	0.09	13.35	22.60	0.51	b.l.d.	76.33	6.05	0.070	365.52	0.014	2.52
	7-18a	50.20	3.78	1.90	b.l.d.	8.63	b.l.d.	0.13	12.45	22.12	0.41	b.l.d.	72.00	2.77	0.063	185.91	0.013	1.42
	7-19a	52.08	2.78	1.06	0.38	6.73	0.10	0.08	14.15	21.93	0.66	b.l.d.	78.95	5.05	0.075	284.85	0.010	2.83
	7-22a	50.78	4.85	0.64	0.03	8.62	0.03	0.14	12.32	21.34	1.30	b.l.d.	71.81	8.11	0.084	408.47	0.013	3.19
BLS7	7-24a	52.16	2.77	0.37	0.03	9.95	b.l.d.	0.18	12.20	20.84	0.97	b.l.d.	68.63	2.60	0.046	238.70	0.008	2.83
	7-24b	48.25	5.42	2.50	0.05	7.10	0.01	0.08	12.59	22.97	0.57	b.l.d.	75.97	2.66	0.046	244.77	0.020	1.20
	7-24d	48.69	5.23	2.46	0.05	7.20	b.l.d.	0.03	12.78	22.76	0.62	b.l.d.	75.99	3.26	0.046	299.55	0.019	1.55
	7-25a	45.91	7.64	3.14	0.06	8.45	0.05	0.13	10.85	22.55	0.72	0.02	69.60	3.18	0.048	280.59	0.033	0.86
	7-27a	47.96	6.40	2.17	0.51	7.02	b.l.d.	0.06	12.50	22.47	0.54	b.l.d.	76.05	6.55	0.054	513.32	0.023	2.23
	7-28a	49.33	4.18	1.82	0.02	8.19	b.l.d.	0.12	13.10	22.38	0.48	0.01	74.03	4.34	0.047	390.54	0.016	2.46
	7-29a	48.99	4.97	1.77	0.34	7.23	b.l.d.	0.12	12.66	22.74	0.60	0.02	75.74	4.12	0.055	316.66	0.017	1.85
	7-34a	49.49	4.52	1.50	b.l.d.	7.29	b.l.d.	0.11	12.77	22.97	0.51	b.l.d.	75.75	5.60	0.059	401.76	0.015	2.74

Table 4-2 (continued)

	Sample	SiO_2	Al_2O_3	TiO_2	Cr_2O_3	FeO	NiO	MnO	MgO	CaO	Na_2O	K_2O	Mg#	A (cm^{-2})	t (mm)	H_2O in cpx (wt. ppm)	$D^{cpx/melt}$	H_2O in melt (wt. %)
BLS7	7-36a	51.14	4.09	1.08	0.35	7.29	b.l.d.	0.11	13.65	21.43	0.76	0.018	76.96	5.02	0.047	452.21	0.013	3.61
	7-37a	51.50	4.68	0.71	0.67	5.60	0.06	0.12	13.89	22.33	0.69	0	81.55	4.32	0.049	373.31	0.013	2.99
BLS8	8-04a	49.24	3.81	1.98	b.l.d.	8.89	0.04	0.12	12.59	22.18	0.44	b.l.d.	71.62	2.38	0.044	228.68	0.008	2.91
	8-09a	50.36	3.18	1.75	0.12	7.37	0.07	0.12	13.63	22.26	0.63	b.l.d.	76.73	1.82	0.042	183.66	0.013	1.43
	8-11a	52.67	1.48	1.14	0.05	6.93	b.l.d.	0.12	14.50	22.32	0.50	0.01	78.87	2.24	0.045	210.61	0.008	2.54
	8-14a	50.72	3.33	1.70	0.04	7.06	b.l.d.	0.08	13.62	22.56	0.59	b.l.d.	77.48	3.21	0.045	302.21	0.012	2.44
	8-15a	49.92	3.95	1.77	0.01	8.30	b.l.d.	0.07	12.83	22.02	0.48	b.l.d.	73.37	3.53	0.049	304.83	0.014	2.20
	8-16a	50.72	2.75	1.58	0.03	7.52	0.01	0.12	13.64	22.49	0.63	b.l.d.	76.37	2.82	0.042	283.90	0.012	2.44
	8-18a	51.83	2.15	1.40	0.06	7.09	0.05	0.13	13.93	22.22	0.59	0.01	77.80	1.97	0.028	297.10	0.010	3.12
	8-18b	50.76	2.69	1.79	0.20	7.39	0.04	0.15	13.65	21.95	0.66	0.02	76.71	1.52	0.028	228.97	0.012	1.96
	8-19a	51.79	2.30	1.10	0.13	7.29	b.l.d.	0.11	14.30	21.81	0.39	b.l.d.	77.76	2.24	0.029	326.10	0.010	3.38
	8-20a	51.01	2.40	1.55	0.26	7.46	0.01	0.15	13.69	21.94	0.60	b.l.d.	76.58	2.43	0.028	367.79	0.011	3.43
	8-21a	51.80	1.59	1.28	0.08	8.69	0.04	0.13	13.26	22.03	0.61	0.01	73.13	1.81	0.027	284.28	0.009	3.22
	8-22a	51.17	2.59	1.37	0.09	8.76	0.05	0.12	13.35	21.86	0.39	0.02	73.10	2.28	0.026	370.99	0.011	3.44
	8-25a	49.97	2.23	1.92	0.07	10.81	b.l.d.	0.21	11.76	21.61	0.43	b.l.d.	65.99	1.59	0.044	152.62	0.011	1.35
	8-27a	50.70	3.78	1.45	0.17	6.88	0.08	0.11	14.01	22.49	0.47	b.l.d.	78.42	4.05	0.048	356.84	0.013	2.66
	8-30a	51.51	2.32	1.07	0.06	7.73	b.l.d.	0.11	14.36	22.24	0.38	0.01	76.81	2.53	0.038	281.82	0.010	2.72
	8-32a	50.06	3.60	1.32	0.42	6.64	b.l.d.	0.08	14.05	21.95	0.39	0.01	79.05	2.02	0.031	276.29	0.013	2.10
	8-36a	45.17	7.19	3.54	0.01	10.68	b.l.d.	0.07	10.68	21.40	0.67	b.l.d.	64.05	2.73	0.028	412.70	0.037	1.13
DHLB4	4-1-02	51.73	1.63	1.29	0.01	10.73	0.06	0.27	12.34	21.78	0.47	b.l.d.	67.21	3.74	0.105	150.76	0.009	1.67
	4-1-05a	51.31	1.87	1.49	b.l.d.	9.77	b.l.d.	0.20	12.90	21.92	0.48	b.l.d.	70.17	2.29	0.094	103.08	0.010	1.04
	4-1-06a	51.42	2.87	1.40	0.32	7.31	0.04	0.18	14.37	22.20	0.39	b.l.d.	77.81	5.36	0.094	241.18	0.012	2.04

Table 4-2 (continued)

	Sample	SiO_2	Al_2O_3	TiO_2	Cr_2O_3	FeO	NiO	MnO	MgO	CaO	Na_2O	K_2O	Mg#	A (cm^{-2})	t (mm)	H_2O in cpx (wt. ppm)	$D^{cpx/melt}$	H_2O in melt (wt. %)
	4-1-06b	52.09	2.28	1.06	0.61	6.79	0.06	0.13	14.25	21.45	0.32	0.01	78.92	4.57	0.094	205.58	0.009	2.22
	4-1-07a	50.58	2.37	1.51	0.04	9.09	0.04	0.22	13.35	21.83	0.39	b.l.d.	72.35	4.17	0.111	158.96	0.011	1.40
	4-1-08a	50.65	3.11	1.86	0.01	8.68	0.08	0.13	13.23	22.02	0.44	b.l.d.	73.11	4.79	0.089	227.68	0.013	1.80
	4-1-08b	51.39	2.34	1.61	0.01	9.39	b.l.d.	0.17	13.27	21.84	0.48	0.01	71.60	5.76	0.089	273.85	0.011	2.52
	4-1-13b	51.34	2.31	1.51	0.05	9.01	0.01	0.16	13.79	21.75	0.47	0.01	73.19	6.09	0.119	216.44	0.011	1.94
	4-1-16b	51.49	2.23	1.21	0.02	8.57	0.05	0.16	13.98	21.87	0.40	b.l.d.	74.42	4.43	0.108	173.41	0.010	1.67
	4-1-19	51.44	2.65	0.88	0.66	6.67	0.01	0.16	14.60	22.26	0.28	b.l.d.	79.60	4.09	0.086	200.99	0.011	1.86
	4-2-02a	50.69	3.69	1.09	0.95	6.50	0.04	0.12	14.19	21.90	0.37	b.l.d.	79.55	3.59	0.083	183.12	0.013	1.40
	4-2-03	50.70	3.90	1.50	0.56	7.51	0.02	0.15	13.06	21.89	0.40	b.l.d.	75.62	3.31	0.086	162.86	0.013	1.27
DHLB4	4-2-04a	51.06	2.38	1.15	0.06	7.45	0.06	0.18	14.32	21.94	0.32	b.l.d.	77.41	5.25	0.092	241.37	0.011	2.29
	4-2-06a	52.00	2.75	0.99	0.65	6.32	0.02	0.13	14.68	22.09	0.36	0.01	80.55	5.00	0.093	227.49	0.010	2.17
	4-2-06d	51.67	2.41	1.58	0.00	9.04	b.l.d.	0.19	13.36	21.77	0.42	b.l.d.	72.48	5.41	0.093	246.28	0.010	2.35
	4-2-08b	51.90	2.60	0.99	0.72	6.53	0.05	0.18	14.83	21.87	0.30	b.l.d.	80.19	7.26	0.101	304.24	0.011	2.86
	4-2-10	52.44	2.20	1.02	0.19	7.16	0.07	0.17	14.83	21.83	0.34	0.02	78.70	2.79	0.090	131.17	0.010	1.37
	4-2-15c	52.71	2.25	1.00	0.44	6.73	b.l.d.	0.11	14.96	21.71	0.32	b.l.d.	79.84	3.73	0.105	150.19	0.009	1.60
	4-2-18a	51.02	3.31	1.59	0.11	7.20	0.02	0.16	14.01	22.03	0.37	b.l.d.	77.62	7.10	0.099	303.59	0.012	2.48
	4-2-19c	51.11	2.83	1.08	0.86	6.47	b.l.d.	0.08	14.60	21.91	0.39	b.l.d.	80.10	4.52	0.098	195.20	0.012	1.69
	4-2-20b	51.64	2.94	1.07	0.86	6.33	0.07	0.12	14.34	22.01	0.37	b.l.d.	80.16	7.10	0.089	337.74	0.011	3.09
	4-2-20c	50.87	3.68	1.45	0.58	6.90	0.07	0.12	13.79	21.94	0.38	0.01	78.09	5.29	0.089	251.64	0.013	1.97
DHLB5	5-1-01c	51.20	3.04	1.12	0.86	6.22	b.l.d.	0.13	14.35	21.96	0.31	b.l.d.	80.44	2.89	0.072	169.88	0.011	1.50
	5-1-02a	51.84	2.25	1.20	0.07	7.67	0.05	0.18	14.11	21.98	0.31	b.l.d.	76.63	3.27	0.073	189.37	0.010	1.95

Table 4-2 (continued)

	Sample	SiO_2	Al_2O_3	TiO_2	Cr_2O_3	FeO	NiO	MnO	MgO	CaO	Na_2O	K_2O	Mg#	A (cm^{-2})	t (mm)	H_2O in cpx (wt. ppm)	$D^{cpx/melt}$	H_2O in melt (wt. %)
DHLB5	5-1-03b	50.45	3.27	1.40	0.53	7.11	0.04	0.12	14.32	22.15	0.39	b.l.d.	78.22	5.15	0.080	272.39	0.013	2.03
	5-1-04a	51.39	2.26	1.10	0.09	7.60	0.07	0.16	14.54	21.80	0.38	b.l.d.	77.33	4.69	0.080	248.06	0.010	2.38
	5-1-05b	51.03	3.00	1.37	0.35	7.03	0.02	0.12	14.19	22.09	0.37	0.01	78.27	2.94	0.076	163.57	0.012	1.39
	5-1-06	50.73	1.82	1.41	0.01	10.04	0.02	0.14	12.62	21.81	0.38	b.l.d.	69.15	3.48	0.075	196.05	0.010	1.99
	5-1-08	50.49	3.69	1.29	0.87	6.45	0.06	0.15	13.96	22.25	0.29	b.l.d.	79.41	4.68	0.077	257.43	0.013	1.94
	5-1-11a	51.22	1.78	1.51	b.l.d.	10.01	b.l.d.	0.23	12.54	21.67	0.43	b.l.d.	69.07	3.38	0.096	148.89	0.009	1.57
	5-1-12	51.56	2.32	0.96	0.58	6.60	0.11	0.16	14.96	21.58	0.37	0.01	80.16	5.50	0.100	232.87	0.010	2.23
	5-1-13b	51.69	1.61	1.34	b.l.d.	10.67	b.l.d.	0.24	12.41	22.08	0.48	b.l.d.	67.47	3.08	0.085	153.07	0.009	1.66
	5-1-14	51.45	2.34	1.19	0.19	7.31	b.l.d.	0.10	14.54	22.07	0.34	b.l.d.	78.00	3.42	0.099	146.34	0.011	1.39
	5-1-15b	52.22	2.29	1.36	0.03	7.95	0.03	0.15	13.75	22.10	0.36	b.l.d.	75.50	6.54	0.089	310.98	0.009	3.28
	5-1-15c	51.47	2.36	1.50	0.04	8.50	0.03	0.17	13.70	21.99	0.40	b.l.d.	74.19	3.80	0.089	180.85	0.011	1.70
	5-2-01	50.85	3.57	1.24	0.95	6.62	b.l.d.	0.14	13.79	21.96	0.32	b.l.d.	78.80	4.48	0.098	193.35	0.012	1.56
	5-2-05b	51.37	3.00	1.03	0.72	6.48	0.06	0.13	14.50	22.10	0.36	b.l.d.	79.97	7.71	0.100	326.43	0.011	2.86
	5-2-06a	50.77	2.90	1.16	0.70	6.55	0.02	0.14	14.47	22.27	0.36	b.l.d.	79.76	5.75	0.102	238.49	0.012	1.98
	5-2-07a	51.44	2.61	0.95	0.69	6.82	0.06	0.19	14.86	21.35	0.31	0.02	79.53	5.98	0.108	234.12	0.011	2.14
	5-2-07b	51.23	1.79	1.55	0.01	10.11	0.02	0.20	11.95	21.80	0.48	b.l.d.	67.83	7.21	0.108	282.52	0.009	3.14
	5-2-08a	50.82	1.96	1.52	b.l.d.	10.03	b.l.d.	0.23	12.70	21.72	0.47	b.l.d.	69.30	4.16	0.106	165.90	0.010	1.61
	5-2-14a	50.66	3.19	1.24	0.42	7.10	b.l.d.	0.15	14.13	22.01	0.40	b.l.d.	78.03	5.48	0.112	206.84	0.012	1.68
	5-2-15	51.62	2.37	1.34	0.03	8.18	0.02	0.14	13.90	22.11	0.39	b.l.d.	75.18	6.14	0.117	222.20	0.010	2.14
	5-2-16b	51.79	2.56	1.17	0.48	6.80	b.l.d.	0.15	14.76	21.74	0.33	b.l.d.	79.47	3.97	0.113	148.81	0.011	1.40
	5-2-19d	51.53	3.12	1.10	0.87	6.47	0.04	0.13	14.37	22.15	0.32	b.l.d.	79.85	5.59	0.108	219.05	0.012	1.90
	5-2-19e	51.04	3.18	1.12	0.94	6.51	0.07	0.11	14.32	22.15	0.39	b.l.d.	79.69	7.76	0.108	303.91	0.012	2.48

Table 4-2 (continued)

	Sample	SiO_2	Al_2O_3	TiO_2	Cr_2O_3	FeO	NiO	MnO	MgO	CaO	Na_2O	K_2O	Mg#	A (cm^{-2})	t (mm)	H_2O in cpx (wt. ppm)	$D^{cpx/melt}$	H_2O in melt (wt. %)
	9-2-01	51.55	1.58	1.26	0.01	11.05	b.l.d.	0.21	11.86	21.82	0.58	0.01	65.67	2.58	0.107	102.18	0.009	1.17
	9-2-02	51.12	3.16	1.40	0.11	7.64	0.06	0.18	13.99	22.08	0.36	b.l.d.	76.55	4.15	0.106	165.66	0.012	1.38
	9-2-06	51.64	2.14	1.14	0.18	6.86	0.04	0.14	14.67	21.91	0.34	b.l.d.	79.22	4.32	0.114	160.23	0.010	1.63
	9-2-07	51.50	2.28	1.61	b.l.d.	8.72	0.01	0.15	13.40	21.85	0.42	0.02	73.26	4.36	0.112	164.76	0.010	1.60
	9-2-09a	52.24	2.11	0.98	0.48	6.95	b.l.d.	0.15	14.88	21.59	0.34	b.l.d.	79.24	6.17	0.114	229.12	0.010	2.39
	9-2-09b	52.19	2.38	1.10	0.41	6.82	0.02	0.17	14.66	21.81	0.35	b.l.d.	79.31	4.04	0.114	150.03	0.010	1.52
	9-2-10	52.25	2.18	1.19	0.16	7.05	b.l.d.	0.11	14.67	21.99	0.30	b.l.d.	78.77	6.28	0.115	231.21	0.010	2.41
	9-2-11	52.71	2.21	0.87	0.58	6.89	0.03	0.18	14.53	21.60	0.22	b.l.d.	78.99	4.29	0.112	161.89	0.009	1.82
	9-2-13	52.38	2.28	1.34	0.01	8.03	0.01	0.12	14.21	21.98	0.29	b.l.d.	75.92	3.69	0.116	134.45	0.010	1.37
	9-2-15a	49.91	4.25	1.53	0.69	6.99	b.l.d.	0.12	13.69	21.57	0.41	b.l.d.	77.73	5.05	0.112	190.90	0.015	1.28
DHLB9	9-2-17	51.48	1.91	1.41	0.01	10.26	b.l.d.	0.19	12.24	21.74	0.45	0.01	68.03	3.71	0.107	146.67	0.009	1.60
	9-2-18	51.66	2.19	1.19	0.08	7.82	0.03	0.14	14.34	21.76	0.36	b.l.d.	76.57	4.30	0.106	171.69	0.010	1.71
	9-2-20a	49.50	5.21	1.25	0.58	6.80	0.01	0.14	13.77	21.44	0.49	b.l.d.	78.32	4.69	0.096	206.58	0.017	1.22
	9-2-20b	50.20	4.81	1.14	0.65	6.48	0.05	0.13	14.33	21.67	0.40	b.l.d.	79.78	7.11	0.096	313.51	0.016	1.99
	9-2-21	50.92	1.66	1.22	0.01	10.61	0.02	0.23	12.13	21.70	0.51	b.l.d.	67.09	2.52	0.095	112.06	0.009	1.22
	9-2-22	51.18	2.86	1.25	0.07	7.47	0.03	0.17	13.89	21.79	0.44	b.l.d.	76.83	3.71	0.096	163.70	0.011	1.52
	9-2-25b	52.09	2.43	1.15	0.12	7.20	0.03	0.12	14.27	21.81	0.33	b.l.d.	77.94	5.10	0.090	239.92	0.010	2.51
	9-2-27b	51.19	2.14	1.67	0.02	9.60	0.03	0.19	13.10	21.70	0.50	0.02	70.87	2.57	0.094	115.46	0.011	1.08
	9-2-28a	51.94	2.58	1.17	0.72	6.92	b.l.d.	0.20	14.68	21.86	0.40	b.l.d.	79.08	3.09	0.078	167.73	0.011	1.53
	9-2-28c	51.86	2.93	1.03	0.84	6.43	0.05	0.11	13.86	22.11	0.38	b.l.d.	79.36	4.19	0.078	227.46	0.010	2.24
	9-2-31a	49.79	3.24	2.32	0.03	10.00	0.04	0.19	11.69	21.65	0.73	b.l.d.	67.58	3.21	0.074	183.60	0.013	1.37

Table 4-2 (continued)

	Sample	SiO_2	Al_2O_3	TiO_2	Cr_2O_3	FeO	NiO	MnO	MgO	CaO	Na_2O	K_2O	Mg#	A (cm^{-2})	t (mm)	H_2O in cpx (wt. ppm)	$D^{cpx/melt}$	H_2O in melt (wt. %)
DHLB9	9-2-31b	51.26	2.35	1.76	0.01	9.55	0.01	0.18	12.91	21.59	0.46	b.l.d.	70.67	2.51	0.074	143.46	0.011	1.34
	9-2-32	51.49	2.46	1.68	0.02	8.20	0.05	0.15	13.48	21.87	0.50	b.l.d.	74.55	2.11	0.064	139.57	0.011	1.33
	9-2-33c	52.38	2.34	1.01	0.22	6.93	0.01	0.13	14.29	21.97	0.43	b.l.d.	78.60	3.87	0.065	251.80	0.009	2.75
	9-2-33d	51.46	2.74	1.20	0.43	7.01	0.04	0.08	14.46	22.15	0.39	0.02	78.62	3.09	0.065	200.82	0.011	1.79
	9-3-01	50.82	3.15	1.47	0.03	7.87	b.l.d.	0.16	13.75	21.96	0.43	b.l.d.	75.71	5.86	0.113	219.32	0.012	1.82
	9-3-05a	51.16	2.40	1.69	b.l.d.	8.97	0.05	0.14	13.31	21.62	0.51	0.01	72.58	3.22	0.122	111.78	0.011	1.02
	9-3-05b	51.12	2.33	1.67	b.l.d.	8.73	0.01	0.17	13.04	21.73	0.47	b.l.d.	72.70	5.32	0.122	184.51	0.010	1.79
	9-3-08	52.65	2.37	0.73	0.58	6.59	0.03	0.10	14.90	22.04	0.40	b.l.d.	80.11	7.42	0.135	232.66	0.009	2.45
DHLB10	10-1-02c	51.16	2.15	1.54	b.l.d.	8.05	0.05	0.18	13.61	21.87	0.44	b.l.d.	75.09	2.91	0.080	153.81	0.010	1.51
	10-1-03c	51.30	3.11	1.24	0.81	6.39	0.04	0.11	14.35	21.85	0.35	b.l.d.	80.01	7.73	0.101	323.76	0.012	2.79
	10-1-03d	51.09	3.27	1.22	0.84	6.49	0.03	0.13	14.29	22.33	0.34	b.l.d.	79.70	8.25	0.101	345.63	0.012	2.80
	10-1-04a	52.69	2.37	1.06	0.35	7.12	0.02	0.15	14.85	21.31	0.33	b.l.d.	78.80	3.88	0.094	174.83	0.010	1.83
	10-1-04b	50.79	3.34	1.24	0.92	6.33	b.l.d.	0.11	14.29	21.97	0.40	b.l.d.	80.11	4.79	0.094	215.66	0.013	1.72
	10-1-05a	51.98	2.23	1.07	0.08	7.44	0.02	0.13	14.49	21.89	0.34	b.l.d.	77.63	4.51	0.088	216.76	0.010	2.24
	10-1-05b	51.26	2.76	1.53	0.13	7.39	b.l.d.	0.23	14.09	21.47	0.39	0.01	77.28	6.47	0.088	311.24	0.011	2.82
	10-1-06a	51.58	2.46	1.52	0.03	8.44	0.03	0.17	13.41	21.45	0.44	b.l.d.	73.92	5.50	0.097	239.92	0.010	2.38
	10-1-06b	51.01	3.35	1.32	0.37	6.96	0.04	0.14	14.25	22.29	0.39	b.l.d.	78.49	5.90	0.097	257.41	0.013	2.05
	10-1-07b	50.19	4.73	1.62	0.74	7.04	0.08	0.12	13.69	21.53	0.44	b.l.d.	77.62	5.55	0.103	228.12	0.016	1.43
	10-1-07e	50.85	3.78	1.35	0.86	6.63	0.04	0.11	14.06	22.11	0.41	b.l.d.	79.10	5.28	0.103	216.70	0.013	1.61
	10-1-07f	51.63	2.33	1.14	0.05	7.94	0.03	0.16	14.03	21.85	0.35	0.01	75.90	11.49	0.103	472.10	0.010	4.74
	10-1-07g	50.30	2.54	1.78	b.l.d.	8.75	b.l.d.	0.19	13.33	21.93	0.40	0.01	73.09	4.26	0.103	174.88	0.012	1.46
	10-1-07h	51.35	2.49	1.54	0.02	8.74	0.04	0.21	13.55	21.52	0.40	b.l.d.	73.44	3.96	0.103	162.64	0.011	1.51

Table 4-2 (continued)

	Sample	SiO_2	Al_2O_3	TiO_2	Cr_2O_3	FeO	NiO	MnO	MgO	CaO	Na_2O	K_2O	Mg#	A (cm^{-2})	t (mm)	H_2O in cpx (wt. ppm)	$D^{cpx/melt}$	H_2O in melt (wt. %)
DHLB10	10-1-08a	51.06	1.68	1.37	b.l.d.	10.04	0.02	0.25	12.40	22.00	0.50	0.01	68.77	3.69	0.092	169.57	0.009	1.81
	10-1-08c	51.01	2.44	1.49	0.01	8.53	0.01	0.15	13.52	22.04	0.40	b.l.d.	73.87	4.31	0.092	198.41	0.011	1.82
	10-1-09	49.81	4.60	1.63	0.72	7.08	0.01	0.12	13.22	21.96	0.47	0.01	76.91	4.44	0.092	204.02	0.016	1.31
	10-1-10a	51.03	2.11	1.37	0.05	9.76	b.l.d.	0.21	12.79	21.39	0.46	b.l.d.	70.02	3.16	0.098	136.27	0.010	1.37
	10-1-11	52.03	2.18	1.17	0.06	8.07	0.08	0.18	13.97	22.18	0.36	b.l.d.	75.52	5.26	0.115	193.61	0.010	2.00
	10-1-13b	51.37	2.97	1.44	0.15	7.62	0.05	0.12	14.14	22.04	0.40	b.l.d.	76.79	7.70	0.104	313.24	0.012	2.68
	10-1-15a	52.63	2.27	0.88	0.41	6.58	0.01	0.15	14.86	22.21	0.35	0.01	80.09	4.46	0.093	202.74	0.009	2.16
	10-1-15b	52.05	2.28	1.13	0.21	7.15	0.04	0.15	14.83	22.13	0.38	0.01	78.72	4.36	0.093	198.51	0.010	1.93
	10-1-15d	52.19	2.60	0.98	0.75	6.68	0.03	0.13	14.68	22.06	0.38	b.l.d.	79.66	5.18	0.093	235.59	0.010	2.26
	10-1-16a	51.70	2.66	1.08	0.81	6.34	0.02	0.09	14.51	21.73	0.38	b.l.d.	80.31	5.38	0.110	206.95	0.013	1.56
	10-2-01b	51.12	1.94	1.44	b.l.d.	9.38	b.l.d.	0.20	12.89	21.82	0.47	b.l.d.	71.02	3.93	0.083	200.35	0.010	2.05
	10-2-01d	50.93	2.46	1.75	b.l.d.	9.26	0.01	0.21	13.14	21.90	0.46	b.l.d.	71.68	7.11	0.083	362.36	0.011	3.18
	10-2-03a	51.00	1.80	1.42	b.l.d.	9.84	0.06	0.20	12.84	21.89	0.48	b.l.d.	69.93	4.02	0.087	195.61	0.010	1.97
	10-2-04a	51.50	1.92	1.51	b.l.d.	9.68	b.l.d.	0.19	12.95	21.86	0.37	b.l.d.	70.46	4.67	0.093	212.48	0.010	2.18
	10-2-04b	51.19	2.25	1.22	0.01	7.77	0.02	0.16	13.94	21.56	0.37	0.01	76.18	7.38	0.093	335.68	0.010	3.41
	10-2-05c	51.60	1.98	1.48	0.01	9.49	0.03	0.23	12.98	21.73	0.45	b.l.d.	70.93	4.04	0.094	181.90	0.010	1.88
	10-2-05d	51.30	3.36	1.11	0.96	6.46	0.07	0.07	14.30	22.03	0.34	b.l.d.	79.78	4.44	0.094	199.91	0.012	1.65
	10-2-06b	50.82	2.46	1.48	0.04	8.41	b.l.d.	0.17	13.71	22.08	0.43	b.l.d.	74.39	4.19	0.092	192.57	0.011	1.70
	10-2-09a	51.44	2.14	1.51	0.02	9.21	0.05	0.16	13.12	21.79	0.47	b.l.d.	71.75	4.04	0.097	176.06	0.010	1.75
	10-2-10a	51.32	1.98	1.47	b.l.d.	9.40	b.l.d.	0.24	12.43	21.95	0.44	b.l.d.	70.21	3.54	0.093	160.93	0.009	1.75
	10-2-10b	51.30	2.00	1.57	0.01	9.65	0.01	0.17	12.94	21.67	0.47	b.l.d.	70.51	3.80	0.093	172.76	0.010	1.72
	10-2-14	51.57	2.93	0.97	0.83	6.30	b.l.d.	0.12	14.46	21.99	0.33	b.l.d.	80.36	5.22	0.077	286.85	0.011	2.64

Table 4-2 (continued)

	Sample	SiO_2	Al_2O_3	TiO_2	Cr_2O_3	FeO	NiO	MnO	MgO	CaO	Na_2O	K_2O	Mg#	A (cm^{-2})	t (mm)	H_2O in cpx (wt. ppm)	$D^{cpx/melt}$	H_2O in melt (wt. %)
DHLB10	10-2-16a	51.96	2.96	0.75	0.81	6.25	0.03	0.09	14.47	22.00	0.38	0.01	80.50	3.79	0.083	193.26	0.010	1.88
	10-2-19a	51.92	2.16	0.98	0.25	7.34	0.02	0.18	14.75	21.50	0.32	b.l.d.	78.17	3.22	0.077	176.95	0.010	1.82
	10-2-19c	50.22	3.42	1.33	0.88	6.37	0.09	0.12	14.30	21.93	0.40	b.l.d.	80.02	4.04	0.077	221.79	0.014	1.64
	10-2-19d	52.33	2.60	1.16	0.41	6.59	0.02	0.12	14.58	22.08	0.36	0.01	79.78	4.98	0.077	273.77	0.010	2.73
XTEJ2	2-4-02a	51.61	2.49	0.85	0.65	7.92	0.02	0.17	15.41	19.66	0.28	b.l.d.	77.61	4.25	0.165	109.07	0.011	0.99
	2-3-03a	51.82	2.20	0.94	0.50	7.89	0.05	0.12	15.03	20.56	0.29	b.l.d.	77.25	5.92	0.167	150.02	0.010	1.46
	2-4-07a	51.27	2.16	0.96	0.18	8.61	b.l.d.	0.09	14.43	20.58	0.30	0.01	74.91	5.72	0.161	150.43	0.010	1.49
	2-4-07b	50.63	2.61	1.42	0.40	9.32	0.08	0.18	14.76	19.91	0.30	0.01	73.85	5.01	0.161	131.59	0.013	1.00
	2-4-09a	51.47	2.29	1.40	0.08	9.06	0.06	0.16	14.10	20.28	0.34	0.01	73.50	4.78	0.175	115.53	0.010	1.10
	2-4-03a	51.23	1.54	1.32	b.l.d.	10.97	0.08	0.18	14.23	19.28	0.31	b.l.d.	69.81	3.03	0.160	80.02	0.010	0.77
	2-5-05a	51.68	1.46	1.17	b.l.d.	11.59	0.01	0.24	14.18	18.89	0.34	b.l.d.	68.56	1.66	0.144	48.72	0.010	0.49
	2-1-02a	50.82	2.29	1.79	0.05	11.36	0.03	0.24	13.31	19.99	0.40	b.l.d.	67.63	2.21	0.131	71.32	0.012	0.59
	2-1-02b	51.80	1.42	0.99	b.l.d.	12.30	0.08	0.22	13.48	19.27	0.34	b.l.d.	66.14	2.26	0.131	72.84	0.009	0.78
	2-5-06a	51.01	1.96	1.36	0.04	12.09	0.05	0.20	12.89	19.50	0.38	0.01	65.53	3.18	0.161	83.44	0.011	0.79
	2-1-03a	50.31	2.02	1.42	0.05	12.48	0.02	0.24	12.97	19.68	0.42	0.01	64.95	3.82	0.143	112.97	0.012	0.95
	2-3-01a	51.29	1.16	1.04	0.02	13.88	b.l.d.	0.31	12.39	19.05	0.41	0.01	61.40	2.72	0.142	81.05	0.009	0.88
XTEJ4	4-1-01a	51.25	1.40	0.87	0.13	12.35	0.01	0.38	13.33	19.05	0.38	b.l.d.	65.81	2.60	0.134	81.94	0.010	0.86
	4-1-01b	51.95	1.50	0.98	b.l.d.	11.28	0.05	0.31	13.77	19.37	0.28	0.01	68.50	3.34	0.134	105.40	0.009	1.16
	4-1-01c	52.47	1.77	1.13	0.02	9.53	b.l.d.	0.23	14.36	20.47	0.29	b.l.d.	72.87	3.08	0.134	97.19	0.009	1.05
	4-1-02a	51.69	1.38	0.91	0.01	12.19	0.02	0.25	13.31	19.08	0.35	0.01	66.06	2.06	0.138	63.29	0.009	0.71
	4-1-04a	51.94	2.05	0.96	0.20	8.39	0.02	0.15	14.96	20.67	0.30	0.01	76.06	4.27	0.157	115.05	0.010	1.14

Table 4-2 (continued)

	Sample	SiO_2	Al_2O_3	TiO_2	Cr_2O_3	FeO	NiO	MnO	MgO	CaO	Na_2O	K_2O	Mg#	A (cm^{-2})	t (mm)	H_2O in cpx (wt. ppm)	$D^{cpx/melt}$	H_2O in melt (wt. %)
XTEJ4	4-1-05a	53.10	1.59	0.94	0.13	8.68	0.04	0.26	15.30	19.78	0.24	0.01	75.87	3.34	0.167	84.68	0.009	0.97
	4-1-10a	52.35	1.89	1.09	0.04	9.17	b.l.d.	0.21	14.62	20.60	0.34	0.07	73.97	3.86	0.162	100.85	0.010	1.04
	4-2-01a	52.40	2.18	1.03	0.10	8.40	b.l.d.	0.16	14.83	20.74	0.26	0.01	75.89	4.85	0.189	108.56	0.010	1.12
	4-4-02a	52.44	2.51	0.84	0.77	8.09	b.l.d.	0.14	15.03	20.00	0.31	0.01	76.81	3.98	0.170	99.01	0.010	0.96
	4-4-05a	52.25	2.33	0.94	0.34	7.84	b.l.d.	0.16	15.06	20.76	0.31	b.l.d.	77.41	5.27	0.173	128.85	0.010	1.27
	4-4-06a	51.62	1.65	1.05	0.03	13.90	0.01	0.35	12.43	18.70	0.45	b.l.d.	61.46	2.48	0.169	62.09	0.010	0.65
	4-4-07a	52.75	2.12	0.92	0.25	7.89	0.07	0.21	14.88	21.01	0.28	b.l.d.	77.08	3.10	0.151	86.92	0.009	0.93
	4-5-02a	52.72	1.68	0.85	0.20	8.24	0.04	0.24	15.51	19.88	0.26	b.l.d.	77.04	2.58	0.152	71.74	0.009	0.79
	4-5-02b	52.67	2.26	0.81	0.77	7.59	b.l.d.	0.14	15.32	20.67	0.28	b.l.d.	78.26	2.28	0.152	63.53	0.010	0.63
	4-5-02c	52.63	2.56	0.76	0.88	7.33	0.03	0.10	15.26	20.50	0.34	b.l.d.	78.78	2.17	0.152	60.46	0.010	0.59
	4-5-02d	52.40	1.87	1.11	0.03	9.01	0.03	0.17	14.74	20.48	0.34	b.l.d.	74.48	1.98	0.152	55.09	0.010	0.58
	4-5-05a	53.54	1.51	0.75	0.17	8.53	0.01	0.25	15.47	20.06	0.29	b.l.d.	76.39	3.26	0.170	81.14	0.008	0.96

Note: b.l.d., below the limit of detection

Table 4-3. Major element composition of olivine phenocrysts in Shuangliao basalts

	Sample	SiO_2	Al_2O_3	TiO_2	Cr_2O_3	FeO	NiO	MnO	MgO	CaO	Total	Mg#
	bb1-01	39.31	0.06	0.01	0.02	17.33	0.28	0.21	42.81	0.22	100.25	81.49
	bb1-02	39.86	0.05	0.03	b.l.d.	15.86	0.17	0.16	43.79	0.21	100.11	83.12
	bb1-03	39.63	0.01	0.02	0.02	16.51	0.27	0.19	42.09	0.11	98.84	81.96
	bb1-04	40.00	0.05	b.l.d.	0.03	14.68	0.22	0.14	44.67	0.21	100.01	84.44
BBT1	bb1-05	39.28	0.04	0.02	0.04	17.35	0.18	0.16	42.15	0.20	99.39	81.24
	bb1-06	38.14	0.04	0.03	b.l.d.	24.27	0.12	0.42	36.36	0.29	99.66	72.76
	bb1-07	40.03	0.05	b.l.d.	b.l.d.	18.26	0.13	0.20	41.40	0.19	100.26	80.17
	bb1-08	39.66	0.07	0.02	0.04	18.63	0.27	0.22	41.09	0.24	100.24	79.73
	bb1-09	38.48	0.08	0.02	0.01	21.23	0.15	0.30	38.94	0.19	99.40	76.58
	bb2-01	39.83	0.06	0.03	0.05	17.73	0.22	0.21	41.71	0.20	100.02	80.75
	bb2-02	37.98	0.01	b.l.d.	0.02	26.52	0.12	0.47	34.85	0.15	100.12	70.08
	bb2-03	39.20	0.04	b.l.d.	0.06	18.30	0.21	0.31	40.97	0.21	99.31	79.96
	bb2-04	38.18	0.02	0.05	0.02	21.39	0.14	0.41	39.07	0.30	99.58	76.51
BBT2	bb2-05	38.53	0.04	0.03	0.01	24.38	0.10	0.41	36.05	0.43	99.99	72.50
	bb2-06	36.64	1.55	0.15	0.44	26.17	0.06	0.50	34.31	0.36	100.17	70.04
	bb2-07	39.89	0.05	b.l.d.	0.02	17.00	0.24	0.17	42.26	0.15	99.79	81.59
	bb2-08	39.93	0.07	0.04	0.04	16.51	0.24	0.15	42.84	0.20	100.02	82.22
	bb2-09	40.17	0.06	0.05	0.07	14.64	0.26	0.12	44.03	0.18	99.57	84.28
	bb3-01	38.39	0.03	b.l.d.	b.l.d.	22.80	0.15	0.46	37.85	0.34	100.01	74.74
	bb3-02	39.84	0.02	0.06	0.02	14.08	0.44	0.17	44.88	0.16	99.67	85.04
	bb3-03	38.68	0.07	0.03	0.02	21.32	0.11	0.30	39.19	0.26	99.98	76.62
	bb3-04	38.20	0.06	b.l.d.	b.l.d.	20.14	0.10	0.34	38.96	0.23	98.03	77.52
BBT3	bb3-05	38.74	0.04	0.01	0.01	23.42	0.10	0.45	35.97	0.48	99.22	73.25
	bb3-06	39.76	0.05	0.01	b.l.d.	16.97	0.23	0.19	42.65	0.23	100.09	81.75
	bb3-07	38.76	0.05	0.02	0.01	22.19	0.13	0.33	38.13	0.29	99.92	75.39
	bb3-08	37.65	0.05	0.06	0.01	23.23	0.14	0.40	37.41	0.38	99.33	74.17
	bb3-09	38.52	0.06	0.01	0.05	22.82	0.12	0.36	37.07	0.35	99.36	74.34
	bb5-01	38.68	0.05	0.02	b.l.d.	20.08	0.24	0.30	39.71	0.24	99.31	77.91
	bb5-02	37.99	0.04	b.l.d.	0.04	20.86	0.20	0.36	38.94	0.29	98.71	76.90
	bb5-03	38.08	0.04	0.03	0.03	22.18	0.21	0.40	37.81	0.31	99.08	75.24
	bb5-04	40.26	0.05	0.03	0.08	14.31	0.29	0.18	44.24	0.20	99.63	84.64
BBT5	bb5-05	39.21	0.03	b.l.d.	0.03	19.13	0.22	0.28	40.26	0.17	99.32	78.96
	bb5-06	40.01	0.04	b.l.d.	0.04	16.91	0.19	0.18	42.54	0.20	100.10	81.77
	bb5-07	38.62	0.04	0.06	b.l.d.	26.47	0.04	0.46	34.08	0.48	100.24	69.66
	bb5-08	39.23	0.05	0.03	b.l.d.	20.67	0.26	0.23	38.72	0.19	99.38	76.96
	bb5-09	39.21	0.05	0.04	0.01	18.25	0.17	0.26	41.00	0.22	99.21	80.02
	bb5-10	39.10	0.06	0.02	0.07	21.05	0.08	0.27	39.24	0.27	100.16	76.87
	bb8-01	37.86	0.03	b.l.d.	0.06	25.05	0.18	0.39	35.87	0.24	99.68	71.86
	bb8-02	37.75	0.02	0.01	0.02	26.46	0.10	0.42	34.23	0.31	99.32	69.76
	bb8-03	38.52	0.04	0.03	0.01	21.45	0.19	0.32	38.11	0.26	98.94	76.01
	bb8-04	37.96	0.04	b.l.d.	0.04	25.59	0.15	0.42	35.14	0.19	99.54	71.00
	bb8-05	37.51	0.05	0.04	0.04	27.65	0.14	0.43	33.33	0.35	99.53	68.25
BBT8	bb8-06	37.13	0.01	b.l.d.	0.02	26.47	0.13	0.49	35.19	0.17	99.60	70.33
	bb8-07	39.40	0.07	0.05	0.01	20.02	0.18	0.31	39.60	0.26	99.90	77.91
	bb8-08	38.91	0.05	0.02	0.02	19.33	0.18	0.29	40.01	0.20	99.02	78.67
	bb8-09	38.96	0.05	0.04	0.03	19.95	0.17	0.30	39.95	0.21	99.65	78.12
	bb8-10	40.53	0.10	b.l.d.	b.l.d.	13.98	0.27	0.14	44.30	0.18	99.49	84.96
	bb8-11	39.63	0.07	b.l.d.	b.l.d.	17.89	0.17	0.23	41.06	0.16	99.21	80.36

Table 4-3. (continued)

	Sample	SiO_2	Al_2O_3	TiO_2	Cr_2O_3	FeO	NiO	MnO	MgO	CaO	Total	Mg#
BLS4	BL4-01	37.92	0.03	0.03	b.l.d.	25.45	0.15	0.42	34.70	0.36	99.06	70.85
	BL4-02	38.40	0.04	0.04	0.05	23.58	0.24	0.43	36.49	0.28	99.55	73.39
	BL4-03	37.83	0.04	0.03	0.02	25.29	0.19	0.41	35.16	0.36	99.33	71.26
	BL4-04	37.46	0.05	0.04	0.01	25.27	0.11	0.39	35.65	0.28	99.27	71.56
	BL4-05	38.00	0.04	0.05	b.l.d.	25.12	0.19	0.35	35.27	0.37	99.38	71.45
	BL4-06	38.58	0.03	b.l.d.	b.l.d.	24.93	0.10	0.46	36.13	0.22	100.44	72.10
	BL4-07	38.14	0.04	0.01	0.03	25.17	0.15	0.43	35.39	0.29	99.64	71.49
	BL4-08	37.91	0.03	0.02	b.l.d.	24.95	0.11	0.39	35.46	0.27	99.14	71.70
	BL4-09	38.88	b.l.d.	b.l.d.	b.l.d.	20.66	0.26	0.26	39.86	0.13	100.04	77.48
BLS6	BL6-01	39.11	0.02	b.l.d.	0.01	18.87	0.27	0.26	40.55	0.14	99.22	79.31
	BL6-02	38.34	0.04	0.03	b.l.d.	25.20	0.10	0.49	35.13	0.29	99.62	71.31
	BL6-03	38.37	0.04	0.04	b.l.d.	26.16	0.08	0.41	34.79	0.23	100.12	70.33
	BL6-04	38.84	0.03	0.03	0.01	22.50	0.08	0.32	37.86	0.13	99.80	75.00
	BL6-05	38.19	0.01	b.l.d.	b.l.d.	25.77	0.09	0.48	34.91	0.36	99.81	70.72
	BL6-06	38.51	0.01	0.02	b.l.d.	24.64	0.14	0.44	35.40	0.25	99.42	71.92
	BL6-07	38.02	0.04	0.08	0.02	24.59	0.17	0.36	36.87	0.18	100.32	72.78
	BL6-08	39.04	0.03	b.l.d.	0.03	21.56	0.12	0.25	39.02	0.22	100.27	76.34
	BL6-09	37.53	0.04	b.l.d.	0.03	23.19	0.20	0.27	38.01	0.18	99.46	74.50
	BL6-10	40.52	0.17	0.05	b.l.d.	14.35	0.31	0.16	44.36	0.19	100.09	84.65
BLS7	BL7-01	37.87	0.02	0.01	0.02	24.13	0.12	0.42	35.83	0.32	98.73	72.59
	BL7-02	38.42	0.02	b.l.d.	b.l.d.	23.81	0.15	0.38	36.70	0.19	99.67	73.32
	BL7-03	38.19	0.04	0.04	b.l.d.	24.21	0.13	0.42	34.60	0.34	97.97	71.81
	BL7-04	38.15	0.02	0.03	0.01	24.82	0.09	0.36	35.17	0.37	99.03	71.64
	BL7-05	37.66	0.04	b.l.d.	0.03	25.45	0.07	0.38	35.42	0.39	99.44	71.28
	BL7-06	38.49	0.04	0.05	b.l.d.	23.72	0.19	0.27	36.82	0.20	99.78	73.45
	BL7-07	38.05	0.03	0.01	b.l.d.	24.82	0.11	0.37	35.41	0.41	99.21	71.78
	BL7-08	38.09	0.02	0.03	b.l.d.	23.41	0.21	0.39	35.96	0.46	98.57	73.25
	BL7-09	37.74	0.04	b.l.d.	0.03	24.17	0.23	0.37	35.90	0.30	98.79	72.59
BLS8	BL8-01	38.57	0.01	b.l.d.	b.l.d.	22.11	0.18	0.38	37.78	0.21	99.23	75.28
	BL8-02	37.86	0.06	0.01	b.l.d.	24.76	0.16	0.42	35.28	0.23	98.81	71.76
	BL8-03	37.45	0.04	0.05	b.l.d.	26.16	0.08	0.45	34.62	0.31	99.17	70.24
	BL8-04	37.87	0.02	0.01	0.01	25.71	0.06	0.48	34.87	0.19	99.20	70.75
	BL8-05	38.30	0.03	0.02	b.l.d.	26.41	0.08	0.45	34.92	0.32	100.53	70.22
	BL8-06	38.52	0.05	b.l.d.	0.03	21.29	0.25	0.26	38.63	0.18	99.21	76.39
	BL8-07	37.72	0.03	0.04	0.05	26.29	0.11	0.44	34.68	0.28	99.64	70.17
	BL8-08	37.58	0.03	0.03	0.07	27.07	0.07	0.42	33.72	0.35	99.34	68.96
	BL8-09	37.49	0.06	0.08	b.l.d.	25.89	0.16	0.35	35.45	0.20	99.69	70.94
	BL8-10	38.60	0.05	b.l.d.	0.03	23.04	0.09	0.29	36.93	0.18	99.21	74.08
	BL8-11	37.41	0.02	0.02	0.03	27.17	0.17	0.40	34.13	0.30	99.64	69.13
DHLB4	d4-01	38.27	0.02	0.02	0.04	24.76	0.07	0.38	36.23	0.33	100.12	72.29
	d4-02	37.60	0.05	0.06	0.02	24.20	0.15	0.38	36.63	0.34	99.42	72.96
	d4-03	37.82	0.02	b.l.d.	0.07	24.08	0.13	0.35	36.64	0.36	99.48	73.06
	d4-04	38.02	0.03	0.06	0.05	23.53	0.15	0.27	37.39	0.30	99.81	73.91
	d4-05	36.61	0.03	b.l.d.	0.04	29.83	0.07	0.49	31.76	0.38	99.20	65.50
	d4-06	38.05	0.03	0.01	0.06	24.43	0.13	0.32	36.37	0.38	99.76	72.64
	d4-07	37.36	0.04	0.06	0.04	24.31	0.11	0.36	36.11	0.41	98.79	72.59
	d4-08	38.26	0.05	b.l.d.	0.04	22.37	0.20	0.31	38.13	0.29	99.65	75.24
	d4-09	39.01	0.03	0.02	b.l.d.	19.18	0.16	0.28	40.70	0.25	99.62	79.09
	d4-10	36.57	0.02	0.01	0.03	29.62	0.11	0.44	32.10	0.37	99.26	65.90

Table 4-3. (continued)

	Sample	SiO_2	Al_2O_3	TiO_2	Cr_2O_3	FeO	NiO	MnO	MgO	CaO	Total	Mg#
DHLB5	d5-01	37.63	0.03	0.04	0.04	26.84	0.14	0.41	33.71	0.35	99.19	69.13
	d5-02	38.00	0.04	0.06	0.07	23.42	0.16	0.26	37.06	0.28	99.32	73.83
	d5-03	37.94	0.04	0.01	0.02	22.79	0.17	0.30	37.61	0.27	99.16	74.63
	d5-04	36.77	0.03	0.03	0.02	29.18	0.15	0.42	32.73	0.40	99.72	66.66
	d5-05	37.87	0.03	0.03	0.04	25.65	0.15	0.35	35.63	0.33	100.07	71.24
	d5-06	38.13	0.04	0.04	b.l.d.	24.59	0.17	0.36	35.79	0.34	99.47	72.18
	d5-07	38.30	0.04	0.03	0.04	21.60	0.17	0.28	38.69	0.28	99.42	76.15
	d5-08	37.55	0.03	b.l.d.	0.03	26.00	0.15	0.38	34.64	0.45	99.23	70.37
	d5-09	38.92	0.05	b.l.d.	b.l.d.	19.25	0.19	0.22	40.15	0.26	99.04	78.81
	d5-10	37.99	0.04	0.01	0.03	22.05	0.12	0.32	38.20	0.32	99.06	75.54
DHLB	d9-01	38.31	0.03	0.02	0.05	25.03	0.21	0.32	35.27	0.40	99.64	71.52
	d9-02	37.79	0.02	0.02	0.05	25.09	0.14	0.35	35.57	0.31	99.34	71.65
	d9-03	38.92	0.06	b.l.d.	b.l.d.	22.35	0.24	0.27	37.86	0.27	99.97	75.12
	d9-04	37.64	0.03	0.02	0.01	25.87	0.19	0.41	35.39	0.34	99.89	70.92
	d9-05	38.31	0.02	0.04	b.l.d.	23.46	0.18	0.34	37.26	0.28	99.90	73.90
	d9-06	37.36	0.03	0.06	0.04	27.52	0.16	0.40	33.80	0.44	99.81	68.65
	d9-07	37.46	0.02	0.02	b.l.d.	27.65	0.14	0.36	33.79	0.34	99.78	68.55
	d9-08	37.72	0.02	b.l.d.	0.02	26.88	0.16	0.40	33.91	0.35	99.45	69.22
	d9-09	38.45	0.03	0.04	0.04	21.48	0.18	0.21	38.89	0.22	99.53	76.35
	d9-10	37.67	0.03	0.08	0.05	26.10	0.13	0.36	35.26	0.28	99.97	70.67
	d9-11	36.94	0.03	0.03	0.04	26.69	0.09	0.32	34.15	0.47	98.77	69.52
	d9-12	38.35	0.05	0.04	0.01	20.98	0.23	0.27	39.33	0.27	99.52	76.97
	d9-13	38.28	0.04	0.06	0.03	22.75	0.18	0.32	38.21	0.27	100.13	74.97
DHLB10	d10-01	36.75	0.03	0.02	0.01	28.49	0.15	0.35	32.80	0.40	99.00	67.24
	d10-02	38.15	0.03	0.07	b.l.d.	24.23	0.15	0.34	35.52	0.33	98.82	72.33
	d10-03	38.44	0.03	0.01	0.02	22.80	0.21	0.35	37.21	0.26	99.33	74.42
	d10-04	38.27	0.03	b.l.d.	0.10	24.82	0.11	0.39	35.97	0.37	100.07	72.10
	d10-05	37.72	0.02	b.l.d.	0.04	23.62	0.12	0.43	35.98	0.34	98.26	73.09
	d10-06	37.62	0.03	0.02	b.l.d.	25.61	0.19	0.33	35.35	0.36	99.50	71.11
	d10-07	38.02	0.03	0.03	b.l.d.	26.33	0.16	0.36	34.68	0.38	99.99	70.14
	d10-08	38.21	0.04	0.01	0.01	25.14	0.11	0.28	35.78	0.27	99.84	71.73
	d10-09	38.43	0.03	0.09	0.04	21.53	0.10	0.31	38.44	0.31	99.30	76.09
	d10-10	39.01	0.02	0.01	0.02	19.81	0.18	0.26	40.39	0.22	99.92	78.43
	d10-11	37.24	0.03	0.02	b.l.d.	32.28	0.08	0.53	30.12	0.45	100.73	62.45
XTEJ2	X2-01	37.11	0.01	0.02	b.l.d.	29.18	0.09	0.33	32.72	0.37	99.82	66.66
	X2-02	36.85	0.02	0.01	b.l.d.	30.19	0.09	0.29	31.85	0.36	99.65	65.29
	X2-03	38.22	0.03	0.05	0.04	29.38	0.12	0.44	33.22	0.34	101.83	66.84
	X2-04	36.12	0.04	0.07	b.l.d.	29.20	0.14	0.35	32.58	0.35	98.86	66.55
	X2-05	37.14	0.02	0.02	0.01	30.14	0.09	0.42	31.99	0.32	100.15	65.43
	X2-06	37.45	0.04	0.01	0.01	28.98	0.16	0.38	32.36	0.35	99.74	66.56
	X2-07	36.50	0.02	0.10	0.01	31.26	0.05	0.37	30.83	0.36	99.51	63.75
	X2-08	37.57	0.03	0.09	0.01	29.88	0.16	0.40	32.41	0.39	100.92	65.91
	X2-09	37.20	0.01	0.03	0.02	29.57	0.16	0.28	32.24	0.33	99.83	66.03
	X2-10	37.30	0.02	b.l.d.	0.05	28.60	0.14	0.36	32.85	0.34	99.64	67.19
	X2-11	36.64	0.01	b.l.d.	0.04	30.97	0.16	0.47	30.97	0.36	99.62	64.07
XTEJ4	X4-01	36.90	0.03	0.03	b.l.d.	29.73	0.12	0.41	32.09	0.33	99.64	65.81
	X4-02	36.87	0.03	0.03	b.l.d.	28.60	0.19	0.39	32.70	0.37	99.18	67.09
	X4-03	37.54	0.03	0.03	0.03	28.16	0.10	0.39	33.49	0.31	100.07	67.95
	X4-04	37.39	0.02	b.l.d.	0.02	28.01	0.11	0.38	33.45	0.35	99.73	68.04

Table 4-3. (continued)

	Sample	SiO_2	Al_2O_3	TiO_2	Cr_2O_3	FeO	NiO	MnO	MgO	CaO	Total	Mg#
XTEJ4	X4-05	36.95	0.03	0.02	b.l.d.	30.18	0.12	0.40	31.35	0.36	99.42	64.94
	X4-06	36.95	0.03	0.02	b.l.d.	30.18	0.12	0.40	31.35	0.36	99.42	64.94
	X4-07	36.99	0.03	b.l.d.	b.l.d.	29.90	0.07	0.39	32.17	0.38	99.92	65.73
	X4-08	37.62	0.03	0.02	0.01	29.37	0.12	0.33	32.55	0.33	100.37	66.40
	X4-09	37.31	0.02	0.06	0.02	30.69	0.10	0.42	31.15	0.33	100.10	64.41
	X4-10	37.42	b.l.d.	b.l.d.	b.l.d.	32.33	0.13	0.44	31.59	0.37	102.28	63.53

Note: b.l.d., below the limit of detection

4.1.1.3 Water content of clinopyroxene phenocrysts and melts

The IR (Infrared) absorption spectra of the Shuangliao cpx phenocrysts in the OH-stretching vibration region (3000-3800 m^{-1}) are mainly composed of three bands: 3630-3620 cm^{-1}, 3540-3520 cm^{-1}, and 3470-3450 cm^{-1} (Fig. 4-4), which are consistent with structural OH bands in both natural and synthetic cpx (e.g. Bell and Rossman, 1992; Denis et al., 2013; Ingrin and Skogby, 2000; Kovács et al., 2012; Li et al., 2008; Peslier et al., 2002; Skogby et al., 1990; Sundvall and Stalder, 2011; Xia et al., 2010, 2013a). The 3620-3640 cm^{-1} band is always predominant. The maximum linear absorbance for all measurements is less than 0.15, implying that the unpolarised method is applicable under these absorbance conditions (Kovács et al., 2008; Withers, 2013). The IR measurement error of unpolarized analysis on single cpx grain is less than 20% (Xia et al., 2013b). Considering additional errors from baseline correction and thickness measurement, the total uncertainty of the calculated water content is estimated to be within 30% (Xia et al., 2013b). IR profiles have been conducted on some big cpx phenocrysts and they turn out to be homogenous, suggesting that water diffusion during their ascent to the surface has not significantly affected the water content in cpx (Fig. 4-4). Variations in water content and Mg# of the Shuangliao cpx phenocrysts are shown in Fig 4-5.

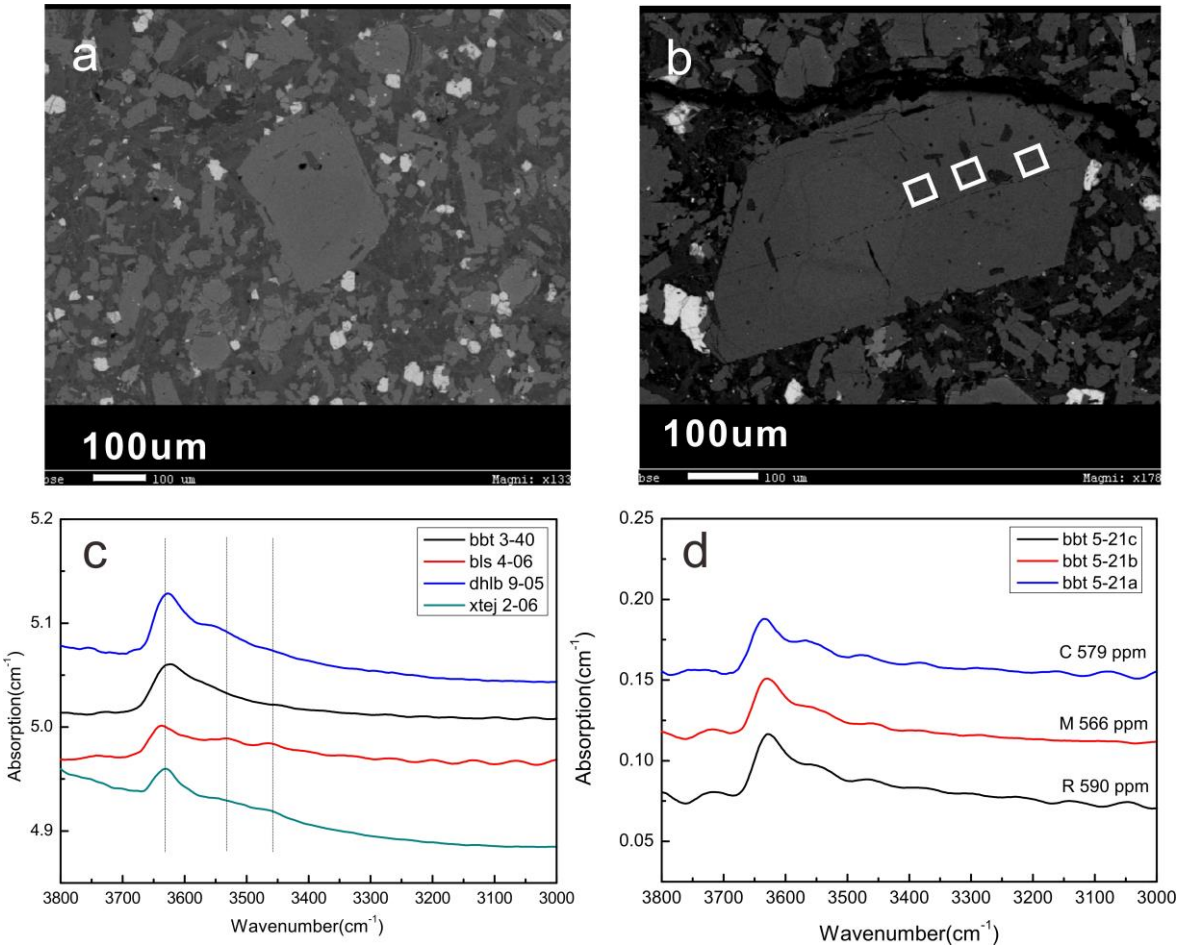

Figure 4-4. a-b) BSE images of cpx phenocrysts in the Shuangliao basalts, the white squares show the positions of the spots for FTIR analysis. c) Representative OH IR absorption spectrum of cpx phenocrysts, dashed lines mark the position of individual OH bands. The absorption intensity has been normalized to 1 cm. d) OH IR absorption profile of the cpx phenocryst (BBT 5-21 listed in Table 4-2) shown in b), C, M and R represent the core, mantle and rim of the phenocryst. Calculated H_2O content are 579, 566, and 590 ppm H_2O, respectively.

The water content of parental melts from which the cpx phenocrysts crystallized can be calculated from the water content of cpx phenocrysts and the H_2O partition coefficient (D) between cpx and basaltic melt. The calculated water contents of cpx and melts with which they equilibrated are listed for each analysed grain in Table 4-2, and plotted versus Mg# of cpx phenocrysts in Fig 4-5.

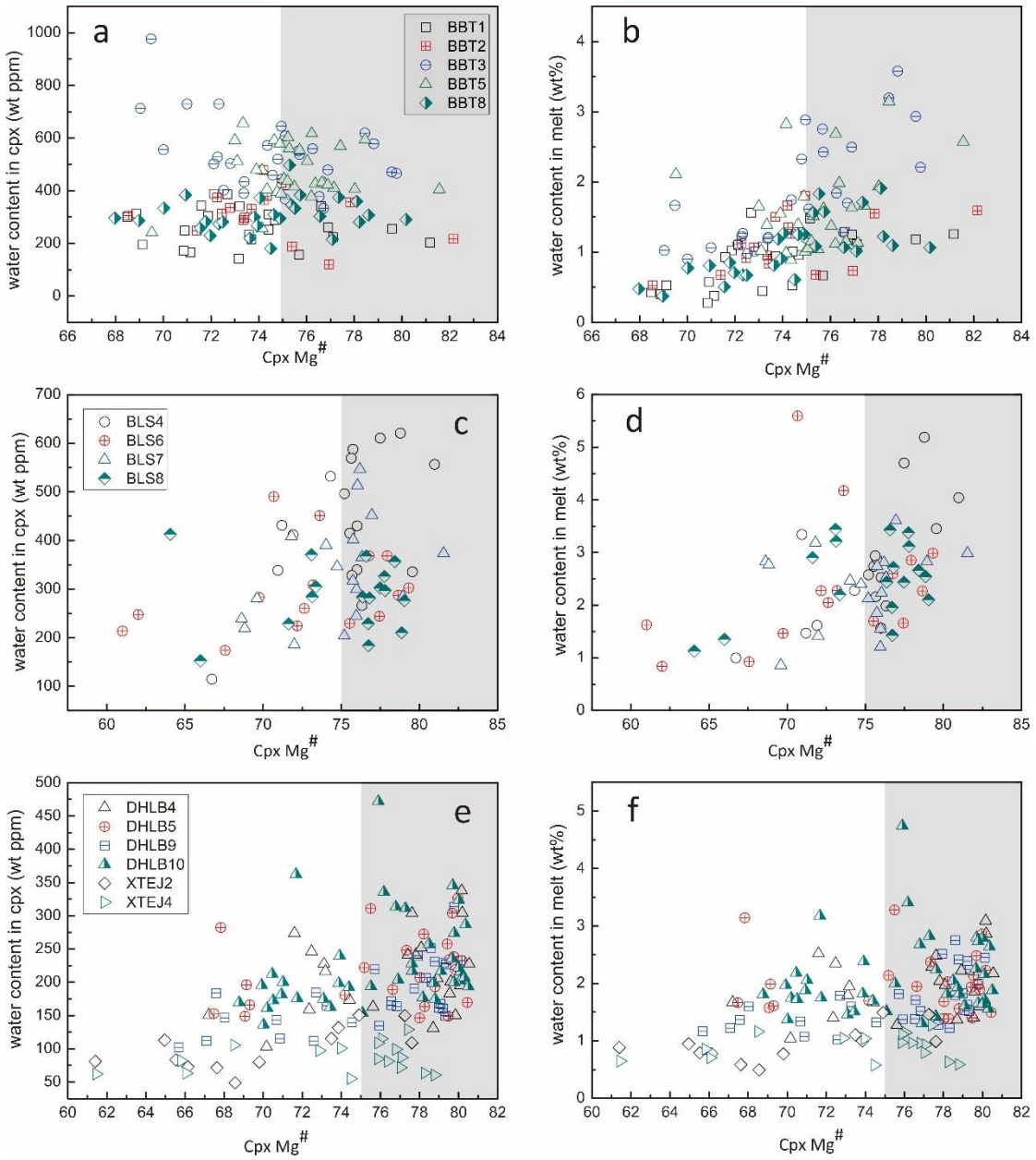

Figure 4-5. H_2O contents measured in cpx phenocrysts and calculated in the parental melts a vs cpx Mg#. The H_2O contents of cpx phenocrysts in a), c) and e) are calculated by Beer-Lambert law; the H_2O water contents of melt in b), d) and f) are calculated from the H_2O content of cpx phenocrysts and the H_2O partition coefficient (D) between cpx and basaltic melt proposed by O'Leary et al. (2010). The gray area with cpx Mg#>75 are data used to calculate the H_2O content of "primary" melts.

H_2O contents of cpx and melts with which they equilibrated vary with Mg# of the cpx phenocrysts (Fig. 4-5), it can be explained by crystal fractionation and degassing during magmatic evolution assuming a homogeneous source. The H_2O contents of the earliest cpx phenocrysts (i.e. cpx with highest Mg#) in the basanites (BBT, BLS) range

from 200 to 800 ppm, and are slightly higher than those of alkaline olivine basalts (DHLB, 200~350 ppm), obviously higher than those of transitional basalts (XTEJ, 50~150 ppm) (Fig. 4-5). The calculated H_2O contents of parental melts equilibrated with the cpx phenocrysts crystallized from basanites (BBT, BLS), alkaline olivine basalts (DHLB) and transitional basalts (XTEJ) are 1~5.6 wt.%, 1~3 wt.% and 0.5~1.5 wt.%, respectively.

4.1.1.4 Oxygen isotope compositions of clinopyroxene phenocrysts

The oxygen isotope compositions of Shuangliao cpx phenocrysts are plotted in Fig. 4-6 and listed in Table 4-4. The $\delta^{18}O$ values of cpx phenocrysts among different samples vary widely, ranging from 4.10‰ to 6.73‰, beyond the range of cpx in typical MORB (mid-ocean ridge basalt) and mantle peridotites (5.4‰-5.8‰) (Eiler et al., 1997; Mattey et al., 1994). Interestingly, this variation is time-dependent. From 51 to 43 Ma, the oxygen isotope compositions of basalts changed from values which are higher than those of normal mantle to values which are lower than those of normal mantle (Fig. 4-6b).

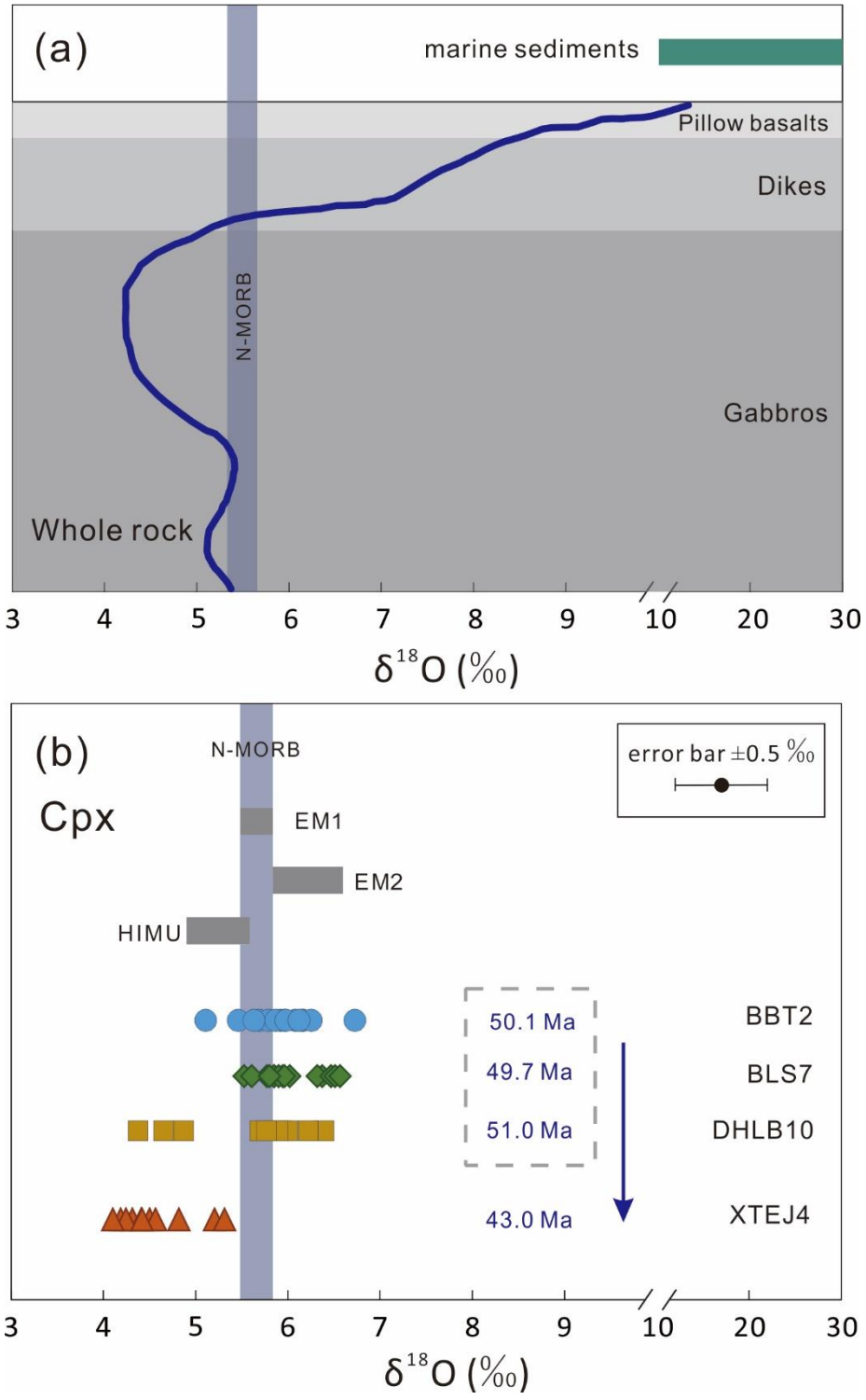

Figure 4-6. a) Typical oxygen isotope profile of altered sediment-covered oceanic crust. The data for oceanic crust are based on the Samail Ophiolite (Gregory and Taylor, 1981), the $\delta^{18}O$ values of marine sediments are from Eiler (2001); b) Oxygen isotope compositions of cpx phenocrysts in Shuangliao basalts. The range of $\delta^{18}O$ values of cpx phenocrysts in N-MORB, EM1, EM2 and HIMU are calculated from the $\delta^{18}O$ values of ol phenocrysts (Eiler et al., 1997), assuming the equilibrium fractionation between cpx and ol is 0.4‰ (Mattey et al., 1994). The erupted ages for Shuangliao basalts are listed in Section 2.2.1.

Table 4-4. The oxygen isotope compositions of cpx phenocrysts in Shuangliao basalts

	Sample	Mg#	$\delta^{18}O$ measured	IMF*	$\delta^{18}O$ corrected by IMF	1SE**
BBT	BBT2-12a	77.8	8.21	2.04	6.16	0.21
	BBT2-14a	71.4	7.96	2.27	5.69	0.17
	BBT2-20	73.4	8.00	2.08	5.92	0.16
	BBT2-25a	68.2	8.18	2.71	5.46	0.12
	BBT2-25b	74.2	8.21	2.04	6.17	0.12
	BBT2-34a	72.3	8.24	2.45	5.79	0.09
	BBT2-26a	73.4	8.11	2.14	5.97	0.10
	BBT2-37a	74.9	8.42	2.17	6.26	0.08
	BBT2-09a	82.2	8.04	1.31	6.73	0.16
	BBT2-07a	74.3	8.52	2.44	6.08	0.27
	BBT2-1a	70.3	8.25	2.61	5.64	0.05
	BBT2-3a	74.9	7.90	2.03	5.87	0.13
	BBT2-5a	76.9	6.79	1.68	5.11	0.21
	BBT2-22a	72.8	8.46	2.48	5.98	0.14
	BBT2-30a	75.4	8.19	2.06	6.12	0.04
BLS	BLS7-24c	68.8	9.05	2.68	6.37	0.07
	BLS7-24d	76.0	7.67	1.82	5.85	0.18
	BLS7-24a	68.6	9.15	2.83	6.32	0.06
	BLS7-24b	76.0	7.88	2.03	5.85	0.13
	BLS7-22a	71.8	8.79	2.32	6.47	0.25
	BLS7-19a	78.9	7.66	1.64	6.02	0.17
	BLS7-04	76.7	7.97	2.19	5.78	0.28
	BLS7-37	81.5	7.89	1.37	6.52	0.13
	BLS7-27a	76.0	8.89	2.94	5.95	0.18
	BLS7-28a	74.0	7.91	2.00	5.90	0.17
	BLS7-36a	77.0	8.56	1.99	6.57	0.28
	BLS7-11a	75.2	7.60	2.07	5.53	0.20
	BLS7-14a	76.3	8.04	2.07	5.97	0.14
	BLS7-18a	72.0	7.97	2.36	5.61	0.12
	BLS7-34a	75.8	7.75	1.94	5.80	0.20
DHLB	DHLB10-1-08b	77.2	9.56	4.91	4.65	0.15
	DHLB10-1-10b	72.9	9.55	5.17	4.37	0.44
	DHLB10-1-15d	79.7	9.07	2.67	6.40	0.16
	DHLB10-1-15b	78.7	8.82	2.89	5.93	0.17
	DHLB10-1-15a	80.1	8.75	2.75	6.00	0.21
	DHLB10-1-15c	78.3	8.89	3.00	5.89	0.14
	DHLB10-1-06a	73.9	9.31	3.62	5.70	0.31
	DHLB10-1-06b	78.5	8.84	3.07	5.77	0.04
	DHLB10-1-03b	71.7	8.82	3.94	4.87	0.09
	DHLB10-1-03c	80.0	9.15	2.93	6.22	0.22
XTEJ	XTEJ4-5-02a	77.0	9.28	4.46	4.82	0.10
	XTEJ4-5-02b	78.3	9.51	4.30	5.21	0.22
	XTEJ4-5-02c	78.8	9.56	4.25	5.32	0.11
	XTEJ4-1-04a	76.1	9.05	4.74	4.32	0.02
	XTEJ4-4-02a	76.8	8.92	4.73	4.19	0.13
	XTEJ4-1-05a	75.9	8.57	4.07	4.50	0.30
	XTEJ4-4-05a	77.4	8.72	4.16	4.57	0.26
	XTEJ4-1-10b	76.1	8.92	4.51	4.41	0.19
	XTEJ4-1-10a	74.0	9.16	4.91	4.25	0.24
	XTEJ4-1-01b	68.5	10.03	5.92	4.10	0.29

Table 4-4. (continued)

	Sample	Mg#	$\delta^{18}O$ measured	IMF*	$\delta^{18}O$ corrected by IMF	1SE**
XTEJ	XTEJ4-1-01c	72.9	9.84	5.42	4.42	0.08

* IMF is the instrumental mass fractionation
** SE the standard error of the mean for the group of measurements in a single cpx grain

4.1.2 Discussion

4.1.2.1 Crustal contamination and crystal fractionation

Crustal contamination and crystal fractionation are common processes that may alter the compositions of "primary" basaltic melt. "Primary" melt in this paper refers to the initial melt formed in the mantle; its composition remains unchanged till the beginning of crystal fractionation. Therefore, the composition of the melt equilibrated with the earliest phenocrysts should be close to that of the "primary" melt. If crustal contamination and crystal fractionation during melt evolution (i.e., magma ascent) can be excluded, the composition of the whole rock is also near that of the "primary" melt. But this is not the case for volatile elements such as H_2O due to degassing upon magma ascent. In other words, the H_2O content of "primary" melt can only be obtained from the earliest phenocrysts, but concentrations of refractory trace elements (e.g., REEs, Ba, Th, Ce, Pb, Nb) can be obtained from whole rock analysis when crustal contamination and crystal fractionation have been excluded.

Abundant peridotite xenoliths in the Shuangliao basalts witness a rapid magma ascent process (generally within a maximum of 50 hours after xenolith entrainment, O'Reilly and Griffin (2010)), leaving limited time for the magma to be influenced by crustal contamination. This is also supported by the trace element signatures; the Shuangliao basalts are enriched in Nb and Ta relative to highly incompatible elements (Rb, Ba, Th, U), which are highly concentrated in the crust. If significant crustal contamination had happened, the Ba/Nb ratios would show positive correlation with the La/Nb ratios, which is not observed in the Shuangliao basalts (Fig. 4-7a). In addition, crustal contamination can also be evaluated through Nb/U and Ce/Pb ratios as the crust has low Nb/U and Ce/Pb ratios than the mantle (Hofmann, 1988; Rudnick and Gao, 2014; Workman and Hart, 2005). The Nb/U ratios of the Shuangliao basalts are slightly lower than the values of MORBs and ocean island basalts (OIBs), and do not change with SiO_2 (Fig. 4-7b). Compared to the basanites which have similar Ce/Pb ratios as

MORBs and OIBs, the Ce/Pb ratios of the alkaline olivine basalts and transitional basalts are low, and the Ce/Pb ratios generally decrease with SiO_2 (Fig.4-7c). If the low Ce/Pb ratios of the low alkaline rocks are caused by crustal contamination, these rocks should be more enriched in incompatible elements than the basanites, which is opposite to our observation. Overall, the Shuangliao basalts have been weakly or not affected by crustal contamination, in agreement with the conclusion of Xu et al. (2012).

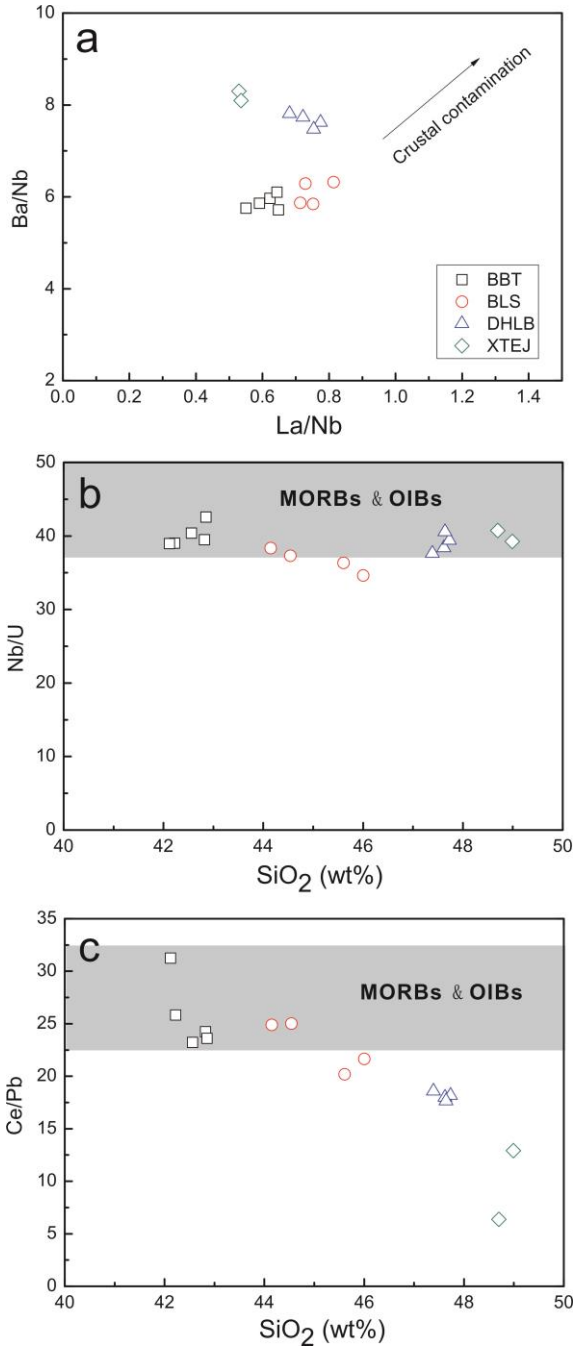

Figure 4-7. a) Ba/Nb vs La/Nb diagram. b-c) Nb/U and Ce/Pb vs SiO_2 in Shuanliao basalts. In a), the arrow represents the contamination trend. The gray zone in b) and c) are variation ranges for Nb/U and Ce/Pb of MORBs and OIBs (Hofmann AW et al., 1986).

The basanites have high Ni and Co contents and high Mg# (65.1-67.9), slightly positive Eu anomaly and no correlation on the plots of major oxides with MgO, suggesting that crystal fractionation was limited. The alkaline olivine basalts and transitional basalts display relatively low Ni (161-209 ppm) and Cr (253-286 ppm) contents and low Mg# (58.8–60.7), implying a small amount of fractionation through olivine and pyroxenes crystallization. It is remarkable that the alkaline olivine basalts and transitional basalts show different major element trends compared with the basanites (Fig 4-2; Xu et al., 2012), so the alkaline olivine basalts and the transitional basalts cannot be the result of basanites evolution via crystal fractionation. Their compositional differences from the basanites can only result from varied degrees of partial melting or distinct magma sources.

4.1.2.2 Heterogeneity of oxygen isotope compositions

The $\delta^{18}O$ values of cpx phenocrysts in the Shuangliao basalts have two primary features: 1) the $\delta^{18}O$ values vary widely, from 4.10‰ to 6.73‰, which is covered by the typical oxygen isotope profile of altered oceanic crust (Eiler, 2001; Gao et al., 2006; Grogory and Taylor, 1981; Hoffman SE et al., 1986); 2) the $\delta^{18}O$ values within individual samples also display considerable variation (1.04‰ to 1.75‰).

During the magma evolution, the oxygen isotope compositions of cpx phenocrysts can be affected by many factors, including alteration on the surface of the Earth, crustal contamination, partial melting, devolatilization, fractional crystallization, assimilation-fractional crystallization (AFC), water-melt interaction.

For Shuangliao basalts, fresh cpx phenocrysts without crack and inclusion were selected by FTIR investigations prior to the oxygen isotope measurement so that the effect of alteration can be ruled out. Previous studies have shown that crustal contamination in the Shuangliao basalts is negligible, so the influence of crustal contamination is limited (Xu et al., 2012). In addition, for basaltic melts with MgO content between 8 and 3 wt.%, the equilibrium oxygen isotope fractionation caused by partial melting, fractional crystallization or devolatilization will be less than 0.1‰ (Eiler, 2001). Thus, partial melting, devolatilization, fractional crystallization are unlikely to be the primary cause responsible for the $\delta^{18}O$ variations of Shuangliao basalts. Theoretically, an AFC process would significantly affect the oxygen isotope

composition of the melt during magma evolution. The AFC process can be evaluated by the equation:

$$\delta^{18}O_m^R = \delta^{18}O_m^0 + (\delta^{18}O_s - \delta^{18}O_m^0 - \mathrm{r}\cdot\Delta^{18}O)\cdot[1 - F^{1/(r-1)}] \quad (4\text{-}2)$$

in which $\delta^{18}O_m^0$, $\delta^{18}O_m^R$ and $\delta^{18}O_s$ are the oxygen isotope compositions of the original melt, residual melt and wall-rocks, respectively; Δ^{18}O is the fractionation of oxygen isotope between the melt and phenocrysts; F is the proportion of the residual melt; and r is the weight percentage ratio of crystallization/assimilation (Taylor, 1974). From this equation, to increase the δ^{18}O value, high degree of fractional crystallization and crustal contamination is required. However, the sample with the highest δ^{18}O value in Shuangliao basalts (BBT and BLS basalts) is characterized by highest Mg# (66.9), highest Ni (525.6 ppm) and Cr (373 ppm) contents, highest Nb/U (38.4) and Ce/Pb (24.9) ratios, which is not consist with the AFC process. High temperature water-melt interaction during crystallization is another candidate accounting for low δ^{18}O values of XTEJ4 (Wang and Eiler, 2008). The equation to assess the influence of water-melt interaction on O isotopes is:

$$\mathrm{W/M} = (\delta^{18}O_M^f - \delta^{18}O_M^i)/[\delta^{18}O_W^i - (\delta^{18}O_M^f - \Delta^{18}O_{MW}] \quad (4\text{-}3)$$

where W/M is the water-rock ratio by atoms; $\delta^{18}O_M^i$, $\delta^{18}O_w^i$ and $\delta^{18}O_M^f$ represent the oxygen isotope compositions of the initial melt, water and final rock; and $\Delta^{18}O_{MW}$ is the fractionation coefficient between the melt and water, which can be calculated using the equation of Zhao and Zheng, (2003):

$$1000\ln\alpha = 4.235\times10^6/T^2 - 7.912\times10^3/T + 2.54 \quad (4\text{-}4)$$

where $\Delta^{18}O_{MW} \approx 1000\ln\alpha$. In fact, the water content of XTEJ4 basalt (with the lowest δ^{18}O value) is lower than those of other basalts in the Shuangliao volcanic field, demonstrating that the high temperature water-melt interaction is not the cause for low δ^{18}O values in XTEJ4.

Overall, the oxygen isotopes of the cpx phenocrysts in the Shuangliao basalts represent the heterogeneity of the mantle source, and the variation in oxygen isotope compositions within each sample is most likely caused by magma mixing. In a complex magma plumbing system, cpx phenocrysts may crystallize in different sources with distinct oxygen isotope compositions and then mix during magma ascent. Another candidate is the sustained injection of magmas with different δ^{18}O values during

crystallization, which would explain the positive correlation between $\delta^{18}O$ values and Mg# of cpx in some samples by the sustained injection of magmas. In fact, the $\delta^{18}O$ features of the cpx phenocrysts in the Shuangliao basalts are consistent with the results of other basalts from Taihang Mountains, eastern China (Liu et al., 2015b) and Canary Island basalts (Gurenko et al., 2011).

4.1.2.3 Water content in the "primary" melts

Estimation of water content in "primary" melt

The composition of the melt equilibrated with the earliest phenocrysts should be close to that of the "primary" melt, so if the mantle source is homogeneous, the H_2O content of the "primary" melt of Shuangliao basalts could be estimated from the cpx phenocrysts with the highest Mg# values (Wade et al., 2008; Xia et al., 2013b). Nevertheless, the heterogeneous oxygen isotope compositions of cpx phenocrysts in individual samples of the Shuangliao basalts suggested that these phenocrysts crystallized from different mantle-derived melts, which had distinct oxygen isotope compositions and mixed during magma ascent. The average H_2O content of all the calculated melts from which the cpx phenocrysts crystallized is, therefore, more representative of "primary" magmas. Considering the effect of fractionation, the H_2O content of the Shuangliao "primary" magmas was estimated by averaging only the H_2O content of melt calculated by cpx phenocrysts with Mg#>75. The choice of this value is supported by the fact that simulation shows that compared with the beginning of cpx crystallization from the magma with Mg# 85, the increase of water content in residual magma would be less than 30% when the Mg# of crystallized cpx is higher than 75 (within the measurement uncertainty, 40%; Fig. 4-8). The H_2O content of the Shuangliao "primary" melts was also estimated from the cpx phenocrysts with the highest Mg# values (assuming a homogeneous source) and by averaging the calculated water content of the equilibrated melts from cpx phenocrysts with relatively low Mg# values, testing two sets of data: Mg# >70 and Mg# >75 (assuming a heterogeneous source and that these high Mg# cpx represent earliest phenocrysts from distinct melts). As shown in Figure 4-9, the average H_2O contents of "primary" melts estimated from the two methods are identical within 30% deviations, similar to the measurement uncertainties. Thus, considering the effect of fractionation and magma mixing, the

averaged water content in melts calculated by cpx phenocrysts with Mg#>75 could represent the H_2O content in the "primary" magmas when 40% uncertainty is considered.

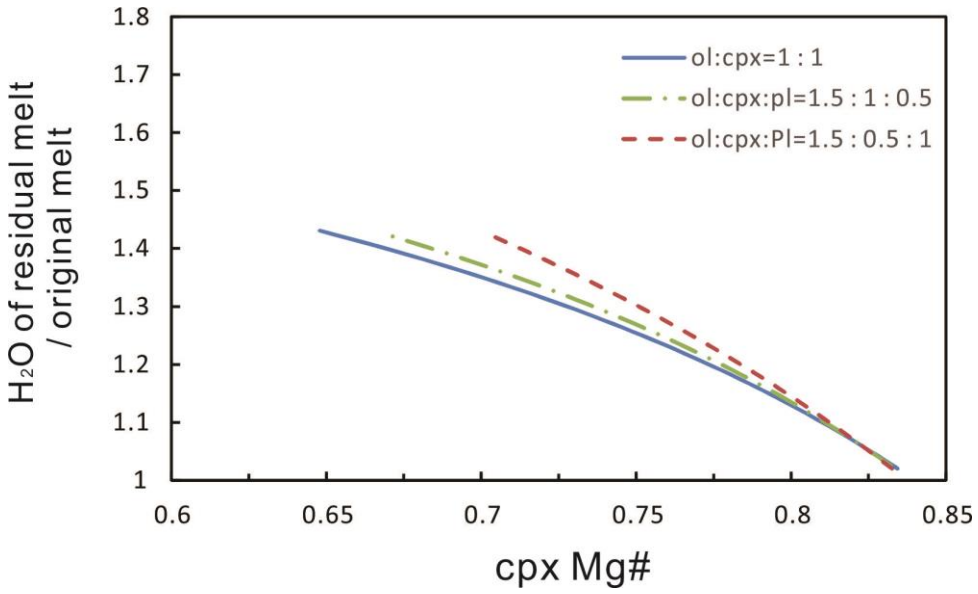

Figure 4-8. Evolution of water content in melt during crystallization of different mineral assemblage vs cpx Mg#. The major element composition of BBT8 was used as the composition of original melt. Assuming that ol, cpx and pl (plagioclase) crystallize at the same time, but have different crystallization ratio. The mineral/melt partition coefficients of water for ol and pl are 0.0002 and 0.004 (Hauri et al., 2006; Johnson et al., 2006) respectively, and 0.02 (average of partition coefficients for BBT8, calculated by equation 10 in O'Leary et al. (2010) for cpx. Kd for ol and cpx are 0.33 and 0.36 respectively (Roeder and Emslie, 1997). The water content of residual melt has been normalized to the original magma water content.

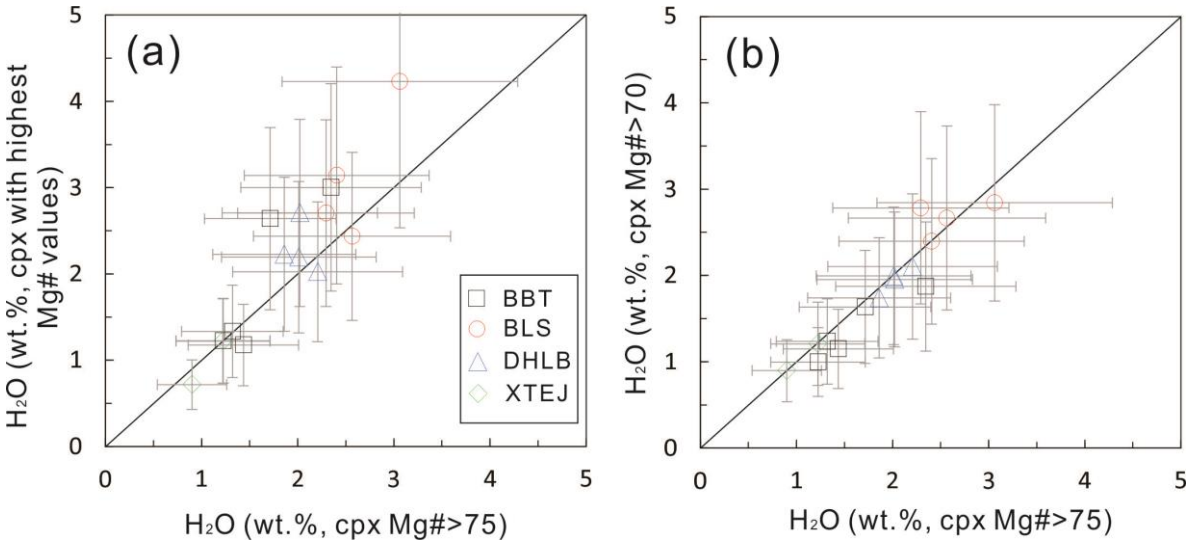

Figure 4-9. Comparison of the H_2O contents of melt calculated from average value of cpx phenocrysts with Mg# > 75 with a) highest Mg#; b) with Mg# > 70. The error bar is 40%. The average H_2O contents of melt obtained by different statistical methods agree within 40%, similar to the measurement uncertainties.

Preservation of water content

The H_2O contents of cpx phenocrysts is mainly affected by degassing during magma ascent coupled with diffusion of H in cpx and crustal contamination.

A great deal of experimental studies on the solubility of water have revealed that alkaline basaltic melts can contain 1 wt.% of H_2O at 0.15 kbar to 12 wt.% at 5 kbar (Botcharnikov et al., 2005; Behrens et al., 2009; Lesne et al., 2011). Whereas the pressure under which Ti-riched pyroxenes will crystallize in alkaline basalts is usually between 5 to 10 kbar (Duda and Schmincke, 1985), even the highest H_2O content in the Shuangliao melts is far below saturation at corresponding pressures. Meanwhile, the Shuangliao basalts are massive without gas bubbles, suggesting no obvious late-stage degassing process.

As mentioned before, H_2O contents on profiles of some large cpx grains have been analysed and no detectable H_2O content variation on profiles of these large cpx grains was found from the core to the rim (Fig. 4-4), demonstrating no measurable H diffusion in cpx. Crustal contamination has been discussed in detail and ruled out in Section 4.1.2.1. In addition, the calculated water contents of magmas display positive correlations with major and trace elements (e.g., K, Rb) (Fig. 4-10), which suggest that

the influence of magma degassing and H diffusion in cpx phenocrysts is negligible and the calculated water content is representive of the primary source. In summary, the H_2O content has been well preserved and the H_2O content plus the H_2O/Ce ratio of the samples can be used to estimate the values of the magma source (Dixon et al., 2002).

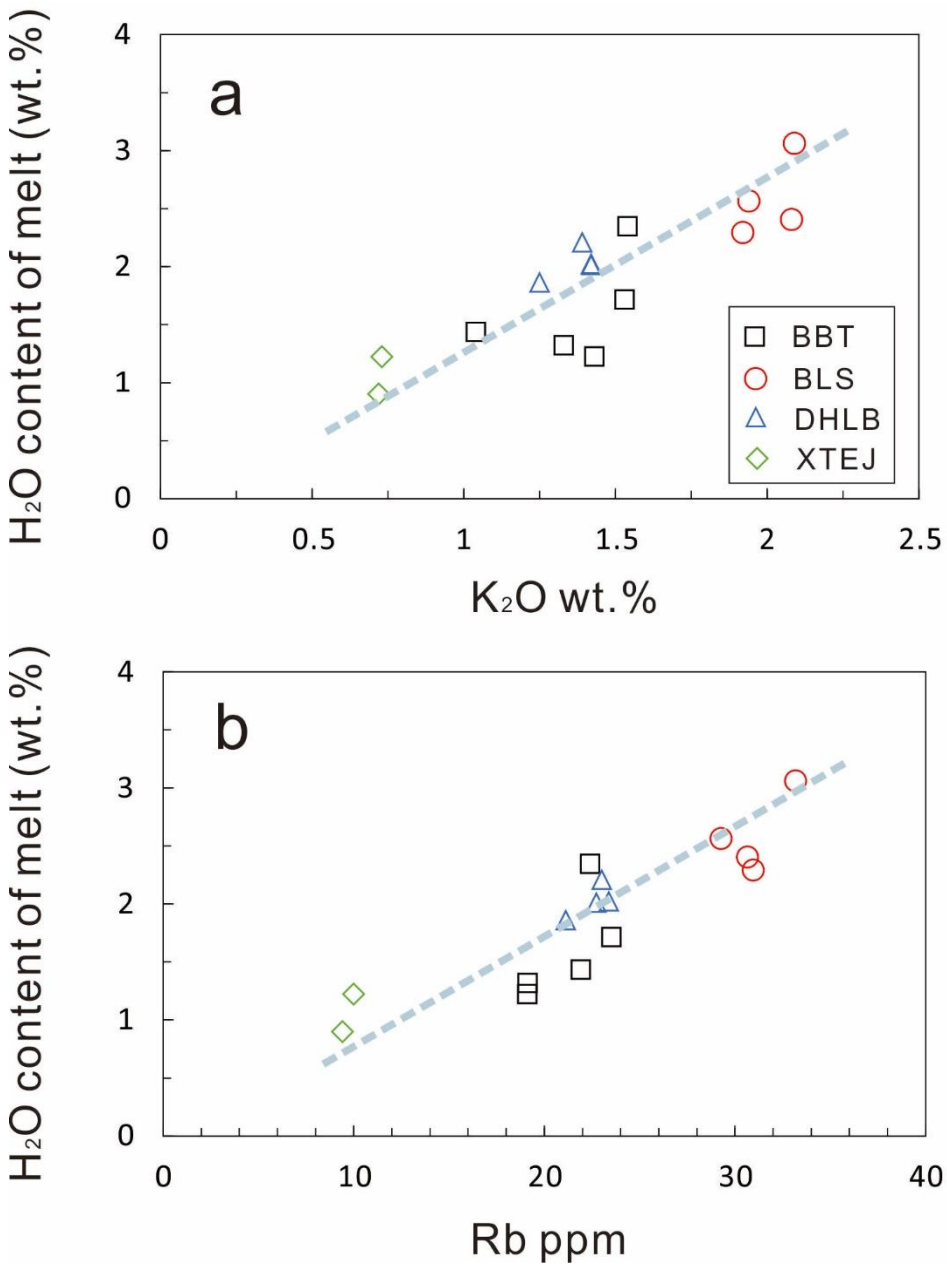

Figure 4-10. The calculated water contents of magmas in the Shuangliao basalts compared with (a) K_2O, (b) Rb concentrations of bulk rocks.

The calculated average H_2O content of the Shuangliao "primary" basalts vary from 0.90 to 3.06 wt.% (Fig. 4-11), falling in the range of back-arc basin basalts (BABBs, 0.2-2.0 wt%, Danyushevsky et al., 1993; Hochstaedter et al., 1990; Stolper and Newmann, 1994) and island arc basalts (IABs, 2.0-8.0 wt%, Dobson et al., 1995; Sisson and Layne, 1993; Wallace, 2005), but are significantly higher than the value of MORBs (0.1-0.3 wt%, Asimow et al., 2004; Danyushevsky et al., 1993, 2000; Dixon, 1988; Michael, 1988, 1995; Sobolev and Chaussidon, 1996; Saal et al., 2002; Simons et al., 2002) and OIBs (0.3-1.0 wt%, Dixon et al., 1997, 2002; Dixon and Clague, 2001; Nichols et al., 2002; Simons et al., 2002; Wallace, 1998).

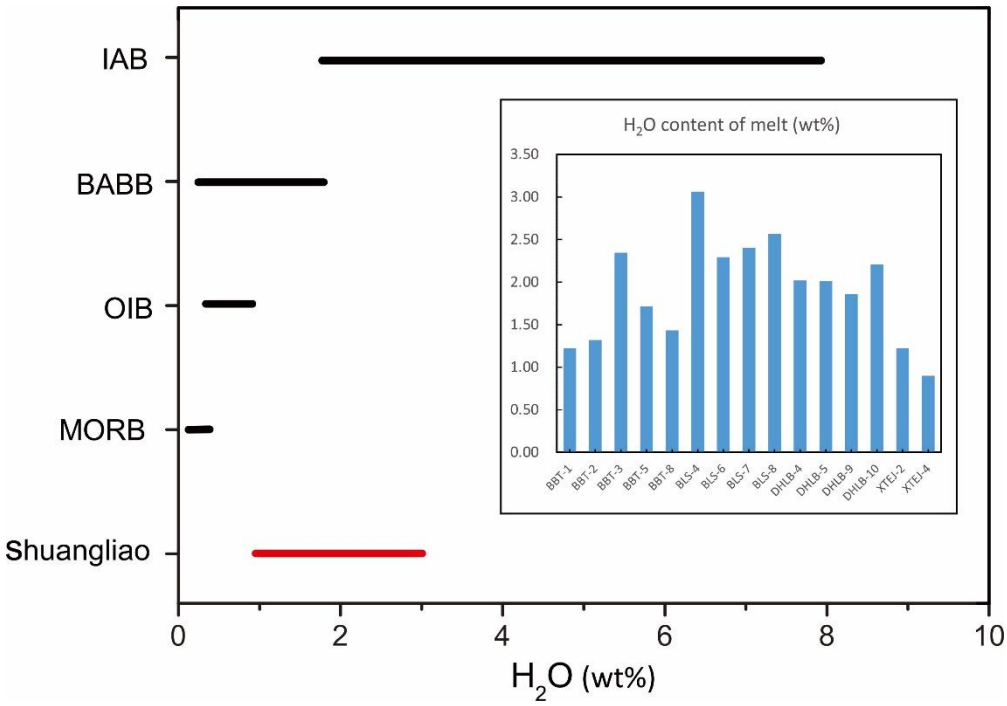

Figure 4-11. Calculated average H_2O content of Shuangliao "primary" melts. The ranges of H_2O content for OIBs, MORBs, BABBs and IABs are from Dixon et al. (2004) and the references therein.

4.1.2.4 Implication for the enriched components in the mantle source

Xu et al. (2012) conducted detailed geochemical studies including major and trace element concentrations, Sr-Nd-Pb isotopes on these basalts. They found that the Shuangliao basalts are characterized by high Fe_2O_3, HIMU (high $^{238}U/^{204}Pb)_{t=0}$) -type trace element pattern and Sr-Nd isotope composition. Based on relatively low $^{206}Pb/^{204}Pb$ ratios (18.13-18.34) than typical HIMU (high $(^{238}U/^{204}Pb)_{t=0}$) OIBs, they

proposed that recycled young oceanic slab component may have been involved in the mantle source.

In Fig 4-12, negative correlations can be observed between the $\delta^{18}O$ values of cpx phenocrysts and Eu anomalies (Eu/Eu*), Sr anomalies (Sr/Sr*) of whole rocks for Shuangliao basalts. Because the Eu and Sr anomalies are typically associated with plagioclase (pl) (Ching-ho et al., 1974; Drake and Weill, 1975) which is rare in the Shuangliao basalts (Xu et al., 2012); feldspars contribution, with the low $\delta^{18}O$ values, should have been present in the mantle source of the basalts. This is consistent with the characteristics of a high temperature hydrothermally altered lower gabbroic oceanic crust (Bach et al., 2001; Gao et al., 2006; Gregory and Taylor, 1981; Hoffman SE et al., 1986). In addition, the basalts with high $\delta^{18}O$ values have no Eu anomaly and relatively weak Sr anomaly which reflect contribution from an upper oceanic crust which has been affected by low temperature hydrothermal alteration (Gao et al., 2006; Gregory and Taylor, 1981; Hoffman SE et al., 1986; Kelley et al., 2003). Therefore, the negative correlations between $\delta^{18}O$ values of cpx phenocrysts and Eu, Sr anomalies correspond to the whole section of the oceanic crust, providing a clear evidence that a whole recycled oceanic crust is involved in the mantle source of these continental intraplate basalts.

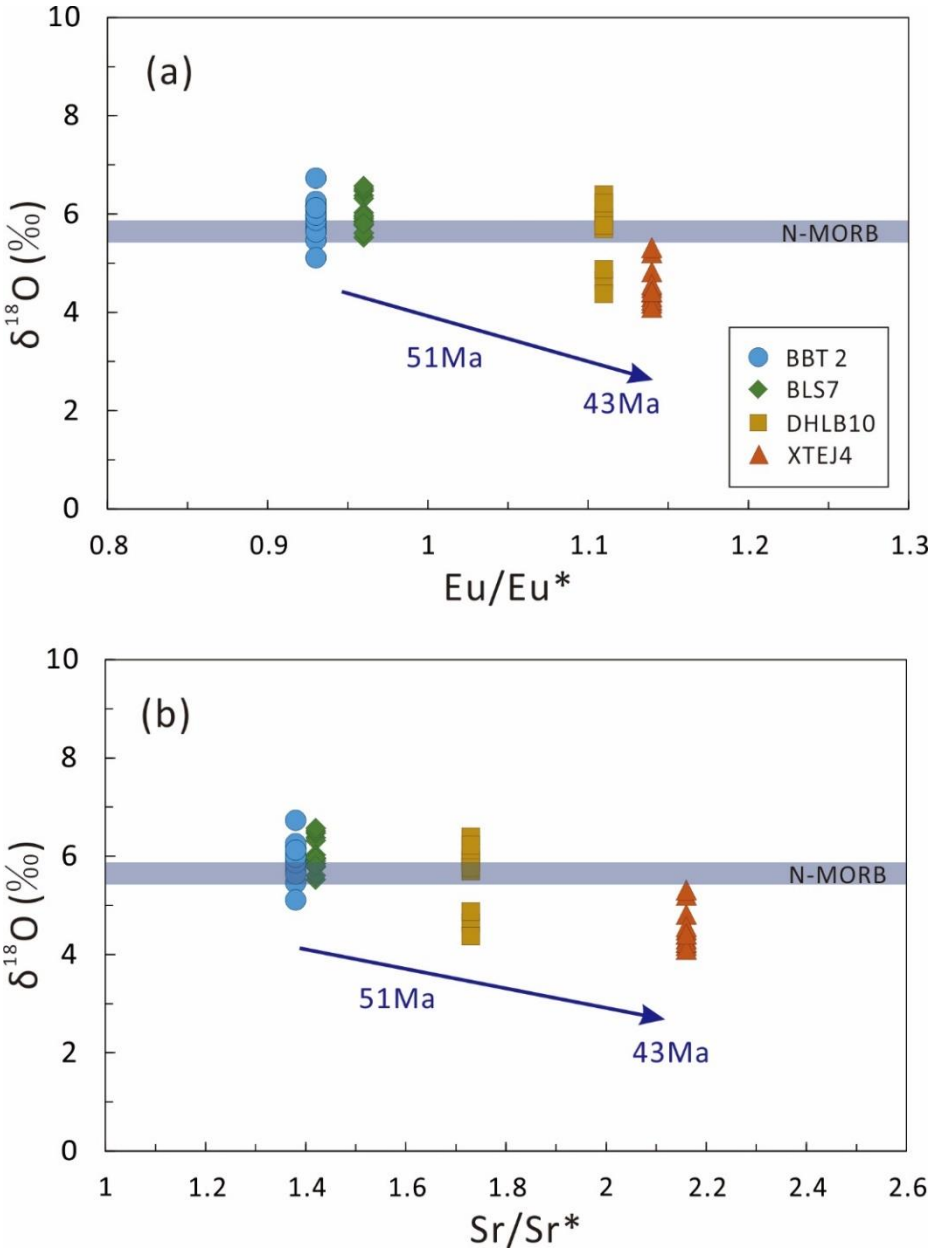

Figure 4-12. Comparison of the range of $\delta^{18}O$ values in cpx phenocrysts and the trace element ratios (Eu/Eu*, Sr/Sr*) of the Shuangliao basalts.

The H_2O/Ce ratios of the Shuangliao basalts (158-737) display also a positive correlation with (Ba/Th)n and a negative correlation with Ce/Pb (Fig. 4-13), suggesting that the presence of a component in the mantle source represented by XTEJ4 (with high H_2O/Ce, (Ba/Th)n ratios and low Ce/Pb ratios). XTEJ4 is also characterized by significant positive K anomaly. Both of these features are consistent with the contribution of recycled marine sediments (Dixon et al., 2002; Plank and Langmuir, 1998).

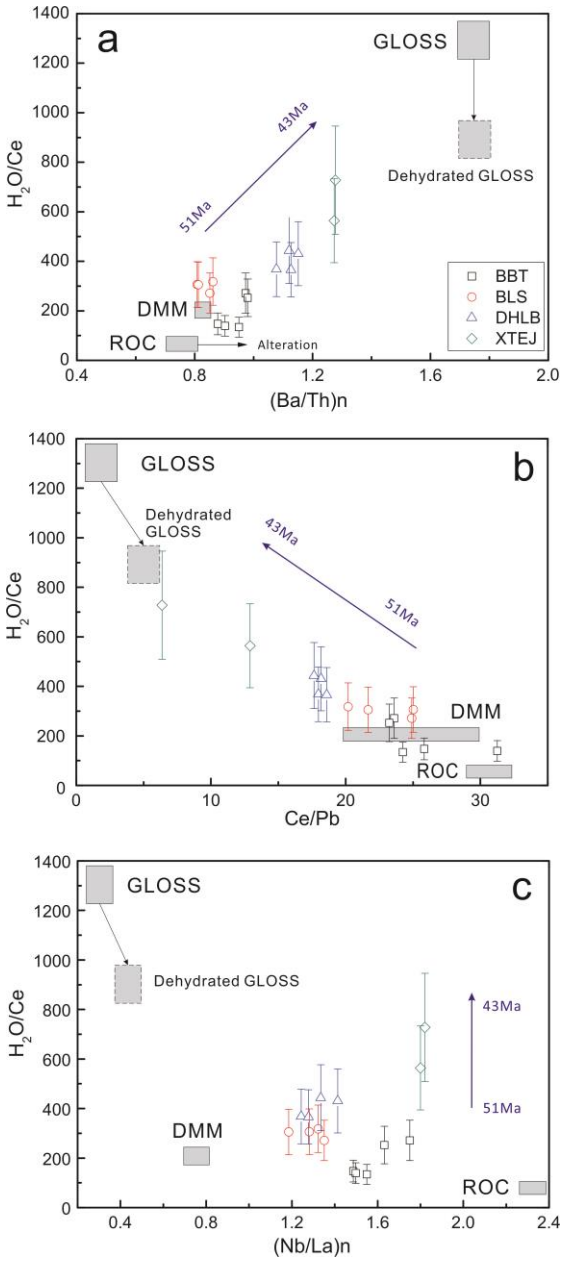

Figure 4-13. Plots of H_2O/Ce vs. (Ba/Th)n, Ce/Pb and (Nb/La)n of the Shuangliao basalts. The gray squares show the possible end members of the mantle source. The H_2O/Ce ratio of GLOSS (~1280), DMM (~200) and ROC (~100) are from Plank and Langmuir (1998); Dixon et al. (2002) and the references therein. The ratios of (Ba/Th)n, Ce/Pb and (Nb/La)n for DMM and GLOSS are from Workman and Hart (2005) and Plank and Langmuir (1998). The (Nb/La)n of ROC are calculated from the concentration of a fresh MORB (5.24 vs 5.21 for Nb and La, Gale et al. (2013)) and the mobility in water (Mobility=$(C_{original}-C_{residual})/C_{original}$*100 %, the water activity of Nb is 20 times the one of La respectively, Kogiso et al., 1997; Kessl et al., 2005). The (Ba/Th)n of ROC would not change much since they have similar fluid mobility, and the Ce/Pb of ROC would increase, due to the high mobility of Pb. The (Nb/La)n and (Ba/Th)n ratios of dehydrated GLOSS would not change because of their similar mobility, and the Ce/Pb ratios of dehydrated GLOSS would increase, due to the high mobility of Pb (Aizawa et al., 1999).

It is worth noting that XTEJ4 has a relatively low $\delta^{18}O$ value (4.10‰-5.32‰) (Table 4-4). However, marine sediments are generally characterized by high $\delta^{18}O$ values. A mass balance calculation was conducted to determine whether there is a sediment component in the mantle source using the equation:

$$\frac{C^i_{melt}}{C^j_{melt}} = (aC^i_{DMM} + bC^i_{LOC} + cC^i_{GLOSS})/(aC^j_{DMM} + bC^j_{LOC} + cC^j_{GLOSS}) \quad (4\text{-}5)$$

where i and j represent the elements involved; C^i_{melt}, C^i_{DMM}, C^i_{LOC} and C^i_{GLOSS} are the concentration of element i in melt, DMM (depleted MORB mantle), LOC (lower oceanic crust) and GLOSS (global subdcting sediments); a, b and c are the proportions of the components (a+b+c=1). The results show that the XTEJ4 basalts with the lowest $\delta^{18}O$ value and highest H_2O/Ce ratio can be the result of the contribution of 72.5% DMM, 26% LOC and 1.5% GLOSS (the element concentrations of DMM, LOC and GLOSS are from Dixon et al. (2002), Plank and Langmuir (1998) and Workman and Hart (2005). This means that the mantle source of the basalts with the low $\delta^{18}O$ values may also contain some fraction of water-rich sediment component. Thus, in addition to recycled oceanic crust, the water-rich sediment component may also contribute to the mantle source of the basalts.

Dixon et al. (2002) proposed that the H_2O/Ce ratio of recycled sediments would be below 100 after highly efficient (>92%) dehydration. However, Shaw et al. (2012) found that the H_2O/Ce ratios of the back-arc basalt glasses from Manus basin, Southwest Pacific ocean, which had been proved to have experienced dehydration during subduction with δD values down to -123‰, are still as high as 500 to 900. As a matter of fact, the dehydration efficiency of recycled sediments during subduction is largely dependent on the geothermal regime, relative cold subducted plate is expected to carry more water into the mantle (Poli and Schmidt 2002, Ohtani. 2005).

In Fig. 4-14 the Shuangliao basalts were compared with the Changbaishan basalts (CBS) for which contribution of recycled sediments (K-hollandite) to the mantle source was proposed by Kuritani et al. (2011). During the subduction, K-hollandite in sediments can be stable within the mantle transitional zone (Rapp et al., 2008). It can release significant amounts of highly incompatible elements through breakdown, which could explain the enrichment of Pb and Ba in the Changbaishan basalts (Kuritani et al., 2011). The Shuangliao and Changbaishan basalts share a same trend on plots of Ba/La vs. Ba/Th, lying on the mixing line between the depleted mantle and recycled sediments

(K-hollandite, Fig. 4-14).

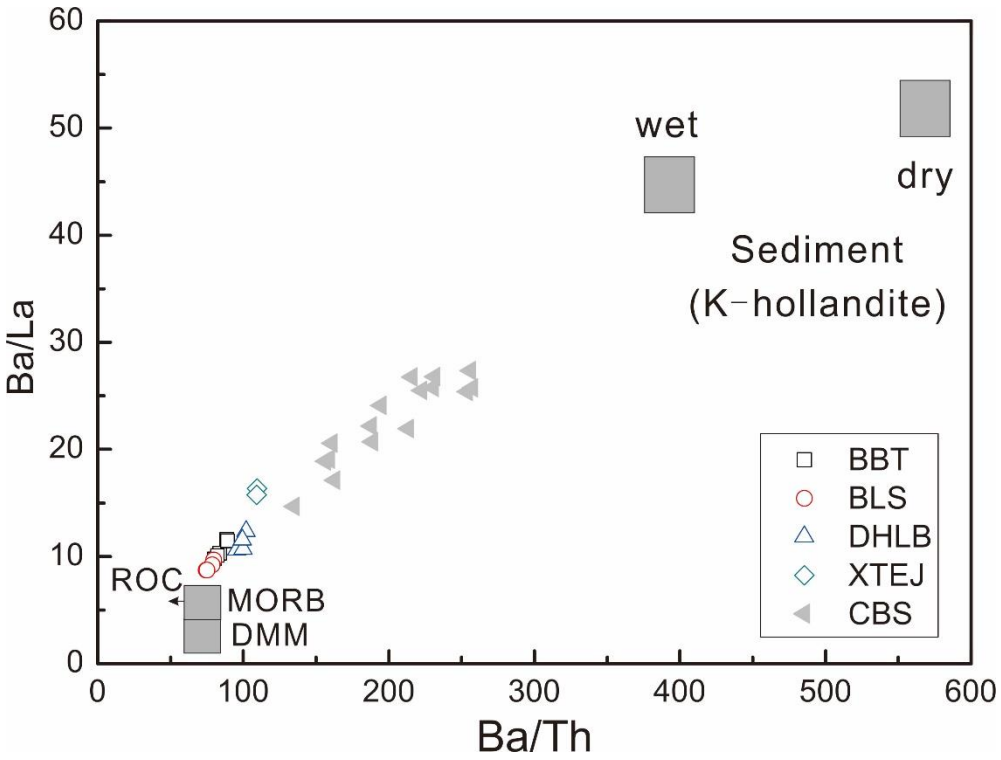

Figure 4-14. Plots of Ba/La vs. Ba/Th ratios of the Shuangliao and Changbaishan basalts. The Changbaishan basalts (CBS) represented by gray triangles are from Kuritani et al. (2009). The Ba/La and Ba/Th ratios of DMM and sediment (K-hollandite) are from Workman and Hart (2005) and Rapp et al. (2008). The trace element ratios of ROC are calculated from their concentration in fresh MORB (Gale et al., 2013), and the mobility in water (Kogiso et al., 1997; Kessl et al., 2005), as proposed in Figure 4-13.

Interestingly, the oxygen isotope compositions, H_2O/Ce ratios and associated trace element ratios of Shuangliao basalts varied significantly with their ages (Figs. 4-12, 4-13), indicating a variation of the recycled oceanic components in the mantle source with time. In combination with the ages of the Shuangliao basalts, the contribution of recycled sediments in the mantle source seems to increase from earlier volcanic events (~51 Ma) to the later (~43 Ma). Considering that the water-rich sediment is more fusible, its addition into the mantle might be a trigger of the melting.

4.1.3 Summary

(1) The H_2O contents of the Shuangliao "primary" basaltic melts vary from 0.90 to 3.06 wt.%, falling in the range of BABBs and IABs and are definitely higher than the value of MORBs and OIBs. The $\delta^{18}O$ values of cpx phenocrysts among different samples vary widely (4.10‰ to 6.73‰), exceeding the value of cpx in typical MORB and mantle peridotites.

(2) The finding that the oxygen isotope variation of cpx in the Shuangliao basalts cover the typical range of oxygen isotope profile of an altered oceanic crust provides a clear evidence that a recycled oceanic slab was involved in the mantle source of these continental basalts.

(3) The significant K positive anomaly and the correlations of H_2O/Ce with (Ba/Th)n and Ce/Pb in the Shuangliao basalts indicate that water-rich sediment component may also have been involved in the mantle source of these basalts.

(4) The relative contribution of the enriched source components in the mantle source has changed with time. More water-rich sediment component is observed in the mantle source of the youngest Shuangliao basalts, which might be the initial trigger for mantle melting.

4.2 Wulanhada basalts

4.2.1 Results

4.2.1.1 Chemical compositions of phenocrysts

The BSE images demonstrate that most of the Wulanhada cpx phenocrysts are euhedral and homogeneous (Fig. 4-15a). The major element contents of cpx phenocrysts are listed in Table 4-5. The cpx are augitic to diopsidic phenocrysts, with Mg# varying from 64.1 to 80.7 and TiO_2 contents ranging from 0.79 to 4.74 wt.%.

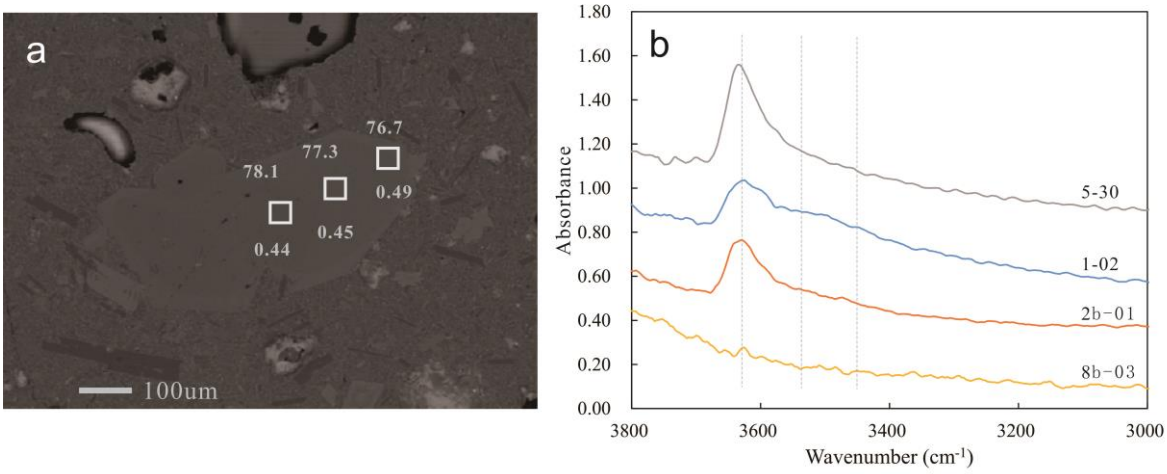

Figure 4-15. a) BSE image of cpx phenocrysts in the Wulanhada basalts, the red squares show the positions of the spots for FTIR analysis. b) Representative OH IR absorption spectra of cpx phenocrysts, dashed lines mark the position of individual OH bands. b) BSE image of cpx phenocrysts in the Wulanhada basalts, the white squares show the positions of the spots for FTIR analysis. The calculated Mg# and H_2O contents are indicated on the image (11NW05-11 listed in Table 4-5).

Table 4-5. Major element compositions of cpx phenocrysts and water contents of cpx phenocrysts and corresponding melts of Wulanhada basalts

		Na_2O	K_2O	SiO_2	Al_2O_3	MgO	CaO	Cr_2O_3	FeO	NiO	MnO	TiO_2	Total	Mg#	$X(^{iv}Al)$	XCa	$D^{cpx/melt}$	$A(cm^{-2})$	t (mm)	H_2O in cpx (wt. ppm)	H_2O in melt (wt. %)
11NW01	1-02	0.63	b.l.d.	46.37	7.93	11.79	21.66	0.06	8.39	b.l.d.	0.14	2.39	99.36	71.47	0.25	0.88	0.032	1.8345	0.066	117.6	0.37
	1-03	0.51	0.01	49.49	5.10	13.34	21.68	0.08	7.79	0.02	0.11	1.65	99.77	75.33	0.15	0.87	0.017	1.6226	0.082	83.7	0.49
	1-03B	0.48	0.01	49.17	5.06	13.13	21.40	0.07	8.27	0.03	0.09	1.92	99.62	73.88	0.16	0.86	0.018	2.1871	0.082	112.9	0.63
	1-04	0.50	b.l.d.	48.65	5.57	12.99	22.18	0.11	7.39	b.l.d.	0.08	1.90	99.36	75.81	0.18	0.89	0.019	1.6179	0.065	105.3	0.55
	1-05	0.76	b.l.d.	45.42	8.55	10.99	20.81	0.01	9.44	0.01	0.14	2.91	99.03	67.49	0.27	0.85	0.038	2.1627	0.065	140.8	0.37
	1-06	0.42	b.l.d.	49.16	4.48	13.50	21.33	b.l.d.	8.06	0.04	0.08	1.89	98.96	74.91	0.15	0.86	0.017	1.7045	0.065	111.0	0.67
	1-07	0.42	0.01	46.93	6.74	12.17	22.40	b.l.d.	8.01	0.03	0.08	2.64	99.42	73.03	0.23	0.91	0.027	1.7788	0.067	112.3	0.42
	1-08	0.39	b.l.d.	48.99	4.93	13.16	22.30	0.03	7.53	b.l.d.	0.05	2.11	99.49	75.70	0.16	0.90	0.018	1.7787	0.113	66.6	0.37
	1-10	0.50	b.l.d.	46.30	7.79	11.86	22.00	0.02	8.15	0.01	0.06	2.79	99.48	72.17	0.25	0.89	0.032	1.5364	0.072	90.3	0.28
	1-12	0.56	0.01	45.76	8.11	11.52	21.88	0.06	8.18	0.02	0.13	2.94	99.16	71.52	0.27	0.89	0.035	1.4459	0.074	82.7	0.24
	1-12B	0.52	b.l.d.	49.79	4.94	13.34	21.68	0.07	7.54	0.07	0.10	1.70	99.75	75.92	0.14	0.87	0.016	1.0874	0.074	56.9	0.35
	1-13	0.60	0.01	47.96	6.80	11.78	21.92	0.10	7.73	0.01	0.10	2.16	99.16	73.11	0.20	0.88	0.022	1.1463	0.066	73.5	0.33
	1-14	0.54	b.l.d.	45.81	8.39	10.76	21.77	0.06	8.47	0.02	0.10	3.29	99.22	69.37	0.27	0.88	0.035	1.1457	0.066	73.5	0.21
	1-15	0.64	b.l.d.	42.87	10.42	9.60	21.39	b.l.d.	9.61	b.l.d.	0.12	4.74	99.40	64.05	0.36	0.87	0.067	1.4357	0.064	94.9	0.14
	1-16	0.52	0.01	47.25	5.92	12.40	21.55	0.05	8.80	b.l.d.	0.07	2.35	98.91	71.53	0.21	0.88	0.024	0.8437	0.072	49.6	0.21
	1-16B	0.67	b.l.d.	46.48	8.04	11.78	21.85	0.06	8.21	0.01	0.10	2.61	99.81	71.91	0.25	0.88	0.033	1.0001	0.072	58.8	0.18
	1-18	0.53	b.l.d.	49.08	4.92	13.28	21.75	0.07	7.90	0.09	0.17	1.74	99.51	74.99	0.16	0.87	0.018	0.9297	0.072	54.6	0.31
	1-19	0.62	b.l.d.	46.45	7.56	11.64	21.71	0.10	8.09	b.l.d.	0.09	2.46	98.73	71.94	0.24	0.88	0.029	1.4917	0.064	98.6	0.34
	1-20	0.46	b.l.d.	50.45	4.53	13.28	21.00	0.04	7.82	0.06	0.13	1.41	99.17	75.17	0.11	0.84	0.014	1.6047	0.074	91.8	0.68
	1-22	0.53	b.l.d.	45.83	8.18	11.31	21.56	0.03	8.43	0.04	0.08	3.20	99.19	70.51	0.27	0.87	0.035	1.5045	0.074	86.0	0.24
11NW02	2-01	0.55	b.l.d.	46.78	7.09	12.25	21.59	0.07	8.59	0.03	0.09	2.50	99.54	71.76	0.24	0.87	0.029	1.0872	0.097	47.4	0.16
	2-02	0.53	b.l.d.	48.41	5.28	12.61	21.67	0.02	8.85	b.l.d.	0.17	2.00	99.55	71.75	0.18	0.87	0.020	0.47	0.097	20.5	0.10
	2-02B	0.53	b.l.d.	47.61	6.70	12.58	21.15	0.11	8.39	0.01	0.12	1.91	99.11	72.76	0.20	0.85	0.024	0.6381	0.097	27.8	0.12
	2-03	0.47	0.01	47.27	7.44	11.90	21.78	0.14	8.69	0.03	0.10	2.32	100.14	70.94	0.23	0.87	0.028	1.4939	0.096	65.8	0.24
	2-04	0.55	b.l.d.	48.14	6.93	11.74	21.89	0.11	8.12	0.02	0.15	2.37	100.00	72.05	0.20	0.88	0.023	0.5892	0.095	26.2	0.11
	2-04B	0.45	0.02	49.45	4.33	13.80	21.35	0.09	8.00	0.04	0.12	1.45	99.11	75.45	0.14	0.86	0.016	0.5696	0.095	25.4	0.16
	2-05	0.35	0.01	50.89	3.71	13.74	21.35	0.13	7.44	b.l.d.	0.10	1.36	99.08	76.70	0.10	0.85	0.012	0.5792	0.099	24.8	0.20
	2-08	0.51	b.l.d.	49.44	5.58	13.43	21.43	0.14	7.90	0.04	0.12	1.55	100.15	75.18	0.16	0.85	0.018	1.2996	0.082	67.1	0.36
	2B-01	0.53	0.01	49.41	4.59	13.75	21.48	0.05	7.78	b.l.d.	0.11	1.46	99.17	75.90	0.15	0.86	0.016	2.774	0.123	95.4	0.59

Table 4-5. (continued)

		Na_2O	K_2O	SiO_2	Al_2O_3	MgO	CaO	Cr_2O_3	FeO	NiO	MnO	TiO_2	Total	Mg#	X(^{iv}Al)	XCa	$D^{cpx/melt}$	A(cm^{-2})	t (mm)	H_2O in cpx (wt. ppm)	H_2O in melt (wt. %)
11NW02	2B-02	0.71	b.l.d.	48.20	7.23	12.95	21.13	0.14	7.65	0.04	0.10	1.94	100.08	75.10	0.21	0.84	0.025	2.628	0.123	90.4	0.36
	2B-03	0.65	0.02	48.48	6.29	13.11	21.50	0.39	7.30	0.01	0.11	1.63	99.48	76.21	0.19	0.86	0.021	1.107	0.128	36.6	0.17
	2B-03B	0.61	b.l.d.	46.87	6.93	12.68	21.93	0.25	7.82	0.01	0.11	2.03	99.23	74.30	0.23	0.89	0.028	1.295	0.128	42.8	0.15
	2B-04B	0.66	b.l.d.	45.38	8.29	11.46	21.41	0.14	8.67	0.03	0.13	2.82	98.99	70.21	0.28	0.87	0.038	1.443	0.118	51.7	0.14
	2B-05	0.71	0.01	45.24	8.14	11.40	21.74	0.04	9.39	b.l.d.	0.09	3.16	99.92	68.40	0.29	0.88	0.040	1.1038	0.104	44.9	0.11
	2B-06	0.59	0.03	46.90	6.81	12.26	22.32	0.15	8.27	b.l.d.	0.07	2.55	99.93	72.54	0.24	0.90	0.028	0.9173	0.103	37.7	0.13
	2B-07B	0.54	b.l.d.	46.86	7.00	12.23	21.98	0.13	8.21	b.l.d.	0.10	2.33	99.38	72.66	0.23	0.89	0.028	1.028	0.114	38.2	0.14
	2B-08	0.55	b.l.d.	47.42	6.81	12.34	22.41	0.12	8.30	0.03	0.08	2.00	100.06	72.60	0.22	0.90	0.026	0.581	0.114	21.6	0.08
	2B-10	0.65	0.03	45.48	8.39	11.76	21.29	0.17	8.59	0.04	0.13	2.69	99.20	70.94	0.28	0.86	0.038	1.7036	0.13	55.4	0.15
	2B-11	0.57	b.l.d.	49.61	4.49	13.64	21.64	0.13	7.89	0.06	0.11	1.38	99.51	75.50	0.14	0.87	0.016	0.782	0.137	24.2	0.15
11NW04	4-01	0.66	b.l.d.	46.43	7.26	12.14	21.61	0.09	8.47	0.03	0.09	2.32	99.10	71.87	0.24	0.88	0.030	1.3056	0.051	108.3	0.36
	4-02	0.53	b.l.d.	47.02	7.05	12.07	21.85	0.11	8.42	0.01	0.11	2.35	99.51	71.87	0.23	0.88	0.027	1.7994	0.056	136.0	0.50
	4-02B	0.61	b.l.d.	46.90	7.28	12.10	21.81	0.12	8.49	0.10	0.15	2.18	99.74	71.76	0.23	0.88	0.029	2.013	0.056	152.1	0.53
	4-03	0.54	b.l.d.	50.02	4.42	12.68	21.96	b.l.d.	8.20	b.l.d.	0.08	1.53	99.44	73.38	0.12	0.88	0.014	1.5046	0.065	97.9	0.70
	4-04	0.51	b.l.d.	49.91	4.09	13.89	21.21	0.09	8.02	0.02	0.15	1.27	99.18	75.53	0.13	0.85	0.015	0.9185	0.06	64.8	0.44
	4-05	0.46	b.l.d.	48.79	4.82	13.84	21.55	0.08	7.97	0.04	0.16	1.53	99.25	75.59	0.16	0.87	0.018	0.9614	0.06	67.8	0.37
	4-06	0.55	0.01	47.34	6.78	12.42	21.92	0.12	8.07	0.06	0.11	2.32	99.71	73.28	0.22	0.88	0.026	1.8498	0.06	130.5	0.50
	4-07	0.51	b.l.d.	49.89	4.32	13.59	21.92	0.06	7.85	0.06	0.12	1.38	99.67	75.54	0.13	0.88	0.015	1.253	0.06	88.4	0.59
	4-08	0.65	b.l.d.	47.07	6.81	12.48	21.99	0.15	8.17	0.01	0.08	1.94	99.35	73.13	0.22	0.89	0.026	1.9719	0.06	139.1	0.53
	4-09	0.65	0.01	47.09	7.16	12.30	21.89	0.11	8.09	b.l.d.	0.09	2.14	99.53	73.05	0.23	0.88	0.027	1.8649	0.06	131.5	0.48
	4-10	0.58	b.l.d.	50.20	4.38	13.86	21.50	0.06	7.73	b.l.d.	0.11	1.33	99.75	76.17	0.13	0.86	0.015	1.0837	0.047	97.6	0.66
	4-11	0.54	0.01	49.80	4.20	13.74	20.92	1.34	7.60	b.l.d.	0.08	1.36	99.57	76.34	0.14	0.84	0.016	1.582	0.062	108.0	0.68
	4-12	0.59	b.l.d.	50.12	4.00	13.66	20.93	0.04	8.60	0.05	0.22	1.25	99.46	73.91	0.12	0.84	0.014	2.1068	0.062	143.8	1.01
	4-13	0.58	b.l.d.	47.25	7.30	12.28	21.80	0.10	8.25	0.04	0.07	2.25	99.91	72.64	0.23	0.88	0.028	2.2301	0.062	152.2	0.55
	4-14	0.56	b.l.d.	48.20	5.87	12.56	21.08	0.02	9.14	b.l.d.	0.14	2.03	99.60	71.00	0.19	0.85	0.022	1.9775	0.062	135.0	0.63
	4-15	0.62	0.01	50.22	4.85	13.88	21.40	0.11	7.50	0.06	0.16	1.33	100.15	76.74	0.14	0.85	0.016	1.8754	0.06	132.3	0.84
	4-16	0.57	b.l.d.	50.06	5.04	13.16	21.64	0.02	8.13	b.l.d.	0.14	1.69	100.45	74.28	0.14	0.86	0.016	1.6619	0.06	117.2	0.72
	4-17	0.52	b.l.d.	49.36	5.01	13.24	21.63	0.08	7.60	0.03	0.16	1.55	99.19	75.64	0.15	0.87	0.016	1.9461	0.063	130.7	0.79

Table 4-5. (continued)

		Na_2O	K_2O	SiO_2	Al_2O_3	MgO	CaO	Cr_2O_3	FeO	NiO	MnO	TiO_2	Total	Mg#	X(^{iv}Al)	XCa	$D^{cpx/melt}$	A(cm^{-2})	t (mm)	H_2O in cpx (wt. ppm)	H_2O in melt (wt. %)
	5-04	0.47	b.l.d.	51.26	3.64	14.16	22.31	0.35	6.03	0.01	0.13	1.29	99.65	80.71	0.10	0.89	0.012	1.069	0.058	78.0	0.65
	5-05	0.43	b.l.d.	49.03	5.90	13.01	22.70	0.47	6.75	b.l.d.	0.08	2.11	100.50	77.45	0.18	0.90	0.020	0.9211	0.058	67.2	0.33
	5-06	0.47	b.l.d.	50.55	5.21	13.72	22.43	0.53	6.01	0.03	0.10	1.42	100.47	80.28	0.14	0.88	0.016	0.6967	0.054	54.6	0.35
	5-07	0.45	b.l.d.	51.03	3.94	13.77	22.63	0.18	6.56	b.l.d.	0.08	1.46	100.10	78.91	0.11	0.90	0.013	1.2159	0.062	83.0	0.65
	5-08	0.57	b.l.d.	46.71	7.41	12.15	22.55	0.37	7.50	0.06	0.10	2.86	100.28	74.28	0.25	0.90	0.032	1.1771	0.062	80.3	0.25
	5-08B	0.46	b.l.d.	50.62	4.09	13.73	22.63	0.18	6.55	b.l.d.	0.13	1.57	99.94	78.90	0.12	0.90	0.014	0.8535	0.062	58.2	0.43
	5-10	0.40	b.l.d.	50.69	3.72	14.31	22.54	0.36	6.15	b.l.d.	0.15	1.35	99.67	80.59	0.12	0.90	0.013	1.5683	0.056	118.5	0.90
	5-11	0.52	b.l.d.	47.64	6.54	12.43	22.43	0.56	6.51	0.04	0.09	2.20	98.97	77.29	0.21	0.90	0.023	1.385	0.056	104.6	0.45
	5-11C	0.50	b.l.d.	48.39	5.72	12.95	22.46	0.63	6.48	0.03	0.09	1.76	99.02	78.08	0.18	0.90	0.020	1.1472	0.056	86.7	0.44
	5-11R	0.50	0.01	48.52	5.80	12.56	22.69	0.54	6.79	0.01	0.08	2.26	99.76	76.72	0.19	0.91	0.020	1.334	0.056	100.8	0.49
	5-12	0.48	b.l.d.	49.99	3.65	13.10	22.11	b.l.d.	7.92	0.01	0.16	1.53	98.98	74.67	0.12	0.89	0.013	0.7801	0.059	55.9	0.43
	5-14	0.38	b.l.d.	51.49	3.84	14.19	22.41	0.27	6.32	0.04	0.12	1.08	100.15	80.01	0.10	0.89	0.012	1.3512	0.058	98.6	0.83
	5-16	0.55	b.l.d.	47.18	6.85	12.44	22.11	0.45	6.92	0.02	0.10	2.42	99.04	76.21	0.22	0.89	0.026	1.2177	0.058	88.8	0.34
11NW05	5-17	0.42	b.l.d.	50.74	3.63	14.33	22.39	0.34	6.30	b.l.d.	0.11	1.38	99.65	80.21	0.11	0.89	0.013	1.7177	0.058	125.3	0.97
	5-18	0.44	0.01	49.00	4.57	13.17	21.88	0.02	8.10	b.l.d.	0.14	1.87	99.19	74.36	0.15	0.88	0.017	1.122	0.053	89.6	0.53
	5-21	0.62	0.01	44.92	8.57	10.96	21.78	0.01	8.68	b.l.d.	0.10	3.61	99.26	69.25	0.29	0.89	0.042	1.3742	0.053	109.7	0.26
	5-22	0.41	b.l.d.	48.52	5.69	13.05	22.33	0.53	6.45	0.02	0.05	1.99	99.05	78.29	0.18	0.90	0.020	1.2954	0.051	107.5	0.55
	5-23	0.43	0.01	49.44	5.00	13.37	22.57	0.42	6.50	b.l.d.	0.13	1.90	99.76	78.58	0.16	0.90	0.017	1.3578	0.051	112.7	0.66
	5-27	0.45	b.l.d.	50.81	3.81	13.98	22.42	0.20	6.46	0.06	0.06	1.40	99.64	79.42	0.11	0.89	0.013	2.6012	0.115	95.7	0.75
	5-28	0.46	0.01	50.00	4.52	13.54	21.99	0.07	7.25	b.l.d.	0.09	1.77	99.69	76.90	0.14	0.88	0.015	4.371	0.115	160.8	1.06
	5-29	0.45	b.l.d.	49.51	4.34	13.57	22.41	0.13	6.88	0.03	0.09	1.73	99.12	77.87	0.14	0.90	0.015	3.0819	0.113	115.4	0.75
	5-30	0.51	b.l.d.	48.58	6.17	12.74	22.75	0.50	6.71	0.06	0.06	2.21	100.30	77.20	0.20	0.91	0.022	4.088	0.102	169.6	0.78
	5-31	0.45	0.03	50.38	4.25	13.70	22.39	0.40	6.35	0.05	0.06	1.48	99.54	79.35	0.13	0.89	0.014	1.1923	0.095	53.1	0.38
	5-31B	0.44	0.01	50.68	3.74	14.10	22.31	0.31	6.24	0.03	0.12	1.11	99.09	80.11	0.11	0.89	0.012	1.2592	0.095	56.1	0.45
	5-32	0.29	0.01	50.97	3.59	14.13	22.24	0.15	7.01	b.l.d.	0.12	1.74	100.24	78.24	0.11	0.88	0.013	1.1108	0.095	49.5	0.38
	5-33	0.40	0.01	51.08	3.79	14.06	22.43	0.39	6.27	0.06	0.07	1.29	99.85	79.99	0.11	0.89	0.012	1.2565	0.095	56.0	0.45
	5-35	0.52	b.l.d.	48.04	6.31	12.00	22.14	b.l.d.	8.65	b.l.d.	0.12	2.32	100.10	71.20	0.20	0.89	0.023	1.0464	0.068	65.1	0.29

Table 4-5. (continued)

		Na_2O	K_2O	SiO_2	Al_2O_3	MgO	CaO	Cr_2O_3	FeO	NiO	MnO	TiO_2	Total	Mg#	X(^{iv}Al)	XCa	$D^{cpx/melt}$	A(cm^{-2})	t (mm)	H_2O in cpx (wt. ppm)	H_2O in melt (wt. %)
11NW06	6-01	0.54	0.01	48.71	5.57	13.49	21.88	0.77	6.42	0.05	0.09	1.48	99.00	78.92	0.17	0.88	0.019	0.4702	0.067	29.7	0.16
	6-02	0.52	b.l.d.	48.08	6.08	13.06	22.16	0.61	6.94	0.04	0.08	1.84	99.40	77.03	0.20	0.89	0.022	0.6395	0.072	37.6	0.17
	6-03	0.53	b.l.d.	48.99	5.34	13.84	22.07	0.68	6.72	b.l.d.	0.05	1.48	99.70	78.58	0.17	0.88	0.019	1.1624	0.062	79.3	0.41
	6-04	0.44	b.l.d.	50.72	3.41	14.48	21.89	0.38	6.87	0.05	0.05	1.08	99.40	78.98	0.11	0.87	0.013	1.2822	0.062	87.5	0.69
	6-05	0.45	b.l.d.	50.37	3.77	14.90	21.72	0.55	6.40	b.l.d.	0.13	0.79	99.08	80.59	0.12	0.87	0.014	1.1817	0.062	80.6	0.59
	6-06	0.39	b.l.d.	51.48	3.26	14.44	21.88	0.37	6.76	0.01	0.09	0.79	99.46	79.19	0.09	0.87	0.011	1.3246	0.062	90.4	0.82
	6-09	0.45	b.l.d.	50.67	3.55	14.65	21.47	0.37	7.01	0.07	0.11	1.08	99.42	78.83	0.11	0.86	0.013	1.4014	0.062	95.6	0.73
	6-11	0.46	b.l.d.	50.43	3.96	14.46	21.58	0.45	6.87	b.l.d.	0.11	1.06	99.36	78.97	0.12	0.86	0.014	1.1604	0.063	77.9	0.57
	6-12	0.55	b.l.d.	51.03	4.40	14.91	21.08	0.19	6.99	b.l.d.	0.12	1.20	100.46	79.19	0.12	0.83	0.015	1.1596	0.063	77.9	0.53
	6-13	0.52	b.l.d.	48.62	5.94	13.32	21.61	0.59	7.12	b.l.d.	0.13	1.57	99.43	76.94	0.18	0.87	0.020	1.3357	0.063	89.7	0.44
	6-14	0.39	0.01	50.35	3.51	14.43	21.73	0.36	7.17	0.01	0.14	1.05	99.15	78.21	0.11	0.87	0.013	0.8522	0.063	57.2	0.43
	6-15	0.51	0.01	48.26	6.09	13.19	21.80	0.58	7.70	0.02	0.15	1.93	100.25	75.33	0.20	0.87	0.023	1.2232	0.061	84.8	0.37
	6-17	0.42	0.01	51.53	3.37	14.83	21.91	0.62	6.55	0.01	0.13	0.86	100.24	80.13	0.10	0.87	0.012	0.7693	0.061	53.4	0.44
	6-19	0.50	0.01	48.90	5.92	13.15	21.76	0.56	7.00	0.11	0.16	1.61	99.66	77.01	0.18	0.87	0.020	0.9246	0.058	67.5	0.34
	6B-05	0.47	0.01	49.69	5.86	13.08	21.50	0.73	7.28	0.01	0.14	1.58	100.33	76.20	0.16	0.85	0.018	0.7065	0.1	29.9	0.16
	6B-06	0.47	b.l.d.	48.49	6.03	13.28	21.69	0.65	7.17	b.l.d.	0.10	1.55	99.42	76.75	0.18	0.87	0.021	1.6118	0.097	70.3	0.34
	6B-06B	0.48	b.l.d.	48.63	5.90	13.34	21.53	0.61	7.28	0.07	0.05	1.49	99.36	76.55	0.18	0.86	0.020	1.4034	0.097	61.2	0.30
	6B-08	0.43	b.l.d.	49.10	5.38	13.48	21.34	0.74	6.94	b.l.d.	0.15	1.58	99.13	77.61	0.16	0.86	0.018	0.4309	0.098	18.6	0.10
	6B-10	0.44	b.l.d.	51.52	3.75	14.22	21.56	0.50	6.45	0.03	0.14	0.99	99.59	79.73	0.09	0.86	0.012	0.2261	0.083	11.5	0.10
	6B-11	0.39	b.l.d.	52.02	3.29	14.60	21.71	0.64	6.48	0.05	0.13	0.99	100.30	80.08	0.09	0.86	0.011	0.5378	0.084	27.1	0.24
11NW09	9-01	0.49	0.01	47.25	6.99	12.05	21.39	0.07	8.77	b.l.d.	0.14	2.60	99.75	71.02	0.22	0.86	0.027	1.535	0.095	68.4	0.25
	9-03	0.36	b.l.d.	48.91	4.84	13.62	21.94	0.12	7.53	b.l.d.	0.12	1.51	98.95	76.34	0.16	0.89	0.017	0.5115	0.092	23.5	0.14
	9-03B	0.52	b.l.d.	48.61	5.82	12.76	21.35	0.06	8.09	b.l.d.	0.11	2.06	99.39	73.78	0.18	0.86	0.020	0.757	0.092	34.8	0.17
	9-04	0.45	0.01	47.98	5.77	12.54	21.89	0.07	8.29	b.l.d.	0.10	2.00	99.10	72.94	0.19	0.89	0.021	1.0896	0.092	50.1	0.24
	9-05	0.47	b.l.d.	47.39	6.50	12.16	21.71	0.01	8.24	0.02	0.17	2.44	99.09	72.47	0.21	0.88	0.024	1.4023	0.095	62.5	0.26
	9-06	0.51	b.l.d.	47.04	6.55	12.26	21.69	0.01	8.71	b.l.d.	0.12	2.52	99.41	71.51	0.22	0.88	0.027	2.427	0.095	108.1	0.41
	9-07	0.55	b.l.d.	46.51	6.75	12.17	22.07	0.06	8.59	0.01	0.07	2.72	99.48	71.64	0.24	0.89	0.029	1.7833	0.095	79.4	0.27
	9-08	0.37	b.l.d.	50.71	3.61	14.58	21.46	b.l.d.	7.41	0.05	0.12	1.22	99.53	77.82	0.11	0.86	0.013	1.0411	0.095	46.4	0.35
	9-09	0.49	0.01	49.10	5.62	13.26	21.87	0.48	7.31	0.04	0.10	1.83	100.09	76.38	0.17	0.87	0.019	1.4856	0.095	66.2	0.34

Table 4-5. (continued)

		Na_2O	K_2O	SiO_2	Al_2O_3	MgO	CaO	Cr_2O_3	FeO	NiO	MnO	TiO_2	Total	Mg#	X(^{iv}Al)	XCa	$D^{cpx/melt}$	A(cm^{-2})	t (mm)	H_2O in cpx (wt. ppm)	H_2O in melt (wt. %)
	9-12	0.61	0.01	47.55	6.56	13.00	21.89	0.22	7.79	0.03	0.09	1.98	99.73	74.85	0.22	0.88	0.025	1.628	0.085	81.0	0.32
	9-13	0.61	b.l.d.	47.34	6.74	12.14	21.90	0.04	8.82	b.l.d.	0.11	2.32	100.03	71.03	0.22	0.88	0.026	1.0408	0.085	51.8	0.20
	9-14	0.47	b.l.d.	50.19	4.27	14.56	20.87	0.12	7.71	0.07	0.08	1.17	99.51	77.11	0.13	0.83	0.015	0.764	0.085	38.0	0.25
	9B-02	0.51	0.01	47.49	6.35	12.20	22.39	0.08	8.03	0.01	0.15	2.35	99.55	73.05	0.21	0.90	0.024	1.1284	0.097	49.2	0.20
	9B-02B	0.40	b.l.d.	51.18	3.54	14.81	21.60	0.10	7.32	0.02	0.09	1.10	100.15	78.30	0.11	0.86	0.013	0.8496	0.097	37.1	0.29
	9B-02C	0.54	0.01	48.39	5.60	12.84	22.41	0.05	8.24	b.l.d.	0.11	2.18	100.37	73.53	0.19	0.90	0.021	1.2467	0.097	54.4	0.25
	9B-03	0.49	0.01	49.55	4.30	14.07	21.96	0.05	7.16	b.l.d.	0.11	1.40	99.09	77.80	0.14	0.88	0.016	0.6684	0.097	29.2	0.19
11NW09	9B-04	0.52	b.l.d.	47.33	6.56	13.02	22.13	0.30	7.69	0.04	0.10	2.25	99.93	75.11	0.23	0.89	0.027	0.7899	0.097	34.5	0.13
	9B-04B	0.59	b.l.d.	46.93	6.64	12.48	22.27	0.11	8.28	0.02	0.07	2.34	99.73	72.89	0.23	0.90	0.028	0.819	0.097	35.7	0.13
	9B-07	0.50	0.01	49.88	4.44	13.63	21.90	0.09	7.68	0.05	0.11	1.20	99.48	76.00	0.13	0.88	0.015	0.4588	0.129	15.0	0.10
	9B-08	0.63	b.l.d.	46.75	6.41	12.09	21.97	0.06	8.72	0.03	0.12	2.47	99.25	71.20	0.23	0.89	0.027	1.0095	0.098	43.6	0.16
	9B-10	0.34	0.01	50.69	3.58	14.60	22.19	0.19	6.81	0.04	0.11	1.21	99.78	79.25	0.12	0.88	0.013	0.721	0.14	21.8	0.17
	9B-11	0.46	b.l.d.	50.33	4.35	14.29	22.28	0.09	6.92	b.l.d.	0.11	1.42	100.24	78.65	0.14	0.88	0.015	0.7793	0.14	23.6	0.16
	9B-12	0.58	0.01	47.93	5.87	12.78	22.20	0.08	8.11	0.02	0.14	1.94	99.65	73.74	0.20	0.89	0.022	1.2053	0.107	47.7	0.22
	9B-12B	0.48	b.l.d.	48.49	5.84	12.92	22.20	0.08	7.80	0.02	0.09	1.68	99.58	74.71	0.18	0.89	0.020	0.4056	0.107	16.0	0.08
	9B-12C	0.56	b.l.d.	47.26	7.15	12.26	21.85	0.15	7.89	0.03	0.10	2.51	99.76	73.48	0.23	0.88	0.028	1.0214	0.107	40.4	0.15
	9B-12D	0.57	b.l.d.	48.24	6.17	12.41	22.18	0.04	8.25	b.l.d.	0.09	2.19	100.14	72.84	0.20	0.89	0.022	0.2986	0.107	11.8	0.05

Note: b.l.d., below the limit of detection

4.2.1.2 Water content of clinopyroxene phenocrysts and melts

Like the Shuangliao basalts, the IR absorption spectra of the Wulanhada cpx phenocrysts in the OH-stretching vibration region (3000-3800 m^{-1}) are mainly composed of three bands: 3630-3620 cm^{-1}, 3540-3520 cm^{-1}, and 3470-3450 cm^{-1}, and the 3620-3640 cm^{-1} band is always predominant (Fig. 4-15b). For some big cpx phenocrysts, profile IR analyses have been conducted. The water contents of these phenocrysts are homogenous from the core to the rim, suggesting that H diffusion during magma ascent to the surface was limited (Fig. 4-15a). The calculated water contents of cpx phenocrysts and corresponding melts are listed in Table 4-5, and plotted versus Mg# of cpx phenocrysts in Fig 4-16. The H_2O contents of cpx phenocrysts and melts range from 10 to 200 ppm and 0.05 to 1 wt.% H_2O, which are significantly lower than those of Shuangliao basalts (50-800 ppm, 0.5-5.6 wt.%). The H_2O contents of cpx phenocrysts and melts vary significantly between different samples (Fig. 4-16).

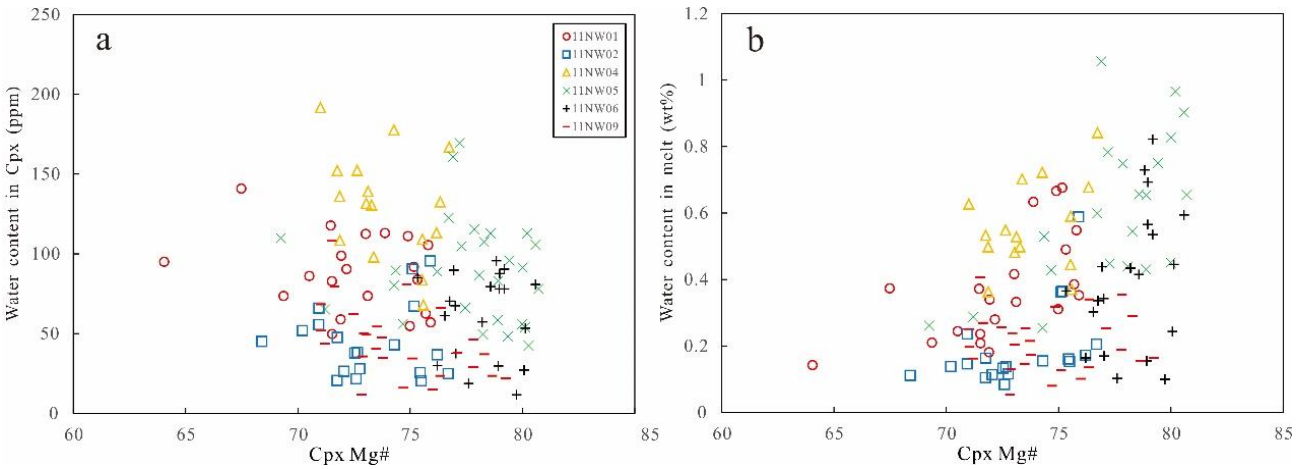

Figure 4-16. H_2O contents of cpx phenocrysts and associated melts vs cpx Mg# of Wulanhada basalts.

4.2.1.3 Oxygen isotope compositions of clinopyroxene phenocrysts

The cpx megacrysts (NSH2, NSH5, NSH8, NSH9, NSH10, NSH14) from Nushan, eastern China were used for instrumental mass fractionation correction. The oxygen isotope compositions of cpx phenocrysts are listed in Table 4-6 and plotted in Fig 4-17. The $\delta^{18}O$ values of cpx phenocrysts range from 5.49‰ to 7.38‰ and are significantly higher than the values of cpx in typical MORB and mantle peridotites (5.4‰-5.8‰) (Eiler et al., 1997; Mattey et al., 1994). The difference in $\delta^{18}O$ values within individual samples varies from 0.52‰ to 1.80‰.

Table 4-6. The oxygen isotope composition of cpx phenocrysts in Wulanhada basalts

	Sample	Mg#	$\delta^{18}O$ measured	IMF*	$\delta^{18}O$ corrected by IMF	1SE**
11NW2	11NW2-07	76.4	8.34	1.96	6.38	0.17
	11NW2-06b	75.8	8.28	2.03	6.26	0.09
	11NW2-06	72.3	8.17	2.38	5.79	0.22
	11NW2b-03	76.2	8.08	1.98	6.10	0.11
	11NW2b-03b	74.3	8.07	2.18	5.89	0.27
	11NW2-03	70.9	8.01	2.52	5.49	0.36
	11NW2-05	76.7	8.20	1.93	6.26	0.30
	11NW2b-07	76.8	8.60	1.92	6.68	0.13
	11NW2b-07b	72.7	8.47	2.34	6.13	0.13
	11NW2-01	71.8	8.20	2.43	5.77	0.25
	11NW2-08	75.2	8.43	2.09	6.34	0.29
	11NW2-04b	75.5	8.51	2.06	6.45	0.06
	11NW2-04	72.1	8.45	2.40	6.05	0.16
11NW9	11NW9b-12d	72.8	8.35	2.33	6.02	0.12
	11NW9b-12c	73.5	8.23	2.26	5.97	0.36
	11NW9b-12b	74.7	7.87	2.14	5.73	0.13
	11NW9b-12	73.7	7.81	2.24	5.58	0.22
	11NW9b-2b	78.3	8.00	1.77	6.23	0.10
	11NW9b-2	73.0	8.51	2.31	6.20	0.20
	11NW9b-2c	73.5	8.23	2.26	5.97	0.12
	11NW9-13	71.0	8.50	2.51	5.99	0.01
	11NW9-14	77.1	9.27	1.89	7.38	0.38
	11NW9-06	71.5	8.61	2.46	6.15	0.17
	11NW9-08	77.8	8.49	1.82	6.67	0.06
	11NW9-07	71.6	8.54	2.45	6.09	0.16
	11NW9-09	76.4	8.48	1.96	6.51	0.14
	11NW9-12	74.8	8.49	2.13	6.36	0.04
11NW5	11NW5-15	76.8	8.31	1.93	6.37	0.20
	11NW5-14	80.0	8.06	1.60	6.46	0.35
	11NW5-16	76.2	8.26	2.00	6.26	0.08
	11NW5-17	80.2	8.23	1.58	6.65	0.16
	11NW5-19	78.3	8.57	1.78	6.79	0.05
	11NW5-21	69.2	8.97	2.73	6.24	0.11
	11NW5-18	74.4	8.49	2.19	6.30	0.25
	11NW5-20	76.6	8.41	1.96	6.45	0.30
	11NW5-13C	72.8	8.67	2.35	6.32	0.20
	11NW5-13	76.0	8.48	2.02	6.46	0.22
	11NW5-13R	75.3	8.61	2.09	6.52	0.04
	11NW5-13RR	73.5	8.41	2.28	6.13	0.17
	11NW5-28	76.9	8.58	1.92	6.66	0.02
	11NW5-11R	76.7	8.34	1.95	6.40	0.07
	11NW5-11	77.3	8.45	1.88	6.56	0.19

Table 4-6. (continued)

	Sample	Mg#	$\delta^{18}O$ measured	IMF*	$\delta^{18}O$ corrected by IMF	1SE**
11NW5	11NW5-11C	78.1	8.31	1.80	6.51	0.09
11NW6	11NW6b-13	73.0	8.24	2.33	5.91	0.11
	11NW6-1a	78.9	8.14	1.72	6.43	0.25
	11NW6-2a	77.3	8.22	1.88	6.34	0.08
	11NW6-2b	79.4	7.97	1.66	6.31	0.22
	11NW6-15	75.3	8.00	2.09	5.91	0.19
	11NW6-19	77.0	8.24	1.91	6.33	0.12
	11NW6-17	80.1	7.86	1.59	6.27	0.19
	11NW6-12	79.2	7.91	1.68	6.22	0.23
11NW1	11NW1-3b	73.9	8.13	2.24	5.89	0.10
	11NW1-3	75.3	8.24	2.09	6.15	0.15
	11NW1-1	66.7	8.64	2.99	5.64	0.09
	11NW1-2	71.5	8.46	2.49	5.97	0.24
	11NW1-21	75.7	8.39	2.05	6.34	0.09
	11NW1-4	75.9	8.11	2.03	6.08	0.09
	11NW1-6	74.9	8.38	2.13	6.25	0.09
	11NW1-19	71.9	8.34	2.45	5.89	0.16
	11NW1-5	67.5	8.12	2.91	5.21	0.24
	11NW1-18	75.0	8.12	2.12	6.00	0.14

* IMF is the instrumental mass fractionation
** SE the standard error of the mean for the group of measurements in a single cpx grain

4.2.2 Discussion

4.2.2.1 Previous study

Geochemical characters of Wulanhada basalts were studied by Fan et al. (2014), including major, trace element concentrations and Sr-Nd-Pb-Hf isotopic compositions. The high Nd/U ratios, low La/Nb ratios and the absence of obvious correlation between SiO_2 and Nb/La ratios suggests that crustal contamination is insignificant. With a low MgO, Ni and Cr contents, the Wulanhada basalts have underwent fractional crystallization of olivine and clinopyroxene. No Eu anomaly and the negative correlation between Al_2O_3 and MgO contents suggest that the fractionation of plagioclase (pl) is limited (Fan et al. 2014). Although the Wulanhada basalts may have underwent significant fractional crystallization, the incompatible element ratios and the isotopic compositions can provide information on the mantle source of these basalts. Based on the negative Zr and Hf anomalies, negative relationship between $^{176}Hf/^{177}Hf$

and $^{143}Nd/^{144}Nd$ (εHf and εNd decoupling) and relatively low $^{87}Sr/^{86}Sr$ ratios, Fan et al. (2014) proposed the presence of carbonated melt in the mantle source. However, no further discussion of this enriched component was presented in their work.

4.2.2.2 High oxygen isotope compositions

The $\delta^{18}O$ values of cpx phenocrysts in Wulanhada basalts are higher than those of cpx in typical MORB and mantle peridotites (Fig. 4-17) (Eiler et al., 1997; Mattey et al., 1994).

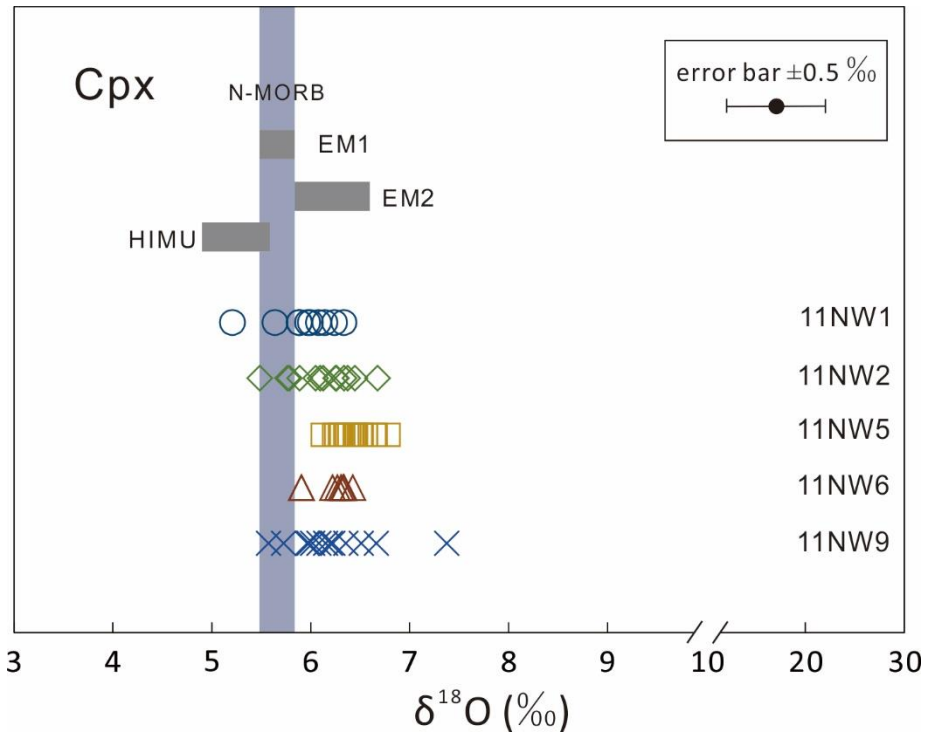

Figure 4-17. Oxygen isotope compositions of cpx phenocrysts in the Wulanhada basalts. The range of $\delta^{18}O$ values of cpx phenocrysts in N-MORB, EM1, EM2 and HIMU are calculated from the $\delta^{18}O$ values of ol phenocrysts (Eiler et al., 1997), assuming the equilibrium fractionation between cpx and ol is 0.4‰ (Mattey et al., 1994).

As discussed in Section 4.1.2.2, the isotopic fractionation of oxygen isotopes caused by fractional crystallization is less than 0.1‰ in basaltic melts (Eiler, 2001). Fresh cpx phenocrysts without crack and inclusion were selected for the oxygen isotope measurements and the crustal contamination in the Wulanhada basalts is limited (Fan

et al. 2014). The sample 11NW05 with relatively high $\delta^{18}O$ values has a low $^{87}Sr/^{86}Sr$ ratio. All of these indicate that the effect of alteration on the surface of the Earth, crustal contamination, partial melting, devolatilization, fractional crystallization, assimilation-fractional crystallization (AFC) process on the oxygen isotope compositions of cpx phenocrysts is limited. Thus, the oxygen isotope compositions of the cpx phenocrysts in the Wulanhada basalts preserve the information of their mantle source. It means that a component with high $\delta^{18}O$ value is needed in the mantle source of Wulanhada basalts.

4.2.2.3 Water content in the "primary" melts

During magma evolution, the Wulanhada basalts underwent significant fractional crystallization (Fan et al., 2014), which had increased the water content of the magma. However, as discussed in Section 4.1.2.3, for a single magma, crystallization process would not lead to a significant elevation of water content in residual melt (<30%, similar to the measurement uncertainties) when the Mg# of crystallized cpx phenocryst is higher than 75 (Fig. 4-8). Thus, considering the magma mixing, the average H_2O content calculated by the cpx phenocrysts with Mg# >75 can represent the H_2O content of the Wulanhada "primary" melts. In Figure 4-18, the calculated water content display good relationship with the $^{87}Sr/^{86}Sr$ and $^{176}Hf/^{177}Hf$ ratios, which means the H_2O content can represent the original information of the mantle source. In addition, the measured water content profiles suggest that H diffusion in cpx phenocryst during magma ascent to the surface is limited (Fan et al., 2014). Thus, the calculated H_2O content from cpx phenocrysts in the Wulanhada basalts has been well preserved.

The calculated average H_2O contents of the Wulanhada basalts range from 0.21 to 0.69 wt.% (Fig. 10, Table 4-7). They fall in the range of MORBs (0.1-0.3 wt%, Asimow et al., 2004; Danyushevsky et al., 1993, 2000; Dixon, 1988; Michael, 1988, 1995; Sobolev and Chaussidon, 1996; Saal et al., 2002; Simons et al., 2002) and OIBs (0.3-1.0 wt%, Dixon et al., 1997, 2002; Dixon and Clague, 2001; Nichols et al., 2002; Simons et al., 2002; Wallace, 1998). The calculated H_2O contents and H_2O/Ce ratios (28-86) of Wulanhada basalts are significantly lower than those of Shuangliao basalts (0.90-3.06 wt.%, 158-737) located more on the east (Fig. 4-19) and are consistent with those of Taihang basalts (Liu et al., 2015b), also located above the edge of the subducted Pacific slab.

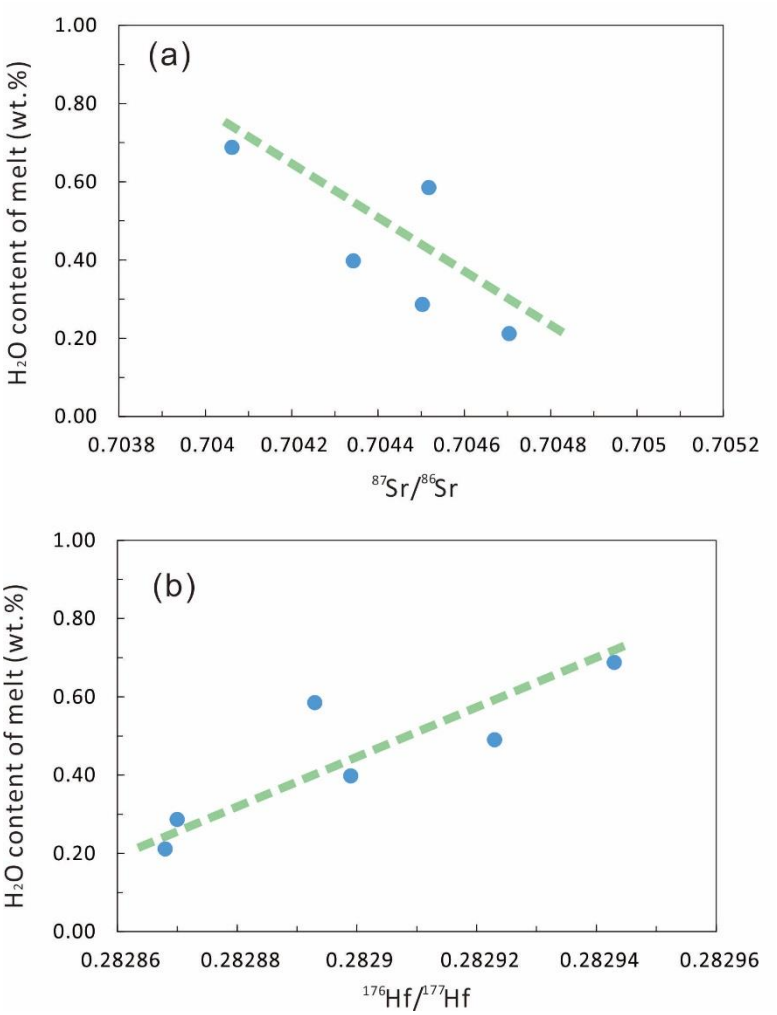

Figure 4-18. The calculated water contents of magmas in the Shuangliao basalts compared with (a) $^{87}Sr/_{86}Sr$, (b) $^{176}Hf/^{177}Hf$ concentrations of bulk rocks.

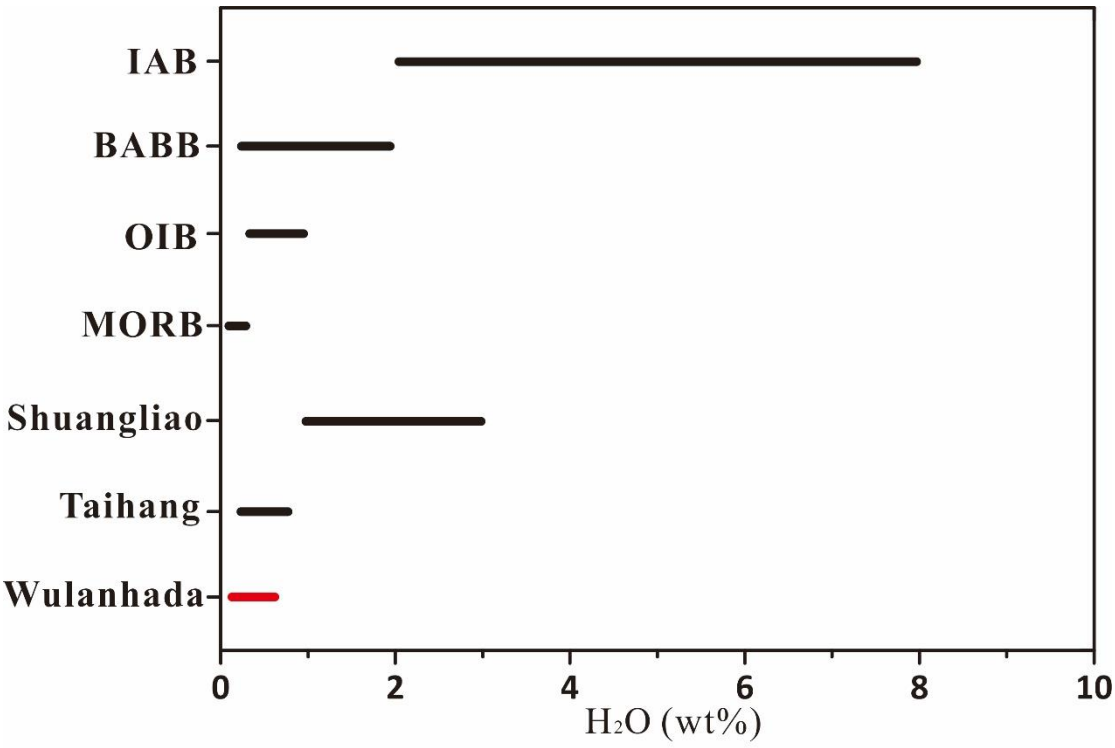

Figure 4-19. Calculated average H_2O content of the Wulanhada "primary" melts. The ranges of H_2O content for OIBs, MORBs, BABBs and IABs are from Dixon et al. (2004) and the references therein. The H_2O content of Taihang basalts is from Liu et al. (2015b).

Table 4-7. The water content and H_2O/Ce of "primary" melt in Wulanhada basalts

	Hongshan	Huoshaoshan	Heinaobao	Zhongliandanlu	Nanliandanlu	8 minitype scoria cones	
Sample	11NW01	11NW02	11NW04	11NW05	11NW06	11NW09	11NW08
H_2O of melt (wt.%)	0.49	0.29	0.58	0.69	0.40	0.21	-**
H_2O/Ce*	59.62	36.42	73.75	85.52	64.95	28.28	-

* Ce content of basalts are from Fan et al. (2014)
** The water content of 11NW08 is very low (Fig. 4-15)

4.2.2.4 The enriched component in the mantle source

As discussed above, the oxygen isotopes of the cpx phenocrysts and the H_2O content of the magma reflect the mantle source. The variable isotopic compositions (e.g., $^{87}Sr/^{86}Sr$ ratio) and highly incompatible trace elements ratios (e.g., variable Ba/Th, Nb/La, Nb/U and Ce/Pb) of Wulanhada basalts also indicate the compositional heterogeneity of the mantle source. Therefore, the $^{87}Sr/^{86}Sr$ ratio, Ba/Th ratio, Nb/La ratio, Nb/U ratio and Ce/Pb ratio and H_2O/Ce ratio can be combined to constrain the enriched component in the mantle source of the Wulanhada basalts (Fig. 4-20).

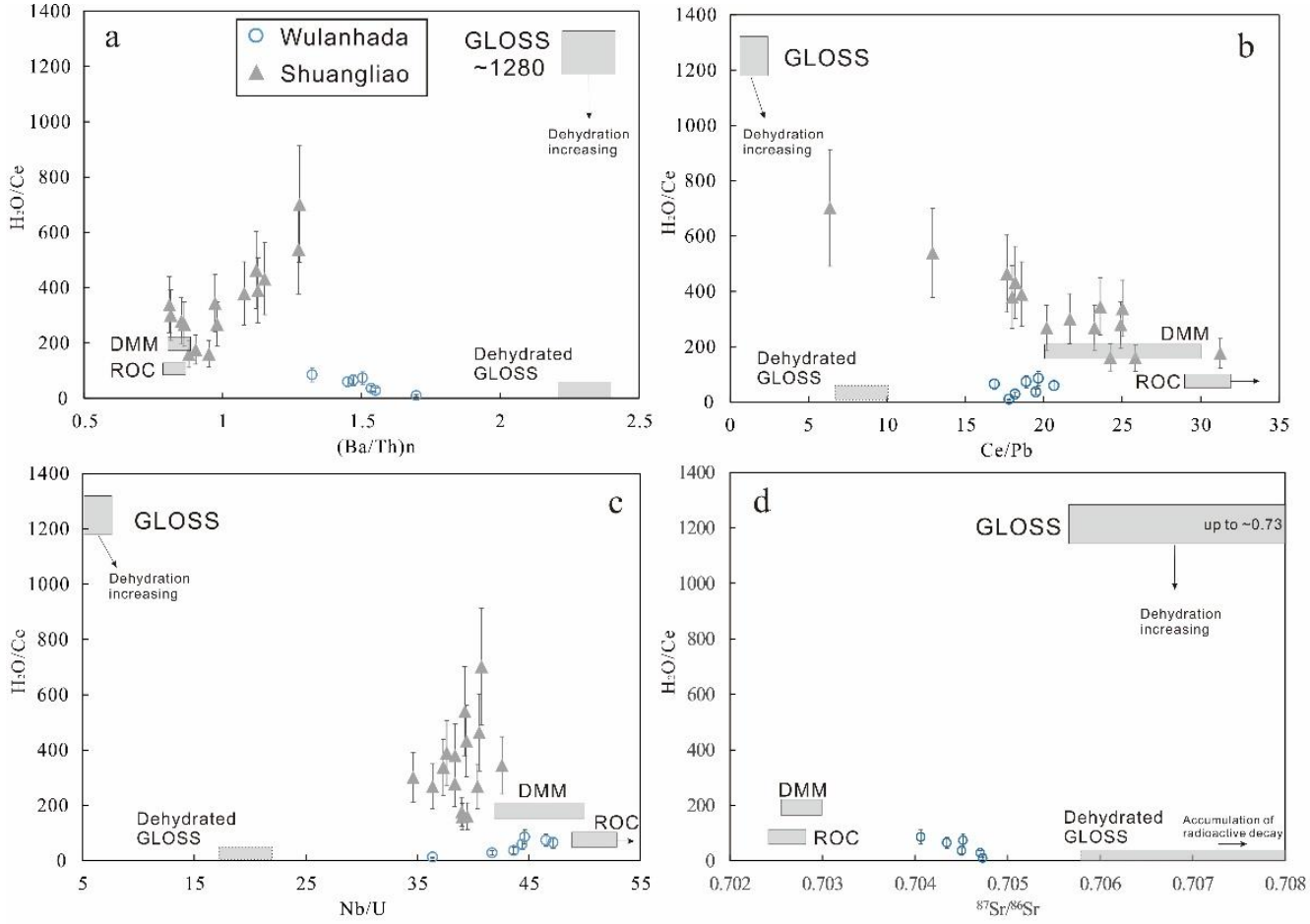

Figure 4-20. Plots of H_2O/Ce vs. Ba/Th, Ce/Pb , Nb/U and $^{87}Sr/^{86}Sr$ of the Wulanhada basalts. The gray squares show the possible end members of the mantle source. The Ce, Nb and U concentrations and $^{87}Sr/^{86}Sr$ values are from Fan et al. (2014). The H_2O/Ce ratios of GLOSS (~1280), DMM (~200) and ROC (~100) are from Plank and Langmuir (1998); Dixon et al. (2002) and the references therein. The ratios of Ba/Th, Ce/Pb, Nb/La and $^{87}Sr/^{86}Sr$ for DMM and GLOSS are from Cale et al. (2013), Plank and Langmuir (1998) and Workman and Hart (2005). Ba/Th of ROC would not change much since the two elements have similar fluid mobility, and the Ce/Pb and Nb/U of ROC would increase, due to the relatively high mobility of Pb and U (Kogiso et al., 1997; Kessl et al., 2005). The Ba/Th ratio of dehydrated GLOSS would not change, and the Ce/Pb and Nb/U ratios of dehydrated GLOSS would increase (Aizawa et al., 1999).

As shown in Fig. 4-20, two components can be identified in the mantle source. One component with normal H_2O/Ce ratio, $^{87}Sr/^{86}Sr$ ratio, Ba/Th ratio, Nb/U ratio and Ce/Pb ratio which are similar to those of normal depleted mantle. The other enriched

component is characterized by low H_2O/Ce ratio, Nb/U ratio and Ce/Pb ratio, high $^{87}Sr/^{86}Sr$ ratio and Ba/Th ratio. The dehydrated marine sediments are characterized by low H_2O/Ce ratios (~100, Dixon et al., 2002) and high $^{87}Sr/^{86}Sr$ ratios (Plank and Langmuir, 1998). For the trace elements, studies of drilled marine sediments has demonstrated that marine sediments have a relatively high Ba/Th ratio, low Nb/U ratio and Ce/Pb ratio (Plank and Langmuir, 1998). Thus, dehydrated marine sediment (GLOSS) is the most likely candidate for this component. In addition, the enriched component in Wulanhada basalts has a high $\delta^{18}O$ value, which is also consistent with the feature of dehydrated GLOSS.

Compared to mantle arrays defined by global OIB and MORB, marine sediments have relatively high $^{176}Hf/^{177}Hf$ ratios for given $^{143}Nd/^{144}Nd$, which also can induce the decoupling of εHf and εNd in Wulanhada basalts (Chauvel et al., 2008). Besides, marine sediments are significantly depleted in Zr and Hf (Plank and Langmuir, 1998), which can account for the negative Zr and Hf anomalies of the Wulanhada basalts.

In the plot of H_2O/Ce vs. (Nb/La)n (Fig. 4-21), the Wulanhada basalts do not display a simple correlation between DMM and dehydrated GLOSS, a ROC component (with high Na/La ratio) is also needed in the source. Overall, three components (DMM, ROC and dehydrated GLOSS) need to be involved in the mantle source of the Wulanhada basalts.

Interestingly, both H_2O content and H_2O/Ce ratio of recycled component in the mantle source of Wulanhada basalts are obviously lower than those of Shuangliao basalts. It emphasizes the regional difference of H_2O content in mantle source. The Wulanhada volcanic field is above the front edge of the subducted Pacific slab and the Shuangliao basalts are located above the subducted Pacific slab (Fig. 1-2). The difference in the H_2O content may reflect the dehydration process of the subducted Pacific plate.

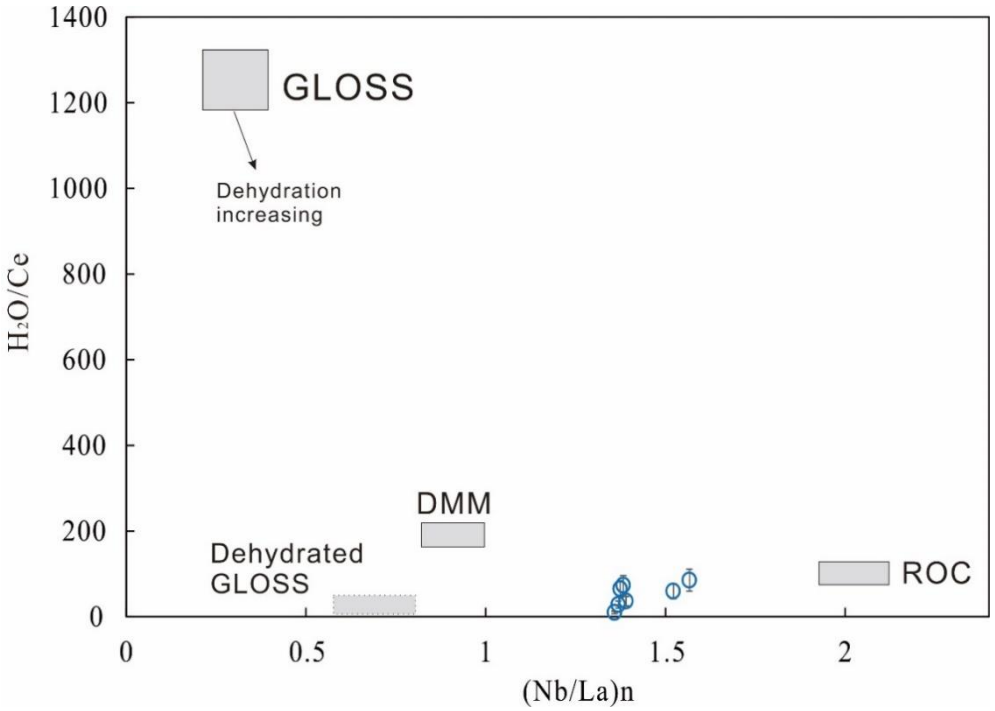

Figure 4-21. Plots of H_2O/Ce vs. (Nb/La)n of the Wulanhada basalts. The Ce, Nb and La concentrations in Wulanhada basalts are from Fan et al. (2014). The H_2O/Ce ratio of each component is the same as in Fig. 4-20. The Nb/La ratios of GOLSS and DMM are from Plank and Langmuir (1998) and Workman and Hart (2005). The (Nb/La)n of ROC is calculated from the concentration of the fresh MORB (5.24 vs 5.21 for Nb and La, Gale et al., 2013) and the mobility in water (Mobility = (Coriginal-Cresidual)/Coriginal*100 %, the water activity of Nb is 20 times the one of La, Kogiso et al., 1997; Kessl et al., 2005). The Nb/La ratio of dehydrated GLOSS would increase, due to the relatively high mobility of La in the sediments (Aizawa et al., 1999).

4.2.3 Summary

(1) The H_2O contents of the Wulanhada basalts vary from 0.21 to 0.69 wt.%, falling in the range MORBs and OIBs. The $\delta^{18}O$ values of cpx phenocrysts vary widely, from 5.49‰ to 7.38‰. They are higher than the values of cpx in typical MORB and mantle peridotites.

(2)The heavy oxygen isotope composition and the correlations of H_2O/Ce with $^{87}Sr/^{86}Sr$, Ba/Th, Nb/La, Nb/U and Ce/Pb in the Wulanhada basalts emphasize the significant contribution of dehydrated marine sediments and ROC to the mantle source.

(3) The H_2O content and H_2O/Ce ratio of recycled component in the mantle source of Wulanhada basalts are obviously lower than those of Shuangliao basalts, which may come from the progressive dehydration of the subducted Pacific plate.

4.3 Chaihe-aershan basalts

4.3.1 Results

4.3.1.1 Major and trace element compositions of bulk rock

Bulk rock major and trace element concentrations of the Chaihe-aershan basalts are presented in Table 4-8. In the TAS (Tasmania) nomenclature of Le Bas et al. (1986), the Chaihe-aershan basalts are in the range of trachybasalt (TFL basalts, high alkalinity) and basalt (low alkalinity) fields (Fig. 4-22a). The basalts with low alkalinity are characterized by high MgO (8.62-12.00 wt.%), CaO (8.68-9.71 wt.%), Mg# (63.2-70.0, Mg#=100*Mg/(Mg+Fe) mol), Ni (213-423 ppm), Co (45.9-58.4 ppm), low TiO_2 (1.88-2.29 wt.%), and P_2O_5 (0.36-0.48 wt.%). DLH basalts have the lowest alkalinity, highest Mg# (67.2-70.0), compared to the TFL basalts, which have relatively low MgO (7.71-8.80 wt.%), Mg# (56.9-62.8) and Ni (176-273 ppm) and high TiO_2 (2.36-2.55 wt.%) and P_2O_5 (0.61-0.75 wt.%). On the plots of major elements compared with MgO, the Chaihe-aershan basalts display distinct compositional trends (Figs. 4-22b-f) which can be divided into three groups (TFL, DLH and other basalts).

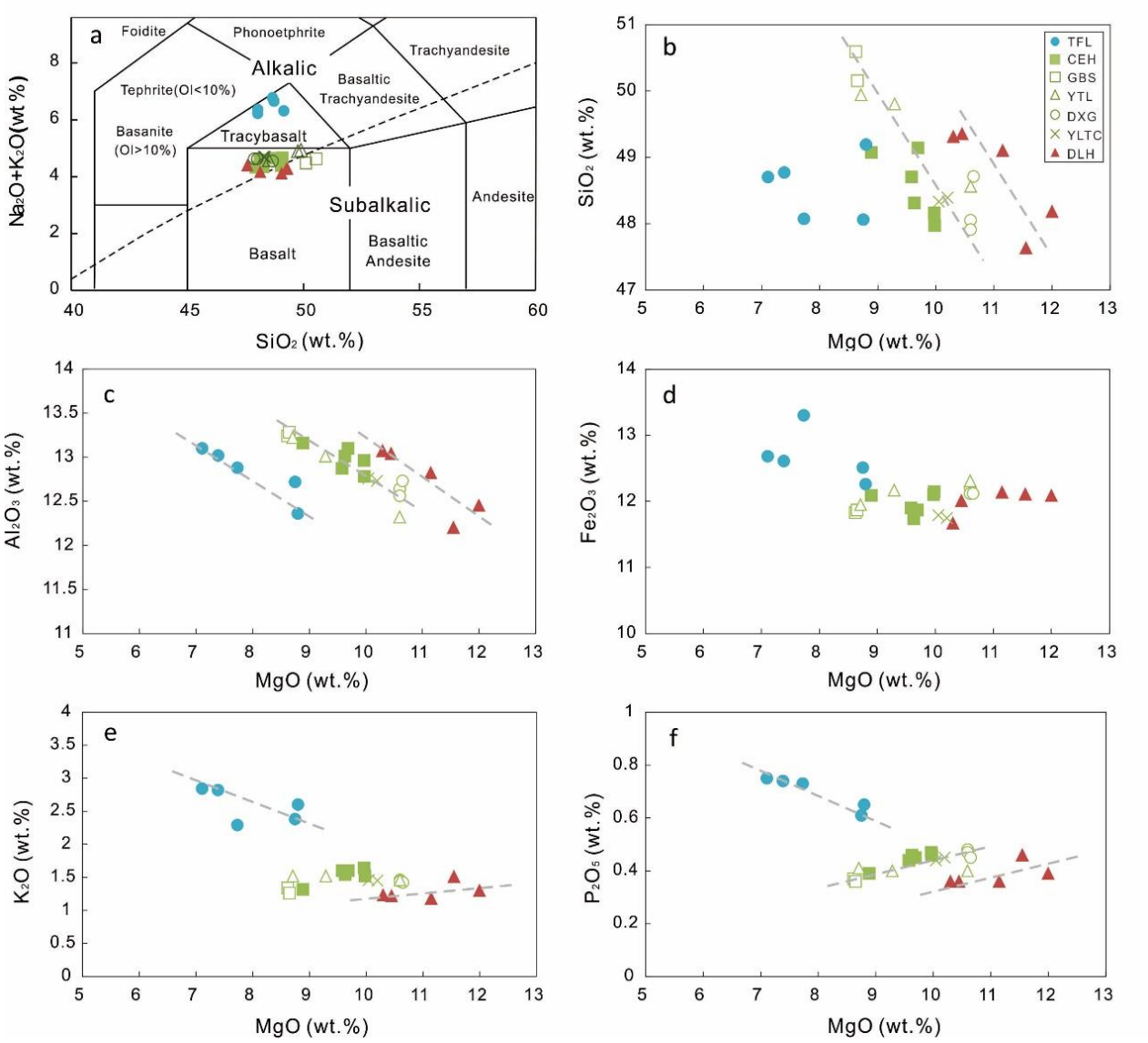

Figure 4-22. a) Total alkali compared with SiO_2 plots for Chaihe-aershan basalts. The classification of rock types is based on Le Bas et al. (1986); b) SiO_2 compared with MgO, c)Al_2O_3 compared with MgO, d) Fe_2O_3 compared with MgO, e) K_2O compared with MgO and f) P_2O_5 compared with MgO for Chaihe-aershan basalts.

The primitive-mantle normalized trace elements and chondrite normalized rare earth element patterns of the Chaihe-aershan basalts show that the concentrations of trace elements vary with the alkalinity of rocks (Fig. 4-23). The TFL basalts have the highest alkali contents and are significantly enriched in light rare earth elements (LREEs) relative to heavy rare earth elements (HREEs), with a high ratio of $(La/Yb)_N$ (18.8-23.7, N denotes normalization to chondrite, Fig. 4-23). The basalts are also enriched in Nb and Ta, relatively depleted in highly incompatible elements (Rb, Ba, Th, U) and have

weak positive Sr anomaly and negative Ti anomaly (Fig. 4-23a).

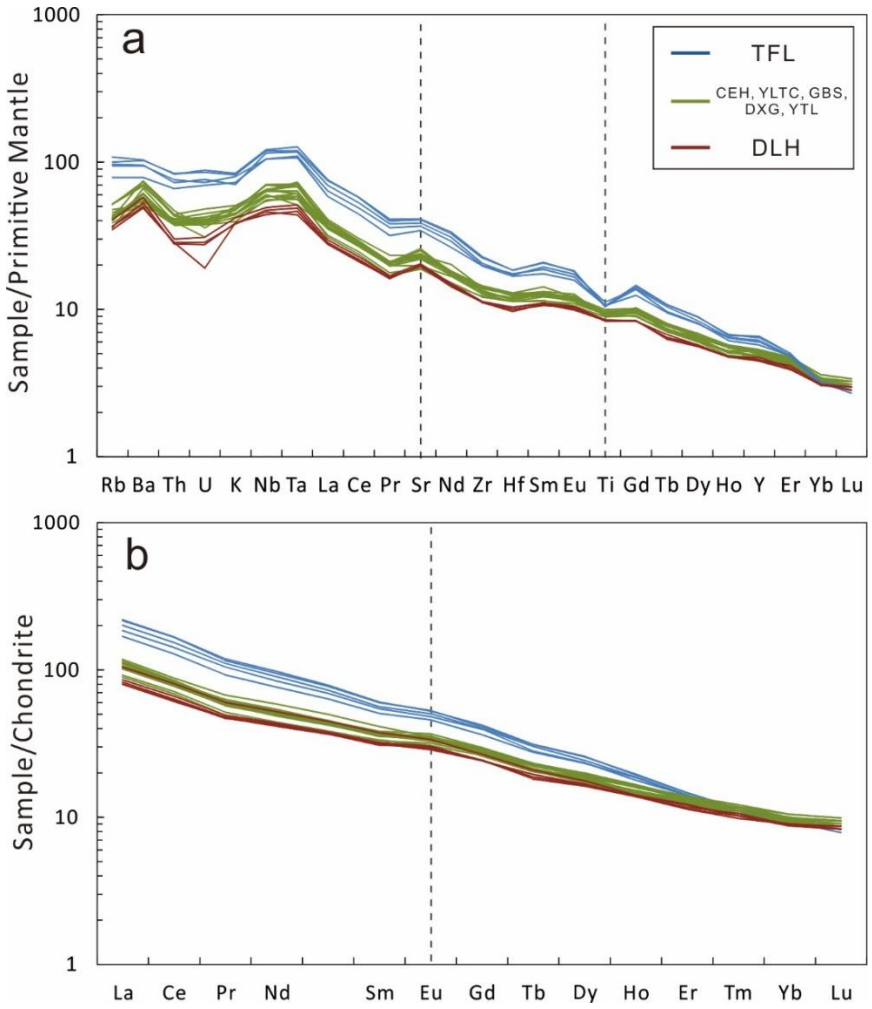

Figure 4-23. Primitive mantle-normalized trace element and the Chondrite-normalized rare earth element concentration diagrams for Chaihe-aershan basalts. Normalization values are based on Sun and McDonough (1989).

The other basalts display similar element patterns, except for identical changes with alkalinity. For the basalts with low alkalinity, the fractionation between LREEs and HREEs decreases ($(La/Yb)_N$ =9.0-12.6), the relative enrichment of Nb, Ta and K increases, the positive Sr and Eu anomalies increase and the Ti anomaly weakens (Fig. 4-23). Because the plagioclase (pl) is rarely present in the samples, the positive Sr and Eu anomalies are unlikely to be caused by the accumulation of pl. In addition, the presence of abundant mantle xenoliths in the Chaihe-aershan basalts demonstrates that the magma ascended rapidly from the mantle.

Table 4-8. Major and trace element compositions of Chaihe-aershan basalts

Location	Chaoerhe						Delehe				
GPS	N 47°26'35.86"; E 121°18'21.96"						N 47°30'23.58"; E 121° 8'35.40"				
sample	CEH-2	CEH-3	CEH-5	CEH-8	CEH-11	CEH-12	DLH-1	DLH-2	DLH-6	DLH-7	DLH-10
SiO_2 (wt.%)	48.16	47.97	48.70	49.07	48.31	49.14	49.31	48.18	49.10	49.35	47.63
TiO_2	2.15	2.29	2.19	2.11	2.08	2.18	1.88	1.91	1.88	1.90	2.10
Al_2O_3	12.96	12.78	12.87	13.16	13.01	13.10	13.07	12.45	12.82	13.04	12.20
$Fe_2O_3^T$	12.10	12.15	11.90	12.09	11.74	11.87	11.67	12.09	12.14	12.01	12.11
MnO	0.17	0.17	0.17	0.17	0.17	0.17	0.16	0.17	0.17	0.16	0.17
MgO	9.97	9.98	9.58	8.89	9.63	9.69	10.30	12.00	11.15	10.45	11.55
CaO	9.59	9.71	9.64	9.59	9.48	9.68	9.11	8.79	9.32	9.18	9.34
Na_2O	2.96	2.82	3.06	3.08	2.82	3.08	3.06	2.88	2.95	3.08	2.91
K_2O	1.64	1.52	1.60	1.32	1.54	1.60	1.23	1.30	1.18	1.22	1.51
P_2O_5	0.47	0.46	0.44	0.39	0.46	0.45	0.36	0.39	0.36	0.36	0.46
LOI	-0.32	-0.02	-0.35	-0.15	0.21	-0.40	-0.47	-0.48	-0.60	-0.55	-0.23
Total	99.85	99.83	99.80	99.72	99.45	100.56	99.68	99.68	100.47	100.20	99.75
Mg#[a]	66.0	65.9	65.4	63.4	65.9	65.8	67.5	70.0	68.4	67.2	69.2
Kˆ(ppm)	12,700	11,900	12,500	10,500	12,100	12,400	9,700	10,500	9,600	9,500	12,000
Tiˆ	12,250	12,950	12,600	11,850	11,800	12,500	10,850	11,050	10,950	10,800	12,350
Liˆ	7.2	7.2	7.1	7.9	10.4	7.3	6.7	7.1	6.6	6.4	8.7
Vˆ	210	220	214	211	192	211	192	197	201	196	201
Crˆ	263	291	270	239	274	272	293	356	349	331	361
Coˆ	50.2	49.5	48.7	47.6	47.1	49.5	50.0	56.1	57.1	53.4	58.4
Niˆ	256	258	248	224	249	260	305	423	386	326	353
Scˆ	22.3	22.8	22.3	21.5	21.1	22.7	21.1	19.8	21.4	21.3	21.9
Ga	20.10	19.40	19.30	19.2	19.30	19.60	18.40	17.90	17.80	18.50	17.80
Gaˆ	18.55	17.40	18.00	18.1	18.30	18.10	17.80	17.00	17.60	17.35	18.10
Rb	32.9	26.5	32.7	22.7	24.9	33.2	22.1	25.7	23.1	23.3	29.8
Rbˆ	32.5	26.2	33.2	23.3	25.1	33.7	22.6	26.1	23.7	23.7	32.1
Sr	547	491	506	417	1040	496	414	430	417	422	505
Srˆ	548	477	486	413	1030	485	407	428	410	403	508
Y	21.6	23.8	22.8	22.9	21.9	23.4	20.3	20.5	20.8	21.5	21.5
Yˆ	21.9	23.0	22.4	22.7	21.5	22.7	19.9	20.0	20.7	20.2	21.8
Nb	46.3	45.6	46.4	41.4	43.5	46.5	31.4	35.0	33.6	32.7	43.8
Nbˆ	43.2	41.9	42.1	37.2	40.5	43.5	28.6	32.5	30.7	28.6	39.6
Ba	479	520	514	462	827	493	340	401	370	347	427
Baˆ	460	480	480	420	790	450	320	380	340	330	410
La	27.1	27.9	26.2	24.1	27.0	26.4	18.9	20.3	19.5	18.9	24.8
Laˆ	27.0	27.1	25.9	23.1	26.9	26.3	18.7	20.1	19.3	18.9	23.8
Ce	51.9	53.8	51.8	47.3	50.0	50.9	37.4	40.5	38.7	38.0	49.4
Ceˆ	51.7	50.0	49.9	44.4	49.3	50.3	36.6	39.7	37.9	37.40	47.2
Pr	5.75	6.42	5.83	5.49	5.99	5.80	4.50	4.67	4.56	4.45	5.71
Nd	24.2	27.4	24.7	22.7	25.2	24.5	19.3	20.3	19.8	19.9	24.3
Zr	3.8	4.0	4.0	3.7	3.9	4.0	3.2	3.2	3.0	3.1	3.6
Hf	160	157	162	143	153	161	125	127	125	125	142
Sm	5.60	6.32	5.76	5.49	5.58	5.66	4.86	4.91	4.83	4.72	5.73
Eu	1.98	2.04	2.03	1.90	2.01	2.00	1.70	1.76	1.67	1.74	1.96
Gd	5.73	6.05	5.93	5.83	5.79	5.92	5.01	4.98	4.96	5.01	5.50
Tb	0.79	0.85	0.85	0.84	0.77	0.84	0.70	0.73	0.70	0.68	0.78
Dy	4.59	5.08	4.71	4.85	4.35	4.81	4.26	4.24	4.18	4.13	4.49
Ho	0.85	0.93	0.91	0.90	0.81	0.91	0.78	0.79	0.79	0.78	0.80
Er	2.05	2.29	2.20	2.21	2.01	2.23	1.88	2.00	1.88	1.93	2.02
Tm	0.28	0.31	0.29	0.30	0.26	0.29	0.26	0.26	0.25	0.27	0.26
Yb	1.59	1.78	1.67	1.78	1.54	1.69	1.51	1.53	1.52	1.50	1.48

Table 4-8. (continued)

Location	Chaoerhe						Delehe				
GPS	N 47°26'35.86"; E 121°18'21.96"						N 47°30'23.58"; E 121° 8'35.40"				
sample	CEH-2	CEH-3	CEH-5	CEH-8	CEH-11	CEH-12	DLH-1	DLH-2	DLH-6	DLH-7	DLH-10
Lu	0.22	0.25	0.24	0.25	0.22	0.24	0.22	0.22	0.21	0.22	0.21
Ta	2.8	3.0	2.9	2.5	2.7	2.8	1.9	2.1	2.0	1.8	2.4
Taˆ	2.72	2.69	2.61	2.29	2.52	2.66	1.76	2.01	1.86	1.79	2.26
Th	3.75	3.97	3.74	3.35	3.77	3.67	2.42	2.56	2.37	2.42	3.24
Thˆ	3.8	4.0	3.7	3.2	3.7	3.7	2.4	2.6	2.4	2.3	3.4
U	1.01	0.75	0.81	0.65	0.94	0.85	0.40	0.65	0.58	0.60	0.85
Uˆ	1.0	0.7	0.7	0.6	0.9	0.8	0.3	0.6	0.5	0.5	0.9
$(La/Yb)_N$[b]	12.23	11.25	11.26	9.72	12.58	11.21	8.98	9.52	9.21	9.04	12.02
Nb/U	45.84	60.80	57.28	63.69	46.28	54.71	78.50	53.85	57.93	54.50	51.53
Ba/Th	127.7	131.0	137.4	137.9	219.4	134.3	140.5	156.6	156.1	143.4	131.8
Eu/Eu*[c]	1.06	0.99	1.05	1.02	1.07	1.05	1.04	1.08	1.03	1.09	1.05

Table 4-8. (continued)

Location	Yueliangtianchi		Tuofengling					Daxiagu		
GPS	N 47°30'31.50"; E 120°52'0.89"		N 47°27'24.72"; E 120°38'49.38"		N 47°27'26.18"; E 120°38'57.89"			N 47°29'50.77"; E 120°37'39.61"		
sample	YLTC-1	YLTC-3	TFL1-3	TFL1-7	TFL2-1	TFL2-2	TFL2-5	DXG-2	DXG-4	DXG-7
SiO_2 (wt.%)	48.39	48.33	48.06	49.19	48.70	48.77	48.07	48.05	47.91	48.71
TiO_2	2.11	2.11	2.37	2.36	2.42	2.40	2.55	2.11	2.10	2.09
Al_2O_3	12.73	12.76	12.72	12.36	13.10	13.02	12.88	12.64	12.56	12.73
$Fe_2O_3^T$	11.75	11.79	12.51	12.26	12.68	12.61	13.30	12.20	12.12	12.12
MnO	0.17	0.17	0.17	0.16	0.17	0.17	0.18	0.17	0.17	0.17
MgO	10.20	10.05	8.75	8.80	7.11	7.39	7.73	10.60	10.60	10.65
CaO	9.50	9.53	8.51	7.84	8.10	8.09	8.48	9.49	9.45	9.30
Na_2O	3.25	3.25	3.86	3.73	3.95	3.85	4.08	3.18	3.20	3.14
K_2O	1.45	1.46	2.38	2.60	2.84	2.82	2.29	1.46	1.44	1.42
P_2O_5	0.45	0.44	0.61	0.65	0.75	0.74	0.73	0.48	0.47	0.45
LOI	-0.11	0.00	-0.34	-0.28	-0.12	-0.06	-0.01	-0.30	-0.46	-0.11
Total	99.89	99.89	99.60	99.67	99.70	99.80	100.28	100.08	99.56	100.67
Mg#[a]	67.1	66.7	62.2	62.8	56.9	58.0	57.8	67.2	67.3	67.4
K^(ppm)	11,300	11,100	18,200	19,900	21,000	20,500	17,600	11,200	11,100	11,000
Ti^	12,350	12,150	13,800	13,700	13,750	13,500	14,550	12,100	12,300	12,050
Li^	6.5	5.8	7.8	8.2	8.7	7.9	7.6	5.0	4.9	5.2
V^	195	232	189	159	159	158	176	190	192	191
Cr^	311	304	212	251	145	148	160	301	297	300
Co^	51.4	49.6	49.3	48.4	43.0	46.1	48.6	51.5	51.7	51.3
Ni^	257	252	244	273	176.0	193.0	206	301	311	314
Sc^	23.2	20.9	16.3	13.1	13.0	12.5	13.7	18.8	20.1	19.8
Ga	18.70	18.90	21.6	21.0	22.5	23.1	21.5	18.9	18.5	18.1
Ga^	18.40	17.50	20.0	20.3	20.9	20.8	20.5	17.7	17.6	18.0
Rb	25.4	26.5	50.0	60.0	68.6	63.5	61.4	27.0	27.7	26.0
Rb^	26.1	25.7	47.5	56.4	61.0	58.0	55.0	27.5	26.9	26.8
Sr	501	534	725	777	867	856	815	526	529	492
Sr^	503	491	699	752	816	802	794	517	523	494
Y	22.4	23.4	27.3	26.1	30.0	29.3	28.1	21.7	22.0	21.6
Y^	21.4	21.6	26.5	25.5	26.1	27.6	26.9	21.7	21.4	22.1
Nb	41.8	42.8	74.9	74.6	86.7	85.0	82.1	46.2	46.0	42.3
Nb^	36.9	36.3	64.5	65.5	70.4	73.6	70.9	40.9	40.0	38.8
Ba	420	429	550	660	723	715	666	397	403	386
Ba^	400	390	520	620	650	640	620	370	380	360
La	24.7	24.7	40.0	43.7	51.8	51.2	47.6	24.8	24.9	24.1
La^	23.4	23.7	38.4	42.5	46.0	48.5	45.3	26.0	24.9	23.8
Ce	48.5	49.2	78.6	86.7	102.5	102.0	93.9	49.4	49.4	47.5
Ce^	47.1	47.5	77.0	86.0	94.6	96.9	91.1	48.7	49.4	46.2
Pr	5.70	5.56	8.77	9.91	11.30	11.00	10.50	5.67	5.71	5.45
Nd	23.6	23.2	35.6	39.3	45.5	44.1	41.9	24.6	24.2	23.5
Zr	3.9	3.9	5.2	5.4	5.7	5.7	5.3	3.7	3.6	3.5
Hf	155	156	221	223	256	250	231	147	151	142
Sm	5.73	5.42	7.75	8.32	9.25	9.18	8.62	5.63	5.62	5.41
Eu	1.90	1.97	2.66	2.79	3.04	3.07	2.92	2.07	2.05	1.97
Gd	5.76	5.34	7.44	8.13	8.68	8.45	8.22	5.68	5.85	5.81
Tb	0.80	0.76	1.03	1.05	1.17	1.16	1.13	0.80	0.77	0.77
Dy	4.53	4.56	5.90	5.95	6.59	6.53	6.18	4.57	4.45	4.46
Ho	0.83	0.86	1.05	1.01	1.09	1.11	1.06	0.85	0.86	0.80
Er	2.08	2.14	2.32	2.33	2.42	2.42	2.35	1.98	2.12	1.99
Tm	0.28	0.27	0.29	0.28	0.29	0.29	0.28	0.27	0.27	0.26
Yb	1.61	1.63	1.53	1.58	1.57	1.59	1.58	1.54	1.57	1.58

Table 4-8. (continued)

Location	Yueliangtianchi		Tuofengling					Daxiagu		
GPS	N 47°30'31.50"; E 120°52'0.89"		N 47°27'24.72"; E 120°38'49.38"		N 47°27'26.18"; E 120°38'57.89"			N 47°29'50.77"; E 120°37'39.61"		
sample	YLTC-1	YLTC-3	TFL1-3	TFL1-7	TFL2-1	TFL2-2	TFL2-5	DXG-2	DXG-4	DXG-7
Lu	0.23	0.24	0.22	0.20	0.21	0.21	0.22	0.22	0.21	0.22
Ta	2.4	2.1	4.4	4.5	5.2	4.9	4.8	2.5	2.6	2.3
Taˆ	2.20	2.11	4.11	4.13	4.57	4.49	4.55	2.61	2.40	2.24
Th	3.34	3.20	5.62	6.44	7.03	7.13	6.15	3.44	3.30	3.31
Thˆ	3.3	3.2	5.8	7.0	6.9	6.6	6.1	3.5	3.4	3.4
U	0.85	0.82	1.46	1.53	1.85	1.79	1.60	0.86	0.84	0.81
Uˆ	0.9	0.9	1.7	1.6	1.9	1.8	1.7	0.9	0.9	0.9
$(La/Yb)_N$[b]	11.01	10.87	18.76	19.85	23.68	23.11	21.62	11.56	11.38	10.95
Nb/U	49.18	52.20	51.30	48.76	46.86	47.49	51.31	53.72	54.76	52.22
Ba/Th	125.7	134.1	97.9	102.5	102.8	100.3	108.3	115.4	122.1	116.6
Eu/Eu*[c]	1.00	1.11	1.06	1.02	1.02	1.05	1.05	1.11	1.08	1.07

Table 4-8. (continued)

Location	Guibeishi		Yantanglin		
GPS	N 47°24'54.20"; E 120°32'4.58"		N 47°22'15.10"; E 120°29'8.91"		
sample	GBS-1	GBS-3	YTL-3	YTL-7	YTL-10
SiO_2 (wt.%)	50.59	50.15	49.94	49.80	48.56
TiO_2	2.00	2.00	1.98	2.04	2.03
Al_2O_3	13.24	13.28	13.22	13.01	12.32
$Fe_2O_3^T$	11.83	11.87	11.95	12.17	12.31
MnO	0.16	0.16	0.16	0.17	0.17
MgO	8.62	8.65	8.71	9.29	10.60
CaO	9.08	9.09	8.68	8.85	8.93
Na_2O	3.30	3.23	3.43	3.38	3.13
K_2O	1.34	1.26	1.52	1.52	1.46
P_2O_5	0.37	0.36	0.41	0.40	0.40
LOI	-0.52	-0.42	-0.52	-0.58	-0.29
Total	100.01	99.63	99.48	100.05	99.62
Mg#[a]	63.2	63.2	63.2	64.2	67.0
K^(ppm)	10,600	9,900	11,800	12,000	11,100
Ti^	11,550	12,100	11,600	12,150	11,800
Li^	5.0	5.2	5.8	5.6	5.1
V^	190	198	184	191	192
Cr^	227	236	239	249	300
Co^	46.6	46.3	45.9	48.9	50.9
Ni^	213	216	234	265	343
Sc^	19.9	19.9	18.9	19.6	18.7
Ga	18.8	18.6	19.8	19.5	19.1
Ga^	18.0	18.4	18.7	18.9	17.5
Rb	27.8	24.5	26.9	30.2	28.9
Rb^	28.1	24.5	26.2	30.0	27.6
Sr	396	402	481	469	463
Sr^	396	400	469	465	453
Y	22.0	22.1	24.3	24.3	23.3
Y^	22.1	22.8	23.2	24.0	22.6
Nb	38.8	39.5	50.3	49.5	45.0
Nb^	34.9	35.5	43.6	44.0	38.1
Ba	350	359	358	356	378
Ba^	330	330	330	340	350
La	21.1	21.8	26.1	25.2	24.1
La^	20.7	21.6	25.0	25.3	24.1
Ce	42.0	43.7	51.2	50.6	48.2
Ce^	41.1	42.4	50.5	49.9	47.8
Pr	4.68	4.89	5.75	5.70	5.42
Nd	19.9	20.6	24.1	24.0	23.0
Zr	3.5	3.5	3.9	3.9	3.6
Hf	138	136	161	158	148
Sm	5.11	5.05	5.87	5.60	5.63
Eu	1.78	1.84	2.13	2.03	1.94
Gd	5.40	5.57	6.11	5.98	5.69
Tb	0.77	0.80	0.87	0.87	0.83
Dy	4.50	4.70	4.93	5.05	4.85
Ho	0.85	0.85	0.92	0.94	0.91
Er	2.08	2.18	2.29	2.25	2.18
Tm	0.27	0.29	0.29	0.30	0.28
Yb	1.64	1.69	1.65	1.70	1.60

Table 4-8. (continued)

Location	Guibeishi		Yantanglin		
GPS	N 47°24'54.20"; E 120°32'4.58"		N 47°22'15.10"; E 120°29'8.91"		
sample	GBS-1	GBS-3	YTL-3	YTL-7	YTL-10
Lu	0.23	0.24	0.24	0.22	0.21
Ta	2.4	2.3	2.9	2.8	2.6
Taˆ	2.22	2.24	2.78	2.78	2.41
Th	3.29	3.16	3.45	3.52	3.25
Thˆ	3.3	3.3	3.7	3.7	3.3
U	0.79	0.79	0.89	0.94	0.81
Uˆ	0.9	0.9	1.0	1.1	0.8
$(La/Yb)_N$[b]	9.23	9.26	11.35	10.64	10.81
Nb/U	49.11	50.00	56.52	52.66	55.56
Ba/Th	106.4	113.6	103.8	101.1	116.3
Eu/Eu*[c]	1.03	1.06	1.08	1.07	1.04

[a] $Mg\#=Mg^{2+}/(Mg^{2+}+Fe^{2+})$, assuming $Fe^{3+}/(Fe^{2+}/Fe^{3+})=0.15$

[b] N denotes normalization to chondrite

[c] Eu/Eu*=2*Eu/(Sm+Gd)

ˆ trace element concentrations which were analyzed for samples digested by HNO_3-HF-$HClO_4$, others were measured by the molten lithium metaborate method

4.3.1.2 Chemical compositions of phenocrysts

The major element compositions of cpx and ol phenocrysts are reported in Tables 4-9 and 4-10. The cpx are augitic to diopsidic in composition, with Mg# ranging from 67.7 to 84.0. The CaO contents of all measured olivines are above 0.1 wt.%, suggesting that they are igneous phenocrysts rather than xenocrysts from peridotite xenoliths (Thompson and Gibson, 2000). The Mg# of ol phenocrysts vary from 64.1 to 85.8, and the highest Mg# values of ol and cpx phenocrysts are generally similar, indicating that they have syn-crystallized.

4.3.1.3 Water content of clinopyroxene phenocrysts and melts

The infrared OH absorption bands of cpx phenocrysts in the Chaihe-aershan can be subdivided into three groups: 3630-3620 cm^{-1}, 3540-3520 cm^{-1}, and 3470-3450 cm^{-1} and the band at 3620-3640 cm^{-1} is always predominant (Fig. 4-24), which is similar to those of other cpx phenocrysts in basalts from Shuangliao and Wulanhada, and other basalts from eastern China (Liu et al., 2015b; Xia et al., 2013b). The calculated water concentrations of cpxs and corresponding melts are listed in Table 4-9 and plotted versus Mg# of cpx phenocrysts in Fig.4-25. The water concentrations of the cpx phenocrysts and the corresponding melts for each sample are clearly different.

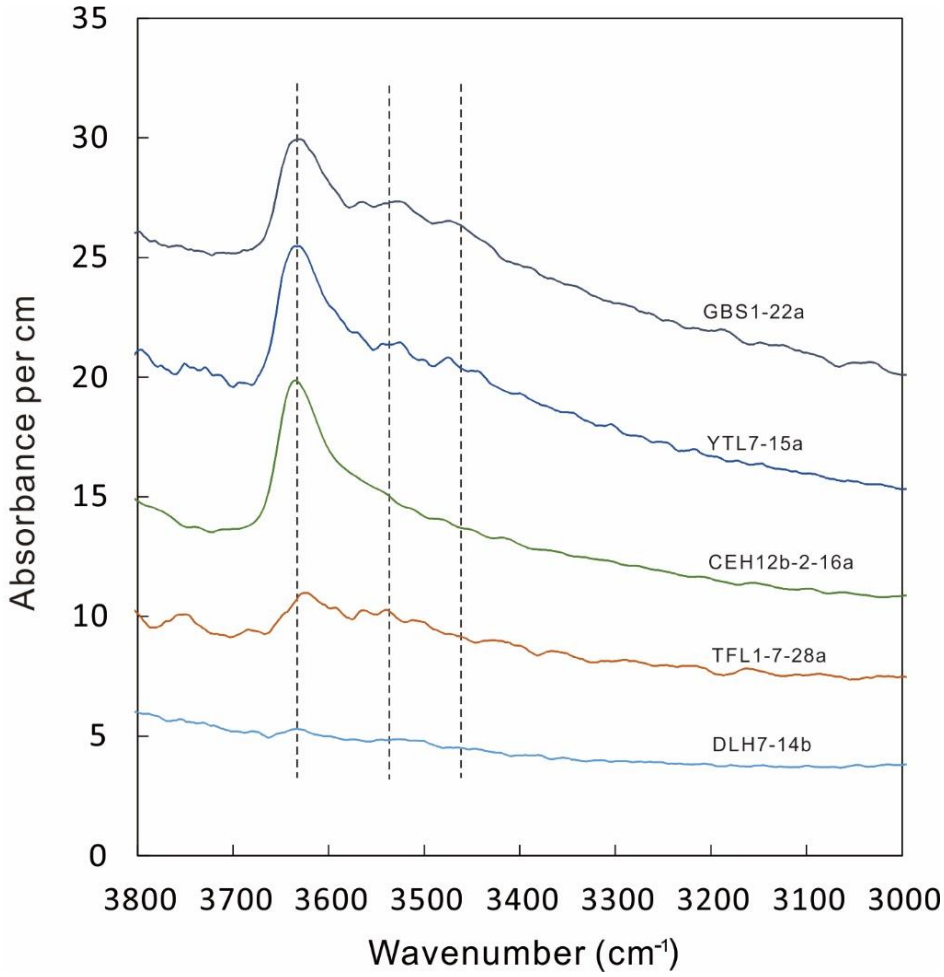

Figure 4-24. Representative IR absorption spectrum of the cpx phenocrysts in the Chaihe-aershan basalts. Dashed lines mark the position of individual OH bands.

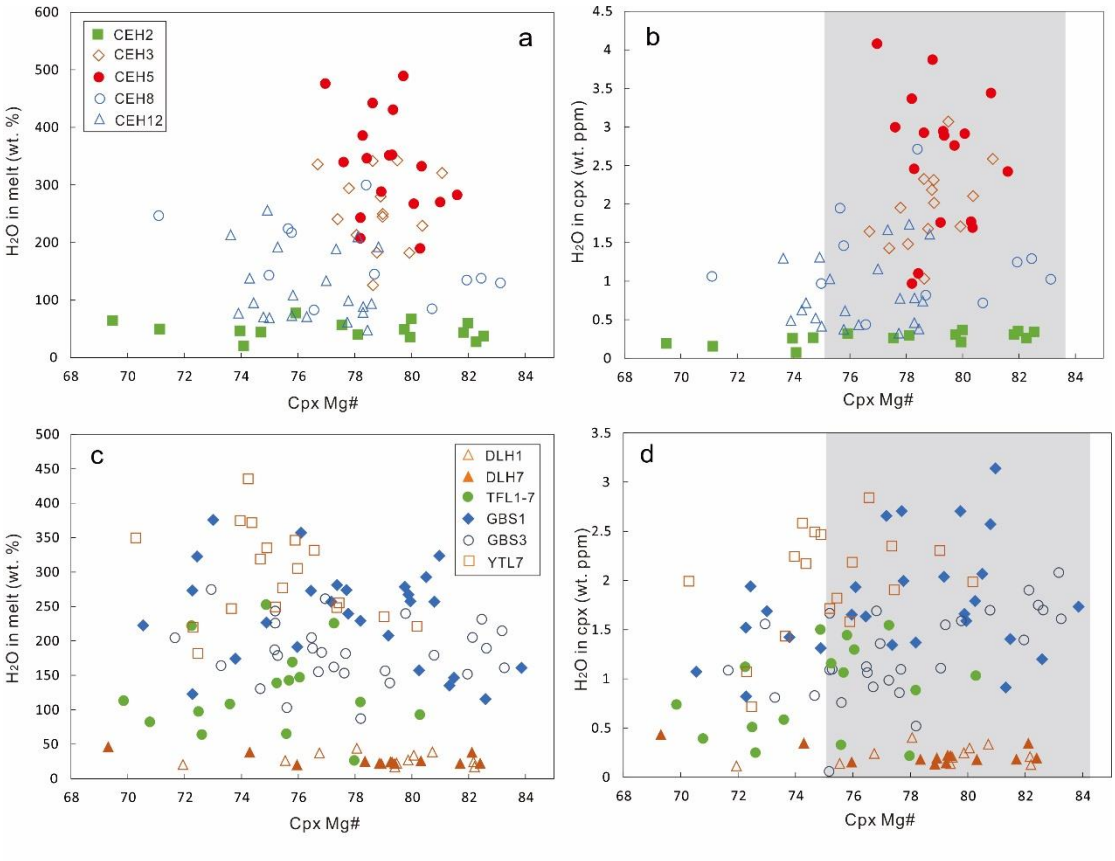

Figure 4-25. H_2O contents of the cpx phenocrysts (a & c) and associated melts (b & d) compared with cpx Mg# in Chaihe-aershan basalts. The labels in b and d are the same as the ones in a and c, respectively. The H_2O contents of the melts do not show any clear trend with Mg#, suggesting that the degassing of magma was limited during magma evolution. The gray area delimit cpx with Mg#>75 which were used to calculate the H_2O content of "primary" melts.

Table 4-9. Major element compositions of cpx phenocrysts and calculated water contents for cpx phenocrysts and corresponding melt of Chaihe-aershan basalts

		SiO_2	Al_2O_3	TiO_2	Cr_2O_3	FeO	NiO	MnO	MgO	CaO	Na_2O	K_2O	Total	Mg#	X(^{iv}Al)	XCa	$D^{cpx/melt}$	A (cm^{-2})	t (cm)	H_2O in cpx (wt. ppm)	H_2O in melt (wt. %)
CEH2	2-05a	49.36	4.50	1.57	1.14	5.62	0.08	0.11	14.33	21.98	0.36	0.01	99.04	81.97	0.15	0.88	0.017	0.709	0.0050	60.02	0.35
	2-22a	48.96	4.53	2.00	0.03	8.55	0.03	0.17	13.63	21.26	0.33	b.l.d.	99.48	73.97	0.16	0.86	0.018	0.551	0.0050	46.64	0.26
	2-22b	50.61	3.35	1.60	0.09	7.28	0.05	0.11	14.56	21.82	0.32	b.l.d.	99.78	78.10	0.12	0.87	0.013	0.472	0.0050	39.95	0.30
	2-23c	51.98	2.19	0.91	0.58	6.18	0.07	0.11	16.39	21.04	0.29	b.l.d.	99.75	82.53	0.08	0.83	0.011	0.471	0.0053	37.61	0.34
	2-23d	52.28	2.51	0.91	0.40	6.15	0.06	0.10	16.01	21.16	0.27	0.01	99.86	82.27	0.07	0.83	0.011	0.345	0.0053	27.52	0.26
	2-35a	45.89	6.96	2.79	0.02	8.83	0.05	0.09	12.21	21.46	0.46	b.l.d.	98.75	71.14	0.25	0.88	0.032	0.611	0.0052	49.73	0.16
	2-35b	46.92	6.13	2.45	0.14	8.16	b.l.d.	0.09	13.09	21.77	0.44	0.02	99.20	74.09	0.23	0.88	0.027	0.250	0.0052	20.33	0.08
	2-35c	47.92	5.37	1.85	0.90	7.01	b.l.d.	0.08	13.57	21.58	0.44	b.l.d.	98.72	77.54	0.19	0.87	0.022	0.701	0.0052	57.03	0.26
	2-35d	49.35	4.53	1.57	0.88	6.51	0.05	0.10	14.59	21.87	0.43	0.01	99.87	79.99	0.16	0.87	0.018	0.824	0.0052	67.04	0.37
	2b-03a	45.59	7.19	2.93	0.03	9.05	0.03	0.07	11.56	22.27	0.44	0.02	99.19	69.48	0.26	0.91	0.034	1.227	0.0081	64.10	0.19
	2b-09a	50.61	3.65	1.06	0.88	6.03	b.l.d.	0.13	15.24	21.82	0.39	b.l.d.	99.80	81.82	0.12	0.87	0.014	0.703	0.0068	43.73	0.31
	2b-10a	49.58	4.14	1.74	0.04	8.35	b.l.d.	0.18	13.83	21.98	0.44	0.01	100.28	74.70	0.15	0.88	0.017	0.754	0.0072	44.28	0.27
	2c-01a	47.43	5.46	2.24	0.75	7.50	b.l.d.	0.13	13.26	22.07	0.45	0.01	99.30	75.92	0.21	0.89	0.024	1.080	0.0059	77.42	0.32
	2c-02a	49.57	4.53	1.50	0.58	6.42	b.l.d.	0.12	14.36	22.37	0.37	b.l.d.	99.83	79.95	0.16	0.89	0.017	0.541	0.0064	35.75	0.21
	2c-05a	50.31	4.38	1.49	0.79	6.55	0.03	0.15	14.47	21.75	0.43	b.l.d.	100.34	79.75	0.14	0.86	0.016	0.728	0.0063	48.90	0.31
CEH3	3-1-02a	51.39	2.65	1.00	1.50	6.46	0.02	0.13	15.52	21.02	0.27	b.l.d.	99.97	81.07	0.10	0.83	0.012	4.623	0.0061	320.69	2.59
	3-1-02b	50.52	4.20	1.73	0.34	7.21	b.l.d.	0.12	14.17	21.83	0.29	0.01	100.43	77.79	0.13	0.86	0.015	4.243	0.0061	294.31	1.95
	3-1-06a	51.72	2.80	1.39	0.25	6.78	0.05	0.11	14.73	21.93	0.30	b.l.d.	100.06	79.49	0.09	0.87	0.011	4.373	0.0054	342.64	3.07
	3-1-06b	52.07	2.55	1.40	0.12	7.05	0.05	0.15	14.85	21.66	0.26	0.02	100.18	78.98	0.08	0.86	0.011	3.124	0.0054	244.80	2.31
	3-1-07a	50.34	4.31	1.62	0.42	6.92	b.l.d.	0.12	13.82	21.59	0.32	b.l.d.	99.46	78.06	0.13	0.86	0.014	3.072	0.0061	213.08	1.48
	3-1-15a	48.16	5.10	2.15	0.28	7.28	0.03	0.14	13.43	22.14	0.36	b.l.d.	99.05	76.70	0.18	0.89	0.020	5.001	0.0063	335.87	1.65
	3-1-16a	51.52	2.69	1.23	0.45	6.46	0.05	0.18	14.84	21.64	0.23	b.l.d.	99.29	80.37	0.08	0.86	0.011	3.357	0.0062	229.10	2.10
	3-2-03a	52.19	2.56	1.22	0.32	6.78	0.05	0.15	15.14	21.61	0.30	0.01	100.31	79.92	0.08	0.85	0.011	2.494	0.0058	181.95	1.71
	3-2-06a	50.35	4.09	1.58	0.43	6.87	0.04	0.09	14.17	21.90	0.39	b.l.d.	99.90	78.63	0.13	0.87	0.015	5.409	0.0067	341.58	2.32
	3-2-14a	51.21	2.64	1.38	0.13	6.95	0.07	0.09	14.46	21.82	0.25	0.01	99.01	78.78	0.08	0.87	0.011	2.412	0.0056	182.25	1.68
	3-3-08a	49.43	4.08	1.68	0.19	7.50	0.04	0.16	14.40	22.02	0.31	0.02	99.82	77.39	0.15	0.88	0.017	4.321	0.0076	240.54	1.43
	3-3-09a	50.75	2.77	1.18	0.17	7.35	0.04	0.12	15.43	21.53	0.27	b.l.d.	99.60	78.91	0.11	0.86	0.013	5.028	0.0076	279.93	2.18
	3-3-15a	51.05	2.68	1.19	0.18	7.29	0.01	0.12	15.37	21.68	0.32	b.l.d.	99.90	78.99	0.10	0.86	0.012	4.776	0.0081	249.51	2.01
	3-3-22a	51.25	3.00	1.11	0.21	7.29	0.03	0.14	15.05	21.66	0.33	b.l.d.	100.06	78.64	0.10	0.86	0.012	2.083	0.0070	125.93	1.03

Table 4-9. (continued)

		SiO_2	Al_2O_3	TiO_2	Cr_2O_3	FeO	NiO	MnO	MgO	CaO	Na_2O	K_2O	Total	Mg#	$X(^{iv}Al)$	XCa	$D^{cpx/melt}$	A (cm^{-2})	t (cm)	H_2O in cpx (wt. ppm)	H_2O in melt (wt. %)
CEH5	5-01a	51.85	1.94	0.91	0.39	6.89	0.05	0.13	16.48	20.65	0.33	0.01	99.61	81.01	0.08	0.82	0.011	2.493	0.0039	270.46	2.47
	5-02a	50.26	3.72	1.60	0.28	7.39	0.01	0.11	13.86	21.97	0.35	b.l.d.	99.56	76.97	0.12	0.88	0.014	4.164	0.0037	476.19	3.44
	5-03a	50.80	2.61	1.21	0.14	6.87	0.06	0.15	15.14	22.02	0.26	b.l.d.	99.26	79.71	0.10	0.88	0.012	4.742	0.0041	489.40	4.08
	5-03b	50.90	3.26	1.47	0.16	7.35	0.03	0.14	14.30	21.48	0.32	b.l.d.	99.40	77.61	0.10	0.86	0.012	3.294	0.0041	339.93	2.76
	5-04a	51.27	2.54	1.33	0.14	7.13	0.01	0.14	15.33	21.53	0.27	b.l.d.	99.67	79.31	0.09	0.86	0.012	3.582	0.0043	352.51	3.00
	5-05a	50.47	3.34	1.54	0.19	7.13	b.l.d.	0.16	14.41	21.62	0.33	b.l.d.	99.18	78.28	0.11	0.87	0.013	3.374	0.0037	385.87	2.94
	5-06a	51.56	2.58	1.12	0.32	6.71	b.l.d.	0.14	15.12	21.55	0.26	0.01	99.38	80.08	0.08	0.86	0.011	2.592	0.0041	267.53	2.46
	5-08a	52.63	2.12	0.91	0.33	6.54	0.07	0.16	16.27	20.13	0.18	b.l.d.	99.33	81.60	0.06	0.80	0.010	2.874	0.0043	282.82	2.91
	5-09a	51.36	2.80	1.43	0.23	7.09	0.05	0.16	14.89	21.81	0.26	b.l.d.	100.07	78.93	0.10	0.87	0.012	2.864	0.0042	288.56	2.42
	5-09b	51.37	2.62	1.25	0.25	6.94	b.l.d.	0.10	14.95	21.59	0.24	b.l.d.	99.31	79.35	0.09	0.86	0.011	4.278	0.0042	430.97	3.87
	5-11a	51.77	2.35	1.04	0.55	7.07	0.05	0.16	16.22	20.12	0.23	b.l.d.	99.57	80.35	0.08	0.80	0.012	3.223	0.0041	332.62	2.89
	5-16a	51.94	2.20	0.90	0.68	7.19	0.07	0.16	16.45	19.61	0.23	b.l.d.	99.43	80.30	0.07	0.78	0.011	2.244	0.0050	189.91	1.69
	5-16b	48.62	4.48	1.84	1.43	6.97	0.06	0.15	14.20	21.05	0.20	b.l.d.	98.98	78.42	0.17	0.85	0.020	4.092	0.0050	346.32	1.77
	5-18a	49.35	5.06	1.60	0.98	7.02	0.06	0.11	14.12	21.19	0.41	b.l.d.	99.91	78.19	0.17	0.84	0.019	2.502	0.0051	207.61	1.10
	5-23a	50.47	2.99	1.47	0.22	7.23	0.03	0.11	14.92	21.44	0.34	0.01	99.20	78.63	0.11	0.86	0.013	4.392	0.0042	442.50	3.37
	5-26a	50.90	2.73	1.35	0.23	7.02	0.05	0.07	15.01	21.53	0.28	0.02	99.17	79.22	0.10	0.86	0.012	3.324	0.0040	351.63	2.93
	5-33a	50.11	3.02	1.44	0.14	7.47	0.01	0.13	15.04	21.35	0.34	0.01	99.05	78.20	0.12	0.86	0.014	2.413	0.0042	243.09	1.76
CEH8	8-02a	50.11	3.45	1.42	0.33	8.50	0.05	0.13	14.29	21.45	0.42	b.l.d.	100.13	74.98	0.13	0.86	0.015	1.287	0.0038	143.30	0.97
	8-03b	47.69	5.71	2.30	0.10	9.35	0.05	0.12	12.90	20.57	0.31	0.01	99.10	71.10	0.20	0.83	0.023	1.808	0.0031	246.78	1.06
	8-05a	49.33	4.42	1.56	0.54	7.04	0.08	0.12	14.59	21.64	0.34	0.01	99.66	78.69	0.16	0.87	0.018	1.511	0.0044	145.26	0.82
	8-06a	48.86	5.10	1.65	0.44	7.53	b.l.d.	0.12	13.79	21.51	0.33	b.l.d.	99.33	76.57	0.17	0.86	0.019	0.783	0.0040	82.80	0.44
	8-07a	51.06	2.86	1.11	0.19	8.11	0.05	0.16	14.14	21.55	0.40	b.l.d.	99.62	75.65	0.09	0.86	0.012	2.703	0.0051	224.24	1.95
	8-09a	51.71	2.26	0.86	0.15	7.80	0.04	0.19	15.88	20.44	0.28	0.01	99.62	78.40	0.08	0.81	0.011	2.622	0.0037	299.90	2.71
	8-11a	49.88	3.75	1.31	0.25	8.13	0.03	0.12	14.26	21.47	0.35	b.l.d.	99.53	75.78	0.13	0.86	0.015	2.106	0.0041	217.29	1.46
	8-12a	51.47	2.83	0.80	0.86	6.00	b.l.d.	0.10	16.58	20.79	0.35	0.01	99.78	83.13	0.10	0.82	0.013	1.383	0.0045	130.03	1.03
	8-12b	52.13	2.11	0.80	0.65	6.53	0.06	0.14	16.61	20.27	0.27	0.01	99.56	81.94	0.07	0.80	0.011	1.435	0.0045	134.90	1.25
	8-12c	52.11	2.15	0.74	0.54	6.23	0.05	0.12	16.41	21.18	0.28	0.01	99.81	82.45	0.08	0.84	0.011	1.466	0.0045	137.88	1.29
	8-13a	51.67	2.23	1.02	0.31	7.02	0.05	0.13	16.49	20.95	0.23	b.l.d.	100.10	80.72	0.09	0.83	0.012	0.804	0.0040	85.05	0.72

Table 4-9. (continued)

		SiO_2	Al_2O_3	TiO_2	Cr_2O_3	FeO	NiO	MnO	MgO	CaO	Na_2O	K_2O	Total	Mg#	$X(^{iv}Al)$	XCa	$D^{cpx/melt}$	A (cm^{-2})	t (cm)	H_2O in cpx (wt. ppm)	H_2O in melt (wt. %)
CEH11	11-1-03a	51.79	2.25	1.14	0.21	6.78	0.05	0.17	16.04	21.15	0.26	0.01	99.85	80.83	0.08	0.84	0.011	1.343	0.0031	183.37	1.63
	11-1-03b	49.09	4.59	1.78	0.36	6.86	b.l.d.	0.12	14.35	22.01	0.36	0.02	99.53	78.87	0.17	0.88	0.018	1.702	0.0031	232.37	1.27
	11-1-03c	51.18	2.92	1.13	0.40	6.30	0.01	0.10	15.35	21.96	0.31	0.02	99.68	81.29	0.10	0.87	0.012	1.834	0.0031	250.29	2.06
	11-1-03d	51.27	3.66	1.31	0.16	7.07	0.03	0.16	14.44	21.78	0.34	b.l.d.	100.21	78.45	0.11	0.86	0.013	1.838	0.0031	250.89	1.99
	11-1-06a	52.58	2.45	0.89	0.30	6.95	0.01	0.11	15.69	20.80	0.29	0.01	100.10	80.09	0.07	0.82	0.010	2.397	0.0028	362.15	3.59
	11-1-07a	51.20	2.52	1.33	0.01	7.92	0.01	0.20	14.67	21.21	0.32	b.l.d.	99.40	76.75	0.09	0.85	0.011	1.617	0.0038	180.10	1.59
	11-1-07b	51.03	2.53	1.36	0.14	6.85	0.07	0.08	15.35	21.68	0.31	b.l.d.	99.39	79.98	0.10	0.87	0.012	3.171	0.0038	353.10	2.95
	11-1-08a	48.14	5.45	2.43	0.44	7.86	0.09	0.16	13.28	21.34	0.44	0.01	99.63	75.08	0.19	0.86	0.022	1.492	0.0032	197.34	0.88
	11-2-02a	50.50	3.59	1.64	0.39	6.45	0.03	0.14	14.62	21.98	0.36	0.02	99.71	80.16	0.12	0.87	0.014	3.148	0.0032	416.29	2.97
	11-2-04a	52.05	2.50	1.15	0.19	6.76	0.03	0.12	15.15	21.26	0.31	b.l.d.	99.52	79.98	0.07	0.84	0.010	2.684	0.0047	241.65	2.36
	11-2-06a	49.87	3.33	1.45	0.33	6.68	0.04	0.09	14.86	22.08	0.36	b.l.d.	99.07	79.87	0.13	0.89	0.014	2.765	0.0031	377.36	2.62
	11-2-07a	51.74	2.45	1.13	0.19	7.02	0.04	0.17	15.45	20.90	0.24	0.01	99.36	79.68	0.08	0.83	0.011	1.755	0.0039	190.41	1.77
	11-2-07b	51.53	2.53	1.20	0.21	7.02	0.02	0.12	15.31	21.04	0.26	b.l.d.	99.23	79.55	0.08	0.84	0.011	1.909	0.0039	207.16	1.88
	11-2-08a	51.74	3.04	1.26	0.17	6.91	0.02	0.13	15.12	21.24	0.30	0.01	99.94	79.61	0.09	0.84	0.012	2.348	0.0032	310.46	2.69
CEH12	12-1-10a	50.20	2.88	1.44	0.04	8.79	b.l.d.	0.18	14.36	20.97	0.36	0.01	99.23	74.44	0.11	0.85	0.013	1.194	0.0053	95.35	0.72
	12-1-11a	49.62	3.56	2.37	0.01	8.49	0.11	0.15	13.49	21.64	0.49	0.01	99.92	73.91	0.14	0.87	0.016	1.093	0.0060	77.05	0.49
	12-1-12a	48.61	5.16	2.46	0.32	7.68	0.03	0.09	12.87	21.77	0.41	0.01	99.42	74.92	0.18	0.88	0.020	1.878	0.0031	256.32	1.31
	12-1-14a	51.50	2.73	1.30	0.15	7.29	0.02	0.10	14.76	21.86	0.28	0.01	99.99	78.29	0.09	0.87	0.011	0.902	0.0043	88.75	0.78

Table 4-9. (continued)

		SiO_2	Al_2O_3	TiO_2	Cr_2O_3	FeO	NiO	MnO	MgO	CaO	Na_2O	K_2O	Total	Mg#	X(^{iv}Al)	XCa	$D^{cpx/melt}$	A (cm^{-2})	t (cm)	H_2O in cpx (wt. ppm)	H_2O in melt (wt. %)
CEH12	12-1-14b	48.55	4.88	2.03	0.31	7.73	0.06	0.15	13.22	21.60	0.40	b.l.d.	98.93	75.29	0.17	0.87	0.019	1.953	0.0043	192.16	1.03
	12-1-14c	51.50	2.90	1.41	0.12	7.68	0.04	0.14	14.42	21.46	0.40	0.01	100.07	76.99	0.09	0.85	0.012	1.358	0.0043	133.62	1.16
	12-2-08a	50.98	3.00	1.34	0.22	7.57	b.l.d.	0.14	14.87	21.51	0.33	0.01	99.95	77.78	0.11	0.86	0.013	1.284	0.0055	98.77	0.78
	12-2-08b	49.59	4.70	1.75	0.61	6.89	0.04	0.15	13.94	21.57	0.35	b.l.d.	99.58	78.29	0.15	0.86	0.017	1.021	0.0055	78.54	0.46
	12-2-09a	48.71	4.85	2.22	0.23	7.71	0.04	0.12	13.53	21.94	0.30	0.01	99.67	75.78	0.18	0.88	0.019	0.928	0.0054	72.74	0.37
	12b-2-12a	51.63	2.65	1.41	0.20	7.60	0.02	0.15	14.55	21.81	0.32	0.01	100.34	77.34	0.09	0.86	0.011	2.855	0.0064	188.76	1.67
	12b-2-16b	49.13	4.06	1.89	0.03	8.59	0.04	0.16	13.46	21.50	0.40	0.02	99.27	73.63	0.15	0.87	0.016	3.076	0.0061	213.35	1.30
	12b-1-05a	49.10	4.77	1.54	0.93	7.31	b.l.d.	0.15	14.32	21.07	0.36	b.l.d.	99.56	77.74	0.17	0.84	0.019	0.918	0.0063	61.64	0.33
	12b-1-09a	51.05	3.15	1.46	0.26	7.07	0.10	0.11	14.55	22.01	0.38	0.01	100.14	78.59	0.11	0.87	0.013	1.263	0.0057	93.78	0.74
	12b-1-11a	49.18	3.89	1.88	0.07	8.34	0.08	0.13	14.02	21.36	0.35	0.01	99.31	74.99	0.15	0.86	0.017	1.001	0.0061	69.46	0.42
	12b-1-05b	49.14	4.23	1.95	0.18	7.86	0.05	0.13	13.82	22.13	0.41	0.01	99.91	75.83	0.16	0.89	0.018	1.618	0.0063	108.66	0.62
	12b-2-08a	49.65	4.49	1.10	0.16	8.04	0.02	0.19	14.52	20.83	0.38	b.l.d.	99.38	76.31	0.14	0.84	0.016	1.159	0.0069	71.05	0.43
	12b-2-10a	51.17	3.17	1.49	0.20	7.22	0.01	0.12	14.74	21.62	0.31	b.l.d.	100.04	78.45	0.10	0.86	0.013	0.781	0.0069	47.88	0.38
	12b-2-12b	50.75	2.82	1.33	0.21	7.07	0.08	0.13	14.77	21.50	0.26	b.l.d.	98.92	78.84	0.10	0.86	0.012	2.912	0.0064	192.51	1.61
	12b-2-13a	47.69	5.12	2.28	0.22	8.09	0.05	0.10	13.11	22.16	0.43	0.01	99.26	74.30	0.20	0.90	0.022	1.695	0.0052	137.95	0.63
	12b-2-14a	50.72	3.25	1.50	0.22	8.54	0.01	0.17	14.20	21.41	0.36	0.01	100.39	74.78	0.12	0.85	0.014	1.083	0.0065	70.47	0.52
	12b-2-16a	51.02	2.93	1.12	0.21	7.48	0.09	0.15	14.96	21.17	0.25	b.l.d.	99.37	78.10	0.10	0.85	0.012	3.020	0.0061	209.48	1.74
DLH1	1-01a	51.82	2.86	0.99	0.15	7.00	0.02	0.17	15.78	20.70	0.26	0.01	99.75	80.07	0.08	0.82	0.011	0.560	0.0070	33.87	0.30
	1-01b	52.35	2.86	0.92	0.29	7.27	0.08	0.17	15.79	20.25	0.25	b.l.d.	100.22	79.47	0.08	0.80	0.011	0.369	0.0070	22.32	0.20
	1-01c	49.87	3.93	1.35	0.56	7.78	0.02	0.14	14.40	21.35	0.32	0.01	99.73	76.75	0.14	0.85	0.016	0.618	0.0070	37.36	0.24

Table 4-9. (continued)

		SiO_2	Al_2O_3	TiO_2	Cr_2O_3	FeO	NiO	MnO	MgO	CaO	Na_2O	K_2O	Total	Mg#	$X(^{iv}Al)$	XCa	$D^{cpx/melt}$	A (cm^{-2})	t (cm)	H_2O in cpx (wt. ppm)	H_2O in melt (wt. %)
DLH1	1-02a	48.93	4.16	1.79	0.12	9.67	0.10	0.15	13.91	20.25	0.34	0.01	99.41	71.95	0.15	0.82	0.018	0.332	0.0069	20.36	0.11
	1-03a	52.12	2.82	0.97	0.26	7.02	0.02	0.16	15.61	20.56	0.25	b.l.d.	99.78	79.87	0.08	0.81	0.011	0.426	0.0067	26.90	0.25
	1-04a	48.73	4.58	1.88	0.42	8.07	b.l.d.	0.15	13.99	20.93	0.40	b.l.d.	99.14	75.55	0.17	0.84	0.019	0.353	0.0057	26.17	0.14
	1-06a	51.65	2.41	1.31	0.22	7.47	0.05	0.15	14.90	21.44	0.31	b.l.d.	99.90	78.07	0.08	0.85	0.011	0.697	0.0067	44.00	0.40
	1-07d	51.09	3.55	0.91	0.75	6.15	b.l.d.	0.11	15.93	20.66	0.49	0.01	99.63	82.21	0.11	0.82	0.014	0.240	0.0059	17.23	0.13
	1-12a	52.29	2.75	0.83	0.27	7.07	0.09	0.14	16.61	19.87	0.28	b.l.d.	100.21	80.72	0.08	0.78	0.012	0.658	0.0072	38.67	0.33
	1b-01a	51.44	3.10	1.07	0.18	7.31	b.l.d.	0.12	15.81	20.71	0.31	b.l.d.	100.05	79.40	0.10	0.82	0.013	0.218	0.0054	17.07	0.13
	1b-02a	48.28	5.34	2.21	0.43	8.50	0.02	0.15	13.59	21.09	0.37	b.l.d.	99.97	74.02	0.19	0.85	0.023	-	-	-	-
	1b-05a	51.02	2.59	1.07	0.23	7.68	b.l.d.	0.14	15.62	20.79	0.33	b.l.d.	99.46	78.37	0.10	0.83	0.012	-	-	-	-
	1b-07a	51.68	2.63	0.96	0.53	6.26	0.07	0.14	16.18	20.96	0.27	0.01	99.67	82.17	0.09	0.83	0.012	0.316	0.0055	24.32	0.21
DLH7	7-03a	51.81	3.03	1.03	0.34	7.09	b.l.d.	0.13	14.90	21.34	0.34	b.l.d.	100.00	78.93	0.09	0.84	0.011	0.331	0.0065	21.55	0.19
	7-04a	52.26	2.50	1.02	0.42	6.87	0.03	0.14	14.85	21.63	0.30	0.01	100.02	79.40	0.07	0.86	0.010	0.342	0.0067	21.62	0.22
	7-04b	51.12	3.05	1.15	0.48	7.46	0.07	0.16	14.94	20.71	0.29	b.l.d.	99.44	78.13	0.10	0.83	0.012	-	-	-	-
	7-05a	49.56	4.35	1.63	0.50	6.79	0.02	0.09	14.20	22.49	0.36	0.02	99.99	78.86	0.16	0.90	0.017	0.304	0.0058	22.18	0.13
	7-07a	50.26	4.73	0.93	0.41	7.43	0.02	0.12	15.92	18.98	0.37	b.l.d.	99.16	79.25	0.13	0.76	0.017	0.386	0.0068	24.04	0.14
	7-08a	50.25	3.75	1.41	0.16	7.88	0.08	0.16	14.11	22.01	0.36	0.01	100.17	76.14	0.13	0.88	0.014	-	-	-	-
	7-09a	50.60	2.80	1.56	0.46	8.16	b.l.d.	0.15	14.45	21.44	0.34	b.l.d.	99.96	75.96	0.11	0.86	0.013	0.355	0.0075	20.03	0.15
	7-11a	51.89	1.99	0.76	0.38	6.88	b.l.d.	0.12	16.28	20.86	0.22	b.l.d.	99.38	80.84	0.07	0.83	0.011	-	-	-	-
	7-13a	51.08	3.86	0.72	0.87	7.07	0.03	0.14	16.18	19.39	0.36	b.l.d.	99.70	80.32	0.11	0.77	0.014	0.435	0.0072	25.55	0.18
	7-14a	50.75	2.92	0.32	0.10	10.15	b.l.d.	0.25	12.85	21.47	0.60	0.01	99.42	69.32	0.08	0.87	0.011	0.814	0.0075	45.90	0.43
	7-14b	51.17	2.97	0.74	0.62	6.27	0.05	0.12	15.71	21.39	0.35	b.l.d.	99.38	81.70	0.10	0.85	0.012	0.389	0.0075	21.97	0.18
	7-14c	51.18	3.33	0.27	0.11	10.66	0.02	0.24	12.51	20.55	0.91	b.l.d.	99.77	67.67	0.07	0.83	0.011	0.753	0.0075	42.49	0.40
	7-16a	49.73	5.16	1.37	0.08	8.30	b.l.d.	0.07	15.01	19.81	0.39	0.01	99.93	76.33	0.15	0.79	0.019	-	-	-	-
	7-17a	51.13	3.81	1.07	0.63	7.52	0.06	0.13	15.26	20.20	0.37	b.l.d.	100.17	78.35	0.11	0.80	0.014	0.315	0.0053	25.12	0.18
	7-22a	50.79	4.35	0.82	0.85	6.99	0.05	0.11	15.30	19.41	0.43	0.02	99.11	79.59	0.11	0.77	0.014	-	-	-	-
	7-23a	52.44	3.02	0.59	0.67	6.28	0.01	0.13	16.18	20.43	0.38	b.l.d.	100.13	82.12	0.08	0.80	0.011	0.547	0.0061	37.96	0.34
	7-24a	52.70	2.82	0.55	0.12	7.91	0.05	0.17	17.01	17.96	0.31	0.01	99.59	79.31	0.06	0.71	0.011	0.365	0.0064	24.14	0.22
	7-24b	52.63	2.69	0.60	0.60	6.60	b.l.d.	0.10	17.35	19.27	0.36	b.l.d.	100.19	82.41	0.08	0.75	0.012	0.334	0.0064	22.05	0.19
	7-27a	50.70	2.13	1.35	b.l.d.	8.75	0.03	0.15	14.18	21.34	0.39	b.l.d.	99.01	74.29	0.09	0.86	0.011	0.427	0.0047	38.41	0.34

Table 4-9. (continued)

		SiO_2	Al_2O_3	TiO_2	Cr_2O_3	FeO	NiO	MnO	MgO	CaO	Na_2O	K_2O	Total	Mg#	$X(^{iv}Al)$	XCa	$D^{cpx/melt}$	A (cm^{-2})	t (cm)	H_2O in cpx (wt. ppm)	H_2O in melt (wt. %)
DXG2	05a	49.12	5.21	2.06	0.35	6.87	0.09	0.13	13.27	21.93	0.28	0.01	99.30	77.50	0.16	0.88	0.018	-	-	-	-
	09a	49.62	3.68	1.50	0.07	9.42	b.l.d.	0.19	14.17	20.06	0.43	b.l.d.	99.14	72.83	0.13	0.81	0.015	-	-	-	-
	13a	52.91	2.37	0.82	0.41	6.13	0.07	0.12	15.68	21.20	0.34	0.01	100.05	82.01	0.06	0.83	0.009	-	-	-	-
	13b	47.97	6.30	2.29	0.43	7.58	0.05	0.11	13.00	21.77	0.48	b.l.d.	99.97	75.36	0.21	0.87	0.024	-	-	-	-
	16a	49.44	5.11	1.89	0.65	6.41	0.08	0.06	13.88	21.64	0.41	b.l.d.	99.57	79.43	0.16	0.86	0.018	-	-	-	-
	21a	52.27	2.41	0.87	0.26	6.27	0.03	0.17	16.19	21.18	0.28	b.l.d.	99.92	82.16	0.07	0.84	0.011	-	-	-	-
	21b	50.98	4.12	1.23	0.61	5.69	b.l.d.	0.12	15.07	22.26	0.40	0.01	100.48	82.53	0.13	0.88	0.014	-	-	-	-
	24a	51.80	2.65	1.17	0.08	7.16	0.03	0.14	15.30	21.31	0.37	0.01	100.00	79.20	0.08	0.84	0.011	-	-	-	-
	34a	50.57	5.15	1.43	0.53	7.48	0.01	0.16	14.92	19.53	0.41	b.l.d.	100.20	78.06	0.14	0.77	0.017	-	-	-	-
	34b	51.47	4.15	0.90	0.96	6.37	0.06	0.16	15.67	20.36	0.39	b.l.d.	100.48	81.44	0.11	0.80	0.014	-	-	-	-
	34c	52.06	3.55	0.65	0.85	5.90	0.06	0.07	15.80	20.28	0.37	b.l.d.	99.61	82.70	0.08	0.80	0.012	-	-	-	-
GBS1	1-01a	48.30	5.85	2.26	0.22	8.55	0.03	0.11	12.97	21.18	0.38	b.l.d.	99.86	73.01	0.19	0.85	0.022	2.664	0.0030	375.78	1.69
	1-02b	48.99	3.28	1.48	0.11	9.81	b.l.d.	0.13	14.46	20.54	0.40	0.01	99.21	72.44	0.14	0.83	0.017	2.135	0.0028	322.62	1.94
	1-03a	49.82	4.16	1.22	0.96	6.65	0.07	0.12	14.86	21.18	0.38	0.02	99.44	79.95	0.14	0.85	0.016	1.583	0.0026	257.67	1.59
	1-03b	48.34	5.45	1.91	0.16	9.58	0.03	0.15	12.87	20.65	0.42	0.01	99.56	70.54	0.18	0.83	0.021	1.368	0.0026	222.66	1.07
	1-04a	49.71	4.49	1.35	0.52	7.90	0.02	0.10	14.39	20.77	0.34	b.l.d.	99.58	76.45	0.14	0.83	0.017	2.192	0.0034	272.84	1.63
	1-07a	50.80	3.91	1.10	1.12	6.35	b.l.d.	0.12	14.70	21.81	0.31	0.01	100.22	80.51	0.12	0.86	0.014	2.630	0.0038	292.81	2.07
	1-09a	49.53	5.06	1.77	0.29	9.13	0.03	0.14	13.36	20.39	0.38	0.02	100.09	72.28	0.15	0.81	0.018	1.873	0.0029	273.28	1.52
	1-10a	49.86	3.67	0.99	1.19	6.08	b.l.d.	0.08	14.86	22.02	0.35	b.l.d.	99.10	81.33	0.13	0.88	0.015	1.469	0.0046	135.08	0.91
	1-10b	52.71	2.23	0.98	0.53	6.60	b.l.d.	0.07	16.28	20.88	0.23	b.l.d.	100.49	81.49	0.07	0.82	0.010	1.592	0.0046	146.39	1.40
	1-11a	51.35	2.79	1.29	0.09	9.29	0.03	0.14	14.67	20.42	0.32	b.l.d.	100.38	73.79	0.09	0.81	0.012	1.564	0.0038	174.17	1.42
	1-12a	49.16	4.74	2.08	0.30	7.80	0.01	0.07	13.04	22.01	0.35	b.l.d.	99.56	74.89	0.16	0.88	0.017	1.769	0.0033	226.88	1.31
	1-14a	51.25	2.30	1.12	0.07	8.80	b.l.d.	0.19	15.60	19.41	0.29	0.01	99.01	75.97	0.08	0.78	0.012	2.080	0.0046	191.33	1.65
	1-16a	50.47	4.22	1.86	0.09	9.47	0.07	0.17	13.85	19.04	0.37	0.03	99.63	72.28	0.12	0.76	0.015	1.105	0.0038	123.00	0.82
	1-21a	53.44	2.17	0.86	0.25	6.81	b.l.d.	0.13	15.52	21.06	0.21	0.01	100.45	80.26	0.04	0.83	0.009	1.488	0.0040	157.45	1.79
	1-22a	48.23	5.17	1.97	0.49	7.21	b.l.d.	0.11	13.82	21.75	0.39	b.l.d.	99.14	77.37	0.19	0.88	0.021	2.991	0.0045	281.23	1.34
	1-23a	52.95	2.11	0.73	0.65	5.51	0.04	0.11	16.07	21.44	0.30	b.l.d.	99.90	83.86	0.06	0.84	0.009	1.483	0.0039	160.87	1.73
	1-24a	51.74	3.50	1.36	0.18	7.41	0.09	0.13	14.54	21.19	0.27	b.l.d.	100.40	77.76	0.09	0.84	0.012	1.812	0.0032	239.61	1.99
	1-25a	52.97	2.08	0.72	0.74	6.07	0.06	0.11	16.17	21.16	0.28	b.l.d.	100.36	82.60	0.06	0.83	0.010	1.093	0.0040	115.62	1.20
	1-27a	52.45	2.41	0.94	0.51	6.61	0.03	0.06	15.77	21.01	0.26	b.l.d.	100.04	80.97	0.07	0.83	0.010	2.753	0.0036	323.58	3.14

Table 4-9. (continued)

		SiO_2	Al_2O_3	TiO_2	Cr_2O_3	FeO	NiO	MnO	MgO	CaO	Na_2O	K_2O	Total	Mg#	$X(^{iv}Al)$	XCa	$D^{cpx/melt}$	A (cm^{-2})	t (cm)	H_2O in cpx (wt. ppm)	H_2O in melt (wt. %)
	1-28a	52.17	2.09	0.77	0.18	8.04	0.03	0.13	15.71	20.36	0.23	b.l.d.	99.69	77.70	0.06	0.81	0.010	2.007	0.0031	273.98	2.70
	1b-01a	52.47	2.24	1.07	0.15	7.95	0.02	0.18	15.08	20.22	0.32	0.01	99.72	77.17	0.06	0.80	0.010	3.465	0.0057	257.22	2.65
GBS1	1b-02a	49.76	4.62	1.78	0.42	8.35	0.05	0.18	14.92	19.49	0.38	b.l.d.	99.94	76.10	0.15	0.78	0.018	2.700	0.0032	357.07	1.93
	1b-05a	49.78	4.63	1.75	0.73	6.92	b.l.d.	0.10	13.91	21.71	0.35	b.l.d.	99.89	78.19	0.15	0.86	0.017	3.521	0.0065	229.21	1.37
	3-02a	48.83	4.69	1.94	0.06	9.39	b.l.d.	0.10	13.31	21.06	0.44	b.l.d.	99.80	71.66	0.17	0.85	0.019	3.093	0.0064	204.48	1.09
	3-02b	49.68	4.62	1.43	0.69	7.15	b.l.d.	0.13	14.39	20.97	0.32	b.l.d.	99.38	78.20	0.15	0.84	0.017	1.320	0.0064	87.24	0.52
	3-03a	49.93	4.55	1.66	0.49	7.66	0.09	0.09	14.15	21.44	0.30	b.l.d.	100.35	76.71	0.15	0.85	0.017	2.016	0.0055	155.10	0.92
	3-06a	48.63	5.06	2.14	0.16	8.68	0.05	0.13	13.35	21.30	0.41	0.02	99.92	73.28	0.18	0.85	0.020	2.597	0.0067	164.01	0.81
	3-06b	49.87	4.71	1.68	0.37	7.20	b.l.d.	0.13	14.05	21.72	0.24	b.l.d.	99.97	77.67	0.15	0.86	0.017	2.876	0.0067	181.63	1.10
	3-06c	49.31	4.91	1.84	0.69	7.00	0.02	0.08	13.61	21.83	0.42	0.01	99.69	77.62	0.16	0.87	0.018	2.427	0.0067	153.27	0.86
	3-07a	52.35	2.24	0.73	0.79	6.30	0.04	0.11	16.24	21.46	0.23	b.l.d.	100.48	82.13	0.08	0.84	0.011	3.343	0.0069	205.00	1.90
	3-08a	51.86	2.48	0.89	0.19	8.15	b.l.d.	0.12	15.16	20.88	0.30	0.04	100.06	76.82	0.08	0.83	0.011	3.205	0.0074	183.26	1.69
	3-10a	52.14	2.30	0.73	0.44	6.82	0.03	0.13	16.08	20.80	0.29	b.l.d.	99.76	80.78	0.07	0.82	0.011	2.372	0.0056	179.23	1.70
	3-12a	49.16	5.00	2.07	0.65	7.25	0.03	0.11	13.22	21.80	0.40	0.03	99.71	76.47	0.16	0.87	0.018	2.565	0.0053	204.78	1.12
	3-15a	52.91	2.40	0.57	0.47	7.14	0.03	0.15	15.27	20.22	0.30	0.01	99.47	79.22	0.04	0.80	0.009	1.773	0.0054	138.93	1.55
	3-16a	50.61	3.69	1.35	0.38	8.17	b.l.d.	0.13	14.19	20.71	0.34	0.01	99.58	75.60	0.11	0.83	0.014	1.243	0.0051	103.13	0.76
	3-18a	49.35	5.04	1.89	0.63	7.47	0.03	0.11	13.99	21.45	0.38	b.l.d.	100.35	76.95	0.17	0.85	0.019	2.594	0.0042	261.28	1.36
GBS3	3-22a	49.72	4.43	1.63	0.49	8.00	0.05	0.11	13.66	21.34	0.40	b.l.d.	99.83	75.28	0.14	0.85	0.016	2.155	0.0051	178.79	1.10
	3-24a	50.46	4.14	1.21	0.75	6.69	0.05	0.10	14.16	21.76	0.35	0.02	99.67	79.06	0.12	0.87	0.014	2.407	0.0065	156.69	1.11
	3-29a	48.59	5.44	2.14	0.41	7.82	0.07	0.13	13.30	21.40	0.37	0.02	99.69	75.19	0.18	0.86	0.021	3.361	0.0063	225.74	1.09
	3-30a	49.21	4.27	1.76	0.17	9.15	b.l.d.	0.12	13.83	20.84	0.45	b.l.d.	99.78	72.94	0.15	0.84	0.018	3.118	0.0048	274.82	1.56
	3b-02a	49.62	4.90	1.75	0.54	7.57	b.l.d.	0.10	13.83	21.55	0.36	b.l.d.	100.23	76.51	0.16	0.86	0.018	2.014	0.0045	189.35	1.06
	3b-04a	51.80	2.25	0.92	0.53	6.34	b.l.d.	0.13	16.16	20.99	0.22	b.l.d.	99.34	81.96	0.08	0.83	0.011	2.224	0.0062	151.79	1.39
	3b-07a	49.90	4.05	1.49	0.32	8.54	b.l.d.	0.16	14.11	20.92	0.36	b.l.d.	99.85	74.67	0.14	0.84	0.016	2.224	0.0072	130.70	0.83
	3b-08a	49.62	4.59	1.14	0.38	7.51	0.03	0.09	14.30	21.56	0.38	b.l.d.	99.60	77.25	0.15	0.86	0.016	2.031	0.0053	162.15	0.98
	3b-09a	52.38	2.01	0.80	0.63	5.82	b.l.d.	0.09	16.23	21.47	0.29	b.l.d.	99.71	83.25	0.07	0.85	0.010	1.901	0.0050	160.89	1.61
	3b-10a	49.72	3.42	1.49	0.02	8.38	b.l.d.	0.15	14.25	21.37	0.41	b.l.d.	99.21	75.19	0.13	0.86	0.015	3.280	0.0057	243.46	1.67
	3b-11a	50.02	4.12	1.23	0.74	6.60	0.02	0.10	14.61	21.44	0.31	0.01	99.21	79.78	0.13	0.86	0.015	2.946	0.0052	239.71	1.59
	3b-12a	52.09	2.32	0.68	0.80	5.77	0.07	0.11	16.00	21.28	0.28	b.l.d.	99.39	83.17	0.07	0.84	0.010	2.335	0.0046	214.78	2.08
	3b-12b	50.59	3.48	0.99	0.99	5.64	0.01	0.16	14.88	22.31	0.33	b.l.d.	99.38	82.46	0.12	0.89	0.013	2.519	0.0046	231.70	1.75
	3b-13a	51.66	2.15	0.84	0.59	6.12	0.02	0.12	16.32	21.50	0.26	b.l.d.	99.57	82.63	0.09	0.85	0.011	1.879	0.0042	189.34	1.70

Table 4-9. (continued)

		SiO_2	Al_2O_3	TiO_2	Cr_2O_3	FeO	NiO	MnO	MgO	CaO	Na_2O	K_2O	Total	Mg#	X(^{iv}Al)	XCa	$D^{cpx/melt}$	A (cm^{-2})	t (cm)	H_2O in cpx (wt. ppm)	H_2O in melt (wt. %)
TFL1-7	05a	49.50	4.34	1.62	0.05	9.36	b.l.d.	0.23	12.17	22.00	0.76	0.02	100.04	69.85	0.14	0.89	0.015	1.123	0.0042	113.14	0.74
	06a	50.66	3.59	1.19	0.23	7.01	0.03	0.12	14.09	21.62	0.62	b.l.d.	99.15	78.19	0.11	0.87	0.013	1.131	0.0043	111.29	0.89
	12a	50.72	4.07	1.27	0.10	7.98	0.02	0.07	13.92	20.65	0.71	0.02	99.52	75.67	0.11	0.82	0.013	1.452	0.0043	142.83	1.06
	12b	50.97	4.79	0.89	0.47	7.60	0.09	0.11	14.47	19.60	0.92	b.l.d.	99.91	77.26	0.12	0.78	0.015	2.295	0.0043	225.83	1.54
	12c	49.33	5.49	1.56	b.l.d.	9.45	b.l.d.	0.16	13.80	19.70	0.78	b.l.d.	100.27	72.24	0.16	0.79	0.020	2.257	0.0043	222.07	1.12
	14a	51.22	2.31	0.84	0.03	8.52	0.02	0.13	15.17	20.85	0.54	b.l.d.	99.63	76.05	0.09	0.83	0.011	1.671	0.0048	147.34	1.30
	16a	49.19	4.94	1.96	0.04	7.71	0.01	0.09	12.89	21.80	0.57	0.01	99.21	74.87	0.15	0.88	0.017	2.629	0.0044	252.82	1.50
	17a	52.85	1.94	0.77	0.37	6.74	0.10	0.11	15.40	21.37	0.35	b.l.d.	100.01	80.28	0.05	0.84	0.009	1.010	0.0046	92.90	1.03
	17b	51.23	2.49	1.19	0.12	8.45	0.04	0.12	14.84	21.16	0.31	0.01	99.97	75.79	0.09	0.84	0.012	1.842	0.0046	169.40	1.44
	18a	50.69	2.84	1.40	b.l.d.	8.12	0.04	0.12	13.85	22.19	0.46	b.l.d.	99.71	75.24	0.10	0.89	0.012	1.543	0.0047	138.91	1.16
	19a	48.12	4.99	2.19	b.l.d.	9.31	0.09	0.11	12.65	22.23	0.54	b.l.d.	100.21	70.78	0.19	0.90	0.021	0.856	0.0044	82.32	0.39
	23a	48.63	4.77	1.94	0.49	8.08	0.03	0.09	14.03	20.48	0.58	b.l.d.	99.13	75.58	0.17	0.83	0.020	0.741	0.0048	65.32	0.33
	27a	46.73	5.39	2.58	0.36	8.51	0.03	0.10	12.65	22.37	0.43	b.l.d.	99.15	72.60	0.22	0.91	0.026	0.788	0.0052	64.14	0.25
	28a	48.83	5.28	1.99	0.02	8.67	0.05	0.13	12.81	21.49	0.61	0.01	99.89	72.49	0.17	0.86	0.019	1.107	0.0048	97.58	0.51
	28b	48.47	4.92	1.70	0.06	8.38	0.04	0.13	13.11	21.53	0.63	b.l.d.	98.96	73.59	0.17	0.87	0.019	1.229	0.0048	108.34	0.59
	32a	50.75	2.73	1.24	0.36	7.36	0.04	0.14	14.61	21.82	0.41	b.l.d.	99.45	77.97	0.10	0.87	0.012	-	-	-	-
YLTC3	3-02a	52.53	2.18	0.90	0.32	6.06	0.03	0.11	16.07	21.06	0.25	0.01	99.51	82.53	0.06	0.83	0.010	-	-	-	-
	3-02b	52.12	2.27	0.95	0.29	6.23	b.l.d.	0.08	16.00	21.29	0.26	0.02	99.51	82.08	0.07	0.84	0.010	-	-	-	-
	3-02c	49.56	4.72	1.45	0.52	6.89	0.04	0.10	14.87	21.13	0.34	0.01	99.63	79.37	0.16	0.84	0.018	-	-	-	-
	3-03a	51.12	1.97	0.83	0.54	5.79	0.05	0.08	16.12	21.22	0.29	b.l.d.	97.99	83.24	0.08	0.85	0.011	-	-	-	-
	3-04a	53.06	2.18	0.70	0.41	5.80	0.05	0.05	16.08	21.23	0.26	b.l.d.	99.81	83.18	0.05	0.83	0.009	-	-	-	-
	3-04b	51.66	3.07	0.99	0.11	7.25	0.02	0.14	15.35	21.23	0.28	b.l.d.	100.09	79.06	0.09	0.84	0.012	-	-	-	-
	3-05a	52.77	2.09	0.73	0.63	5.80	0.03	0.13	16.62	21.04	0.30	0.01	100.14	83.64	0.07	0.83	0.010	-	-	-	-
	3-05b	51.49	2.56	0.76	0.26	6.39	0.01	0.14	16.25	20.95	0.25	b.l.d.	99.05	81.93	0.08	0.83	0.011	-	-	-	-
	3-08a	53.00	2.17	0.46	0.46	5.45	b.l.d.	0.09	16.04	21.16	0.35	b.l.d.	99.17	84.00	0.04	0.84	0.009	-	-	-	-
YTL7	01a	49.19	3.86	1.54	0.07	8.79	0.01	0.15	14.01	21.70	0.44	0.01	99.76	73.96	0.15	0.87	0.017	2.836	0.0032	375.00	2.24
	01b	50.96	2.35	0.82	0.21	8.39	0.03	0.21	15.39	20.41	0.32	b.l.d.	99.10	76.57	0.09	0.82	0.012	2.510	0.0032	331.88	2.84
	02a	49.91	3.40	1.40	0.04	8.06	0.05	0.10	14.29	21.43	0.36	b.l.d.	99.04	75.98	0.12	0.86	0.014	2.453	0.0034	305.25	2.18
	06a	50.98	2.90	1.24	0.08	8.99	0.01	0.14	14.87	20.41	0.35	0.02	99.99	74.67	0.10	0.81	0.013	3.393	0.0045	319.04	2.49

Table 4-9. (continued)

		SiO_2	Al_2O_3	TiO_2	Cr_2O_3	FeO	NiO	MnO	MgO	CaO	Na_2O	K_2O	Total	Mg#	$X(^{iv}Al)$	XCa	$D^{cpx/melt}$	A (cm^{-2})	t (cm)	H_2O in cpx (wt. ppm)	H_2O in melt (wt. %)
	07a	51.92	2.50	0.84	0.36	7.09	0.06	0.07	14.98	21.47	0.30	b.l.d.	99.60	79.03	0.07	0.85	0.010	2.335	0.0042	235.22	2.30
	07b	50.57	3.65	1.18	0.59	7.41	0.05	0.12	14.27	21.37	0.33	b.l.d.	99.55	77.44	0.11	0.85	0.013	2.533	0.0042	255.22	1.90
	08a	49.86	3.19	1.37	0.14	8.53	0.04	0.13	14.51	21.44	0.36	b.l.d.	99.57	75.20	0.13	0.86	0.015	2.181	0.0037	249.42	1.71
	10a	49.96	3.95	1.51	0.30	8.07	0.04	0.10	13.91	21.89	0.32	b.l.d.	100.04	75.45	0.14	0.87	0.015	3.405	0.0052	277.07	1.82
	11a	49.25	4.09	1.83	0.22	8.88	0.05	0.15	13.93	20.78	0.37	0.04	99.59	73.65	0.15	0.84	0.017	2.860	0.0049	246.95	1.43
	12a	50.07	3.16	1.28	0.14	8.55	b.l.d.	0.11	14.31	21.16	0.41	b.l.d.	99.19	74.89	0.12	0.85	0.014	3.880	0.0049	335.05	2.47
	14a	47.42	5.94	2.20	0.37	8.91	b.l.d.	0.09	13.15	20.94	0.45	b.l.d.	99.46	72.47	0.21	0.85	0.025	2.150	0.0050	181.95	0.72
YTL7	15a	47.89	4.55	1.98	0.14	9.09	0.02	0.12	13.31	21.86	0.42	b.l.d.	99.38	72.30	0.19	0.89	0.021	2.550	0.0049	220.19	1.07
	16a	48.83	4.17	1.47	0.38	8.42	0.03	0.14	13.70	21.58	0.37	0.02	99.10	74.36	0.16	0.87	0.017	3.604	0.0041	371.90	2.17
	16b	49.12	3.86	1.85	0.06	10.47	0.04	0.22	13.89	19.67	0.37	b.l.d.	99.54	70.29	0.15	0.79	0.018	3.389	0.0041	349.76	1.99
	16c	48.27	5.45	2.15	0.52	7.61	b.l.d.	0.09	13.45	21.84	0.39	b.l.d.	99.77	75.90	0.19	0.88	0.022	3.356	0.0041	346.35	1.58
	17a	51.76	2.51	1.04	0.42	6.93	0.02	0.10	15.71	20.94	0.20	0.01	99.63	80.18	0.08	0.83	0.011	2.091	0.0040	221.15	1.98
	17b	49.49	4.32	1.66	0.35	8.43	0.06	0.16	13.63	21.48	0.45	0.01	100.05	74.24	0.15	0.86	0.017	4.115	0.0040	435.30	2.58
	18a	51.73	2.18	0.88	0.34	8.02	0.03	0.12	15.37	20.53	0.27	b.l.d.	99.47	77.36	0.07	0.82	0.011	2.643	0.0045	248.52	2.35

Note: b.l.d., below the limit of detection

Table 4-10. Major element compositions of ol phenocrysts in Chaihe-aershan baslats

	OXIDE	SiO_2	Al_2O_3	TiO_2	Cr_2O_3	FeO	NiO	MnO	MgO	CaO	Total	Mg#
CEH2	ceh2-01	38.70	0.01	0.03	0.07	19.85	0.22	0.24	40.67	0.27	100.06	78.51
	ceh2-02	39.17	b.l.d.	b.l.d.	0.09	20.46	0.22	0.23	38.86	0.18	99.22	77.20
	ceh2-03	37.58	0.06	0.03	0.68	23.75	0.15	0.33	36.28	0.30	99.15	73.14
	ceh2-04	38.33	0.05	0.03	0.09	21.65	0.21	0.31	38.76	0.23	99.66	76.14
	ceh2-05	37.82	0.02	0.07	0.04	24.80	0.16	0.29	35.99	0.31	99.50	72.13
	ceh2-06	37.33	0.04	b.l.d.	0.04	26.48	0.11	0.35	34.77	0.31	99.44	70.07
	ceh2-07	39.88	0.05	0.01	0.26	16.64	0.18	0.12	42.93	0.24	100.31	82.14
	ceh2-08	38.63	0.03	0.01	0.04	21.61	0.19	0.27	38.40	0.29	99.48	76.01
	ceh2-09	39.11	0.05	0.02	0.09	18.66	0.22	0.20	40.62	0.25	99.21	79.52
	ceh2-10	37.94	0.03	0.01	0.37	24.66	0.12	0.32	35.75	0.31	99.52	72.10
CEH3	ceh3-01	39.50	0.04	0.03	0.09	16.71	0.25	0.22	42.30	0.42	99.57	81.86
	ceh3-02	39.66	0.04	0.07	0.03	15.73	0.31	0.14	43.07	0.27	99.32	83.00
	ceh3-03	40.17	0.01	b.l.d.	0.05	16.07	0.27	0.19	43.55	0.28	100.60	82.85
	ceh3-04	39.51	0.03	b.l.d.	0.04	18.29	0.24	0.22	41.40	0.29	100.02	80.14
	ceh3-05	40.37	0.05	0.05	0.06	16.28	0.34	0.20	41.61	0.25	99.20	82.01
	ceh3-06	38.83	0.02	0.05	0.06	21.17	0.19	0.29	38.50	0.35	99.45	76.43
	ceh3-07	39.08	b.l.d.	0.01	0.03	20.29	0.17	0.28	39.42	0.37	99.64	77.60
	ceh3-08	39.18	0.02	0.03	0.04	20.27	0.16	0.31	39.63	0.33	99.96	77.71
	ceh3-09	39.49	0.03	0.01	0.04	16.79	0.25	0.21	42.58	0.25	99.65	81.89
	ceh3-10	39.24	0.04	0.01	0.04	20.72	0.12	0.32	39.65	0.37	100.50	77.34
	ceh3-11	39.25	0.06	0.07	0.19	19.40	0.18	0.24	40.25	0.32	99.96	78.72
	ceh3-12	40.20	0.05	b.l.d.	0.05	14.83	0.33	0.17	42.31	0.29	98.22	83.57
CEH5	ceh5-01	39.89	0.03	0.02	0.08	16.61	0.31	0.12	42.51	0.22	99.78	82.02
	ceh5-02	39.62	0.02	0.04	0.03	18.19	0.33	0.16	41.15	0.24	99.77	80.13
	ceh5-03	39.34	0.01	b.l.d.	0.06	17.69	0.24	0.16	41.40	0.28	99.18	80.67
	ceh5-04	43.32	2.97	0.48	0.08	18.45	0.14	0.22	32.60	1.52	99.79	75.91
	ceh5-05	39.08	0.02	0.02	0.03	20.86	0.15	0.17	39.07	0.24	99.63	76.96
	ceh5-06	38.71	0.03	0.02	0.02	22.05	0.18	0.27	37.89	0.29	99.45	75.39
	ceh5-07	39.75	0.03	b.l.d.	0.03	17.84	0.26	0.18	41.74	0.23	100.06	80.66
	ceh5-08	39.46	0.03	b.l.d.	0.04	18.72	0.24	0.16	41.12	0.26	100.03	79.65
	ceh5-09	39.13	0.03	0.06	0.01	20.15	0.17	0.20	39.90	0.29	99.93	77.93
	ceh5-10	38.81	0.02	0.05	0.01	21.35	0.18	0.23	39.14	0.27	100.07	76.58
CEH8	ceh8-01	38.46	0.05	0.04	0.19	17.80	0.37	0.12	42.11	0.23	99.37	80.83
	ceh8-02	38.48	0.04	0.01	0.04	21.51	0.18	0.22	38.37	0.30	99.14	76.08
	ceh8-03	38.89	0.03	0.05	0.03	21.50	0.23	0.22	39.06	0.25	100.23	76.41
	ceh8-04	39.30	0.06	0.04	0.13	17.08	0.25	0.18	41.96	0.23	99.23	81.41
	ceh8-05	39.28	0.03	b.l.d.	0.03	18.72	0.25	0.17	40.43	0.25	99.14	79.38
	ceh8-06	38.27	0.03	0.01	0.03	21.74	0.22	0.20	39.07	0.37	99.93	76.21
	ceh8-07	39.73	0.04	b.l.d.	0.10	17.43	0.27	0.19	42.14	0.23	100.14	81.17
	ceh8-08	38.68	0.03	0.01	0.02	21.08	0.25	0.22	39.25	0.29	99.83	76.85
	ceh8-09	38.81	0.02	b.l.d.	0.02	20.25	0.21	0.25	39.91	0.26	99.72	77.85
	ceh8-10	38.74	0.03	b.l.d.	0.04	21.88	0.20	0.25	38.46	0.30	99.91	75.81
CEH12	ceh12-01	38.41	0.02	b.l.d.	0.05	22.96	0.24	0.29	37.71	0.32	100.00	74.55
	ceh12-02	38.07	0.03	0.01	b.l.d.	24.90	0.16	0.38	35.67	0.29	99.51	71.86
	ceh12-03	39.52	0.04	b.l.d.	0.05	19.72	0.22	0.29	40.06	0.27	100.15	78.37
	ceh12-04	39.95	0.01	0.01	0.01	15.71	0.25	0.21	43.47	0.14	99.74	83.15
	ceh12-05	38.17	0.04	0.03	b.l.d.	25.13	0.13	0.37	35.82	0.31	100.00	71.76
	ceh12-06	39.06	0.01	0.05	b.l.d.	20.59	0.25	0.28	39.32	0.31	99.88	77.29
	ceh12-07	38.12	0.03	b.l.d.	0.03	24.88	0.17	0.29	36.25	0.24	100.01	72.21

Table 4-10. (continued)

	OXIDE	SiO_2	Al_2O_3	TiO_2	Cr_2O_3	FeO	NiO	MnO	MgO	CaO	Total	Mg#
CEH12	ceh12-08	39.72	0.04	0.03	0.03	16.27	0.29	0.20	43.24	0.18	100.00	82.57
	ceh12-09	38.69	0.02	0.02	0.03	22.00	0.28	0.25	37.85	0.27	99.42	75.41
	ceh12-10c	38.65	0.03	b.l.d.	b.l.d.	20.64	0.25	0.25	39.62	0.25	99.68	77.39
	ceh12-10mc	38.58	0.04	0.01	0.05	20.23	0.25	0.19	39.47	0.21	99.03	77.67
	ceh12-10mr	38.28	0.03	0.04	0.03	21.12	0.23	0.24	38.94	0.25	99.15	76.68
	ceh12-10r	37.74	0.02	0.01	0.04	24.56	0.18	0.26	36.16	0.30	99.27	72.42
DLH1	dlh1-01	39.73	0.05	b.l.d.	0.04	14.93	0.26	0.14	44.23	0.18	99.56	84.08
	dlh1-02	39.42	0.05	b.l.d.	0.03	17.71	0.15	0.20	41.74	0.24	99.52	80.78
	dlh1-03	39.89	0.04	b.l.d.	0.04	14.92	0.26	0.12	43.75	0.23	99.25	83.94
	dlh1-05	39.37	0.07	0.04	0.13	14.33	0.34	0.14	44.55	0.22	99.19	84.72
	dlh1-06	40.09	0.03	b.l.d.	0.08	14.78	0.38	0.10	44.68	0.22	100.35	84.35
	dlh1-07	39.83	0.07	b.l.d.	0.27	15.21	0.22	0.15	43.96	0.19	99.88	83.75
	dlh1-08	40.36	0.03	0.01	0.03	13.36	0.32	0.13	45.23	0.14	99.62	85.78
	dlh1-10	40.32	0.03	b.l.d.	0.08	14.71	0.34	0.07	44.36	0.21	100.11	84.32
DLH7	dlh7-01	37.87	0.02	0.01	b.l.d.	25.91	0.12	0.28	35.57	0.25	100.03	70.99
	dlh7-02	36.95	0.03	0.01	b.l.d.	29.02	0.14	0.31	33.06	0.29	99.81	67.01
	dlh7-03	37.33	0.03	0.06	b.l.d.	30.17	0.11	0.32	30.81	0.26	99.10	64.55
	dlh7-04	37.78	0.01	b.l.d.	0.02	27.14	0.12	0.32	34.04	0.23	99.66	69.10
	dlh7-05	37.55	0.01	0.02	0.05	27.00	0.15	0.32	35.16	0.17	100.43	69.90
	dlh7-06	38.00	0.02	b.l.d.	b.l.d.	28.19	0.14	0.35	33.56	0.24	100.49	67.98
	dlh7-07	38.44	0.06	0.01	0.04	20.15	0.34	0.20	39.66	0.20	99.10	77.82
	dlh7-08	36.91	0.02	0.03	0.04	29.85	0.12	0.31	31.99	0.25	99.51	65.64
	dlh7-09	37.35	0.02	0.03	0.05	27.58	0.17	0.33	34.19	0.19	99.89	68.85
	dlh7-11	36.78	0.01	0.06	0.01	30.95	0.13	0.45	30.94	0.27	99.60	64.06
DXG2	dxg2-01	38.32	0.01	0.01	0.02	20.94	0.22	0.17	39.95	0.16	99.80	77.28
	dxg2-02	37.58	0.03	b.l.d.	b.l.d.	26.00	0.13	0.34	35.85	0.29	100.22	71.08
	dxg2-03	38.90	b.l.d.	0.01	b.l.d.	22.16	0.22	0.25	38.63	0.12	100.29	75.65
	dxg2-04	38.12	0.01	0.07	b.l.d.	26.87	0.07	0.39	33.88	0.28	99.68	69.21
	dxg2-05	39.25	0.02	b.l.d.	0.02	20.03	0.26	0.21	40.39	0.02	100.20	78.24
	dxg2-06	39.79	0.03	0.04	0.03	17.41	0.26	0.14	42.04	0.10	99.83	81.15
	dxg2-07	38.25	0.02	0.04	0.01	24.61	0.10	0.28	35.87	0.26	99.43	72.21
	dxg2-08	39.13	0.01	b.l.d.	0.04	21.07	0.14	0.25	38.67	0.16	99.45	76.60
	dxg2-09	38.13	0.11	b.l.d.	0.05	25.09	0.16	0.34	35.66	0.29	99.83	71.70
	dxg2-10	39.04	0.01	b.l.d.	b.l.d.	20.86	0.27	0.22	39.45	0.10	99.96	77.12
GBS1	gbs1-01	39.86	0.03	0.03	0.04	16.95	0.26	0.13	42.75	0.21	100.25	81.81
	gbs1-02	39.93	0.01	b.l.d.	0.05	15.97	0.31	0.19	43.47	0.24	100.17	82.91
	gbs1-03	38.84	0.04	b.l.d.	0.05	17.50	0.17	0.22	42.26	0.31	99.40	81.15
	gbs1-04	39.01	0.03	b.l.d.	0.07	18.57	0.31	0.17	41.11	0.22	99.49	79.78
	gbs1-05	39.63	0.07	0.01	0.03	15.40	0.21	0.14	43.73	0.28	99.50	83.51
	gbs1-06	39.08	0.04	0.03	0.06	19.26	0.17	0.25	40.61	0.24	99.73	78.99
	gbs1-07	39.82	0.02	b.l.d.	0.04	16.13	0.23	0.13	42.68	0.25	99.28	82.51
	gbs1-08	38.59	0.04	0.03	0.06	22.24	0.19	0.26	37.45	0.27	99.11	75.02
	gbs1-09	39.00	0.03	b.l.d.	0.04	19.41	0.22	0.16	40.52	0.25	99.62	78.82
	gbs1-10	39.69	0.04	0.05	0.09	16.78	0.23	0.17	42.22	0.24	99.51	81.77
GBS3	gbs3-01	39.88	0.03	0.06	0.06	17.37	0.24	0.19	41.84	0.23	99.88	81.12
	gbs3-02	39.55	0.02	0.01	0.01	17.21	0.24	0.18	41.74	0.21	99.15	81.22
	gbs3-03	39.77	0.03	0.03	0.06	15.20	0.44	0.15	43.64	0.21	99.51	83.66

Table 4-10. (continued)

	OXIDE	SiO_2	Al_2O_3	TiO_2	Cr_2O_3	FeO	NiO	MnO	MgO	CaO	Total	Mg#
GBS3	gbs3-04	39.52	0.03	0.01	0.04	17.11	0.28	0.18	42.01	0.24	99.41	81.41
	gbs3-05	39.91	0.03	b.l.d.	0.04	15.34	0.34	0.17	43.70	0.20	99.72	83.55
	gbs3-06	39.11	0.03	b.l.d.	0.01	19.99	0.22	0.20	39.36	0.29	99.20	77.83
	gbs3-07	39.60	0.04	0.02	0.01	16.25	0.19	0.17	42.58	0.26	99.10	82.37
	gbs3-08	39.91	0.04	0.02	0.03	15.01	0.31	0.12	43.91	0.22	99.58	83.91
	gbs3-09	39.27	0.03	0.04	0.04	20.56	0.25	0.16	39.26	0.26	99.88	77.29
	gbs3-10	39.18	0.03	b.l.d.	0.06	18.26	0.25	0.20	40.94	0.28	99.21	80.00
TFL1-7	tfl1-7-01	39.60	0.03	0.03	0.03	19.25	0.29	0.18	40.65	0.19	100.25	79.02
	tfl1-7-02	38.35	0.03	0.05	0.05	23.61	0.08	0.23	37.31	0.29	100.00	73.80
	tfl1-7-03	39.56	0.04	0.05	0.10	17.87	0.20	0.16	41.46	0.20	99.65	80.53
	tfl1-7-04	39.17	0.02	0.06	0.01	20.60	0.27	0.23	39.55	0.23	100.14	77.39
	tfl1-7-05	39.69	0.11	0.08	0.12	19.76	0.32	0.24	39.72	0.36	100.41	78.18
	tfl1-7-06	39.64	0.02	0.04	0.03	16.66	0.47	0.14	42.80	0.03	99.84	82.08
	tfl1-7-07	39.19	0.01	0.08	0.08	21.96	0.21	0.23	38.24	0.26	100.25	75.64
	tfl1-7-08	38.81	0.02	0.06	0.03	22.45	0.20	0.32	37.43	0.28	99.59	74.83
YLTC3	yltc3-02	39.52	0.02	0.02	0.06	16.16	0.22	0.21	43.28	0.25	99.75	82.68
	yltc3-03	40.05	0.02	0.02	0.04	15.00	0.20	0.14	44.41	0.24	100.11	84.07
	yltc3-04	39.19	0.02	0.01	0.05	19.88	0.28	0.34	40.33	0.24	100.34	78.34
	yltc3-06	39.78	0.01	0.05	0.08	16.11	0.31	0.15	43.54	0.13	100.15	82.82
	yltc3-07	39.77	0.03	0.03	0.03	14.86	0.26	0.19	43.68	0.21	99.05	83.97
	yltc3-09	40.22	0.03	0.02	0.03	15.87	0.32	0.16	43.37	0.23	100.24	82.97
	yltc3-10	39.70	0.03	b.l.d.	0.14	18.50	0.25	0.27	40.34	0.27	99.49	79.54
YTL7	ytl7-01	38.54	0.04	b.l.d.	0.03	21.96	0.19	0.28	38.10	0.24	99.37	75.57
	ytl7-03	39.79	0.05	0.02	0.02	16.08	0.31	0.17	43.21	0.21	99.86	82.73
	ytl7-04	39.36	0.04	b.l.d.	0.05	18.87	0.28	0.16	40.97	0.21	99.94	79.47
	ytl7-05	39.93	0.01	0.01	0.05	16.81	0.30	0.16	42.20	0.23	99.70	81.73
	ytl7-08	38.55	0.04	0.01	b.l.d.	23.40	0.15	0.34	36.87	0.26	99.63	73.75
	ytl7-09	39.34	0.05	0.02	0.19	19.83	0.28	0.16	40.39	0.22	100.46	78.41
	ytl7-10	38.52	0.02	0.05	0.05	21.83	0.25	0.25	38.17	0.23	99.37	75.72

Note: b.l.d., below the limit of detection

4.3.1.4 Oxygen isotope compositions of clinopyroxene phenocrysts

The correlations between IMF and the Mg# of standards (NSH2, NSH5, NSH8, NSH9, NSH10, NSH14) in each session are listed in Fig. 3-3, and the calculated oxygen isotope compositions of cpx phenocrysts are listed in Table 4-11 and plotted in Figs. 4-26 and 4-27. The cpx phenocrysts of Chaihe-aershan basalts show wide variations in $\delta^{18}O$ values (4.28‰ to 8.57‰), apparently beyond the range of normal mantle-derived cpx (5.6±0.2‰, Eiler et al., 1997; Mattey et al., 1994). The difference in $\delta^{18}O$ values within individual samples is also wide (1.28‰-2.3‰). In some samples, a positive correlation between $\delta^{18}O$ values and Mg# of cpx can be identified.

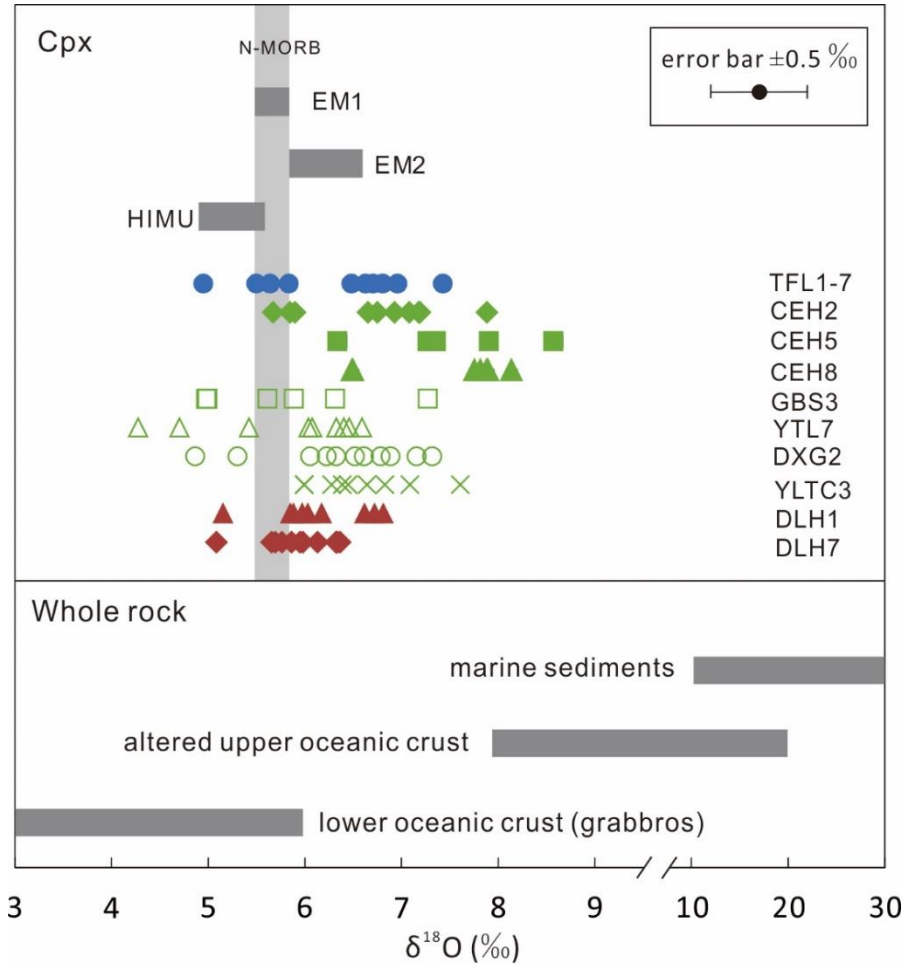

Figure 4-26. Oxygen isotope compositions of cpx phenocrysts in Chaihe-aershan basalts. The range of $\delta^{18}O$ values of cpx phenocrysts in N-MORB, EM1, EM2 and HIMU are calculated from the $\delta^{18}O$ values of ol phenocrysts (Eiler et al., 1997), assuming the equilibrium fractionation between cpx and ol is 0.4‰ (Mattey et al., 1994). The $\delta^{18}O$ values of bulk rock (marine sediments, altered upper oceanic crust and lower oceanic crust) are based on Eiler (2001).

Table 4-11. The oxygen isotope compositions of cpx phenocrysts in Chaihe-aershan basalts

	Mg#	$\delta^{18}O$ measured	IMF*	$\delta^{18}O$ corrected by IMF	1SE**
ceh2-05a	81.97	12.31	4.42	7.89	0.09
ceh2-22a	73.97	12.21	6.36	5.85	0.09
ceh2-22b	78.10	12.04	5.38	6.65	0.04
ceh2-23c	82.53	11.73	4.64	7.09	0.13
ceh2-23d	82.27	11.97	4.78	7.19	0.02
ceh2b-09a	81.82	11.82	5.06	6.75	0.07
ceh2b-10a	74.70	12.45	6.55	5.90	0.06
ceh2c-01a	75.92	11.93	6.25	5.68	0.06
ceh2c-02a	79.95	12.23	5.30	6.93	0.16
ceh2c-05a	79.75	12.57	5.39	7.18	0.02
ceh5-03a	79.71	10.29	2.93	7.36	0.14
ceh5-05a	78.28	10.85	2.94	7.91	0.08
ceh5-09b	79.35	11.14	2.57	8.57	0.09
ceh5-26a	79.22	9.50	3.16	6.34	0.09
ceh5-33a	78.20	10.21	2.93	7.27	0.02
ceh8-02a	74.98	11.08	4.59	6.49	0.33
ceh8-09a	78.40	11.42	3.66	7.76	0.09
ceh8-11a	75.78	10.78	4.28	6.50	0.09
ceh8-12a	83.13	11.12	3.22	7.90	0.42
ceh8-12b	81.94	11.22	3.40	7.82	0.27
ceh8-12c	82.45	11.10	3.22	7.88	0.07
ceh8-13a	80.72	11.60	3.46	8.14	0.01
DLH1-01a	80.07	10.03	3.22	6.81	0.09
DLH1-01b	79.47	10.04	3.42	6.62	0.03
DLH1-01c	76.75	9.71	3.82	5.89	0.14
DLH1-03a	79.87	9.28	3.43	5.85	0.05
DLH1-12a	80.72	9.59	3.42	6.18	0.12
DLH1b-01a	79.40	9.51	3.53	5.98	0.16
DLH1b-02a	74.02	9.62	4.46	5.15	0.17
DLH1b-05a	78.37	9.81	3.77	6.03	0.10
DLH1b-07a	82.17	9.94	3.21	6.72	0.09
DLH7-04a	79.40	9.68	3.35	6.33	0.28
DLH7-04b	78.13	9.88	3.54	6.34	0.07
DLH7-07a	79.25	9.19	3.43	5.76	0.13
DLH7-08a	76.14	9.65	3.99	5.66	0.16
DLH7-09a	75.96	9.76	4.06	5.70	0.11
DLH7-11a	80.84	9.67	3.30	6.37	0.21
DLH7-14b	81.70	8.88	2.90	5.98	0.16
DLH7-16a	76.33	8.98	3.89	5.09	0.16
DLH7-17a	78.35	9.40	3.53	5.87	0.06
DLH7-22a	79.59	9.42	3.47	5.95	0.24
DLH7-24a	79.31	9.59	3.45	6.13	0.19
DXG2-05a	77.50	11.04	4.71	6.33	0.00
DXG2-09a	72.83	9.57	4.70	4.87	0.53
DXG2-13a	82.01	9.95	3.16	6.78	0.37
DXG2-13b	75.36	9.58	4.28	5.31	0.12
DXG2-16a	79.43	9.82	3.60	6.23	0.19
DXG2-21a	82.16	11.09	3.77	7.32	0.19

Table 4-11. (continued)

	Mg#	$\delta^{18}O$ measured	IMF*	$\delta^{18}O$ corrected by IMF	1SE**
DXG2-21b	82.53	10.76	3.60	7.16	0.08
DXG2-24a	79.20	10.47	3.95	6.52	0.08
DXG2-34a	78.06	9.88	3.82	6.06	0.16
DXG2-34b	81.44	9.88	3.26	6.62	0.02
DXG2-34c	82.70	9.94	3.05	6.89	0.17
gbs3-06a	73.28	10.65	5.65	4.99	0.16
gbs3-06b	77.67	11.05	4.88	6.17	0.22
gbs3-06c	77.62	10.41	4.80	5.62	0.29
gbs3-10a	80.78	10.84	3.56	7.28	0.05
gbs3-30a	72.94	10.34	5.36	4.98	0.14
gbs3b-04a	81.96	9.86	3.55	6.31	0.14
gbs3b-08a	77.25	10.53	4.40	6.13	0.41
gbs3b-11a	79.78	9.78	3.89	5.89	0.10
TFL1-7-12a	75.67	10.89	4.08	6.81	0.07
TFL1-7-12b	77.26	10.61	3.90	6.71	0.06
TFL1-7-12c	72.24	11.19	4.56	6.63	0.23
TFL1-7-14a	76.05	9.77	4.13	5.64	0.11
TFL1-7-17a	80.28	10.43	3.47	6.96	0.09
TFL1-7-18a	75.24	8.90	3.95	4.95	0.08
TFL1-7-27a	72.60	9.82	4.32	5.50	0.17
TFL1-7-28a	73.59	10.72	4.24	6.48	0.01
TFL1-7-28b	72.49	10.20	4.36	5.84	0.08
TFL1-7-32a	77.97	11.13	3.70	7.43	0.03
YL3h-02a	82.53	9.85	3.85	6.00	0.15
YL3h-02b	82.08	10.16	3.88	6.28	0.05
YL3h-02c	79.37	10.71	4.26	6.45	0.03
YL3h-03a	83.24	10.31	2.70	7.61	0.03
YL3h-04a	83.18	9.61	3.21	6.39	0.21
YL3h-04b	79.06	9.83	3.84	6.00	0.15
YL3h-05a	83.64	9.50	2.67	6.83	0.05
YL3h-05b	81.93	10.00	2.91	7.09	0.06
YL3h-08a	84.00	9.33	2.68	6.65	0.07
YTL7-01a	73.96	8.74	4.47	4.28	0.10
YTL7-01b	76.57	8.86	4.15	4.71	0.07
YTL7-02a	75.98	10.22	4.18	6.04	0.07
YTL7-06a	74.67	10.93	4.47	6.46	0.06
YTL7-07a	79.03	10.34	3.93	6.41	0.06
YTL7-07b	77.44	10.75	4.15	6.59	0.25
YTL7-11a	73.65	10.09	4.67	5.42	0.15
YTL7-12a	74.89	10.86	4.53	6.33	0.08
YTL7-16a	74.36	10.70	4.62	6.08	0.11

* IMF is the instrumental mass fractionation

** SE the standard error of the mean for the group of measurements in a single cpx grain

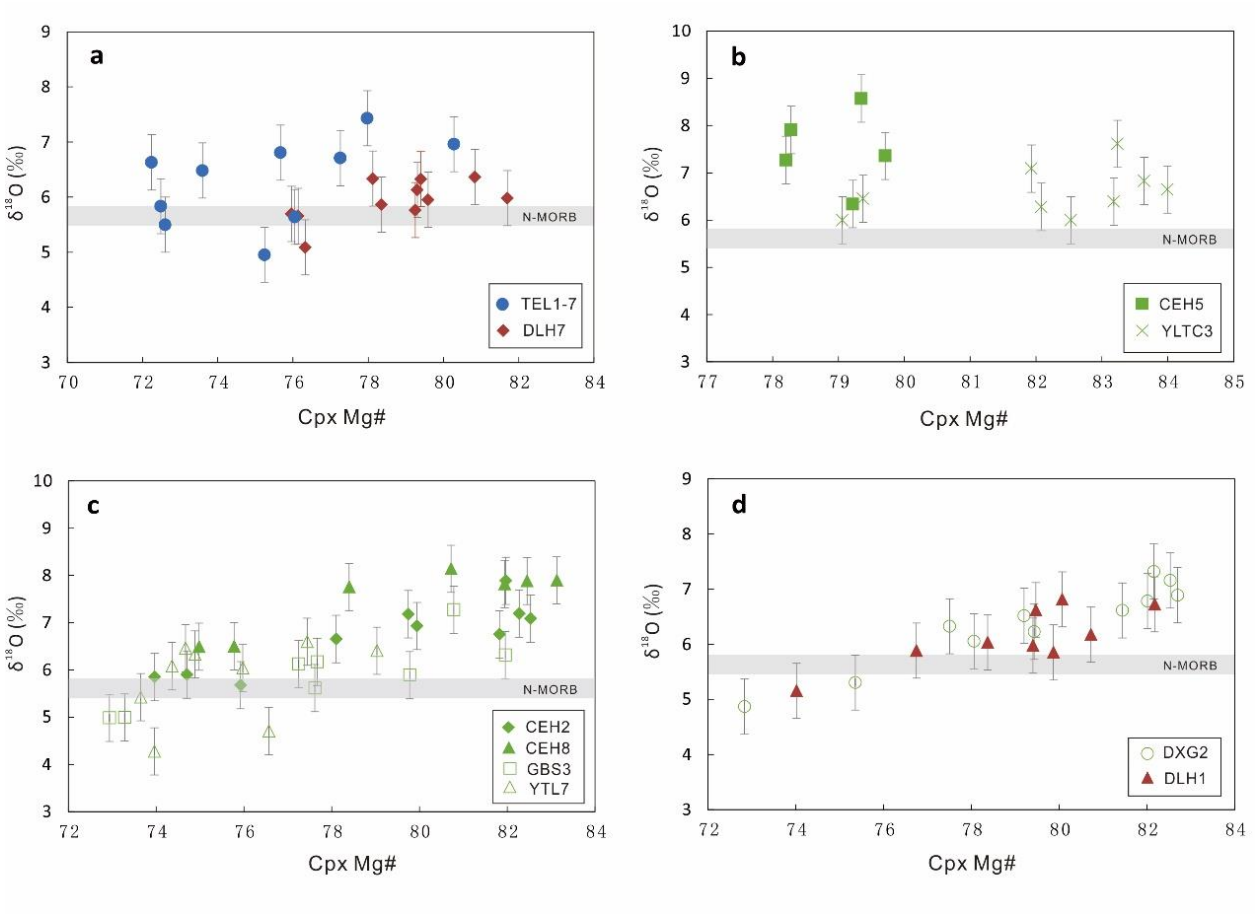

Figure 4-27. Oxygen isotope compositions of the cpx phenocrysts in the Chaihe-aershan basalts compared with their cpx Mg#.

4.3.2 Discussion

4.3.2.1 Crustal contamination and crystal fractionation

Abundant mantle xenoliths in the Chaihe-aershan basalts suggests that the host magma ascent was fast (generally less than 50 h after xenolith entrainment, O'Reilly and Griffin, 2010), leaving limited time for the magma to be contaminated by the continental crust. The continental crust is characterized by low Nb/U ratio; however, the Chaihe-aershan basalts have high Nb/U ratios (45.8-78.5), falling primarily into the range of MORBs and OIBs (Fig. 4-28a; Hofmann AW et al., 1986), and there is no negative correlation between the Nb/U ratios and SiO_2 contents. In addition, as the continental crust is enriched in Ba relative to Nb (Rudnick and Gao, 2014), if crustal contamination had occurred, Ba/Nb ratios would have displayed a positive correlation with SiO_2, which was not observed in the Chaihe-aershan basalts (Fig. 4-28b).

Therefore, the crustal contamination was limited during the ascent of the Chaihe-aershan basaltic magmas, which is consistent with the conclusions of Ho et al. (2013) and Zhao and Fan (2012).

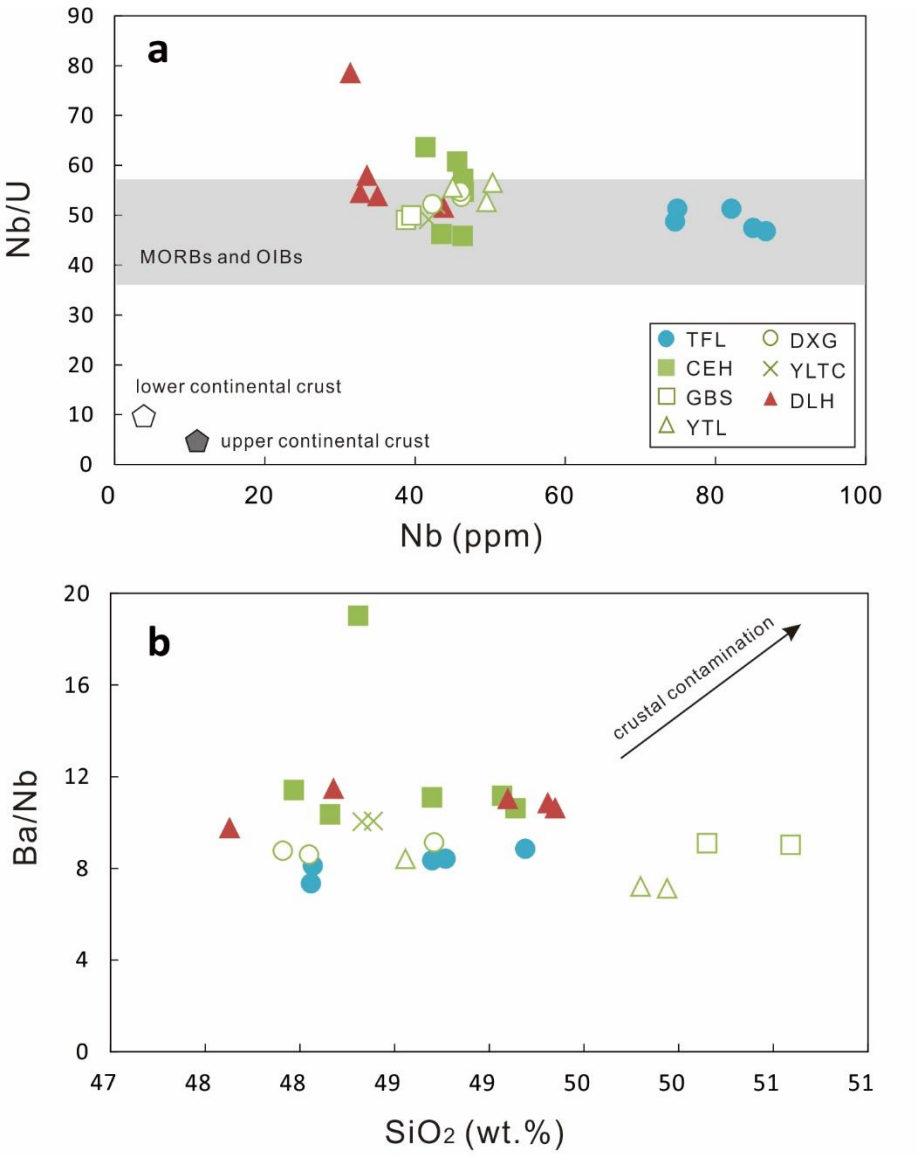

Figure 4-28. a) Nb/U compared with Nb, b) Ba/Nb compared with SiO_2 in Chaihe-aershan basalts. In a), the gray zone is Nb/U of MORBs and OIBs (Hofmann AW et al., 1986). Data for the upper continental crust and lower continental crust are from Rudnick and Gao (2014). The arrow in b) represents the crustal contamination trend.

The majority of the Chaihe-aershan basalts (except the TFL basalts) have high Mg# (63.2-70.0), identical to those of other basalts in eastern China (e.g., Chen et al., 2007;

Zou et al., 2000), high Ni and Co contents, and weak positive Eu anomaly, suggesting no significant crystal fractionation of the basalts. TFL basalts display relatively low Mg# (56.9-62.8) as well as low Ni (176-273 ppm) and Cr (145-251 ppm) contents, indicating a small amount of fractional crystallization of ol and cpx. The negative correlation between Al_2O_3 and MgO contents and no negative Eu anomaly suggest that the fractionation of pl in the TFL basalts was limited. As the compositional trends between TFL, DLH and other basalts are distinct (Figs. 4-22b-f), the compositional differences among these three basalt groups cannot be simply caused by fractional crystallization. In Figs. 4-22e and 4-22f, the compositional trends of red symbols (DLH) and green symbols (CEH, GBS, YTL, DXG and YLTC) show positive correlations between K_2O, P_2O_5 and MgO. Given that K and P are incompatible for the main fractionation phases (ol, cpx, pl and Cr-spinel) (e.g., Brunet and Chazot. 2001; Salters and Stracke. 2004), the contents of K and P in the melts should display a slight increase during crystal fractionation. Therefore, these positive trends in the Chaihe-aershan basalts are more likely to be caused by magma mixing (high-MgO and low-MgO components) rather than crystal fractionation.

4.3.2.2 Heterogeneity of oxygen isotope composition

The $\delta^{18}O$ values of cpx phenocrysts in the Chaihe-aershan basalts have two primary features (Fig. 4-26): (1) the $\delta^{18}O$ values vary widely, ranging from 4.27‰ to 8.57‰ suggesting both an enrichment and a depletion of $\delta^{18}O$ of cpx compared with typical MORB and mantle peridotites (5.4‰-5.8‰; Eiler et al., 1997; Mattey et al., 1994); (2) the $\delta^{18}O$ values within individual samples also display considerable variation (1.28‰-2.31‰), and for the CEH2, CEH8, DLH1, DXG2 and GBS2 basalts, the $\delta^{18}O$ values decrease linearly with the decrease of Mg# in cpx (Fig. 4-27).

Oxygen isotope compositions of cpx phenocrysts are affected by many factors, including systematic deviation caused by analytical artifact, alteration on the surface of the Earth, crustal contamination, fractional crystallization (or assimilation-fractional crystallization [AFC] process), partial melting, devolatilization, water-melt interaction during crystallization (decreasing the oxygen isotope ratio) and heterogeneity of the mantle source. In particular, analytical artifact, AFC process or water-melt interaction might induce a positive correlation between $\delta^{18}O$ and Mg# of cpx phenocrysts.

As shown in Fig. 3-3, the analytical oxygen isotope results for standards appear to be reasonable. The same suit of standards were also used to correct the oxygen isotope data of cpx phenocrysts from the Shuangliao basalts. The $\delta^{18}O$ values show a nearly flat trend with the Mg#, implying that an analytical artifact involving matrix effect might not be the main reason for the positive correlations between $\delta^{18}O$ and Mg# of cpx phenocrysts.

The LOIs of the Chaihe-aershan basalts are less than 0.1 wt.% and do not display any correlation with the $\delta^{18}O$ values. In addition, fresh, crack- and inclusion-free areas of the cpx phenocrysts were selected by FTIR investigation before oxygen isotope measurement. Thus, the effect of alteration near the surface of the Earth after eruption on the selected cpx phenocrysts can be ruled out.

As discussed in Section 4.3.2.1, the crustal contamination in the Chaihe-aershan basalts is weak. The fractionation of oxygen isotopes caused by partial melting, fractional crystallization or devolatilization is expected to be less than 0.1‰ in basaltic melt with MgO content between 8 and 3 wt.% (Eiler, 2001 and references therein), indicating that these factors are unlikely to be the primary cause of the $\delta^{18}O$ variations of the Chaihe-aershan basalts.

Taking CEH5 basalts as an example, the simulation of the AFC process shows that, to increase $\delta^{18}O$ in CEH5 basalt from 5.6‰ to 8.6‰, the magma must undergo extensive crystallization (~32%) and crustal assimilation (~16%) (Equation 4-1). However, considering that continental crust is characterized by low MgO, low Nb/U and Nb/La ratios (Rudnick and Gao, 2014), the high concentration of MgO (9.58 wt.%), Mg# (65.4), Nb/U (57.3) and Nb/La (1.77) of CEH5 basalt are clearly inconsistent with the results of the AFC model. However, with the low $\delta^{18}O$ value of the surrounding rock in the continental crust (~5‰, Kempton and Harmin, 1992), the AFC process could explain the positive correlation between $\delta^{18}O$ and Mg# of cpx phenocrysts. The calculated results show that the magma requires extensive crystallization (~80%) and crust assimilation (~40%) to decrease the $\delta^{18}O$ value of CEH5 basalt from 8.6‰ to 5.6‰; however, it is also in contradiction with the observation of CEH5 basalt (high MgO, Mg#, Nb/U and Nb/La). Therefore, both the high $\delta^{18}O$ value of cpx phenocrysts and the positive correlation between $\delta^{18}O$ and Mg# in the same samples cannot be simply explained by AFC process.

Water-melt interaction during crystallization may also account for the positive correlation between $\delta^{18}O$ and Mg#. Assuming a temperature of 1100℃， the calculated results show that ~10% meteoric water in weight is required to decrease the $\delta^{18}O$ value from 7.3‰ to 4.9‰ (Equation 4-2). A lower temperature requires more meteoric water. It is difficult to imagine that such an amount of meteoric water could be involved during the evolution of magma. In such a situation, the high water content would be recorded by cpx phenocrysts. In fact, the water contents of cpx phenocrysts in samples which show a positive correlation between $\delta^{18}O$ and Mg# are very low (DLH1; Fig. 4-25).

Overall, the oxygen isotopes of the cpx phenocrysts in the Chaihe-aershan basalts represent the heterogeneity of the mantle source, and the variation in oxygen isotope compositions within each sample is most likely caused by magma mixing. This is consistent with the results of basalts from the Shuangliao and Wulanhada basalts in this work and Taihang and Canary basalts in previous studies (Gurenko et al., 2011; Liu et al., 2015b). As mentioned above, the positive correlations between K_2O, P_2O_5 and MgO suggest that magma mixing occurred between high-MgO and low-MgO components, which are also consistent with the $\delta^{18}O$ features of the cpx phenocrysts. However, there are no significant correlations between the major element contents (e.g., MgO and K_2O) and trace element ratios (e.g., Ba/Th, Nb/La, Th/La), which hinder us to further discriminate the high-MgO and low-MgO components.

To compare oxygen isotope ratios with the water content and trace elements of the magma, the range of isotope compositions in each sample was used to discuss the oxygen isotopic information of the mantle source.

4.3.2.3 Water content in "primary" magmas

As mentioned above, the variation of H_2O content in magmas during crystal fractionation is within the measurement uncertainty when the cpx phenocrysts with Mg# >75 are used to estimate the H_2O content in magmas. There is little or no crustal contamination in the Chaihe-aershan basalts and no correlation between H_2O and SiO_2, which suggest that the influence of crustal contamination on the H_2O content of the magmas was limited. The calculated water content of magmas displays positive correlations with major and trace elements (e.g., K, Ce, Th, Ta), except for CEH2.CEH12 and TFL basalts (Fig. 4-29), which are the same as the results in Dixon

et al. (2002). These good correlations suggest that the influence of magma degassing and H diffusion in cpx phenocrysts on these samples is not significant and the calculated water content represents the primary source contribution. As discussed above, TFL basalts display distinct compositional trends compared with other basalts, which could explain the different correlations in Fig. 4-29. CEH2 and CHE12 basalts have similar compositions as other basalts from CEH but significantly low H_2O contents, which suggest that these samples might have undergone H diffusion during the degassing of the magma. Petrographic investigations have shown that the crystallinities of the matrix in the CEH2 and CHE12 basalts are obviously higher than those of the matrix in other basalts, which implies that the cooling rate of these basalts was slower and the diffusion of the H could have been relatively more significant. Therefore, these samples were ignored in the following discussion.

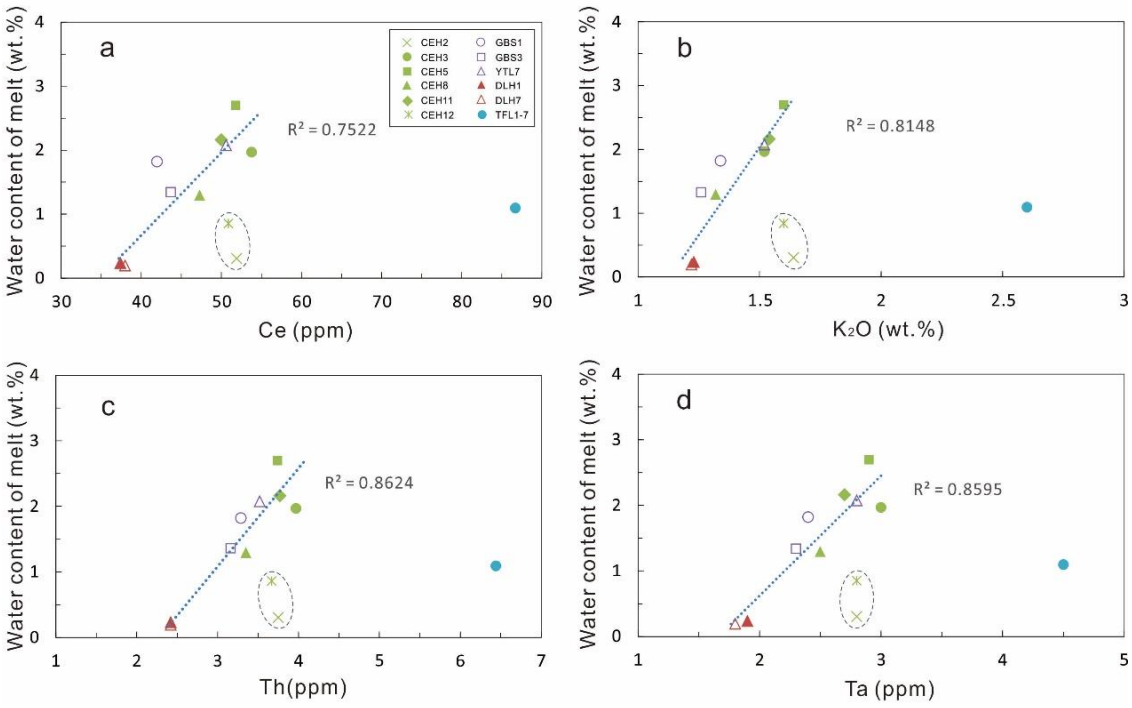

Figure 4-29. Calculated water contents of magmas in Chaihe-aershan basalts compared with (a) Ce, (b) K_2O, (c) Th and (d) Ta concentrations.

The calculated H_2O contents of the Chaihe-aershan "primary" magmas (0.19 to 2.70 wt.%, Table 4-12) cover the range of MORBs (0.1-0.3 wt.%), OIBs (0.3-1.0 wt.%, and back-arc basin basalts (BABBs, 0.2-2.0 wt.%) (Dixon et al., 2004 and references

therein). H_2O has a compatibility similar to Ce, and the H_2O/Ce ratios generally remain unchanged during magma processes such as partial melting and crystal fractionation (Michael, 1995). The calculated H_2O/Ce ratios for each basalt vary substantially, indicating mainly heterogeneity in the mantle source (Table 4-12).

In Fig. 4-25, the H_2O contents of cpx phenocrysts and the corresponding melts of each basalt vary widely (obviously beyond measurement uncertainty). Combined with the large variations in oxygen isotope compositions, the widely varying H_2O contents of cpx phenocrysts also indicates the mixing of magmas. However, H is a highly mobile element, and the H_2O content in cpx phenocrysts will be homogenized by diffusion after residence in melts for a long time (Ingrin and Blanchard, 2006), which suggests that the magma mixing occurs shortly before eruptions. In other words, the each eruption might be triggered by a magma mixing process.

Table 4-12. The average oxygen isotope compositions of cpx phenocrysts and the water contents of melt in Chaihe-aershan basalts

Sample	CEH-2^	CEH-3	CEH-5	CEH-8	CEH-11	CEH-12^	DLH-1	DLH-7	YLTC-3	TFL1-7	DXG-2	GBS-1	GBS-3	YTL-7
H_2O of melt (wt. %)	0.30	1.97	2.70	1.30	2.16	0.86	0.23	0.19	-	1.09	-	1.82	1.36	2.07
Grain number*	10	14	17	9	14	14	10	6	-	8	-	16	7	9
2SE	0.05	0.52	0.79	0.69	0.74	0.50	0.09	0.06	-	0.38	-	0.59	0.22	0.39
H_2O/Ce of melt	58	365	521	274	432	170	62	51	-	126	-	433	310	410
$\delta^{18}O$ value's range of cpx (‰)	5.68 - 7.89	-	6.34 - 8.57	6.49 - 8.14	-	-	5.15 - 6.81	5.09 - 6.37	6.00 - 7.61	4.95 - 7.43	4.87 - 7.32	-	4.98 - 7.28	4.28 - 6.59
Average $\delta^{18}O$ value of cpx (‰)	6.70	-	7.49	7.50	-	-	6.14	5.92	6.59	6.31	6.37	-	5.92	5.81

* The number of cpx grain involved in calculation

^ CEH2 and CHE12 basalts may underwent significant H diffusion during the degassing of magma

4.3.2.4 Enriched components in the mantle source

As discussed above, the oxygen isotopes of the cpx phenocrysts and the H_2O/Ce ratios of magma mainly reflect the original basaltic source. The trace elements of the Chaihe-aershan basalts show different degrees of enrichment for highly incompatible trace elements (e.g., variable Ba/Th ratio), indicative of the compositional heterogeneity of the mantle source. The Ba/Th ratio, Eu anomaly, H_2O/Ce ratio of the whole rock and the $\delta^{18}O$ values of the cpx phenocrysts were combined to constrain the heterogeneity in the mantle source of the Chaihe-aershan basalts. As shown in Fig. 4-30, three components can be identified (Components I, II and III). Among them, Component I, with normal $\delta^{18}O$ values, H_2O/Ce ratio, Ba/Th ratio, and Eu anomaly related to the depleted mantle, would be the ambient mantle in the mantle source (DMM, Fig. 4-30).

Component II: Altered upper oceanic crust and GLOSS

Component II is represented by the CEH basalts, characterized by high $\delta^{18}O$ values (~7.5‰) and H_2O/Ce ratios (~600), relatively high Ba/Th, and no Eu anomaly (Fig. 4-30).

The $\delta^{18}O$ value of Component II is higher than the value of normal mantle, indicating the involvement of recycled crustal materials. Generally, the origin of this recycled crustal component could be from the recycled continental crust (Eiler, 2001), fluids or melts liberated from a subducted slab (e.g., Auer et al., 2009) or subducted upper oceanic crust and/or marine sediments (GLOSS) (Eiler, 2001; Gregory and Taylor, 1981). The CEH basalts are characterized by high MgO contents, Mg#, Nb/La (>1.7) and Nb/U (>47) ratios, however, the continental crust has low MgO and is significantly depleted in Nb (Rudnick and Gao, 2014) which is against the contribution of continental crust. Similarly, the relative enrichment in Nb, Ta, and the high Nb/U ratios demonstrate that the component with high $\delta^{18}O$ values was unlikely to be from the fluids or melts released from subducted slab, which would be relatively depleted in Nb and Ta (Kessel et al., 2005). Thus, the recycled oceanic crust, particularly the upper altered crust and marine sediments with $\delta^{18}O$ up to 20‰ (Eiler, 2001; Gregory and Taylor, 1981), is the most likely candidate for this component.

In addition, the altered oceanic crust and marine sediments are characterized by high H_2O/Ce ratios (up to ~5000 and ~1280, respectively, Dixon et al., 2002). For the trace

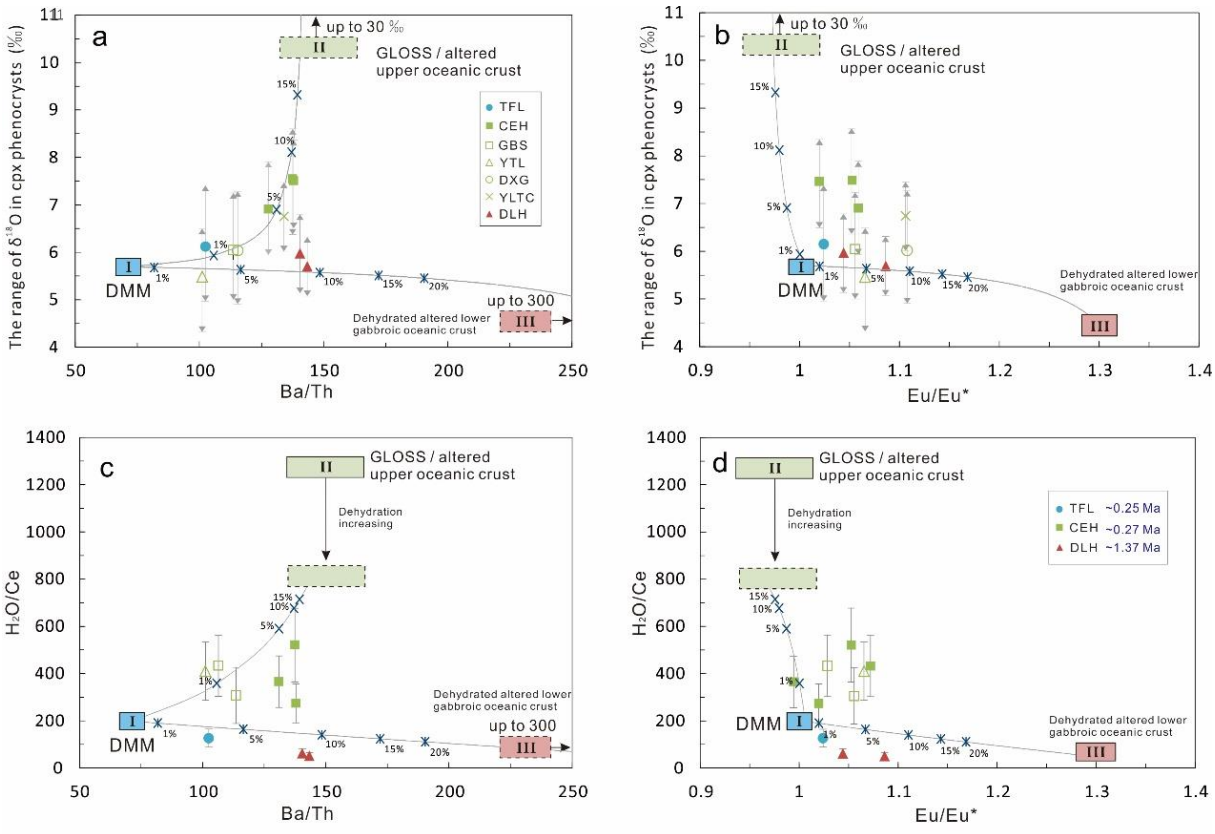

Figure 4-30. Comparison of the range of $\delta^{18}O$ values in cpx phenocrysts and the trace element ratios (H_2O/Ce, Ba/Th and Eu/Eu*) in Chaihe-aershan basalts. The squares show the possible end members of mantle sources. In a) and b), the $\delta^{18}O$ values of DMM, GLOSS, altered upper oceanic crust and altered lower gabbroic oceanic crust are from Eiler (2001). The H_2O/Ce ratios of DMM, GLOSS, altered upper oceanic crust and altered lower gabbroic oceanic crust are from Dixon et al. (2002) and Plank and Langmuir (1998). The ratios of Ba/Th and Eu/Eu* for DMM, GLOSS, altered upper oceanic crust and altered lower gabbroic oceanic crust are calculated from Bach et al. (2001), Kelley et al. (2003), Plank and Langmuir (1998) and Workman and Hart (2005). The ratios of Ba/Th in dehydrated altered lower oceanic crust are calculated based on the element mobility in water (Kessl et al., 2005; Kogiso et al., 1997). The grey lines are mix lines calculated between components I and II and components I and III. In order to let all points match the mix lines, the component II should be a mixture between the marine sediments and altered oceanic crust. The ages of the CEH, TFL and DLH basalts are from Fan et al. (2011).

elements, studies of the drilled marine sediments and oceanic crust demonstrated that the marine sediments have a relatively high Ba/Th ratio (Plank and Lagmuir, 1988) and that the abundance of Ba in the altered basaltic upper crust should increase relative to

Th (Bach et al., 2001; Kelley et al., 2003). These are consistent with the characteristics of Component II.

Thus, Component II is most likely from hydrothermally altered upper oceanic crust/marine sediments.

Component III: Dehydrated altered lower gabbroic oceanic crust

Component III, best represented by the DLH basalts, has a relatively high Ba/Th ratio, a positive Eu anomaly, relatively low $\delta^{18}O$ value and low H_2O/Ce ratio (Fig. 4-30).

Experimental studies have shown that the mobility of Ba is identical to that of Th in fluid (Kessel et al., 2005; Kogiso et al., 1997); thus, the Ba/Th ratio remains relatively constant in subducted oceanic crust during dehydration. As mentioned above, the Ba/Th ratio of oceanic crust will increase during oceanic crust alteration (Bach et al., 2001; Kelley et al., 2003). Therefore, the dehydrated altered oceanic crust is characterized by high Ba/Th ratio. The H_2O/Ce ratio of this dehydrated oceanic crust can be as low as 100 (depending on the efficiency of dehydration, Dixon et al., 2002; Shaw et al., 2012), which is consistent with the H_2O/Ce ratio of Component III (Figs. 4-30c, 29d).

Eu anomalies are typically associated with plagioclase (pl), in which Eu is highly compatible. Because of the rare presence of pl phenocrysts in the DLH basalts, the positive Eu anomaly of Component III is unlikely to be caused by the accumulation of pl. Thus, the positive Eu anomaly may indicate the presence of a pl-bearing signature in the mantle source, which suggests that the dehydrated altered oceanic crust discussed above is likely the lower gabbroic oceanic crust. Similar to the Chaihe-aershan basalts, the Shuangliao basalts of NE China have a positive Eu anomaly, which can be explained by the lower gabbroic oceanic crust in the mantle source (Figs. 4-12, 4-30; Xu et al., 2012). In addition, the depleted oxygen isotope compositions relative to the normal mantle of Component III also indicate the contribution of the lower oceanic crust, which has undergone high-T water–rock interaction (Eiler, 2001; Gregory and Taylor, 1981).

Overall, Component III should be from a dehydrated altered lower gabbroic oceanic crust.

The mixing lines between these components were calculated. The relative contributions of these recycled oceanic components in the mantle source changed

significantly within a limited time (Fig. 4-30). For example, in the mantle source of relatively old basalts (DLH basalts, 1.37 Ma), the recycled altered lower gabbroic oceanic crust component and ambient normal mantle sources dominated (with a positive Eu anomaly and relatively low $\delta^{18}O$ values and low H_2O/Ce ratios). One million years later (0.25-0.27 Ma), marine sediments and altered upper oceanic crust became major source components, triggering melting and eruption of the water-rich CEH and TFL basalts (with high $\delta^{18}O$ values and H_2O/Ce ratios). Notably, the proportion of the fusible components (marine sediments and/or altered upper oceanic crust) in the mantle source of Chaihe-aershan basalts increased over time.

4.3.2.5 Mass-balance modeling of partial melting of proposed source components

As discussed above, three primary components (hydrothermally altered upper oceanic crust and marine sediments, altered lower gabbroic oceanic crust, and ambient mantle) are identified in the mantle source of Chaihe-aershan basalts. The mass-balance modeling of the partial melting of these source components was conducted to attempt to match the trace element patterns of the samples.

The depleted mantle (DMM) in Workman and Hart (2005) and GLOSS in Plank and Langmuir (1998) were assumed to represent the ambient mantle and marine sediment. The trace elements compositions of altered upper oceanic crust (UOC) were estimated from the drilled upper oceanic crust at ODP site 801 (Kelly et al., 2003), calculated by mixing of highly altered TAB (40%) and MORB (60%). To fit the model, the abundance of U was lowered by 30% and the abundance of Sr was increased by 30%, which are within the range of the results in Kelly et al. (2003). The composition of the altered lower gabbroic oceanic crust (LOC) was evaluated by the most altered sample at ODP Hole 735B (Bach et al., 2001). The compositions of these components are shown in Table 4-13.

The trace element concentrations of the marine sediment and oceanic crust would vary by dehydration during subduction. The residual trace element concentration of marine sediment was calculated by:

$$C_{Sed}^{residual} = C_{Sed}^{0} \times (1 - Mob.\%) \quad (4\text{-}6)$$

where the C_{Sed}^{0} and $C_{Sed}^{residual}$ are the element concentrations of marine sediment

before and after dehydration, and the Mob.% is the elemental mobility during subduction (Table 4-13), which are calculated from Johnson and Plank. (2000). Kessel et al. (2005) and Kogiso et al. (1997) have estimated the partition coefficient between fluid/rock ($D^{fluid/rock}$) during the subduction of oceanic crust. The residual element concentrations of recycled oceanic crust was calculated by:

$$C_{Cust}^{residual} = C_{Crust}^{0} / \left[1 + \left(D^{fluid/rock} \times f\right) - f\right] \quad (4\text{-}7)$$

where the C_{Crust}^{0} and $C_{Crust}^{residual}$ are the elements concentrations of oceanic crust before and after the dehydration. The $D^{fluid/rock}$ of oceanic crust was calculated by averaging the experimental data (shown in Table 4-13) from Kessel et al. (2005) and Kogiso et al. (1997).

The mineral/melt partition coefficients ($D^{mineral/melt}$) for each element is displayed in Table 4-13. The $D^{mineral/melt}$ used for olivine and orthopyroxene were estimated by experimental data from Salters and Longhi. (1999) and Salters et al. (2004). The $D^{mineral/melt}$ of clinopyroxene and garnet were the average values from Johnson (1998), Salters and Longhi. (1999) and Salters et al. (2004). In order to fit the data better, the $D^{garnet/melt}$values of Zr and Hf were increased by 30% from the averages, which are within the range of the experimental results in Johnson (1998), Salters and Longhi. (1999) and Salters et al. (2004).

The hydrothermally altered upper oceanic crust, marine sediment and altered lower gabbroic oceanic crust in the mantle source would undergo dehydration during subduction. Considering that the hydrothermally altered upper oceanic crust and marine sediment in the mantle source of Chaihe-aershan basalts have high H_2O/Ce ratios, the H_2O/Ce ratio of the altered lower gabbroic oceanic crust is low, the dehydrated degree of hydrothermally altered upper oceanic crust and marine sediments was assumed to be 1% and that for altered lower gabbroic oceanic crust was assumed to be 4%. According to these degrees of dehydration, the compositions of the hydrothermally altered upper oceanic crust, marine sediments and dehydrated altered lower gabbroic oceanic crust in the mantle source were calculated. During the melting of mantle source, the mineralogy of the mantle source was assumed to be composed of 60% olivine, 18% orthopyroxene, 15% clinopyroxene and 7% garnet, and that the total mineral/melt partition coefficient estimated by this type of mineral assemblage remains constant during the partial melting progress. The batch melting model was used to simulate the trace elements of

the partial melt mixed with hydrothermally altered upper oceanic crust or marine sediment, altered lower gabbroic oceanic crust, and ambient mantle. The composition of melt was calculated by:

$$C_{melt} = C_o/(f + D(1 - f) \quad (4\text{-}8)$$

where C_o and C_{melt} are the element concentrations of melt and initial source, f is the degree of partial melting and D is the total mineral/melt partition coefficient. The proportion of different components and the degree of partial melting were adjusted to make the composition of the calculated melt consistent with the Chaihe-aershan basalts.

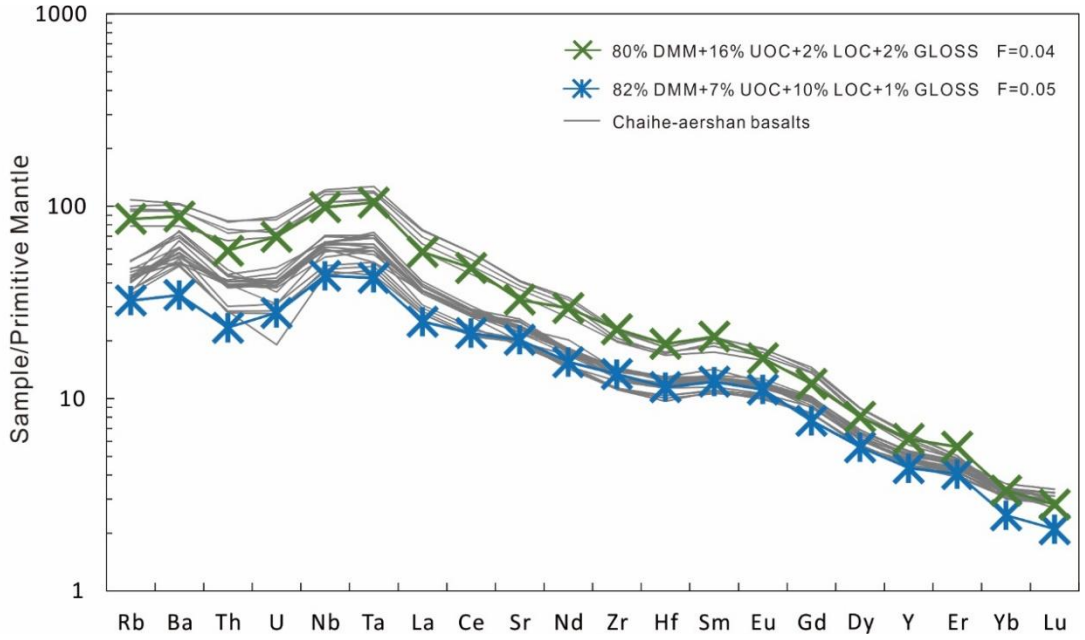

Figure 4-31. Mass-balance modeling of the partial melting of the proposed source components. All the trace element concentrations are normalized to primitive mantle (Sun and McDonough. 1989). The trace element concentration of the DMM, GLOSS, altered upper oceanic crust (UOC) and altered lower gabbroic oceanic crust (LOC) are from Workman and Hart (2005), Plank and Langmuir (1998), Kelley et al. (2003) and Bach et al. (2001). The dehydrated compositions of GLOSS, UOC and LOC in the mantle source are calculated through the trace element mobility in the water and assumed dehydration degree. The batch melting model was used to simulate the progress of partial melting. Partial melting of these sources with the variable proportion of different components and the partial melting degree results in the compositions of the model melts (blue and green crosses). F is the degree of partial melting. The detailed parameters used and model calculation are discussed in the Text.

The result shows that the trace element composition of Chaihe-aershan basalts can be matched by 4% partial melting of mantle source mixed with 80% depleted mantle (DMM), 16% hydrothermally altered upper oceanic crust (UOC), 2% dehydrated altered lower gabbroic oceanic crust (LOC) and 2% marine sediment (GLOSS), and 5% partial melting of mantle source mixed by 82% DMM, 7% UOC, 10% LOC and 1% GLOSS (Fig. 4-31).

The results of the modeling are in good agreement with the samples (Fig. 4-31), indicating that Chaihe-aershan basalts could come from the partial melting of these three components recognized before. In addition, Component II might be a mixture of marine sediments and altered upper oceanic crust. There are 1 to 2 wt.% marine sediments in the mantle source.

Table 4-13. The parameters used in the modeling trace element pattern calculation

	DMM	UOC	LOC	GLOSS	$D^{fluid/rock}$ (oceanic crust)	Mob $\%^{sediment}$	$D^{ol/melt}$	$D^{cpx/melt}$	$D^{opx/melt}$	$D^{gt/melt}$
Rb	0.05	28.2	0.75	57.2	200	43.5	0.0003	0.0004	0.0002	0.0002
Ba	0.563	162.14	11.57	776	30	49.6	0.000005	0.00049	0.000006	0.00007
Th	0.0079	1.0474	0.041	6.91	25	32.6	0.00005	0.0058	0.002	0.009
U	0.0032	0.40852	0.018	1.68	25	45.9	0.00038	0.010	0.002	0.028
Nb	0.149	17.176	2.54	8.94	0.1	35.4	0.0005	0.0092	0.004	0.0091
Ta	0.0096	1.0478	0.067	0.63	0.1	36.4	0.0005	0.0125	0.004	0.015
La	0.192	10.332	1.02	28.8	20	32.1	0.0005	0.0369	0.00355	0.0012
Ce	0.55	25.524	3.09	57.3	18	31.7	0.0005	0.0685	0.004	0.011
Sr	7.66	256.62	167.9	327	30	52.8	0.00004	0.101	0.0007	0.0016
Nd	0.581	15.726	2.54	27	12	30.6	0.00042	0.135	0.012	0.058
Zr	5.08	135.8	33.3	130	1.2	34.1	0.0005	0.121	0.14	0.27
Hf	0.157	3.176	0.729	4.06	1.2	35.3	0.00165	0.220	0.027	0.32
Sm	0.239	4.094	0.83	5.78	8	31.4	0.0011	0.258	0.02	0.24
Eu	0.096	1.38	0.59	1.31	2	29.5	0.00095	0.32	0.03	0.4
Gd	0.358	4.882	1.18	5.26	1	29.4	0.0011	0.255	0.036	1.2
Dy	0.505	5.068	1.41	4.99	0.3	29.2	0.0027	0.348	0.038	2.1
Y	3.33	29.84	7.6	29.8	0.02	29.4	0.009	0.440	0.07	3.1
Er	0.348	2.922	0.84	2.92	0.01	29.2	0.013	0.329	0.055	3.3
Yb	0.365	2.75	0.8	2.76	0.01	29.2	0.02	0.383	0.08	6.05
Lu	0.058	0.4282	0.12	0.413	0.01	28.9	0.02	0.417	0.12	7.05

Note: The parameters for each element were estimated as described in the Text

4.3.3 Summary

(1) The large variations of the H_2O contents in the "primary" magmas of the Chaihe-aershan (0.23-2.70 wt.%) and the $\delta^{18}O$ values of cpx phenocrysts (4.27 to 8.57‰) imply the compositional heterogeneity of the source.

(2) The $\delta^{18}O$ values of cpx phenocrysts within individual samples display considerable variation (1.28-2.31‰ for $\delta^{18}O$ value), indicating that cpx phenocrysts crystallized in a complex magma plumbing system and mixed during magma ascent or sustained injection of magmas during crystallization. The wide variations of the H_2O contents also suggest that magma mixing occurred shortly before eruptions.

(3) The relations between the $\delta^{18}O$ values of cpx phenocrysts and the H_2O/Ce ratio, Ba/Th ratio and Eu anomaly of whole rocks demonstrate the contributions of three components to the mantle source (hydrothermally altered upper oceanic crust and marine sediments, altered lower gabbroic oceanic crust, and ambient mantle). The proportions of these three components have varied widely over a short time (~1.27 Ma to ~0.25 Ma).

4.4 Xiaogulihe basalts

4.4.1 Results

4.4.1.1 Chemical compositions of phenocrysts

The BSE images show that most of the cpx are euhedral and homogeneous (Fig. 4-32). The Mg# values of cpx vary from 82.4-89.2, similar to those of the coexisting olivine phenocrysts (Sun et al., 2015), demonstrating that they are syn-crystallized products. The TiO_2 contents of cpx phenocrysts vary form 0.68 w to 2.23 wt.%.

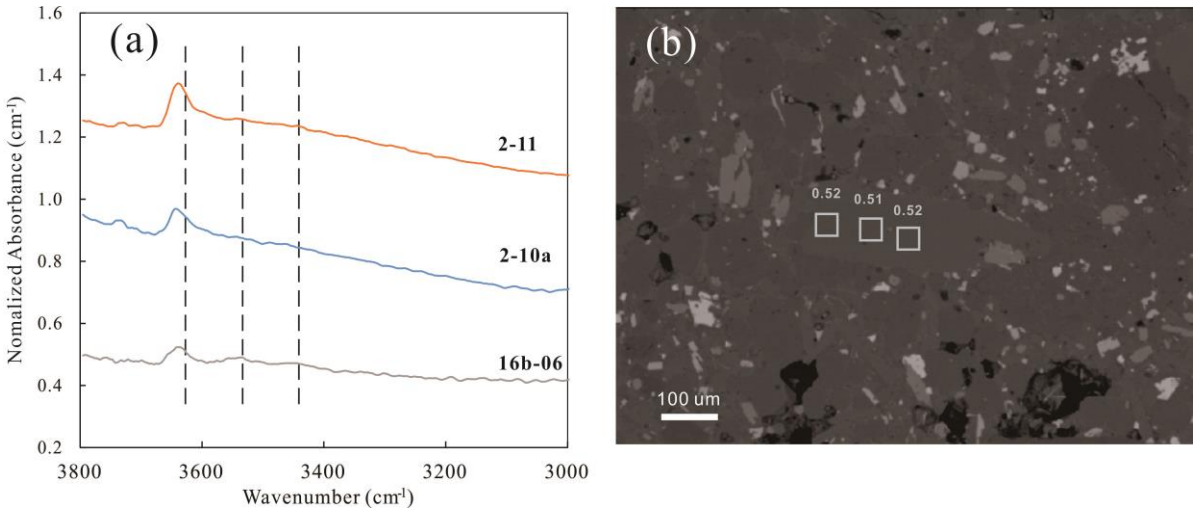

Figure 4-32. a) Representative OH IR absorption spectrum of cpx phenocrysts, dashed lines mark the position of individual OH bands. The absorption intensity has been normalized to 1 cm; b) BSE image of cpx phenocryst in Xiaogulihe ultrapotassic volcanic rocks. The red squares show the positions of the spots for profile analysis, from the core to the rim, the H_2O content of correspond melt is 0.52, 0.51, 0.52 wt% (GLH12-03 listed in Table 4-14).

4.4.1.2 Water content of clinopyroxene phenocrysts and melts

The IR absorption spectra of the Xiaogulihe cpx phenocrysts in the OH-stretching vibration region are composed of three bands: 3630-3620 cm^{-1}, 3540-3520 cm^{-1}, and 3470-3450 cm^{-1}(Fig. 4-32a) which are consistent with those of the Shuangliao, Wulanhada and Chaihe-aershan baslats. Some profile analyses were conducted in cpx phenocrysts and it shows that water content is homogeneous from the core to the rim

(Fig. 4-32b). The calculated H_2O contents of cpx phenocrysts and corresponding equilibrated melts are listed in Table 4-14 and plotted versus Mg# values of cpx in Fig. 4-33. The H_2O content of cpx phenocrysts and corresponding melts are relatively low (18.3-56.6 ppm, 0.24-0.74 wt.%).

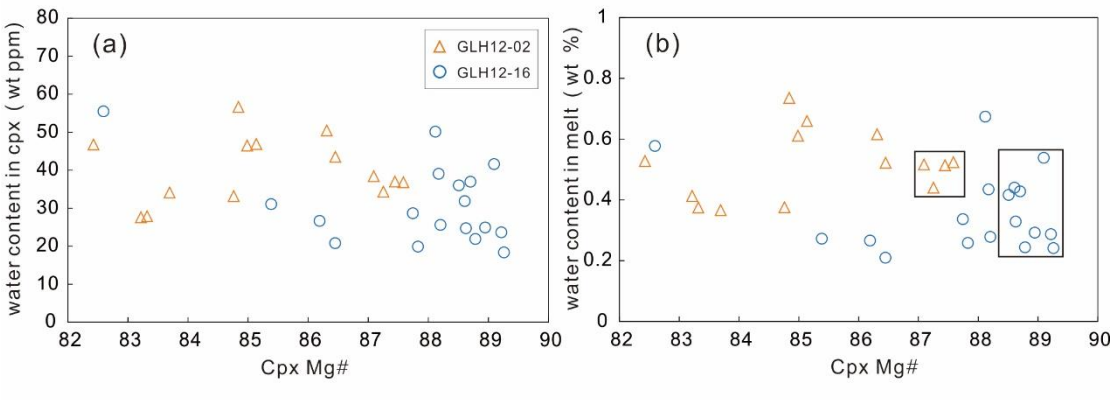

Figure 4-33. H_2O content in cpx phenocrysts (a) and melts with which they were equilibtated (b) vs cpx Mg#. The points in squares in (b) are data used to calculate the H_2O content of the "primary" magmas.

Table 4-14. Major element compositions of cpx phenocrysts and calculated water contents of cpx phenocrysts and corresponding melts

		Na_2O	K_2O	SiO_2	Al_2O_3	MgO	CaO	Cr_2O_3	FeO	NiO	MnO	TiO_2	Total	Mg#	$X(^{iv}Al)$	XCa	$D^{cpx/melt}$	$A(cm^{-2})$	t (mm)	H_2O in cpx (wt ppm)	H_2O in melt (wt %)
GLH12-02	2-01a	0.29	0.01	53.19	0.96	15.94	23.45	0.33	4.15	b.l.d.	0.05	1.35	99.71	87.25	0.042	0.92	0.0078	0.7143	0.088	34.3	0.44
	2-01b	0.79	0.01	51.50	1.25	15.27	22.10	0.22	5.80	b.l.d.	0.13	2.23	99.31	82.43	0.055	0.88	0.0089	0.9724	0.088	46.8	0.53
	2-02	0.35	b.l.d.	52.76	0.87	15.77	23.39	0.01	4.97	0.06	0.09	1.36	99.64	84.99	0.038	0.93	0.0076	1.1861	0.108	46.5	0.61
	2-03a	0.36	0.01	52.78	1.15	15.85	23.12	0.43	4.43	b.l.d.	0.09	1.40	99.60	86.45	0.050	0.91	0.0083	1.0283	0.100	43.5	0.52
	2-03b	0.26	b.l.d.	53.64	0.68	16.20	23.33	0.20	4.15	b.l.d.	0.08	1.06	99.59	87.44	0.028	0.92	0.0072	0.8747	0.100	37.0	0.51
	2-03c	0.27	0.04	53.41	0.64	15.70	23.72	0.41	3.97	0.04	0.10	1.09	99.39	87.59	0.028	0.94	0.0070	0.8702	0.100	36.8	0.52
	2-06	0.24	b.l.d.	53.29	0.77	16.01	23.28	0.28	4.23	0.04	0.08	1.17	99.38	87.09	0.034	0.92	0.0074	0.9169	0.101	38.4	0.52
	2-07a	0.39	0.01	53.23	0.53	15.07	23.43	b.l.d.	5.42	0.05	0.18	0.79	99.09	83.22	0.019	0.93	0.0067	0.7113	0.109	27.6	0.41
	2-07b	0.35	0.01	52.71	0.80	15.39	23.40	0.01	5.49	0.02	0.13	1.11	99.43	83.32	0.035	0.93	0.0074	0.718	0.109	27.9	0.38
	2-08	0.37	b.l.d.	52.69	0.90	15.63	23.25	0.08	4.98	0.01	0.15	1.36	99.42	84.84	0.039	0.92	0.0077	1.499	0.112	56.6	0.74
	2-09	0.26	b.l.d.	52.69	0.64	15.94	23.33	b.l.d.	4.96	0.01	0.11	1.21	99.13	85.14	0.028	0.93	0.0071	0.8531	0.077	46.9	0.66
	2-10a	0.41	b.l.d.	51.85	1.59	15.19	23.42	0.20	5.28	0.04	0.08	2.00	100.05	83.69	0.069	0.93	0.0093	1.0724	0.133	34.1	0.37
	2-10b	0.36	0.01	52.07	1.38	15.51	23.15	0.02	4.97	0.07	0.10	1.64	99.27	84.76	0.060	0.92	0.0088	1.043	0.133	33.2	0.38
	2-11	0.38	0.01	52.57	1.11	15.42	23.22	0.52	4.36	0.02	0.05	1.62	99.28	86.31	0.049	0.92	0.0082	1.9071	0.160	50.4	0.62
GLH12-16	16-01b	0.35	b.l.d.	53.82	0.81	16.57	23.42	0.16	3.98	0.03	0.11	0.89	100.15	88.12	0.033	0.92	0.0074	0.8171	0.069	50.1	0.67
	16-05b	0.37	0.01	52.78	1.41	15.91	23.16	0.83	3.96	0.01	0.06	0.94	99.43	87.74	0.054	0.92	0.0085	0.5012	0.074	28.7	0.34
	16-07	0.36	0.01	53.00	1.18	16.20	23.44	0.73	3.49	0.04	0.05	1.01	99.50	89.22	0.050	0.92	0.0082	0.4523	0.081	23.6	0.29
	16-08	0.44	0.01	51.84	1.73	15.58	22.78	0.99	4.35	0.06	0.09	1.66	99.51	86.45	0.075	0.90	0.0099	0.3979	0.081	20.8	0.21
	16-09	0.39	0.01	52.44	1.31	16.18	23.36	0.83	3.68	0.06	0.04	1.11	99.41	88.70	0.057	0.92	0.0086	0.7421	0.085	36.9	0.43
	16-13	0.29	0.01	54.02	0.81	16.73	23.23	0.51	3.83	0.03	0.11	0.85	100.42	88.63	0.033	0.91	0.0075	0.6009	0.103	24.7	0.33
	16-15	0.41	b.l.d.	51.83	1.45	15.91	23.25	0.82	3.81	0.05	0.09	1.33	98.96	88.17	0.064	0.93	0.0090	0.9685	0.105	39.0	0.43
	16-18	0.47	0.01	51.09	2.22	15.59	22.78	0.73	4.76	0.05	0.09	1.37	99.14	85.39	0.098	0.91	0.0114	0.7334	0.100	31.0	0.27
	16-20	0.44	0.01	52.31	1.43	15.89	23.21	0.91	3.58	b.l.d.	0.10	1.14	99.03	88.78	0.063	0.92	0.0090	0.4909	0.095	21.9	0.24
	16-24	0.25	0.01	53.61	0.87	16.76	23.20	0.63	3.60	0.04	0.09	0.68	99.74	89.26	0.036	0.91	0.0076	0.4073	0.094	18.3	0.24
	16b-03	0.33	b.l.d.	53.31	1.27	16.45	23.36	0.80	3.65	0.05	0.06	1.00	100.28	88.95	0.054	0.91	0.0085	0.559	0.095	24.9	0.29
	16b-05	0.37	b.l.d.	52.28	1.82	15.69	23.26	0.50	4.48	0.07	0.08	1.73	100.28	86.19	0.079	0.91	0.0100	0.7239	0.115	26.6	0.27
	16b-06	0.25	b.l.d.	53.81	0.96	16.21	23.06	0.60	3.72	b.l.d.	0.09	0.89	99.58	88.61	0.027	0.91	0.0072	0.9028	0.12	31.8	0.44
	16b-10	0.40	b.l.d.	52.33	1.51	15.90	23.15	0.78	3.79	b.l.d.	0.04	1.34	99.24	88.20	0.066	0.92	0.0092	0.5803	0.096	25.6	0.28

Table 4-14. (continued)

	Na_2O	K_2O	SiO_2	Al_2O_3	MgO	CaO	Cr_2O_3	FeO	NiO	MnO	TiO_2	Total	Mg#	$X(^{iv}Al)$	XCa	$D^{cpx/melt}$	$A(cm^{-2})$	t (mm)	H_2O in cpx (wt ppm)	H_2O in melt (wt %)
16b-11	0.37	0.01	52.86	1.52	15.87	23.20	0.95	3.67	0.04	0.07	1.04	99.59	88.51	0.056	0.91	0.0086	0.8332	0.098	36.0	0.42
16b-12	0.30	b.l.d.	53.68	1.02	16.35	23.05	0.49	4.04	0.04	0.10	0.95	100.02	87.83	0.036	0.90	0.0077	0.3852	0.082	19.9	0.26
16b-13	0.32	0.01	53.33	0.86	16.54	22.94	0.63	3.61	0.01	0.04	1.05	99.32	89.10	0.037	0.90	0.0077	0.8058	0.082	41.6	0.54

Note: Mg#=100*Mg/(Mg+Fe)

b.l.d., below the limit of detection

4.4.2 Discussion

4.4.2.1 Previous studies

Sun et al. (2014) and Sun et al. (2015) conducted detailed geochemical studies on the Xiaogulihe ultrapotassic volcanic rocks, including major and trace element compositions, Sr-Nd-Pb-Hf isotopic compositions and oxygen isotope compositions of olivine phenocrysts. The Xiaogulihe ultrapotassic volcanic rocks are characterized by extremely high K_2O contents (>7 wt.%) and K_2O/NaO ratios (>3) (Sun et al., 2014). The positive correlation between $^{187}Os/^{188}Os$ and 1/Os suggests insignificant crustal contamination (less than 1%) (Sun et al., 2014). Considering the low $^{206}Pb/^{204}Pb$ ratios, moderately high $^{87}Sr/^{86}Sr$ ratios of bulk rocks and high $\delta^{18}O$ values of olivine phenocrysts, Sun et al. (2014) and Sun et al. (2015) proposed that the potassium-rich component in the mantle source came from phlogopite-bearing peridotites in SCLM which have been metasomatized by potassium-rich silicate melts derived from ancient (>1.5 Ga) subducted continental-derived sediments.

4.4.2.2 Water content in the "primary" melts

The main factors affecting the H_2O content in cpx phenocrysts are crustal contamination, crystal fractionation and degassing coupled with diffusion of H in cpx. Os isotope compositions indicate that the Xiaogulihe ultrapotassic rocks have not been significantly affected by crustal materials during magma ascent (Sun et al., 2014). The Mg# values of these ultrapotassic rocks are 69.1 to 71.6 (Sun et al., 2014), close to the so-called primitive mantle magmas, suggesting that crystal fractionation is limited. The water content profile on some cpx phenocrysts is homogeneous from the core to the rim, demonstrating that no measurable H diffusion in cpx phenocrysts occurred (Fig. 3-30). Moreover, with the decrease of Mg# of cpx phenocrysts, H_2O contents of melts with which cpx equilibrated remain unchanged (Fig. 3-31), suggesting that the degassing or water enrichment was not significant during magma evolution. In summary, the H_2O contents of the samples can reflect the values of magma source.

"Primary" magmas refer to the initial melts equilibrated with earliest crystallized phenocrysts. As mention above, for the Xiaogulihe ultrapotassic rocks, cpx and ol phenocrysts crystallized simultaneous and the crystal fractionation is limited, suggesting the cpx with high Mg# are earliest phenocrysts, so we can use the cpx

phenocrysts with Mg# >87 in the sample GLH12-02 and Mg# >88.5 in the sample GLH12-16 to estimate the water content of the "primary" magmas (Fig. 3-31b). The calculated water contents of the "primary" magmas are 0.36±0.11 and 0.50±0.15 wt%, which are within the range of mid-ocean ridge basalts (MORBs, 0.1-0.3 wt%, Asimow et al., 2004; Danyushevsky et al., 1993, 2000; Dixon, 1988; Michael, 1988, 1995; Sobolev and Chaussidon, 1996; Saal et al., 2002; Simons et al., 2002) and ocean island basalts (OIBs, 0.3-1 wt%, Dixon et al., 1997, 2002; Dixon and Clague, 2001; Nichols et al., 2002; Simons et al., 2002; Wallace, 1998), and obviously lower than those of most back-arc basin basalts (BABBs, 0.2-2.0 wt%, Danyushevsky et al., 1993; Hochstaedter et al., 1990; Stolper and Newmann, 1994) and island arc basalts (IABs, 2.0-8.0 wt%, Dobson et al., 1995; Sisson and Layne, 1993; Wallace, 2005) (Fig. 3-32a). The calculated H_2O/Ce ratio of the "primary" magmas is about 15, much lower than that of the normal depleted mantle (DMM, 150-210, Bizimis and Peslier, 2015; Dixon et al., 2002) and primitive mantle (PM, ~200, calculated by McDonough and Sun, (1995) and Dixon and Clague, (2001)) (Fig. 3-32b).

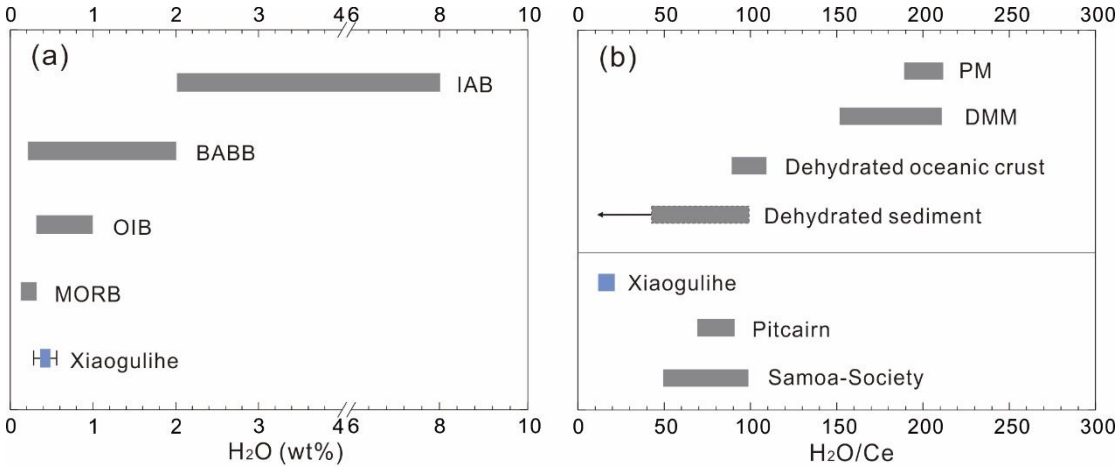

Figure 4-34. a) Calculated H_2O content of the Xiaogulihe ultrapotassic "primary" magmas. The ranges of H_2O content for OIBs, MORBs, BABBs and IABs are from Dixon et al. (2004) and references therein. b) Comparison of the H_2O/Ce ratio of the Xiaogulihe ultrapotassic "primary" magmas with that of PM, DMM, dehydrated oceanic crust and sediment, Pitcarin and Samoa-society basalts (Bizimis and Peslier, 2015; Dixon et al., 2002; Kendrick et al., 2014, 2015; Workman et al., 2006).

4.4.2.3 Source of the K-rich component

The low H_2O/Ce ratio of the Xiaogulihe "primary" magmas suggests that the H_2O content of K-rich component is especially low. Dixon et al. (2002) proposed that the H_2O/Ce ratio of the recycled sediments would be below 100 after highly efficient (>92%) dehydration and the Samoa-Society and Pitcairn seamounts basalts, which are interpreted to contain dehydrated sedimentary or lithospheric components, also have low H_2O/Ce ratios (50-100 and 80, Fig. 4-34b) (Kendrick et al., 2014, 2015; Workman et al., 2006). High-Pressure experiments demonstrated that the continental sediments would transform to K-hollandite, garnet, stishovite, etc. at 15-23 GPa (Rapp et al., 2008). Among them, K-hollandite (particularly the dry K-hollandite), with K_2O>15%, has a broad P-T stability field and will be stable until the mantle transition zone (MTZ) (Rapp et al., 2008), and then releases abundant potassium when it breaks down. The ancient sediments can also account for the low $^{206}Pb/^{204}Pb$ ratios, moderately high $^{87}Sr/^{86}Sr$ ratios high $\delta^{18}O$ values in the Xiaogulihe ultrapotassic volcanic rocks. Thus, the ancient sediments which have been dehydrated significantly during subduction (e.g., dry K-hollandite) could be a candidate for the K-rich component in the mantle source of the Xiaogulihe ultrapotassic volcanic rocks.

4.4.3 Summary

(1) The Xiaogulihe ultrapotassic volcanic rocks are characterized by low H_2O contents (0.36-0.50 wt%, within the range of MORBs and OIBs) and low H_2O/Ce ratio (~15, observably much lower than that of the DMM), suggesting that the K-rich component is "dry".

(2) Combined with the low $^{206}Pb/^{204}Pb$ ratios, moderately high $^{87}Sr/^{86}Sr$ ratios of the bulk rock and the high $\delta^{18}O$ values of olivine phenocrysts, the ancient sediments which underwent significant dehydration could be a candidate for the K-rich component in the mantle source of the Xiaogulihe ultrapotassic volcanic rocks.

Chapter 5. Implications for the genesis of eastern China Cenozoic basalts

5.1 MTZ source constrained by water content

5.1.1 The proposed sources

In the last 30 years, a lot of work has been carried out to study the continental intraplate basalts in eastern China. There are controversial opinions on the origins where basalts sourced: the lithospheric mantle (e.g., Chu et al., 2013; Wang et al., 2011; Zhang et al., 2009), the asthenospheric mantle (e.g., Choi et al., 2005; Niu, 2005; Zou et al., 2000) and the mantle transition zone (MTZ) (e.g., Sakuyama et al., 2013; Xu et al., 2012; Kuritani et al., 2011, 2013). Recently, the signal of a recycled oceanic crust has been recognized in the mantle source of these basalts by new geochemical approaches, including H_2O content of magma (Liu et al., 2015a), O isotopic compositions of the phenocrysts (Liu et al., 2015a; Wang et al., 2015), Mg isotopic compositions of bulk rock (Huang et al., 2015), and composition of melt inclusions (Li et al., 2016). Considering that the seismic tomography imaging has shown the remnants of the subducted Pacific slab in the MTZ beneath eastern China (e.g., Huang and Zhao, 2006; Liu et al., 2017b; Wei et al., 2012), the enriched components with the signal of a recycled oceanic crust were associated with this remnant Pacific slab in the MTZ. The interpretation was supported by the recent study conducted by Wang et al. (2015). Combined oxygen isotope compositions with the Ar/Ar ages and other geochemical features, they identified the signal of an altered subducted oceanic crust in the mantle source of the Chifeng continental flood basalts in eastern China. Considering the existence of a stagnant Pacific slab in the MTZ, they proposed that these basalts have their origin from the MTZ. Another evidence was the high water content of Chifeng basalts, which is in agreement with a hydrous MTZ. However, the water content of Chifeng basalts was estimated by a non-analytical approach (modeling calculations on MELTS, Hong et al., 2013). Thus, they are indirect evidences for whether the mantle source of these basalts is water rich and located in the MTZ.

Natural samples and experimental studies have demonstrated that the water contents in different layers of mantle vary greatly: the H_2O content of the upper mantle is 50-250 ppm typically, the H_2O content in MTZ can be as high as 1% and the lower mantle

might be similar to upper mantle (e.g. Bodnar et al., 2013; Hirschmann et al., 2005; Ohtani, 2015; Panero et al., 2015). A hydrous MTZ suggest that the water content in the source of continental basalts can be a direct evidence for whether these basalts come from the MTZ. In some continental lithospheric mantle, the impact of multi-stage metasomatism would produce hydrous minerals (amphibole, phlogopite), which are rich in water (Hawkesworth et al., 1987). The H_2O contents of lithosphere in eastern China have been studied in detail by Hao et al. (2014), Hao et al. (2016), Xia et al. (2010), Xia et al. (2013a), Yang et al. (2008) and Yu et al. (2011), which provide convinced references for comparison with water content of the source for continental basalts.

5.1.2 Estimating water content in the mantle source

Based on mass-balance, the water content of the source can be calculated from the H_2O content of "primary" magma, degree of partial melting and partition coefficient of H_2O.

For the modal batch melting modeling, the H_2O content of the mantle source can be calculated by equation:

$$C_o^{H2O} = C_m^{H2O} * (D + f * (1 - D)) \quad (5\text{-}1)$$

And for the modal fractional melting modeling, the equation is

$$C_o^{H2O} = \frac{C_m^{H2O}}{f} * (1 - (1 - f)^{1/D}) \quad (5\text{-}2)$$

where C_o^{H2O} and C_m^{H2O} are the concentrations of the H_2O in the mantle source and melt, respectively, f is the degree of partial melting and D is the bulk partition coefficient of H_2O. H_2O contents of "primary" magma for continental basalts have been already estimated in this work and previous studies (Liu et al., 2015a, b; Liu et al., 2016), and the experimental studies have constrained the partition coefficient of H_2O between peridotites and the basaltic melts (0.005-0.013, Aubaud et al., 2004; Hirchmann et al., 2009; O'Leary et al., 2010; Tenner et al., 2009). Now, only the partial melting degree of the continental basalts is needed to determine the H_2O content of the mantle source.

Maaløe, (1994) and Zou and Zindler, (1996) proposed that the partial melting degree

of basalts can be estimated by the ratios of trace elements (e.g., La/Sm). In their calculation, two magmas with same source and different partial melting degree were compared (magma 1 and magma 2). Based on the modal batch melting modeling, the equations for the concentrations of the two trace elements (a, b) in magma 1 (melting degree is f) are:

$$C_1^a = \frac{C_0^a}{D^a + f*(1-D^a)} \tag{5-3}$$

$$C_1^b = \frac{C_0^b}{D^b + f*(1-D^b)} \tag{5-4}$$

and the concentrations of the two trace elements (a, b) in magma 2 (melting degree is g) are:

$$C_2^a = \frac{C_0^a}{D^a + g*(1-D^a)} \tag{5-5}$$

$$C_2^b = \frac{C_0^b}{D^b + g*(1-D^b)} \tag{5-6}$$

where C_0^a, C_0^b, C_1^a, C_1^b, C_2^a and C_2^b are the concentrations of trace element a and b in the source and magma 1 and 2. f and g are the partial melting degree of magma 1 and 2, D^a and D^b are the bulk partition coefficients of trace element a and b, which are calculated by the weighted average of the partition coefficient in each mineral.

$$D = \sum K^i D^i \tag{5-7}$$

Then, combining equations 5-3 with 5-5 and 5-4 with 5-6, the trace element content in the source can be offset, which are:

$$Q_a = \frac{C_1^a}{C_2^a} = \frac{D^a + g*(1-D^a)}{D^a + f*(1-D^a)} \tag{5-8}$$

$$Q_b = \frac{C_1^b}{C_2^b} = \frac{D^b + g*(1-D^b)}{D^b + f*(1-D^b} \tag{5-9}$$

According to equations 5-8 and 5-9, the partial melting degree f for magma 1 and g for magma 2 can be calculated.

In the same way, the equations for the modal fractional melting modeling are:

$$Q_a = \frac{C_1^a}{C_2^a} = \frac{g*(1-(1-f)^{\frac{1}{Da}})}{f*(1-(1-g)^{\frac{1}{Da}})} \tag{5-10}$$

$$Q_b = \frac{C_1^b}{C_2^b} = \frac{g*(1-(1-f)^{\frac{1}{Db}})}{f*(1-(1-g)^{\frac{1}{Db}})} \quad (5\text{-}11)$$

Using the Newton's method for the system of nonlinear equations, f and g in equation system 5-10 and 5-11can be solved.

In order to satisfy the assumption that the two magmas are from the same source and the variable trace element compositions are only caused by different partial melting extent; the basalts, with the largest difference in compositions, from the same volcano were chosen for calculations. Then, the partial melting degree of the remaining basalts from this volcano were calculated on the basis of this approach. Because the La/Sm ratios of basalts from the same source are primarily affected by the degree of partial melting (e.g., Schiling et al., 1978; Wood, 1979; Xu et al., 2012), La and Sm were selected to calculate partial melting degree of basalts. Maaløe and Pedersen, (2003) calculated the partial melting degree of Kauai basalts based on the Nd and Sm. For comparison, the Nd and Sm were also used to estimate the partial melting degree of the basalts in this work.

However, the method of the trace element ratio will not work on the basalts with close compositions (e.g., XTEJ in the Shuanliao basalts). Kelley et al. (2006) proposed that the TiO_2 content in the trace element-rich source of BABBs (back arc basin basalts) with MgO >8 wt.%, can be estimated by the TiO_2/Y ratio based on the equation:

$$C_{Ti}^o = \frac{(TiO_2/Y)_{sample}}{(TiO_2/Y)_{MORB}} * C_{Ti}^{DMM} \quad (5\text{-}12)$$

in which C_{Ti}^o is the concentration of TiO_2 in the source, C_{Ti}^{DMM} is the concentration of Ti in DMM (depleted MORB mantle, 0.133 wt.%, Salters and Stracke, (2004)), $(TiO_2/Y)_{sample}$ is the TiO_2/Y ratio of basalts and $(TiO_2/Y)_{MORB}$ is the TiO_2/Y ratio of DMM, which is 0.04 (Kelley et al., 2006). Thus, the partial melting degree of basalts can be directly estimated by the concentration of TiO_2 in the source. The equation on the modal batch melting modeling is:

$$f = \frac{\frac{C_{Ti}^o}{C_{Ti}^l} - D_{Ti}}{1 - D_{Ti}} \quad (5\text{-}13)$$

And for the modal fractional melting modeling, the equation is:

$$C_{Ti}^l = \frac{C_{Ti}^o}{f} * (1 - (1 - f)^{1/DTi}) \quad (5\text{-}14)$$

where C_{Ti}^{l} is the concentration of TiO_2 in the basalts. With this method, Kelley et al. (2006) successfully reproduced the original trend between the H_2O content and partial melting extent in BABBs. This method is applicable to the basalts with similar compositions.

In this work, both methods were used to calculate the partial melting extent of the basalts. During the calculation, the bulk partition coefficient of La, Nd, Sm and Ti were calculated on the mineralogy of the mantle source assumed as the composition of 60% olivine, 20% orthopyroxene, 15% clinopyroxene and 5% garnet (Salters and Stracke, 2004). The results show that the estimated partial melting degree using the two approaches are close for most samples. The range from 4% to 20%, is consistent with that of normal continental basalts (Table 5-1).

The H_2O content in the source of the basalts from eastern China (Shuangliao, Wulanhada, Chaihe-aershan, Xiaogulihe, Taihang, Shandong, Zhejiang, Fujian and Guangdong) were calculated. The minimum (based on the lowest partition coefficient of H_2O and the partial melting degree) results of H_2O contents in the mantle source for each sample are listed in Table 5-1. The conservatively estimated water contents of mantle source for basalts in eastern China approximately range from 200 to 6000 ppm for bath melting modeling and from150 to 4000 ppm for fractional melting modeling, and most of them are higher than 500 ppm (Table 5-1).

Table 5-1. The calculated partial melting degrees and H_2O contents in the source of the basalts from eastern China

	Sample	TiO_2 (wt.%)	MgO (wt.%)	La (ppm)	Nd (ppm)	Sm (ppm)	Y (ppm)	H_2O (wt%)	F^{batch} (La-Sm)	F^{batch} (Nd-Sm)	$F^{fractional}$ (La-Sm)	$F^{fractional}$ (Nd-Sm)	F(Ti)	H_2O^{batch} (ppm)	$H_2O^{fractional}$ (ppm)
Shuangliao	BBT-1	2.78	11.41	37.2	36.0	7.18	19.4	1.22	18.2	11.8	11.1	11.8	13.6	1502	1358
	BBT-2	2.91	11.18	42.3	40.2	8.03	21.5	1.32	16.0	10.4	9.7	10.5	12.0	1434	1287
	BBT-3	2.89	11.60	34.9	34.1	6.97	20.4	2.35	18.8	12.6	11.8	12.4	12.8	3060	2773
	BBT-5	2.49	15.47	32.9	31.5	6.50	18.9	1.71	20.2	13.8	12.5	13.5	14.2	2442	2149
	BBT-8	2.82	12.19	41.6	39.0	7.55	20.8	1.44	17.2	10.8	9.9	10.9	12.5	1611	1424
	BLS-4	2.23	11.98	47.4	42.8	8.29	19.7	3.06	8.3	10.0	6.1	7.9	13.4	2679	1876
	BLS-6	2.21	11.11	44.7	40.1	8.02	18.9	2.29	8.6	10.8	6.4	8.4	14.1	2083	1487
	BLS-7	2.28	11.92	44.6	41.2	8.12	19.3	2.41	8.5	10.5	6.5	8.2	13.8	2156	1563
	BLS-8	2.13	10.51	45.0	40.0	7.92	19.5	2.57	8.8	10.9	6.4	8.5	13.6	2367	1653
	DHLB-4	2.06	7.71	27.4	26.9	5.76	20.1	2.02	13.5	13.7	12.4	11.9	13.0	2723	2410
	DHLB-5	2.05	8.12	23.8	23.8	5.15	18.4	2.01	15.3	15.7	14.3	13.5	14.7	3036	2708
	DHLB-9	1.92	8.79	24.3	23.8	5.17	18.1	1.86	15.3	15.7	14.0	13.5	15.0	2861	2505
	DHLB-10	2.04	8.28	24.5	24.1	5.06	18.6	2.21	15.6	15.4	13.9	13.3	14.5	3291	2936
	XTEJ-2	1.84	8.11	7.83	10.6	3.10	15.4	1.22	-	-	-	-	18.3	2285	2235
	XTEJ-4	1.78	8.49	7.48	9.98	2.83	14.8	0.90	-	-	-	-	19.3	1774	1738
Chaihe-aershan	CEH-3	2.29	9.98	27.9	27.4	6.32	23.8	1.97	8.8	3.8	16.4	7.3	10.4	842	1438
	CEH-5	2.19	9.58	26.2	24.7	5.76	22.8	2.70	9.8	4.4	17.5	8.2	11.0	1324	2204
	CEH-8	2.11	8.89	24.1	22.7	5.49	22.9	1.30	10.4	5.0	19.0	8.9	11.0	708	1156
	CEH-11	2.08	9.63	27.0	25.2	5.58	21.9	2.16	10.2	4.3	17.0	8.0	11.6	1034	1729
	DLH-1	1.88	10.30	18.9	19.3	4.86	20.3	0.23	9.9	10.2	9.5	12.2	12.9	248	221
	DLH-7	1.90	10.45	18.9	19.9	4.72	21.5	0.19	10.2	9.9	9.5	11.8	11.9	199	184
	TFL1-7	2.36	8.80	43.7	39.3	8.32	26.1	1.09	6.3	11.2	7.2	12.0	9.1	736	1317
	GBS-1	2.00	8.62	21.1	19.9	5.11	22.0	1.82	7.4	4.2	7.9	8.2	11.6	850	1441
	GBS-3	2.00	8.65	21.8	20.6	5.05	22.1	1.73	7.5	4.0	7.7	7.9	11.5	774	1329
	YTL-7	2.04	9.29	25.2	24.0	5.60	24.3	2.07	3.9	15.5	5.2	12.7	10.1	899	1088

Table 5-1. (continued)

	Sample	TiO_2 (wt.%)	MgO (wt.%)	La (ppm)	Nd (ppm)	Sm (ppm)	Y (ppm)	H_2O (wt%)	F^{batch} (La-Sm)	F^{batch} (Nd-Sm)	$F^{fractional}$ (La-Sm)	$F^{fractional}$ (Nd-Sm)	F(Ti)	H_2O^{batch} (ppm)	$H_2O^{fractional}$ (ppm)
Wulanhada	11NW01	2.58	4.12	43.1	38.3	8.1	21.9	0.49	6.9	14.3	7.0	12.2	-	360	345
	11NW02	2.54	4.02	40.8	37	7.9	22.6	0.29	7.1	14.9	7.4	12.6	-	217	213
	11NW04	2.51	4.03	41.1	37.4	7.9	23.4	0.58	7.1	14.7	7.4	12.5	-	443	431
	11NW05	2.6	4.76	41.8	37.7	8.1	22.7	0.69	6.9	14.6	7.2	12.4	-	506	500
	11NW06	2.3	5.97	31.1	29.9	6.8	21.9	0.40	8.6	18.9	9.7	15.6	-	359	387
	11NW09	2.45	4.12	38.7	35.3	7.6	21.5	0.21	7.5	15.7	7.8	13.2	-	168	165
Xiaogulihe	GLH12-02	3.2	7.74	163	120	18.6	23.7	0.36	6.1	5.7	6.6	8.7	10.4	223	237
	GLH12-16	3.03	9.13	137	104	16.6	22.2	0.50	7.1	6.9	7.8	10.1	11.4	368	391
Shandong	07FYS01	1.9	8.8	19	22	4.7	18	1.40	7.0	8.1	8.0	11.2	15.0	1041	1122
	07FYS02	2.0	8.2	20	23	4.9	19	2.16	6.6	7.6	7.7	10.7	13.9	1526	1658
	07FYS04	2.1	9.2	29	30	6.0	20	0.67	5.0	5.4	5.3	8.0	13.4	366	359
	07FYS07	2.4	10.7	22	23	5.0	19	0.58	6.4	7.4	7.2	10.5	14.2	398	418
	07FYS09	2.0	9.0	28	28	5.7	21	2.98	5.4	5.8	5.6	8.6	12.6	1738	1668
	07FYS10	2.0	9.4	27	27	5.7	21	3.89	5.5	5.9	5.7	9.0	12.6	2308	2211
Taihang	FS-38	2.26	8.91	24.7	28.3	6.31	19.8	1.07	11.0	6.6	9.9	10.4	0.0	759	1055
	FHS-1	2.68	7.83	33.6	37.6	9.15	25	0.20	9.7	12.2	7.5	10.1	0.0	203	150
	JD-1	2.74	6.48	27.3	31.8	7.24	22.1	0.24	12.8	14.7	9.2	12.0	0.0	317	221
	MAS-1	2.74	6.47	39	43.3	10.08	25.6	0.34	8.6	10.3	6.4	8.7	0.0	309	219
	ZQ-1	2.22	7.17	23.1	26.6	6.17	18.6	0.84	15.3	18.0	10.9	15.8	0.0	1322	913
	ZQ-2	2.27	7.09	23.5	27.1	6.43	19	0.48	14.6	17.6	10.7	15.5	0.0	722	513
	ZQ-4	2.22	6.67	24.9	28.1	6.38	19.9	0.62	14.7	16.9	10.1	15.0	0.0	941	626
Zhejiang	XL-1	2.68	12.32	93	74	14	34	1.32	9.7	12.0	8.0	11.0	6.0	851	791
	XL-2	2.50	14.48	79	65	13	30	1.71	10.9	13.8	9.4	12.4	7.4	1339	1261
	XL-3	2.73	14.82	81	68	13	29	2.67	10.5	13.2	9.2	12.0	7.7	2175	2053
	XL-4	2.44	13.20	86	69	13	31	1.69	10.4	12.9	8.6	11.8	6.8	1239	1161

Table 5-1. (continued)

	Sample	TiO_2 (wt.%)	MgO (wt.%)	La (ppm)	Nd (ppm)	Sm (ppm)	Y (ppm)	H_2O (wt%)	F^{batch} (La-Sm)	F^{batch} (Nd-Sm)	$F^{fractional}$ (La-Sm)	$F^{fractional}$ (Nd-Sm)	F(Ti)	H_2O^{batch} (ppm)	$H_2O^{fractional}$ (ppm)
Zhejiang	XL-5	2.56	12.10	96	76	15	35	1.38	9.3	11.6	7.7	10.7	5.7	853	790
	XL-6	2.90	14.57	72	61	12	25	1.11	11.5	14.9	10.3	13.3	9.5	1103	1053
	XL-7	2.94	15.27	73	59	12	26	1.86	11.8	15.4	10.2	13.7	9.1	1769	1684
	XL-8	2.77	12.62	75	59	11	27	1.69	12.4	15.5	9.8	13.8	8.5	1508	1431
	XL-9	2.73	12.47	80	60	13	29	1.72	11.2	15.1	9.3	13.5	7.9	1428	1349
	XL-10	2.87	14.96	71	59	12	25	1.36	11.5	15.4	10.4	13.7	9.8	1399	1337
	XL-11	2.85	13.13	72	56	12	27	1.84	12.1	16.3	10.3	14.4	8.9	1721	1638
	XL-12	2.43	13.02	89	65	13	31	2.04	10.9	13.9	8.3	12.6	6.9	1504	1410
	XL-13	2.64	14.21	75	58	12	27	1.59	12.4	15.8	9.9	14.1	8.9	1482	1409
	GP-1	2.75	10.35	31	32	8	26	2.45	9.1	8.8	8.8	11.2	9.1	2336	2145
	GP-2	2.83	10.04	31	33	8	26	2.12	8.9	8.5	8.5	11.0	9.0	1987	1809
	GP-3	3.06	10.67	32	34	8	27	2.50	8.6	8.3	8.4	10.7	8.8	2315	2107
	GP-4	2.84	9.93	33	34	8	27	1.32	8.6	8.2	8.1	10.6	8.7	1200	1077
	GP-5	3.01	10.46	35	37	9	28	2.31	7.8	7.3	7.6	9.7	8.2	1920	1756
	GP-6	3.02	10.43	38	39	9	29	1.65	7.6	7.0	7.1	9.4	7.8	1332	1172
	GP-7	2.97	10.31	33	36	8	28	1.68	8.2	7.7	8.0	10.1	8.4	1445	1340
Fujian	BL-6	2.13	10.11	45.3	34.2	7.37	22.2	2.11	8.6	9.9	7.2	10.9	11.4	1916	1530
	BL-7	2.11	10.72	41.5	32.2	7.05	21.4	2.41	9.1	10.6	7.9	11.6	12.0	2298	1903
	BL-9	2.14	9.99	48.2	35.8	7.66	23.0	2.27	8.2	9.4	6.8	10.4	10.9	1971	1547
	BL-11	2.14	10.21	43.7	33.6	7.23	22.0	2.52	8.8	10.1	7.5	11.1	11.5	2335	1893
	MX-1	2.97	15.00	77.5	68.6	12.8	30.3	0.43	7.3	14.4	7.2	12.2	7.3	332	309
	MX-2	3.00	17.15	68.5	62.0	11.6	28.0	0.38	8.2	16.1	8.2	13.5	8.2	326	308
	MX-3	2.84	17.04	68.6	61.5	11.5	28.5	0.46	8.3	16.3	8.2	13.6	8.0	408	380
	MX-4	3.03	16.46	76.6	64.1	12.4	28.9	0.20	7.6	15.6	7.3	13.1	7.8	160	145
	MX-6	3.07	16.39	82.7	67.7	13.0	30.6	0.45	7.2	14.6	6.8	12.4	7.1	346	308
	MX-7	2.92	14.48	68.2	62.1	11.7	27.9	0.27	8.1	16.1	8.2	13.5	8.2	230	220
	MX-8	3.13	13.05	88.9	84.2	15.9	34.8	0.42	4.6	7.3	6.0	10.1	5.8	215	244

Table 5-1. (continued)

	Sample	TiO_2 (wt.%)	MgO (wt.%)	La (ppm)	Nd (ppm)	Sm (ppm)	Y (ppm)	H_2O (wt. %)	F^{batch} % (La-Sm)	F^{batch} % (Nd-Sm)	$F^{fractional}$ % (La-Sm)	$F^{fractional}$ % (Nd-Sm)	F % (Ti)	H_2O^{batch} (ppm)	$H_2O^{fractional}$ (ppm)
Fujian	MX-9	2.93	12.34	92.5	86.1	16.1	35.2	0.31	4.5	7.1	5.8	9.9	5.7	155	175
	MX-10	2.99	13.20	96.1	88.9	16.7	36.5	0.28	4.3	6.8	5.8	9.6	5.3	133	148
	MX-12	3.16	12.90	99.7	84.3	16.4	35.1	0.36	4.5	7.3	5.6	10.1	5.7	178	206
	SH-1	2.62	8.52	64.2	56.0	10.7	28.2	3.36	19.7	13.5	10.9	11.8	-	4682	3646
	SH-2	2.70	7.31	56.5	49.7	9.73	26.8	1.46	21.8	15.5	12.3	13.3	-	2311	1795
	SH-3	2.79	7.29	57.5	49.9	9.64	27.3	3.78	22.1	15.4	12.1	13.3	-	5976	4587
	SH-4	2.89	8.12	55.5	48.7	9.44	26.3	2.64	22.6	15.8	12.5	13.6	-	4292	3317
	SH-5	2.70	7.80	62.1	53.4	10.30	27.3	1.62	20.5	14.2	11.2	12.4	-	2375	1816
Guangdong	GD12CJ-B-1	2.19	8.36	82.6	68.0	12.5	34.2	2.83	11.3	8.2	7.8	8.9	6.0	1816	1687
	GD12CJ-B-3	2.18	11.21	50.6	43.8	8.59	28.0	2.14	17.4	13.8	12.8	14.0	8.2	1855	1757
	GD12CJ-B-4	2.18	10.78	48.2	42.2	8.34	27.7	2.76	18.0	14.4	13.4	14.5	8.3	2425	2299
	GD12CJ-B-12	2.16	11.05	46.1	40.8	8.12	27.6	2.01	15.0	18.5	14.0	15.0	8.4	1774	1682
	GD12CJ-B-13	2.17	10.19	56.6	48.1	9.29	28.5	3.25	12.4	15.9	11.4	12.7	8.0	2751	2602
	GD12CJ-B-14	2.20	10.73	50.5	43.3	8.56	27.0	1.78	14.0	17.5	12.9	14.1	8.7	1621	1540
	JCD-3	2.11	10.60	53.4	45.9	8.48	24.9	2.84	11.8	7.3	7.9	9.5	9.7	2187	2252
	JCD-4	2.13	10.80	47.6	41.7	7.83	24	3.67	12.9	8.2	8.9	9.5	10.3	3166	3267
	JCD-5	2.12	11.00	51.5	45.1	8.3	24.6	1.60	12.1	7.4	8.2	8.8	9.9	1262	1320
	JCD-6	2.22	11.40	50.4	44.6	8.25	24.2	3.53	12.2	7.5	8.4	8.9	10.1	2817	2970
	JCD-7	2.16	11.80	48.4	42.7	7.97	24.1	4.24	12.7	7.9	8.8	9.3	10.2	3557	3711
	PUZ-1	2.31	10.10	59.3	51.4	9.72	27.6	2.58	4.8	4.3	6.1	8.1	8.4	1232	1568
	PUZ-7	2.32	10.10	60.2	52.5	9.84	28	3.16	4.7	4.2	6.0	7.9	8.2	1467	1891
	PUZ-13	2.33	10.50	60.3	52.3	9.81	28.2	2.87	4.8	4.2	6.0	7.9	8.1	1338	1713

Note: Major, trace element compositions and H_2O contents of Taihang, Shandong, Zhejiang, Fujian and Guangdong basalts are from Liu et al. (2015a, b), Liu et al. (2016, 2017a)

5.1.3 MTZ source of Cenozoic basalts of eastern China.

The H_2O contents in the peridotite xenoliths from the same region were collected for comparison (Hao et al., 2014; 2016; Xia et al., 2010; 2013; Yang et al., 2008; Yu et al., 2011). It is clearly evidenced that the H_2O contents in the source of these basalts are significantly higher than those of the lithospheric mantle in each region (Fig. 5-1a). In addition, it appears that the water contents in the mantle source of the basalts decrease from the east to the west (except for the Chaihe-aershan basalts in the Northwest NEC) (Fig. 5-1b). It is in contrast with the variation trend of water contents in the lithospheric mantle (decreasing from the south to the north) (Hao et al., 2016). It clearly demonstrates that the lithospheric mantle is not the source of the continental basalts in eastern China.

Actually, mantle plumes derived from the LLSVPs (Large low-shear-velocity provinces) in lower mantle could involve materials from the recycled oceanic crust (Li et al., 2014), which might also have high water content. However, no signal of deeper mantle plume was recognized by geophysical observations beneath the eastern China, except for the Hainan Island (Fukao et al., 1992; Huang and Zhao et al., 2006; Wei et al., 2012; Zhang et al., 2016) and the stagnated slabs in the MTZ beneath the eastern China probably block the rising of deeper mantle plume (e.g., Fukao et al., 1992; Huang and Zhao et al., 2006; Wei et al., 2012).

Overall, the water-rich source of Cenozoic basalts in eastern China is probably in the hydrous MTZ.

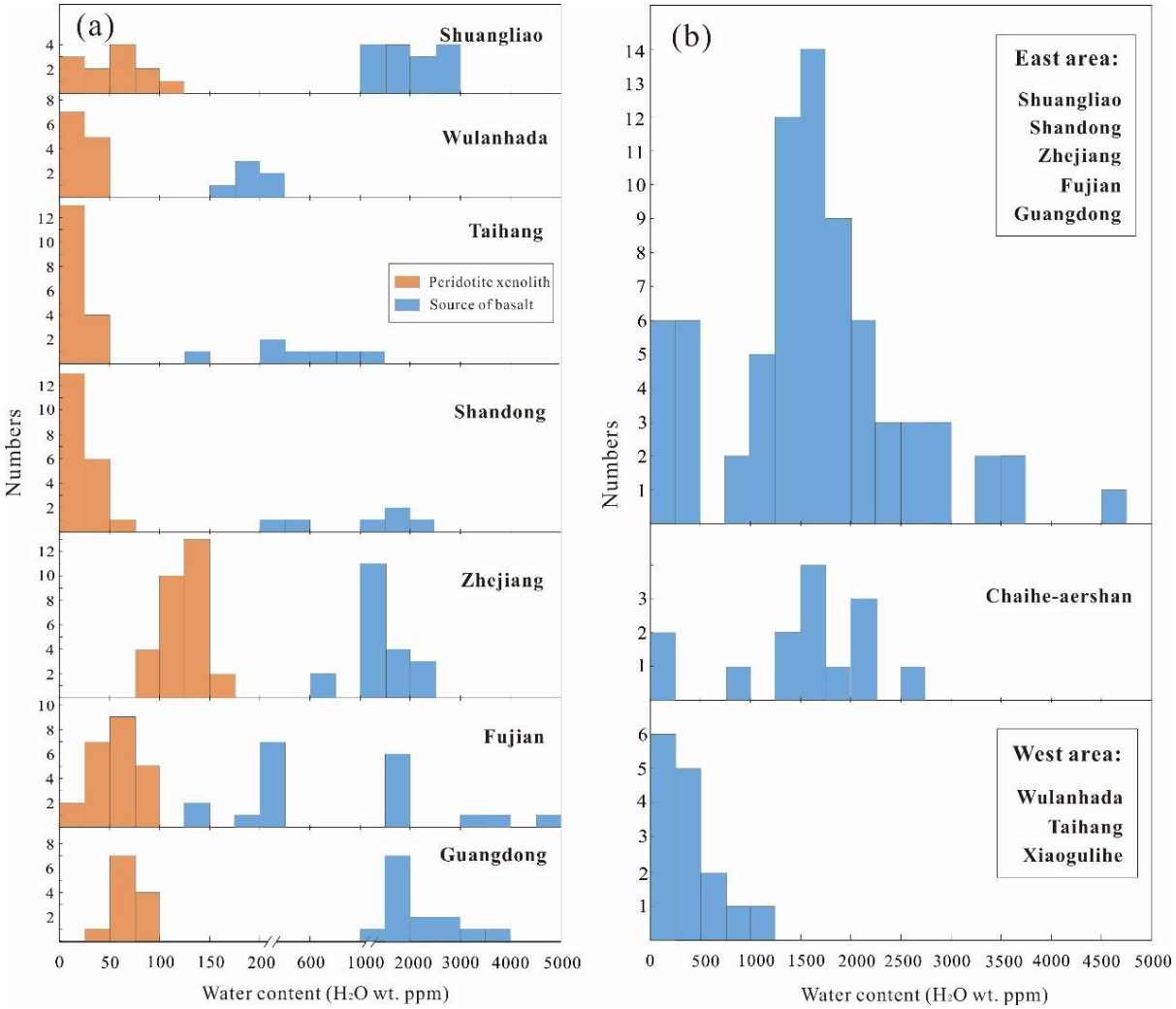

Figure 5-1. a) Comparison of the calculated water contents in the sources of Cenozoic eastern China basalts with those in peridotite xenoliths from same regions. (b) The spatial variation of H_2O content in the sources of basalts from eastern China. The H_2O content of peridotite xenoliths are from Hao et al. (2014), Hao et al. (2016), Xia et al. (2010), Xia et al. (2013a), Yang et al. (2008) and Yu et al. (2011). The water content in the sources is calculated using modal fractional melting modeling with the lowest partition coefficient of H_2O and the partial melting degree and is listed in Table 4-15.

5.2 The role of the ongoing Pacific subduction

5.2.1 Recycled materials from the Pacific plate

As discussed in the Chapter 4, the components of the recycled marine sediments and oceanic crust have been identified in the mantle source of basalts from eastern China. It worth noting that, the relative contributions of these recycled oceanic components in the mantle source of a single volcano field changed significantly within a limited time

(Figs. 4-12, 4-13, 4-30). For example, in the mantle source of earlier basalts from the Chaihe-aershan volcanic field (DLH basalts, 1.37 Ma), the recycled altered lower gabbroic oceanic crust component and ambient normal mantle sources dominate (with a positive Eu anomaly and relatively low $\delta^{18}O$ values and low H_2O/Ce ratios). One million years later (0.25-0.27 Ma), marine sediments and altered upper oceanic crust became major enriched components in the source, forming water-rich CEH basalts (with high $\delta^{18}O$ values and H_2O/Ce ratios). Similarly, the Shuangliao basalts present a similar scenario: the upper oceanic crust component and ambient normal mantle were involved during the older eruptive cycle (~51 Ma), whereas recycled marine sediments were involved in the later (~43 Ma) (Xu et al., 2012). Liu et al., (2016) studied the Zhejiang basalts (26-17 and 11 Ma) in SE China and also identified an additional recycled dehydrated sediment component in the source of the younger basalts.

The Pacific slab was constantly subducting under eastern Asia for at least the last 80 million years (Maruyama et al., 1997), a process that continuously transports recycled materials into the deep mantle. The proportion of recycled components in the MTZ was affected by the ongoing subduction of the Pacific slab. Thus, the ongoing subduction of the Pacific slab is a reasonable explanation for the variations of recycled components in the mantle source of basalts over time. In other words, the Pacific slab located in the MTZ is likely the source of the enriched components in the continental basalts from eastern China. On the other hand, the ongoing subduction of the Pacific slab (with cold P-T path, Poli and Schmidt, 2002) can continuously transport H_2O to the deep mantle, and maintain the high H_2O content in the MTZ beneath eastern China, which is consistent with the geophsical oberviation (e.g., Karato, 2011).

5.2.2 The heterogeneous distribution of recycled materials in the mantle source of eastern China basalts

The study of different volcanic fields allows us to investigate the heterogeneity of the mantle source and the spatial influence of the Pacific slab. Figure 5-2 illustrates the comparison of H_2O contents and H_2O/Ce ratios of the basalts from the different volcanic regions in eastern China (Shuangliao, Wulanhada, Chaihe-aershan, Taihang, Shandong, Zhejiang and Xiaogulihe) (Liu et al., 2015a, b; Liu et al., 2016; this study). The H_2O contents and H_2O/Ce ratios of these basalts encompass a large domain (0.19 to 3.89

wt.%, 12 to 737), emphasizing the heterogeneity of the mantle sources. Interestingly, the basalts close to the Pacific trench (Shuangliao (0.90-3.06 wt.%, 165-737), Shandong (0.58-3.89 wt%, 113-696) and Zhejiang (1.11-2.67 wt.%, 79-407)) have high H_2O contents and H_2O/Ce ratios than those located above the front edge of Pacific slab (Wulanhada (0.21-0.69 wt.%, 28-86), Xiaogulihe (0.36-0.5 wt.%, 12-19) and Taihang (0.2-1.07 wt.%, 28-198)), except for the Chaihe-aershan basalts, which are far away from Pacific trench and spread wide range in H_2O contents and H_2O/Ce ratios (0.19-2.7 wt.%, 51-521) (Fig. 5-2). This behavior is likely related to the dehydration process of the subducted Pacific plate.

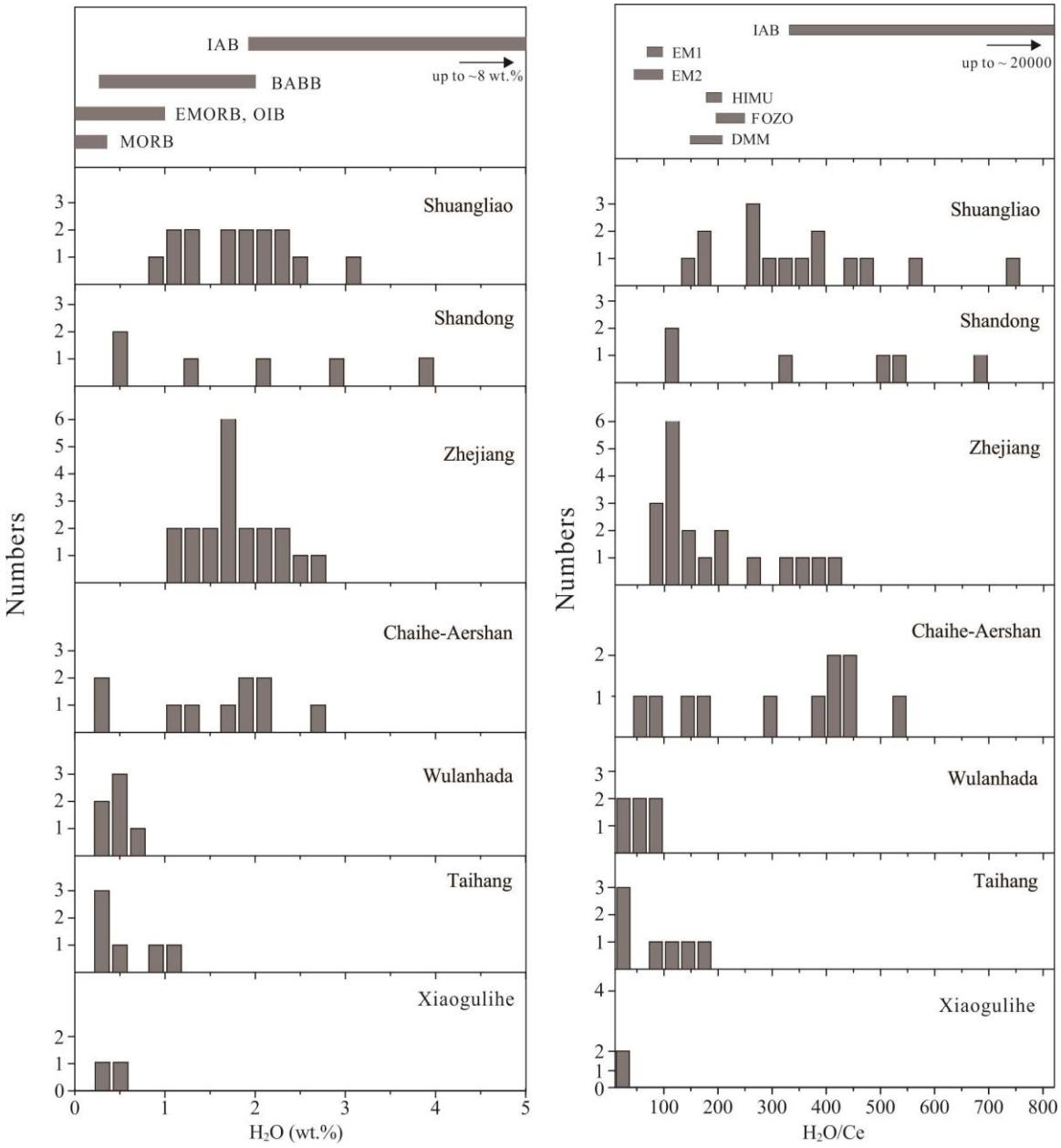

Figure 5-2. The water contents and H_2O/Ce ratios of the Cenozoic alkali basalts in eastern China. The water content data of the Cenozoic basalts in eastern China are from Liu et al. (2015a, b), Liu et al. (2016) and this study. The data source of IAB, BABB, OIB, MORB and E-MORB is Asimow et al. (2004), Danyushevsky et al. (1993, 2000), Dixon and Clague (2001), Dixon et al. (1988, 1997, 2002), Dobson et al. (1995), Hochstaedter et al. (1990), Michael, (1988, 1995), Nichols et al. (2002), Saal et al. (2002), Simons et al. (2002), Sisson and Layne (1993), Sobolev and Chaussidon (1996), Stolper and Newman (1994) and Wallace (1998; 2005). The H_2O/Ce ratio of PM is calculated with H_2O content from Dixon and Clague (2001) and Ce concentration from Sun and McDonough (1989), and the H_2O/Ce ratios of the EM1, EM2, HIMU, FOZO, DMM and IAB are from Cabral et al. (2014), Dixon et al. (2002), Kendrick et al. (2014, 2015), Workman et al. (2006), and Ruscitto et al. (2012).

Many studies have shown that Cenozoic basalts in eastern China have major elements, trace elements and Sr-Nd-Pb isotope compositions similar to EM (enriched mantle)-type or HIMU (high $(^{238}U/^{204}Pb)_{t=0}$)-type OIBs (ocean island basalts) (Chauvel et al., 1992; Chen et al., 2007; Hofmann, 1997; Le Roex et al., 1990; Workman et al., 2004; Xu et al., 2012; Zou et al., 2000; this study). Although some basalts from eastern China show H_2O contents similar to OIBs and H_2O/Ce ratios similar to EM1, EM2 and HIMU, there are many samples with high H_2O content and H_2O/Ce ratio in each locality (Fig. 5-2). The H_2O contents and high H_2O/Ce ratios of basalts in eastern China may suggest that the recycled (enriched) components in the mantle sources of basalts in eastern China contained more water than components of typical EM- and HIMU-type OIBs by subduction. It is worth noting that the H_2O/Ce ratios of the Xiaogulihe volcanic rocks from NE China are quite low (~15), which may suggest that the K-rich component in the mantle source came from ancient continent-derived sediments that dehydrated significantly during subduction (e.g., dry K-hollandite).

Because the H_2O/Ce ratio of basalt is a good indicator of recycled components, we compiled the H_2O/Ce and Ba/Th ratios of basalts (Shuangliao, Wulanhada, Chaihe-aershan, Shandong, Taihang and Zhejiang basalts) in Fig. 5-3 to illustrate the heterogeneous mantle source. Most data are distributed between typical OIBs and IABs, and the three primary components can be identified (GLOSS (global subducting sediments) / altered upper oceanic crust, dehydrated altered oceanic crust and DMM) (Fig. 5-3). The influence of these components varies from one region to another. For example, the H_2O/Ce ratios of the Shuangliao basalts display a positive correlation with the Ba/Th ratios, suggesting mixture of DMM and GLOSS / altered upper oceanic crust (high H_2O/Ce ratio); however, the correlations between H_2O/Ce and Ba/Th of the Wulanhada and Taihang basalts indicate mixture of DMM and significantly dehydrated marine sediment or altered oceanic crust (low H_2O/Ce ratio). The mantle sources of the Chaihe-aershan, Shandong and Zhejiang basalts are more complex, presenting mixture of the three components. The variability of components in the mantle sources among different Cenozoic volcano fields suggest that the contribution of recycled components from the Pacific slab to the different areas vary widely. Before and during subduction, the proportions of sediment, upper oceanic crust and lower gabbro oceanic crust are varied, and the oceanic slab undergoes variable degrees of alteration and dehydration, which can cause the observed spatial variations in the composition of source(e.g.,

Pietruszka et al., 2013).

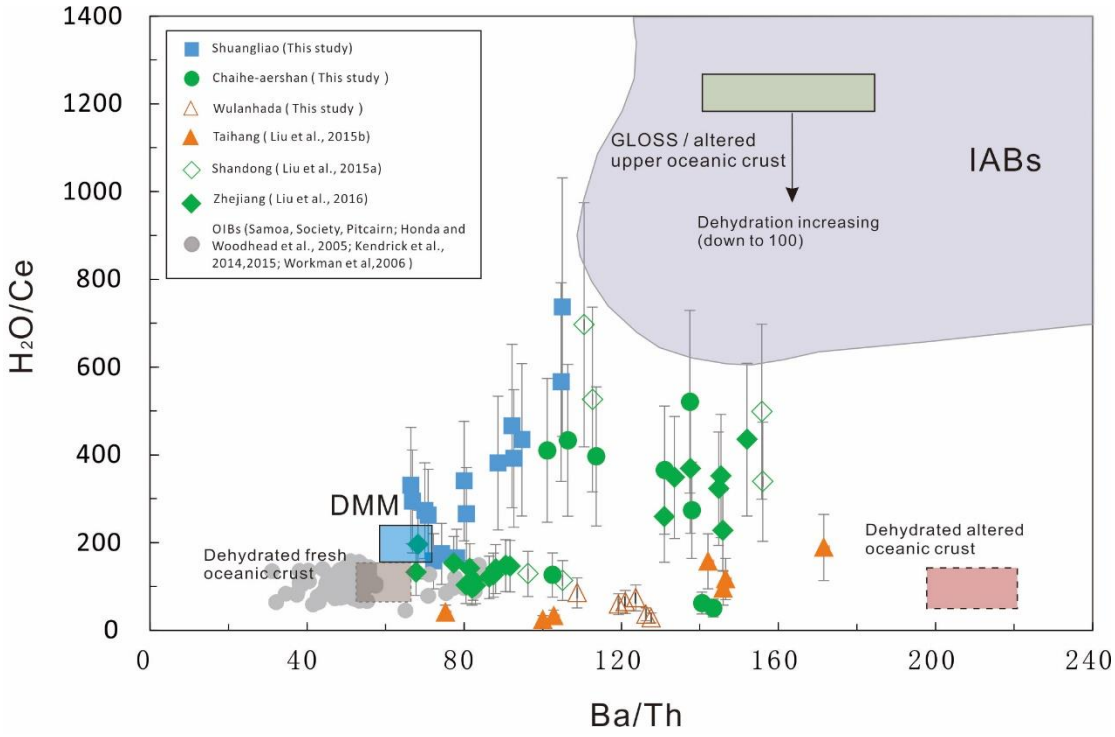

Figure 5-3. The H_2O/Ce ratios compared with the Ba/Th ratios of eastern China Cenozoic basalts. Data from Shuangliao basalts (this study), Chaihe-aershan basslts (this study), Wulanhada (this study), Taihang basalts (Liu et al., 2015b), Shandong basalts (Liu et al., 2015a) and Zhejiang basalts (Liu et al., 2016) are included for comparison. The squares indicate the possible end members of the mantle sources. The H_2O/Ce and Ba/Th ratios of DMM, GLOSS, altered upper oceanic crust and dehydrated altered oceanic crust are the same as in Fig. 4-30. The H_2O/Ce and Ba/Th ratios of the dehydrated fresh oceanic crust are from Dixon et al. (2002) and Workman and Hart (2005). The data for typical OIBs (Samoa, Society, Pitcarin; Honda and Woodhead et al., 2005; Kendrick et al., 2014, 2015; Workman et al, 2006) and IABs (Ruscitto et al., 2012 and references therein) were used for comparison.

5.2.3 A model for the role of the ongoing Pacific subduction on Cenozoic magmatism in eastern China (Asia)

Figure 5-4 illustrates the possible influences of the ongoing Pacific slab subduction on the genesis of Cenozoic basalts in eastern China. The Pacific slab is constantly subducted under eastern Asia and the rollback of the subducting slab might induce the convective circulation process in the large mantle wedge. Numerical models showed

that the focused mantle upwelling can be generated ahead of the slab from the mantle transition zone (Faccenna et al., 2010; black arrow in Fig. 5-4a), and the Wulanhada, Chaihe-aershan, Taihang and Xiaogulihe volcanic fields are just above the front edge of the subducted Pacific slab. In addition, Richard et al. (2010) discovered that the presence of water at the top of the Pacific slab can induce wet upwelling in a few million years through their numerical model (blue arrows in Fig. 5-4a). Moreover, recent seismic tomography studies identified a small gap in the stagnant slab beneath southern NE China (Liu et al., 2015c; Tang et al., 2014). When a gap is present in the subducting slab, the low velocity sub-lithospheric mantle carried down to the transition zone beneath the subducting slab will escapes from the slab sealing and rise up to form mantle upwelling (Tang et al., 2014; red arrow in Fig. 8a). Overall, all of these mechanisms might lead to the rising of material from the oceanic slab with mantle upwelling, and then decompression melting in the shallow areas.

As shown in Fig. 5-4a, the proportion and composition of recycled components in different mantle sources are variable during subduction, alteration and dehydration (e.g., Pietruszka et al., 2013), which could account for the heterogeneous mantle source of the intraplate basalts in eastern China. In Fig. 5-4b, the Chihe-aershan volcanic field was taken as an example. The rising rectangles represent the proportion of the different recycled components in the mantle sources of Chaihe-aershan basalts. The recycled components (~1.37 Ma) in the mantle sources of the DLH basalts were dominated by recycled altered lower gabbroic oceanic crust components; then the marine sediments and altered upper oceanic crust became a major source component at 0.25 Ma. Because the Pacific slab was continuously subducted and transported the recycled materials into the mantle during this period, the mantle source changed continuously, and the contributions of the marine sediments and altered upper oceanic crust have probably increased during this period.

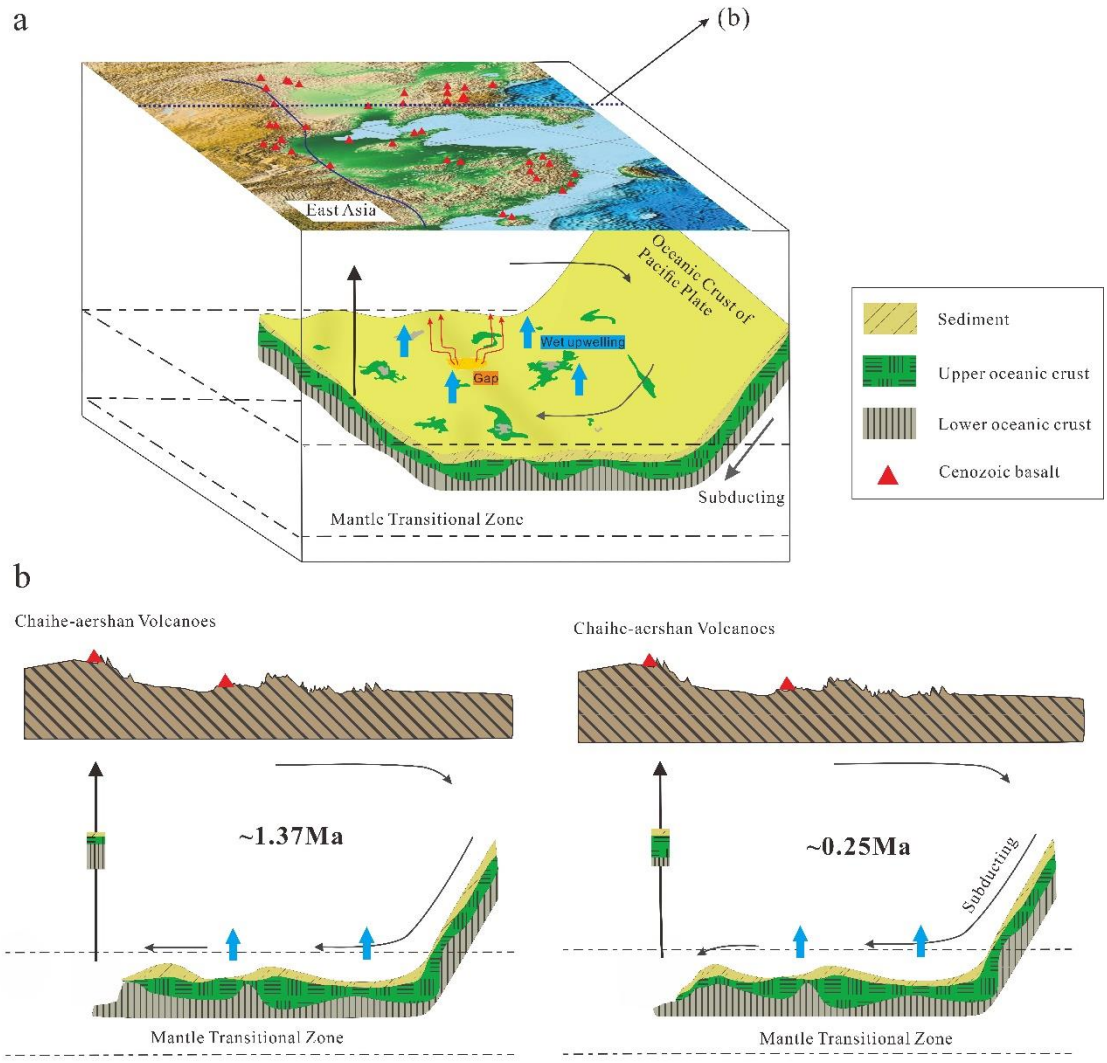

Figure 5-4. Cartoon illustrating the heterogeneity and evolution of mantle sources for the Cenozoic intraplate basalts from eastern China. (a) The red triangles represent the Cenozoic basalts in eastern China, and the subducted Pacific slab stagnates in the MTZ beneath eastern China. The proportions and compositions of marine sediments, upper oceanic crust and lower gabbro oceanic crust in different areas are variable because of the variable alterations and dehydration before and during subduction. The black and blue arrows represent mantle upwelling ahead of slab and wet upwelling (Faccenna et al., 2010; Richard et al., 2010). There is a gap in the slab that will cause upwelling of the low-velocity sub-lithosphere beneath the subducting slab (Liu et al., 2015c). (b) Evolution of mantle sources for Chaihe-aershan basalts. The rectangles represent the proportion of the different recycled components in the mantle source. At ~1.37 Ma, the recycled altered lower gabbroic oceanic crust component dominated the mantle source. The ongoing subduction of the Pacific slab may affect the composition of the mantle source, the proportion of marine sediments and altered upper oceanic crust components increased in mantle sources (~0.25 Ma).

Chapter 6. Conclusions

In this work, the water content and oxygen isotope composition of clinopyroxene (cpx) phenocrysts in basalts associated with the major and trace element compositions of bulk rocks were conducted to study the influence of the subducted Pacific slab on the genesis of the Cenozoic continental basalts in eastern China. The major and trace element compositions of bulk rocks and the O isotope compositions, water contents and major element compositions in clinopyroxene (cpx) phenocrysts have been investigated in detail. Several major conclusions have been drawn, including:

For the Shuangliao basalts, the $\delta^{18}O$ values of cpx phenocrysts range from 4.10‰ to 6.73‰, beyond the value of cpx in typical MORB and mantle peridotites and covered by typical oxygen isotope profile of altered oceanic crust, which provides a clear evidence that the recycled oceanic slab is the main enriched component in the mantle source of these continental basalts. The calculated H_2O contents of the "primary" magma vary from 0.90 to 3.06 wt.%, falling in the range of BABBs and IABs and are definitely higher than the values of MORBs and OIBs. The significant K positive anomaly and the correlations of H_2O/Ce with Ba/Th and Ce/Pb in the Shuangliao basalts indicate that water-rich sediment component may also be needed in the mantle source. In combination with the ages of the Shuangliao basalts, more recycled marine sediments were involved in the mantle source for later (~43 Ma) basalts than earlier (~51 Ma) basalts.

Unlike the Shuangliao basalts, the Wulanhada basalts have low H_2O contents (0.21-0.69 wt.%), falling in the range of MORBs and OIBs. The $\delta^{18}O$ values of cpx phenocrysts vary from 5.49‰ to 7.38‰, and are apparently higher than the values of cpx in typical MORB and mantle peridotites. The heavy oxygen isotope compositions and the correlations of H_2O/Ce with $^{87}Sr/^{86}Sr$, Ba/Th, Nb/La, Nb/U and Ce/Pb indicate the contributions of a significantly dehydrated marine sediments and ROC to the mantle source of the Wulanhada basalts.

In the Chaihe-aershan volcanic field, the large variations in the H_2O contents of "primary" magmas (0.23-2.70 wt.%) and the $\delta^{18}O$ values of cpx phenocrysts (4.27 to 8.57‰) imply the compositional heterogeneity of the mantle source. The $\delta^{18}O$ values and H_2O content within individual samples also display considerable variation, implying the mixing of magmas occurred shortly before the eruption. Three

components (hydrothermally altered upper oceanic crust and marine sediments, altered lower gabbroic oceanic crust, ambient mantle) have been identified in the mantle source based on the relations between $\delta^{18}O$ values of the cpx phenocrysts, H_2O/Ce and Ba/Th ratios and the Eu anomaly of bulk rock.

The Xiaogulihe ultrapotassic volcanic rocks are characterized by low H_2O contents (0.36-0.50 wt%, within the range of MORBs and OIBs) and low H_2O/Ce ratio (~15, much lower than that of the DMM), suggesting the low water content of K-rich component in the mantle source. Considering the high $\delta^{18}O$ values of olivine phenocrysts, low $^{206}Pb/^{204}Pb$ ratios and moderately high $^{87}Sr/^{86}Sr$ ratios of the bulk rock, the K-rich component in the mantle source could be derived from a significantly dehydrated ancient sediments (e.g., dry K-hollandite).

The conservatively estimated water contents of mantle source for the basalts in eastern China (Shuangliao, Wulanhada, Chaihe-aershan, Xiaogulihe, Shandong, Taihang, Zhejiang, Fujian, Guangdong) approximately range from 150 to 4500 ppm, which are significantly higher than those of the lithospheric mantle from the same region. The water-rich source of these basalts provides clear evidences that the Cenozoic continental basalts in eastern China originated from the hydrous MTZ.

In Shuangliao and Chaihe-aershan volcanic fields, the proportions of the recycled oceanic components in the mantle source changed significantly within a limited time. The Pacific slab is constantly subducting under eastern China and continuously transports recycled materials to the deep mantle. The temporal heterogeneity of the source components is likely to be caused by ongoing Pacific slab subduction, which means that the enriched components in the mantle source of these basalts may be derived from the Pacific slab itself located in the MTZ.

The H_2O contents and H_2O/Ce ratios of basalts in eastern China encompass a large domain (0.19 to 3.89 wt.%, 12 to 737). For most basalts, the H_2O contents and H_2O/Ce ratios are higher than those of typical OIBs. It is worth noting that, the basalts close to the Pacific trench (Shuangliao, Shandong and Zhejiang) have higher H_2O contents and H_2O/Ce ratios than those located above the front edge of Pacific slab (Wulanhada, Xiaogulihe and Taihang), except for the Chaihe-aershan basalts. This scenario may be related to the continuous dehydration process of the subducted Pacific plate.

Basalts from different areas of eastern China (Shuangliao, Wulanhada, Xiaogulihe,

Shandong, Taihang and Zhejiang) show wide variability of the contributions of recycled components from the Pacific slab among their mantle sources, which could be caused by varying degrees of alterations and dehydration before and during subduction.

Chapter 7. Perspectives

In this work, the subducted Pacific slab in the mantle transition zone (MTZ) has been identified as a primary source for the enriched components of continental basalts in eastern China. More work is also needed to further constrain the effect of the Pacific slab on the genesis of the continental basalts, especially from the dynamic view.

The available data indicates that the H_2O contents and H_2O/Ce ratios of basalts in eastern China decrease from the east to the west, along the subducting direction of the Pacific slab. To examine this characteristic of the spatial distribution of water content and to explore its possible relationship with the dehydration of the Pacific slab, systemtic work is needed.

The Xiaogulihe ultrapotassic basalts are characterized by low water contents relative to the sodic alkaline basalts in eastern China. However, there are just two samples in this work that more researches on the other potassic basalts volcanic rocks in NE China (e.g., Wudalianchi, Erkeshan and Keluo) should be conducted to constrain H_2O content of the ultrapotassic basalts and compare with the sodic alkaline basalts.

The data of the H_2O contents for the basalts in eastern China were estimated from the cpx phenocrysts. However, this method is limited to basalts with cpx phenocrysts and the uncertainty is relatively large. New analytical method should be developed.

The continental intraplate basalts are widely spread in continents (Fig. 1-1), which have similar geochemical features. The new approaches in this work may provide further constrains on the genesis of these basalts. Some work has been conducted on the basalts from French Massif Central (FMC) and was presented in the Appendix.

References

Aizawa, Y., Tatsumi, Y., Yamada, H., 1999. Element transport by dehydration of subducted sediments: Implication for arc and ocean island magmatism. *Island Arc 8*, 38-46.

Asimow, P., Dixon, J., Langmuir, C., 2004. A hydrous melting and fractionation model for mid-ocean ridge basalts: Application to the Mid-Atlantic Ridge near the Azores. *Geochemistry, Geophysics, Geosystems 5*. doi: 10.1029/2003GC000568.

Aubaud, C., Hauri, E. H., Hirschmann, M. M., 2004. Hydrogen partition coefficients between nominally anhydrous minerals and basaltic melts. *Geophysical Research Letters 31*. doi: 10.1029/2004GL021341.

Auer, S., Bindeman, I., Wallace, P., Ponomareva, V., Portnyagin, M., 2009. The origin of hydrous, high-$\delta^{18}O$ voluminous volcanism: diverse oxygen isotope values and high magmatic water contents within the volcanic record of Klyuchevskoy volcano, Kamchatka, Russia. *Contributions to Mineralogy and Petrology 157*, 209-230.

Bach, W., Alt, J.C., Niu, Y., Humphris, S.E., Erzinger, J., Dick, H.J., 2001. The geochemical consequences of late-stage low-grade alteration of lower ocean crust at the SW Indian Ridge: Results from ODP Hole 735B (Leg 176). *Geochimica et Cosmochimica Acta 65*, 3267-3287.

Bai, Z.D., Wang, J.M., Xu, G.L., Liu, L., Xu, D.B., 2008. Quaternary volcano cluster of Wulanhada, right-back-banner, Chahaer, Inner Mongolia. *Acta Petrologica Sinica 24*, 2585-2594 (in Chinese).

Behrens, H., Misiti, V., Freda, C., Vetere, F., Botcharnikov, R.E., Scarlato, P., 2009. Solubility of H_2O and CO_2 in ultrapotassic melts at 1200 and 1250 °C and pressure from 50 to 500 MPa. *American Mineralogist 94*, 105-120.

Bell, D.R., Ihinger, P.D., Rossman, G.R., 1995. Quantitative analysis of trace OH in garnet and pyroxenes. *American Mineralogist 80*, 465-474.

Bell, D.R., Rossman, G.R., 1992. Water in Earth's mantle: The role of nominally anhydrous minerals. *Science 255*, 1391-1397.

Bizimis, M., Peslier, A.H., 2015. Water in Hawaiian garnet pyroxenites: Implications for water heterogeneity in the mantle. *Chemical Geology 397*, 61-75.

Bodnar, R. J., Azbej, T., Becker, S. P., Cannatelli, C., Fall, A., Severs, M. J., 2013. Whole Earth geohydrologic cycle, from the clouds to the core: The distribution of

water in the dynamic Earth system. *Geological Society of America Special Papers 500*, 431-461.

Botcharnikov, R., Freise, M., Holtz, F., Behrens, H., 2005. Solubility of COH mixturesin natural melts: new experimental data and application range of recent models. *Annals of Geophysics*. doi: 10.4401/ag-3224

Brunet, F., Chazot, G., 2001. Partitioning of phosphorus between olivine, clinopyroxene and silicate glass in a spinel lherzolite xenolith from Yemen. *Chemical Geology 176*, 51-72.

Cabral, R.A., Jackson, M.G., Koga, K.T., Rose-Koga, E.F., Hauri, E.H., Whitehouse, M.J., Kelley, K.A., 2014. Volatile cycling of H_2O, CO_2, F, and Cl in the HIMU mantle: A new window provided by melt inclusions from oceanic hot spot lavas at Mangaia, Cook Islands. *Geochemistry, Geophysics, Geosystems 15*, 4445-4467.

Chauvel, C., Hofmann, A.W., Vidal, P., 1992. HIMU-EM: the French Polynesian connection. *Earth and Planetary Science Letters 110*, 99-119.

Chauvel, C., Lewin, E., Carpentier, M., Arndt, N. T., Marini, J. C., 2008. Role of recycled oceanic basalt and sediment in generating the Hf–Nd mantle array. *Nature geoscience 1*, 64-67.

Chen, L.H., Zeng, G., Jiang, S.Y., Hofmann, A.W., Xu, X.S., Pan, M.B., 2009. Sources of Anfengshan basalts: subducted lower crust in the Sulu UHP belt, China. *Earth and Planetary Science Letters 286*, 426-435.

Chen, Y., Zhang, Y., Graham, D., Su, S., Deng, J., 2007. Geochemistry of Cenozoic basalts and mantle xenoliths in Northeast China. *Lithos 96*, 108-126.

Ching-oh, S., Williams, R. J., Shine-soon, S., 1974. Distribution coefficients of Eu and Sr for plagioclase-liquid and clinopyroxene-liquid equilibria in oceanic ridge basalt: an experimental study. *Geochimica et Cosmochimica Acta 38*, 1415-1433.

Choi, S. H., Kwon, S. T., Mukasa, S. B., Sagong, H., 2005. Sr–Nd–Pb isotope and trace element systematics of mantle xenoliths from Late Cenozoic alkaline lavas, South Korea. *Chemical Geology 221*, 40-64.

Chu, Z.Y., Harvey, J., Liu, C.Z., Guo, J.H., Wu, F.Y., Tian, W., Zhang, Y.L., Yang, Y.H., 2013. Source of highly potassic basalts in northeast China: Evidence from Re–Os, Sr–Nd–Hf isotopes and PGE geochemistry. *Chemical Geology 357*, 52-66.

Clayton, R.N., Mayeda, T.K., 1963. The use of bromine pentafluoride in the extraction of oxygen from oxides and silicates for isotopic analysis. *Geochimica et Cosmochimica Acta 27*, 43-52.

Danyushevsky, L., Falloon, T., Sobolev, A., Crawford, A., Carroll, M., Price, R., 1993. The H_2O content of basalt glasses from Southwest Pacific back-arc basins. *Earth and Planetary Science Letters 117*, 347-362.

Danyushevsky, L.V., Eggins, S.M., Falloon, T.J., Christie, D.M., 2000. H_2O abundance in depleted to moderately enriched mid-ocean ridge magmas; Part I: incompatible behaviour, implications for mantle storage, and origin of regional variations. *Journal of Petrology 41*, 1329-1364.

Denis, C.M., Demouchy, S., Shaw, C.S. 2013. Evidence of dehydration in peridotites from Eifel Volcanic Field and estimates of the rate of magma ascent. *Journal of Volcanology and Geothermal Research 258*, 85-99.

Dixon, J.E., Clague, D.A., 2001. Volatiles in basaltic glasses from Loihi Seamount, Hawaii: Evidence for a relatively dry plume component. *Journal of Petrology 42*, 627-654.

Dixon, J.E., Clague, D.A., Wallace, P., Poreda, R., 1997. Volatiles in alkalic basalts form the North Arch Volcanic Field, Hawaii: extensive degassing of deep submarine-erupted alkalic series lavas. *Journal of Petrology 38*, 911-939.

Dixon, J.E., Dixon,T.H., Bell,D.R., Malservisi,R., 2004. Lateral variation in upper mantle viscosity: role of water. *Earth and Planetary Science Letters 222*, 451–467.

Dixon, J.E., Leist, L., Langmuir, C., Schilling, J.-G., 2002. Recycled dehydrated lithosphere observed in plume-influenced mid-ocean-ridge basalt. *Nature 420*, 385-389.

Dixon, J.E., Stolper, E., Delaney, J.R., 1988. Infrared spectroscopic measurements of CO_2 and H_2O in Juan de Fuca Ridge basaltic glasses. *Earth and Planetary Science Letters 90*, 87-104.

Dobson, P.F., Skogby, H., Rossman, G.R., 1995. Water in boninite glass and coexisting orthopyroxene: concentration and partitioning. *Contributions to Mineralogy and Petrology 118*, 414-419.

Drake, M.J., Weill, D.F., 1975. Partition of Sr, Ba, Ca, Y, Eu^{2+}, Eu^{3+}, and other REE between plagioclase feldspar and magmatic liquid: an experimental study. *Geochimica et Cosmochimica Acta 39*, 689-712.

Duda, A., Schmincke, H.-U., 1985. Polybaric differentiation of alkali basaltic magmas: evidence from green-core clinopyroxenes (Eifel, FRG). *Contributions to Mineralogy and Petrology 91*, 340-353.

Eiler, J.M., 2001. Oxygen isotope variations of basaltic lavas and upper mantle rocks.

Reviews in Mineralogy and Geochemistry 43, 319-364.

Eiler, J.M., Farley, K.A., Valley, J.W., Hauri, E., Craig, H., Hart, S.R., Stolper, E.M., 1997. Oxygen isotope variations in ocean island basalt phenocrysts. *Geochimica et Cosmochimica Acta 61*, 2281-2293.

Eiler, J.M., Schiano, P., Kitchen, N., Stolper, E.M., 2000. Oxygen-isotope evidence for recycled crust in the sources of mid-ocean-ridge basalts. *Nature 403*, 530-534.

Faccenna, C., Becker, T.W., Lallemand, S., Lagabrielle, Y., Funiciello, F. and Piromallo, C., 2010. Subduction-triggered magmatic pulses: A new class of plumes? *Earth and Planetary Science Letters 299*, 54-68.

Fan, Q., Hooper, P.R., 1991. The Cenozoic basaltic rocks of eastern China: petrology and chemical composition. *Journal of Petrology 32*, 765-810.

Fan, Q.-C., Zhao, Y.-W., Li, D.-M., Wu, Y., Sui, J.-L., Zheng, D.W., 2011. Studies on Quaternary volcanism stages of Halaha river and Chaoer river in the Great Xing'an Range: Evidence from K-Ar dating and volcanic geology features. *Acta Petrologica Sinica 27*, 2827-2832 (in Chinese).

Fan, Q. C., Chen, S. S., Zhao, Y. W., Zou, H. B., Li, N., & Sui, J. L. (2014). Petrogenesis and evolution of Quaternary basaltic rocks from the Wulanhada area, North China. *Lithos*, *206*, 289-302.

Farmer, G.L., 2014. Continental basaltic rocks. *Treatise on geochemistry (Second Edition) 4*, 75-110. doi:10.1016/B978-0-08-095975-7.00303-X

Fitzsimons, I.C.W., Harte, B., Clark, R.M., 2000. SIMS stable isotope measurement: counting statistics and analytical precision. *Mineralogical Magazine 64*, 59-59.

Foley, S., Venturelli, G., Green, D.H., Toscani, L., 1987. The ultrapotassic rocks: characteristics, classification, and constraints for petrogenetic models. *Earth-Science Reviews 24*, 81-134.

Fukao, Y., Obayashi, M., Inoue, H., & Nenbai, M. (1992). Subducting slabs stagnant in the mantle transition zone. *Journal of Geophysical Research: Solid Earth*, *97*, 4809-4822.

Gaetani, G.A., O'Leary, J. A., Shimizu, N., Bucholz, C. E., Newville, M., 2012. Rapid reequilibration of H_2O and oxygen fugacity in olivine-hosted melt inclusions. *Geology 40*, 915-918.

Gale, A., Dalton, C.A., Langmuir, C.H., Su, Y., Schilling, J.G., 2013. The mean composition of ocean ridge basalts. *Geochemistry, Geophysics, Geosystems 14*, 489-518.

Gao, Y., Hoefs, J., Przybilla, R., Snow, J. E., 2006. A complete oxygen isotope profile through the lower oceanic crust, ODP Hole 735B. *Chemical Geology 233*, 217-234.

Gregory R.T., Taylor H.P., 1981. An oxygen isotope profile in a section of Cretaceous oceanic crust, Samail ophiolite, Oman: evidence for $\delta^{18}O$ buffering of the oceans by deep (>5 km) seawater-hydrothermal circulation at mid-ocean ridges. *Journal of Geophysical Research: Solid Earth* doi: 10.1029/86iB04p02737.

Gurenko A.A, Bindeman I.N, Chaussidon M., 2011. Oxygen isotope heterogeneity of the mantle beneath the Canary Islands: insights from olivine phenocrysts. *Contributions to Mineralogy and Petrology 162*, 349-363.

Hao, Y., Xia, Q., Li, Q., Chen, H., Feng, M., 2014. Partial melting control of water contents in the Cenozoic lithospheric mantle of the Cathaysia block of South China. *Chemical Geology 380*, 7-19.

Hao, Y.T., Xia, Q.K., Jia, Z.B., Zhao, Q.C., Li, P., Feng, M., Liu, S.C., 2016. Regional heterogeneity in the water content of the Cenozoic lithospheric mantle of Eastern China. *Journal of Geophysical Research: Solid Earth.* doi: 10.1002/2015JB012105

Hartley, M.E., Thordarson, T., Taylor, C., Fitton, J. G., 2012. Evaluation of the effects of composition on instrumental mass fractionation during SIMS oxygen isotope analyses of glasses. *Chemical Geology 334*, 312-323.

Hauri, E.H., Gaetani, G.A., Green, T.H., 2006. Partitioning of water during melting of the Earth's upper mantle at H2O-undersaturated conditions. *Earth and Planetary Science Letters 248*, 715-734.

Hawkesworth, C., Rogers, N., van Calsteren, P., Menzies, M., 1987. Mantle enrichment processes and the origin of basalts. In Menzies, M. A. and Hawkesworth, C. J. eds. *Mantle Metasomatism*. London, UK: Academic Press, 365-388.

Hirschmann, M.M., Aubaud, C., Withers, A.C., 2005. Storage capacity of H_2O in nominally anhydrous minerals in the upper mantle. *Earth and Planetary Science Letters 236*, 167-181.

Hirschmann, M.M., Tenner, T., Aubaud, C., Withers, A.C., 2009. Dehydration melting of nominally anhydrous mantle: The primacy of partitioning. *Physics of the Earth and Planetary Interiors 176*, 54-68.

Ho, K.S., Chen, J.C., Lo, C.H., Zhao, H.L., 2003. ^{40}Ar–^{39}Ar dating and geochemical characteristics of late Cenozoic basaltic rocks from the Zhejiang–Fujian region,

SE China: eruption ages, magma evolution and petrogenesis. *Chemical Geology, 197,* 287-318.

Ho, K.-S., Ge, W.-C., Chen, J.-C., You, C.-F., Yang, H.-J., Zhang, Y.-L., 2013. Late Cenozoic magmatic transitions in the central Great Xing'an Range, Northeast China: Geochemical and isotopic constraints on petrogenesis. *Chemical Geology 352,* 1-18.

Ho, K.S., Liu, Y.A.N., Chen, J.C., Yang, H.J., 2008. Elemental and Sr--Nd--Pb isotopic compositions of late Cenozoic Abaga basalts, Inner Mongolia: Implications for petrogenesis and mantle process. *Geochemical Journal 42,* 339.

Hochstaedter, A.G., Gill, J.B., Kusakabe, M., Newman, S., Pringle, M., Taylor, B., Fryer, P., 1990. Volcanism in the Sumisu Rift, I. Major element, volatile, and stable isotope geochemistry. *Earth and Planetary Science Letters 100,* 179-19

Hofmann, A.W., 1988. Chemical differentiation of the Earth: the relationship between mantle, continental crust, and oceanic crust. *Earth and Planetary Science Letters 90,* 297-314.

Hofmann, A.W., 1997. Mantle geochemistry: the message from oceanic volcanism. *Nature 385,* 219-229.

Hofmann, A.W., Jochum, K.P., Seufert, M., White, W.M., 1986. Nb and Pb in oceanic basalts: new constraints on mantle evolution. *Earth and Planetary Science Letters 79,* 33-45.

Hoffman, S.E., Wilson, M., Stakes, D.S., 1986. Inferred oxygen isotope profile of Archaean oceanic crust, Onverwacht Group, South Africa. *Nature 321,* 55-58.

Honda, M., Woodhead, J.D., 2005. A primordial solar-neon enriched component in the source of EM-I-type ocean island basalts from the Pitcairn Seamounts, Polynesia. *Earth and Planetary Science Letters 236,* 597-612.

Hong, L.B., Zhang, Y.H., Qian, S.P., Liu, J.Q., Ren, Z.Y., Xu, Y.G., 2013. Constraints from melt inclusions and their host olivines on the petrogenesis of Oligocene-Early Miocene Xindian basalts, Chifeng area, North China Craton. *Contributions to Mineralogy and Petrology, 165,* 305-326.

Hou, Z., Wang, C., 2007. Determination of 35 trace elements in geological samples by inductively coupled plasma mass spectrometry. *Journal of University of Science and Technology of China 37,* 940-944.

Huang, J., Li, S.-G., Xiao, Y., Ke, S., Li, W.-Y., Tian, Y., 2015. Origin of low δ^{26}Mg Cenozoic basalts from South China Block and their geodynamic implications.

Geochimica et Cosmochimica Acta 164, 298-317.

Huang, J., Zhao, D., 2006. High-resolution mantle tomography of China and surrounding regions. *Journal of Geophysical Research: Solid Earth*. doi: 10.1029/2005JB004066.

Ingrin, J., Blanchard, M., 2006. Diffusion of hydrogen in minerals. *Reviews in Mineralogy and Geochemistry 62*, 291-320.

Ingrin, J., Skogby, H., 2000. Hydrogen in nominally anhydrous upper-mantle minerals concentration levels and implications. *European Journal of Mineralogy 12*, 543-570.

Johnson, E.A., 2006. Water in nominally anhydrous crustal minerals: Speciation, concentration, and geologic significance. *Reviews in Mineralogy and Geochemistry 62*, 117-154.

Johnson, K.T., 1998. Experimental determination of partition coefficients for rare earth and high-field-strength elements between clinopyroxene, garnet, and basaltic melt at high pressures. *Contributions to Mineralogy and Petrology 133*, 60-68.

Johnson, M.C., Plank, T., 2000. Dehydration and melting experiments constrain the fate of subducted sediments. *Geochemistry, Geophysics, Geosystems 1*. doi: 10.1029/1999GC000014.

Karato, S.I., 2011. Water distribution across the mantle transition zone and its implications for global material circulation. *Earth and Planetary Science Letters 301*, 413-423.

Kelley, K.A., Plank, T., Grove, T.L., Stolper, E.M., Newman, S., Hauri, E., 2006. Mantle melting as a function of water content beneath back-arc basins. *Journal of Geophysical Research: Solid Earth 111*. doi: 10.1029/2005JB003732.

Kelley, K.A., Plank, T., Ludden, J., Staudigel, H., 2003. Composition of altered oceanic crust at ODP Sites 801 and 1149. *Geochemistry, Geophysics, Geosystems*, *4*, 8910. doi:10.1029/2002GC000435.

Kempton, P.D., Harmon, R.S., 1992. Oxygen isotope evidence for large-scale hybridization of the lower crust during magmatic underplating. *Geochimica et Cosmochimica Acta 56*, 971-986.

Kendrick, M.A., Jackson, M.G., Kent, A.J., Hauri, E.H., Wallace, P.J., Woodhead, J., 2014. Contrasting behaviours of CO_2, S, H_2O and halogens (F, Cl, Br, and I) in enriched-mantle melts from Pitcairn and Society seamounts. *Chemical Geology 370*, 69–81.

Kendrick, M.A., Jackson, M.G., Hauri, E.H., Phillips, D., 2015. The halogen (F, Cl, Br, I) and H_2O systematics of Samoan lavas: Assimilated-seawater, EM2 and high-$^3He/^4He$ components. *Earth and Planetary Science Letters 410,* 197-209.

Kessel, R., Schmidt, M.W., Ulmer, P., Pettke, T., 2005. Trace element signature of subduction-zone fluids, melts and supercritical liquids at 120–180 km depth. *Nature 437,* 724-727.

Kita, N.T., Ushikubo, T., Fu, B., Valley, J.W., 2009. High precision SIMS oxygen isotope analysis and the effect of sample topography. *Chemical Geology 264,* 43-57.Kita, N.T., Nagahara, H., Tachibana, S., Tomomura, S., Spicuzza, M.J., Fournelle, J.H., Valley, J.W., 2010. High precision SIMS oxygen three isotope study of chondrules in LL3 chondrites: Role of ambient gas during chondrule formation. *Geochimica et Cosmochimica Acta 74,* 6610-6635.

Kogiso, T., Tatsumi, Y., Nakano, S., 1997. Trace element transport during dehydration processes in the subducted oceanic crust: 1. Experiments and implications for the origin of ocean island basalts. *Earth and Planetary Science Letters 148,* 193-205.

Kokfelt, T., Hoernle, K., Hauff, F., Fiebig, J., Werner, R., Garbe-Schönberg, C., 2006. Combined Trace Element and Pb-Nd-Sr-O Isotope Evidence for Recycled Oceanic Crust (Upper and Lower) in the Iceland Mantle Plume. *Journal of Petrology 47,* 1705-1749.

Kovács, I., Green, D.H., Rosenthal, A., Hermann, J., O'Neill H. St. C., Hibberson, W.O., Udvardi, B., 2012. An experimental study of water in nominally anhydrous minerals in the upper mantle near the water saturated solidus. *Journal of Petrology 53,* 2067-2093.

Kovács, I., Hermann, J., O'Neill, H.S.C., Gerald, J.F., Sambridge, M., Horváth, G., 2008. Quantitative absorbance spectroscopy with unpolarized light: Part II. Experimental evaluation and development of a protocol for quantitative analysis of mineral IR spectra. *American Mineralogist 93,* 765-778.

Kuritani, T., Kimura, J.-I., Miyamoto, T., Wei, H., Shimano, T., Maeno, F., Jin, X., Taniguchi, H., 2009. Intraplate magmatism related to deceleration of upwelling asthenospheric mantle: Implications from the Changbaishan shield basalts, northeast China. *Lithos 112,* 247-258.

Kuritani, T., Kimura, J.-I., Ohtani, E., Miyamoto, H., Furuyama, K., 2013. Transition zone origin of potassic basalts from Wudalianchi volcano, northeast China. *Lithos 156,* 1-12.

Kuritani, T., Ohtani, E., Kimura, J.-I., 2011. Intensive hydration of the mantle transition zone beneath China caused by ancient slab stagnation. *Nature Geoscience 4*, 713-716.

Le Bas, M., Le Maitre, R., Streckeisen, A., Zanettin, B., 1986. A chemical classification of volcanic rocks based on the total alkali-silica diagram. *Journal of Petrology 27*, 745-750.

Le Roex, A.P., Cliff, R.A., Adair, B.J.I., 1990. Tristan da Cunha, South Atlantic: geochemistry and petrogenesis of a basanite-phonolite lava series. *Journal of Petrology 31*, 779-812.

Lei, J., Xie, F., Fan, Q., Santosh, M., 2013. Seismic imaging of the deep structure under the Chinese volcanoes: An overview. *Physics of the Earth and Planetary Interiors 224*, 104-123.

Lesne, P., Scaillet, B., Pichavant, M., Iacono-Marziano, G., Beny, J.-M., 2011. The H_2O solubility of alkali basaltic melts: an experimental study. *Contributions to Mineralogy and Petrology 162*, 133-151.

Li, H.Y., Xu, Y.G., Ryan, J.G., Huang, X.L., Ren, Z.Y., Guo, H., Ning, Z.G. 2016. Olivine and melt inclusion chemical constraints on the source of intracontinental basalts from the eastern North China Craton: Discrimination of contributions from the subducted Pacific slab. *Geochimica et Cosmochimica Acta 178*, 1-19.

Li, J.Y., 2006. Permian geodynamic setting of Northeast China and adjacent regions: closure of the Paleo-Asian Ocean and subduction of the Paleo-Pacific Plate. *Journal of Asian Earth Sciences 26*, 207-224.

Li, Z.X.A., Lee, C.T.A., Peslier, A.H., Lenardic, A., Mackwell, S.J., 2008. Water contents in mantle xenoliths from the Colorado Plateau and vicinity: Implications for the mantle rheology and hydration-induced thinning of continental lithosphere. *Journal of Geophysical Research: Solid Earth 113*, B09210. doi:10.1029/2007JB005540.

Libowitzky, E., Rossman, G.R., 1996. Principles of quantitative absorbance measurements in anisotropic crystals. *Physics and Chemistry of Minerals 23*, 319-327.Liu, J., Xia, Q.-K., Deloule, E., Chen, H., Feng, M., 2015a. Recycled oceanic crust and marine sediment in the source of alkali basalts in Shandong, eastern China: Evidence from magma water content and oxygen isotopes. *Journal of Geophysical Research: Solid Earth.* doi:10.1002/2015JB012476.

Liu, J., Xia, Q.-K., Deloule, E., Ingrin, J., Chen, H., Feng, M., 2015b. Water content

and oxygen isotopic composition of alkali basalts from the Taihang Mountains, China: Recycled oceanic components in the mantle source. *Journal of Petrology*. doi: 10.1093/petrology/egv013.

Liu, S.C., 2017a. *Water content and geochemistry of Cenozoic basalts in SE China: implications for enrichment in the mantle source of intra-plate basalts.* (Doctoral dissertation, Hefei: University of Science and Technology of China).

Liu, S.C., Xia, Q.K., Choi, S.H., Deloule, E., Li, P., Liu, J., 2016. Continuous supply of recycled Pacific oceanic materials in the source of Cenozoic basalts in SE China: the Zhejiang case. *Contributions to Mineralogy and Petrology 171*, doi: 10.1007/s00410-016-1310-4.

Liu, X., Zhao, D., Li, S., Wei, W., 2017b. Age of the subducting Pacific slab beneath East Asia and its geodynamic implications. *Earth and Planetary Science Letters 464*, 166-174.

Liu, Z., Niu, F., Chen, Y.J., Grand, S., Kawakatsu, H., Ning, J., Tanaka, S., Obayashi, M. and Ni, J., 2015c. Receiver function images of the mantle transition zone beneath NE China: New constraints on intraplate volcanism, deep subduction and their potential link. *Earth and Planetary Science Letters 412*, 101-111.

Maaløe, S., 1994. Estimation of the degree of partial melting using concentration ratios. *Geochimica et Cosmochimica Acta 58*, 2519-2525.

Maaløe, S., Pedersen, R.B., 2003. Two methods for estimating the degree of melting and trace element concentrations in the sources of primary magmas. *Chemical Geology 193*, 155-166.

Maruyama S, Isozaki Y, Kiruma G, Terabayashi M., 1997. Paleogeographic maps of the Japanese Islands: Plate tectonic synthesis from 750 Ma to the present. *Island Arc 6*, 121-142.

Mattey, D., Lowry, D., Macpherson, C., 1994. Oxygen isotope composition of mantle peridotite. *Earth and Planetary Science Letters 128*, 231-241.

McDonough, W.F., Sun, S.S., 1995. The composition of the Earth. *Chemical Geology 120*, 223-253.

Menzies, M.A., Rogers, N., Tindle, A.G., Hawkesworth, C.J., 1987. Metasomatic and enrichment processes in lithospheric peridotites, an effect of asthenosphere-lithosphere interaction. In: Menzies, M. A. and Hawkesworth, C. J. eds. *Mantle Metasomatism*. London, UK: Academic Press, 313-361.

Michael, P.J., 1988. The concentration, behavior and storage of H_2O in the suboceanic

upper mantle: Implications for mantle metasomatism. *Geochimica et Cosmochimica Acta 52*, 555-566.

Michael, P., 1995. Regionally distinctive sources of depleted MORB: Evidence from trace elements and H_2O. *Earth and Planetary Science Letters 131*, 301-320.

Muehlenbachs, K., Clayton, R.N., 1976. Oxygen isotope composition of the oceanic crust and its bearing on seawater. *Journal of Geophysical Research 81*, 4365-4369.

Müller, R.D., Sdrolias, M., Gaina, C., Steinberger, B., Heine, C., 2008. Long-term sea-level fluctuations driven by ocean basin dynamics. *Science 319*, 1357-1362.

Murphy, D.T., Collerson, K.D., Kamber, B.S., 2002. Lamproites from Gaussberg, Antarctica: possible transition zone melts of Archaean subducted sediments. *Journal of Petrology 43*, 981-1001.

Nichols, A., Carroll, M., Höskuldsson, A., 2002. Is the Iceland hot spot also wet? Evidence from the water contents of undegassed submarine and subglacial pillow basalts. *Earth and Planetary Science Letters 202*, 77-87.

Niu, Y., 2005. Generation and evolution of basaltic magmas: some basic concepts and a new view on the origin of Mesozoic–Cenozoic basaltic volcanism in eastern China. *Geological Journal of China Universities 11*, 9-46.

Niu, Y., Wilson, M., Humphreys, E.R., O'Hara, M.J., 2012. A trace element perspective on the source of ocean island basalts (OIB) and fate of subducted ocean crust (SOC) and mantle lithosphere (SML). *Episodes 35*, 310-327.

Ohtani, E., 2005. Water in the Mantle. *Elements 1*, 25-30.

Ohtani, E., 2015. Hydrous minerals and the storage of water in the deep mantle. *Chemical Geology 418*, 6-15.

O'Leary, J.A., Gaetani, G.A., Hauri, E.H., 2010. The effect of tetrahedral Al^{3+} on the partitioning of water between clinopyroxene and silicate melt. *Earth and Planetary Science Letters 297*, 111-120.

O'Reilly, S.Y., Griffin, W.L., 2010. Rates of magma ascent, constraints from mantle-derived Xenoliths. In: Dosseto A., Turner S.P., Van Orman J.A., (Eds.), Timescales of magmatic processes, from core to atmosphere. John Wiley & Sons, Ltd, Chichester, UK, 116-124.

Page, F., Kita, N.T., Valley, J.W. 2010. Ion microprobe analysis of oxygen isotopes in garnets of complex chemistry. *Chemical Geology 270*, 9-19.

Panero, W.R., Pigott, J.S., Reaman, D.M., Kabbes, J.E., Liu, Z., 2015. Dry (Mg, Fe) SiO_3 perovskite in the Earth's lower mantle. *Journal of Geophysical Research:*

Solid Earth 120, 894-908.

Pearson, D.G., Brenker, F.E., Nestola, F., McNeill, J., Nasdala, L., Hutchison, M.T., Matveev, S., Mather, K., Silversmit, G., Schmitz, S. and Vekemans, B., 2014. Hydrous mantle transition zone indicated by ringwoodite included within diamond. *Nature 507*, 221-224.

Peslier, A.H., Luhr, J.F., Post, J., 2002. Low water contents in pyroxenes from spinel-peridotites of the oxidized, sub-arc mantle wedge. *Earth and Planetary Science Letters 201*, 69-86.

Pietruszka, A.J., Norman, M.D., Garcia, M.O., Marske, J.P., Burns, D.H., 2013. Chemical heterogeneity in the Hawaiian mantle plume from the alteration and dehydration of recycled oceanic crust. *Earth and Planetary Science Letters 361*, 298-309.

Plank, T., Kelley, K.A., Zimmer, M.M., Hauri, E.H., Wallace, P.J. 2013. Why do mafic arc magmas contain~ 4wt% water on average? *Earth and Planetary Science Letters 364*, 168-179.

Plank T., Langmuir C.H., 1998. The chemical composition of subducting sediment and its consequences for the crust and mantle. *Chemical Geology 145*, 325-394.

Poli, S., Schmidt, M.W., 2002. Petrology of subducted slabs. *Annual Review of Earth and Planetary Sciences 30*, 207-235.

Portnyagin, M., Almeev, R., Matveev, S., Holtz, F. 2008. Experimental evidence for rapid water exchange between melt inclusions in olivine and host magma. *Earth and Planetary Science Letters 272*, 541-552.

Putlitz, B., Matthews, A., Valley, J.W., 2000. Oxygen and hydrogen isotope study of high-pressure metagabbros and metabasalts (Cyclades, Greece): implications for the subduction of oceanic crust. *Contributions to Mineralogy and Petrology 138*, 114-126.

Rapp, R.P., Irifune, T., Shimizu, N., Nishiyama, N., Norman, M.D., Inoue, T., 2008. Subduction recycling of continental sediments and the origin of geochemically enriched reservoirs in the deep mantle. *Earth and Planetary Science Letters 271*, 14-24.

Richard, G.C., Iwamori, H., 2010. Stagnant slab, wet plumes and Cenozoic volcanism in East Asia. *Physics of the Earth and Planetary Interiors 183*, 280-287.

Roeder, P.L., Emslie, R.F., 1970. Olivine-liquid equlibrium. *Contributions to Mineralogy and Petrology 29*, 275-289.

Rudnick, R., Gao, S., 2014. Composition of the continental crust. *Treatise on geochemistry (Second Edition) 4*, 1-51. doi:10.1016/B978-0-08-095975-7.00301-6.

Ruscitto, D.M., Wallace, P.J., Cooper, L.B. and Plank, T., 2012. Global variations in H_2O/Ce: 2. Relationships to arc magma geochemistry and volatile fluxes. *Geochemistry, Geophysics, Geosystems 13*. doi: 10.1029/2011GC003887

Saal, A.E., Hauri, E.H., Langmuir, C.H., Perfit, M.R., 2002. Vapour undersaturation in primitive mid-ocean-ridge basalt and the volatile content of Earth's upper mantle. *Nature 419*, 451-455.

Salters, V.J. Longhi, J., 1999. Trace element partitioning during the initial stages of melting beneath mid-ocean ridges. *Earth and Planetary Science Letters 166*, 15-30.

Salters, V. J., Stracke, A., 2004. Composition of the depleted mantle. *Geochemistry, Geophysics, Geosystems 5*. doi: 10.1029/2003GC000597

Sambridge, M., Gerald, J.F., Kovács, I., O'Neill, H. S. C., Hermann, J., 2008. Quantitative absorbance spectroscopy with unpolarized light: Part I. Physical and mathematical development. *American Mineralogist 93*, 751-764.

Sakuyama, T., Tian, W., Kimura, J.I., Fukao, Y., Hirahara, Y., Takahashi, T., Senda, R., Chang, Q., Miyazaki, T., Obayashi, M. Kawabata, H., 2013. Melting of dehydrated oceanic crust from the stagnant slab and of the hydrated mantle transition zone: constraints from Cenozoic alkaline basalts in eastern China. *Chemical Geology 359*, 32-48.

Schilling, J. G., Sigurdsson, H., Kingsley, R. H., 1978. Skagi and western neovolcanic zones in Iceland: 2. Geochemical variations. *Journal of Geophysical Research: Solid Earth 83*, 3983-4002.

Sengör, A. M. C., Natalin, B. A. 1996. Paleotectonics of Asia: fragments of a synthesis. In *Tectonic evolution of Asia* (edited by: Yin, A., Harrison, M.). 486-640.

Sengör, A., Natal'In, B., Burtman, V., 1993. Evolution of the Altaid tectonic collage and Palaeozoic crustal growth in Eurasia. *Nature 364*, 299-307.

Shaw, A.M., Hauri, E.H., Behn, M.D., Hilton, D.R., Macpherson, C.G., Sinton, J.M., 2012. Long-term preservation of slab signatures in the mantle inferred from hydrogen isotopes. *Nature Geoscience 5*, 224-238.

Simons, K., Dixon, J., Schilling, J.G., Kingsley, R., Poreda, R., 2002. Volatiles in basaltic glasses from the Easter-Salas y Gomez Seamount Chain and Easter

Microplate: Implications for geochemical cycling of volatile elements. *Geochemistry, Geophysics, Geosystems 3,* 1-29.

Sisson, T., Layne, G., 1993. H_2O in basalt and basaltic andesite glass inclusions from four subduction-related volcanoes. *Earth and Planetary Science Letters 117,* 619-635.

Skogby, H., Bell, D.R., Rossman, G.R., 1990. Hydroxide in pyroxene: variations in the natural environment. *American Mineralogist 75,* 764-774.

Sobolev, A.V., Chaussidon, M., 1996. H_2O concentrations in primary melts from supra-subduction zones and mid-ocean ridges: implications for H_2O storage and recycling in the mantle. *Earth and Planetary Science Letters 137,* 45-55.

Stolper, E., Newman, S., 1994. The role of water in the petrogenesis of Mariana trough magmas. *Earth and Planetary Science Letters 121,* 293-325.

Sun S.S., McDonough W.F., 1989. Chemical and isotopic systematics of oceanic basalts: implications for mantle composition and processes. *Geological Society, London, Special Publications 42,* 313-345.

Sun, Y., Ying, J., Zhou, X., Shao, J.A., Chu, Z., Su, B. 2014. Geochemistry of ultrapotassic volcanic rocks in Xiaogulihe NE China: Implications for the role of ancient subducted sediments. *Lithos 208,* 53-66.

Sun, Y., Ying, J., Su, B., Zhou, X., Shao, J.A. 2015. Contribution of crustal materials to the mantle sources of Xiaogulihe ultrapotassic volcanic rocks, Northeast China: New constraints from mineral chemistry and oxygen isotopes of olivine. *Chemical Geology 405,* 10-18.

Sundvall, R., Stalder, R., 2011. Water in upper mantle pyroxene megacrysts and xenocrysts: A survey study. *American Mineralogist 96,* 1215-1227.

Tang, Y., Obayashi, M., Niu, F., Grand, S.P., Chen, Y.J., Kawakatsu, H., Tanaka, S., Ning, J., Ni, J.F., 2014. Seismic evidence of a subduction-induced mid-mantle plume for the origin of Changbaishan volcanism in northeast China. *Nature Geoscience 7,* 470–475.

Tang, Y.J., Zhang, H.F., Ying, J.F., 2006. Asthenosphere–lithospheric mantle interaction in an extensional regime: implication from the geochemistry of Cenozoic basalts from Taihang Mountains, North China Craton. *Chemical Geology 233,* 309-327.

Taylor, H.P., 1974. The application of oxygen and hydrogen isotope studies to problems of hydrothermal alteration and ore deposition. *Economic geology 69,* 843-883.

Tenner, T.J., Hirschmann, M.M., Withers, A.C., Hervig, R.L., 2009. Hydrogen

partitioning between nominally anhydrous upper mantle minerals and melt between 3 and 5 GPa and applications to hydrous peridotite partial melting. *Chemical Geology 262*, 42-56.

Thompson, R., Gibson, S., 2000. Transient high temperatures in mantle plume heads inferred from magnesian olivines in Phanerozoic picrites. *Nature 407*, 502-506.

Valley, J.W., Graham, C.M., 1991. Ion microprobe analysis of oxygen isotope ratios in granulite facies magnetites: diffusive exchange as a guide to cooling history. *Contributions to Mineralogy and Petrology 109*, 38-52.

Valley, J.W., Kita, N.T. 2009. In situ oxygen isotope geochemistry by ion microprobe. *Mineralogical Association of Canada Short Course 41*, 19-63.

Valley, J.W., Kitchen, N., Kohn, M.J., Niendorf, C.R., Spicuzza, M.J., 1995. UWG-2, a garnet standard for oxygen isotope ratios: strategies for high precision and accuracy with laser heating. *Geochimica et Cosmochimica Acta 59*, 5223-5231.

Wade, J.A., Plank, T., Hauri, E.H., Kelley, K.A., Roggensack, K. and Zimmer, M., 2008. Prediction of magmatic water contents via measurement of H_2O in clinopyroxene phenocrysts. *Geology 36*, 799-802.

Wallace, P.J., 1998. Water and partial melting in mantle plumes: Inferences from the dissolved H_2O concentrations of Hawaiian basaltic magmas. *Geophysical Research Letters 25*, 3639-3642.

Wallace, P.J., 2005. Volatiles in subduction zone magmas: concentrations and fluxes based on melt inclusion and volcanic gas data. *Journal of Volcanology and Geothermal Research, 140*, 217-240.

Wang, X.-C., Wilde, S.A., Li, Q.-L., Yang, Y.-N., 2015. Continental flood basalts derived from the hydrous mantle transition zone. *Nature Communication.* doi:10.1038/ncomms8700.

Wang, Y., Zhao, Z.F., Zheng, Y.F., Zhang, J.J., 2011. Geochemical constraints on the nature of mantle source for Cenozoic continental basalts in east-central China. *Lithos 125*, 940-955.

Wang, Z., Eiler, J.M. 2008. Insights into the origin of low-$\delta^{18}O$ basaltic magmas in Hawaii revealed from in situ measurements of oxygen isotope compositions of olivines. *Earth and Planetary Science Letters 269*, 377-387.

Wei, W., Xu, J., Zhao, D., Shi, Y., 2012. East Asia mantle tomography: New insight into plate subduction and intraplate volcanism. *Journal of Asian Earth Sciences 60*, 88-103.

Windley, B.F., Maruyama, S., Xiao, W.J., 2010. Delamination/thinning of sub-continental lithospheric mantle under Eastern China: The role of water and multiple subduction. *American Journal of Science 310,* 1250-1293.

Withers, A.C., 2013. On the use of unpolarized infrared spectroscopy for quantitative analysis of absorbing species in birefringent crystals. *American Mineralogist 98,* 689-697.

Woodhead, J. D., Greenwood, P., Harmon, R.S., Stoffers, P., 1993. Oxygen isotope evidence for recycled crust in the source of EM-type ocean island basalts. *Nature 362,* 809-813.

Workman R.K., Hart S.R., 2005. Major and trace element composition of the depleted MORB mantle (DMM). *Earth and Planetary Science Letters 231,* 53-72.

Workman, R.K., Hart, S.R., Jackson, M., Regelous, M., Farley, K.A., Blusztajn, J., Staudigel, H. 2004. Recycled metasomatized lithosphere as the origin of the Enriched Mantle II (EM2) end-member: Evidence from the Samoan Volcanic Chain. *Geochemistry, Geophysics, Geosystems 5,* Q04008. doi: 10.1029/2003GC000623.

Workman, R.K., Hauri, E., Hart, S.R., Wang, J., Blusztajn, J., 2006. Volatile and trace elements in basaltic glasses from Samoa: implications for water distribution in the mantle. *Earth and Planetary Science Letters 241,* 932-951.

Wood, D.A., 1979. Dynamic partial melting: its application to the petrogeneses of basalts erupted in Iceland, the Faeroe Islands, the Isle of Skye (Scotland) and the Troodos Massif (Cyprus). *Geochimica et Cosmochimica Acta 43,* 1031-1046.

Xia, Q.-K., Dallai, L., Deloule, E., 2004. Oxygen and hydrogen isotope heterogeneity of clinopyroxene megacrysts from Nushan Volcano, SE China. *Chemical Geology 209,* 137-151.

Xia, Q.-K., Hao, Y.-T, Li, P., Deloule, E., Coltorti, M., Dallai, Li, P., Deloule, E., Coltorti, M., Dallai, L., Yang, X.-Z., Feng, M., 2010. Low water content of the Cenozoic lithospheric mantle beneath the eastern part of the North China Craton. *Journal of Geophysical Research: Solid Earth 115,* 1-22. doi: 10.1029/2009JB006694

Xia, Q.-K., Hao, Y.-T., Liu, S.-C., Gu, X.-Y., Feng, M., 2013a. Water contents of the Cenozoic lithospheric mantle beneath the western part of the North China Craton: Peridotite xenolith constraints. *Gondwana Research 23,* 108-118.

Xia, Q.-K., Liu, J., Liu, S.-C., Kovács, I., Feng, M., Dang, L., 2013b. High water

content in Mesozoic primitive basalts of the North China Craton and implications on the destruction of cratonic mantle lithosphere. *Earth and Planetary Science Letters 361*, 85-97.

Xu, Y.G., 2014. Recycled oceanic crust in the source of 90–40Ma basalts in North and Northeast China: evidence, provenance and significance. *Geochimica et Cosmochimica Acta 143*, 49-67.

Xu, Y.-G., Zhang, H.-H., Qiu, H.-N., Ge, W.-C., Wu, F.-Y., 2012. Oceanic crust components in continental basalts from Shuangliao, Northeast China: Derived from the mantle transition zone? *Chemical Geology 328*, 168-184.

Yang, X.-Z., Xia, Q.-K., Deloule, E., Dallai, L., Fan, Q.C., Feng, M., 2008. Water in minerals of the continental lithospheric mantle and overlying lower crust: a comparative study of peridotite and granulite xenoliths from the North China Craton. *Chemical Geology 256*, 33-45.

Yu, S.Y., Xu, Y.-G., Huang, X.-L., Ma, J.-L., Ge, W.-C., Zhang, H.-H., Qin, X.-F., 2009. Hf–Nd isotopic decoupling in continental mantle lithosphere beneath Northeast China: effects of pervasive mantle metasomatism. *Journal of Asian Earth Sciences 35*, 554-570.

Yu, Y., Xu, X.S., Griffin, W.L., O'Reilly, S.Y., Xia, Q.-K., 2011. H_2O contents and their modification in the Cenozoic subcontinental lithospheric mantle beneath the Cathaysia block, SE China. *Lithos 126*, 182-197.

Zeng, G., Chen, L.-H., Hofmann, A.W., Jiang, S.-Y., Xu, X.-S., 2011. Crust recycling in the sources of two parallel volcanic chains in Shandong, North China. *Earth and Planetary Science Letters 302*, 359-368

Zhang, J.B. 1992. *Source's characteristics of ultra-potassium basaltic rocks from northeast China and research on regional mantle geochemistry* (Doctoral dissertation, Beijing: Institute of Geology, Chinese Academy of Sciences, 1992: 3-29 (in Chinese)).

Zhang, J.J., Zheng, Y.F., Zhao, Z.F., 2009. Geochemical evidence for interaction between oceanic crust and lithospheric mantle in the origin of Cenozoic continental basalts in east-central China. *Lithos 110*, 305-326.

Zhang, M., Suddaby, P., Thompson, R.N., Thirlwall, M.F., Menzies, M.A., 1995. Potassic volcanic rocks in NE China: geochemical constraints on mantle source and magma genesis. *Journal of Petrology 36*, 1275-1303.

Zhang, Y., Wang, Y., Zhao, L., Jin, Z. 2016. On velocity anomalies beneath

southeastern China: An investigation combining mineral physics studies and seismic tomography observations. *Gondwana Research 31*, 200-217.

Zhao, Y.-W., Fan, Q.-C., 2012. Mantle Sources and magma genesis of Quaternary volcanic rocks in the Halaha River and Chaoer River area, Great Xing'an Range. *Acta Petrologica Sinica 28*, 1119-1129 (in Chinese).

Zhao, Z.-F., Zheng, Y.-F., 2003. Calculation of oxygen isotope fractionation in magmatic rocks. *Chemical Geology 193*, 59-80.

Zhi, X., Song, Y., Frey, F.A., Feng, J., Zhai, M., 1990. Geochemistry of Hannuoba basalts, eastern China: constraints on the origin of continental alkalic and tholeiitic basalt. *Chemical Geology 88*, 1-33.

Zhou, X., Armstrong, R.L., 1982. Cenozoic volcanic rocks of eastern China-secular and geographic trends in chemistry and strontium isotopic composition. *Earth and Planetary Science Letters 58*, 301-329.

Zou, H., Fan, Q., Yao, Y., 2008. U–Th systematics of dispersed young volcanoes in NE China: asthenosphere upwelling caused by piling up and upward thickening of stagnant Pacific slab. *Chemical Geology 255*, 134-142.

Zou, H., Reid, M.R., Liu, Y., Yao, Y., Xu, X., Fan, Q., 2003. Constraints on the origin of historic potassic basalts from northeast China by U–Th disequilibrium data. *Chemical Geology 200*, 189-201.

Zou, H., Zindler, A., 1996. Constraints on the degree of dynamic partial melting and source composition using concentration ratios in magmas. *Geochimica et Cosmochimica Acta 60*, 711-717.

Zou, H., Zindler, A., Xu, X., Qi, Q., 2000. Major, trace element, and Nd, Sr and Pb isotope studies of Cenozoic basalts in SE China: mantle sources, regional variations, and tectonic significance. *Chemical Geology 171*, 33-47.

Published papers

Chen H., Xia Q.-K., Ingrin J., Jia Z.-B., Feng M. 2015. Changing recycled oceanic components in the mantle source of the Shuangliao Cenozoic basalts, NE China: New constraints from water content. *Tectonophysics. 650,* 113-23. Doi: 10.1016/j.tecto.2014.07.022.

Chen, H., Xia, Q.-K., Ingrin, J. 2015. Water content of the Xiaogulihe ultrapotassic volcanic rocks, NE China: implications for the source of the potassium-rich component. *Science Bulletin, 60,* 1468-1470. Doi:10.1007/s11434-015-0862-4.

Chen, H., Xia, Q.-K., Ingrin, J., Deloule, E., Bi, Y. 2017. Heterogeneous source components of intraplate basalts from NE China induced by the ongoing Pacific slab subduction. *Earth and Planetary Science Letters. 459,* 208-220. Doi: 10.1016/j.epsl.2016.11.030.

Related manuscripts

Chen, H., Xia, Q.-K., Deloule, D., Ingrin, J., Typical oxygen isotope profile of altered oceanic crust recorded in continental intraplate basalts

Chen, H., Xia, Q.-K., Kuritani, T., Liu, J., Liu, S.-C., Ingrin, J., Mantle transition zone source of intraplate basalts from eastern China constrained by water content

Chen, H., Xia, Q.-K., Ingrin, J., Liu, J., Liu, S.-C., Continuous dehydration process of the subducted Pacific plate: Constraints by the alkali basalts from north China

Auxiliary part

Allègre basalts from French Massif Central

The Cenozoic continental basalts in Western Europe are mainly distributed in French Massif Central (FMC) (Fig. 8-1), and have similar geochemical characteristics with the Cenozoic basalts in eastern China (Chauvel and Jahn, 1984; Downes, 1987; Lustrino and Wilson, 2007; Michon and Merle, 2001; Wilson and Downes, 1991). Recently, the full-waveform tomographic model showed the presence of subducted African slab in the mantle transition zone beneath the area of FMC (Fichtner and Villaseñor, 2015), which is more or less comparable to the situation in eastern China. Thus, comparing the basalts from the French Massif Central with those form eastern China will be helpful to better understand the common source of the enriched components and the evolution of mantle source worldwide. In this work, six samples from Allègre have been studied, which is located at south part of The FMC.

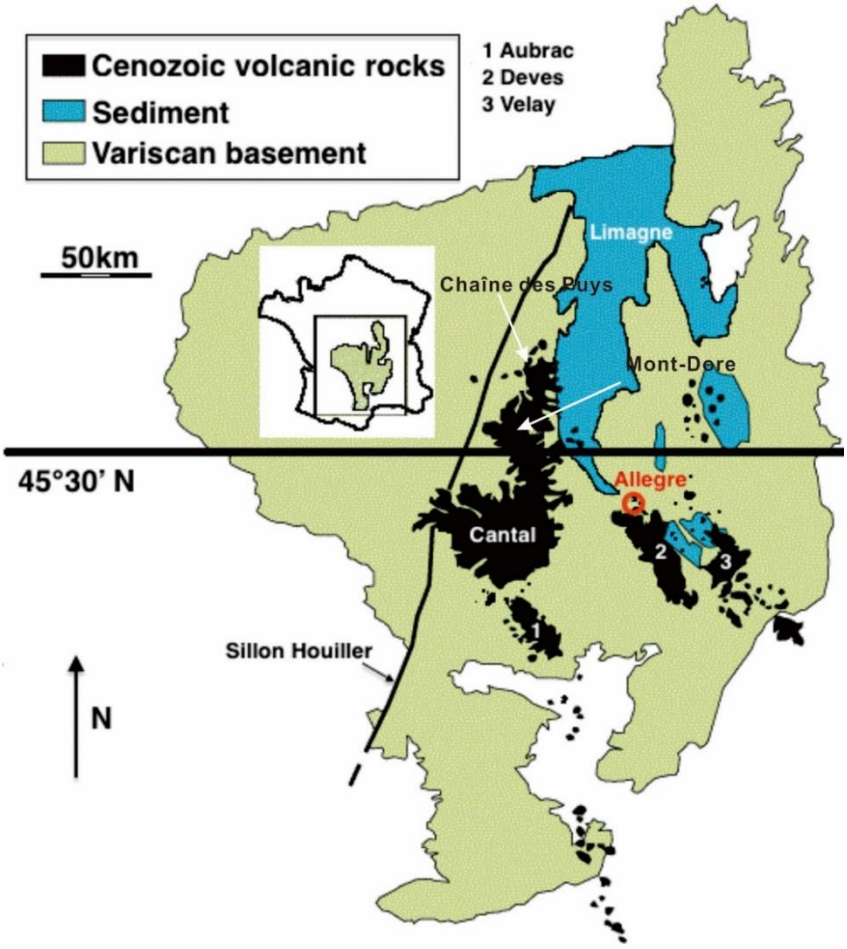

Figure 8-1. Simplified geological map of the FMC and the spatial distribution of Cenozoic volcanoes (modified from Gu (2016)).

The French Massif Central (FMC) is a part of the Variscan belt in Western Europe and belongs to the north Gondwana margin (Faure et al., 2009). The tectonic evolution history of the FMC is still controversial. It can be result from the closure of the Rheic Ocean and related oceanic basins between the Laurussia and Gondwana plate during the early Carboniferous or formed by a single north-directed subduction process (e.g., Faure et al., 2005, 2009; Lardeaux et al., 2001).

Since the Cenozoic alkaline magmatism is widely spread in FMC area, which forms the largest magmatic province in the Western Europe (Fig. 8-1) (Chauvel and Jahn, 1984; Downes, 1987; Lustrino and Wilson, 2007; Michon and Merle, 2001). The volcanic activity lasted from 65 Ma until ~6900 yr ago, which occurred in three phases: 1) pre-rift magmatic event (~65-38 Ma); 2) rifting magmatic event (~38-15 Ma) and 3) major magmatic event (early Miocene to recent) (Juvigne, 1992; Michon and Merle, 2001). The basalts are mainly distributed in Cantal (~8,000 km^2, the largest tertiary volcano in Western Europe), Mont-Dore, Aubrac, Chaîne des Puys, Velay and Devès. The basalts in FMC carried plenty of peridotite xenoliths. Based on the compositions of peridotite, the FMC has been divided into northern domain (more refractory) and southern domain (more fertile) (Downes et al., 2003; Granet et al., 1995; Lenoir et al., 2000). The Allègre volcanic field studied in this work belongs to the southern domain, and is located at the north of Devès. The HIMU-like (high $(^{238}U/^{204}Pb)_{t=0}$) signal is largely recognized in the mantle source of basalts from FMC (e.g., Hamelin et al., 2009; Lustrino and Wilson, 2007; Négrel et al., 2015; Wilson and Downes, 1991). Recently, a seismic tomography has suggested the presence of a subducted African slab in the mantle transition zone beneath the area of FMC (Fichtner and Villaseñor, 2015).

The Allègre basalts is located in the southern FMC domain (Fig. 8-1) and carried abundant mantle xenoliths, which suggests a rapid magma ascent. These basalts have a typical porphyritic texture and contain ~15% phenocrysts, which are primarily olivine. The amount of clinopyroxene and plagioclase phenocrysts are relatively low. The diameter of the phenocrysts varies from 100 to 400 μm. The matrix primarily comprises olivine, clinopyroxene and plagioclase.

Results

Major and Trace element concentrations of bulk rock

Bulk rock major and trace element concentrations of the Allègre basalts are presented in Table 8-1. The basalts have a similar compositions of MgO (8.50-8.83 wt.%), $Fe_2O_3^T$ (11.77-12.03); CaO (8.77-8.94 wt.%), Mg# (62.4-63.8, Mg#=100*Mg/(Mg+Fe) mol), Ni (190.5-204 ppm), Co (41.9-44.7 ppm) and Cr (202-217 ppm) to the basalts in eastern China, and fall in the range of basanite in the TAS nomenclature of Le Bas et al. (1986) (Fig. 8-2). On the plots of major elements versus MgO, the compositions of Allègre basalts are relatively homogeneous (Fig. 8-3).

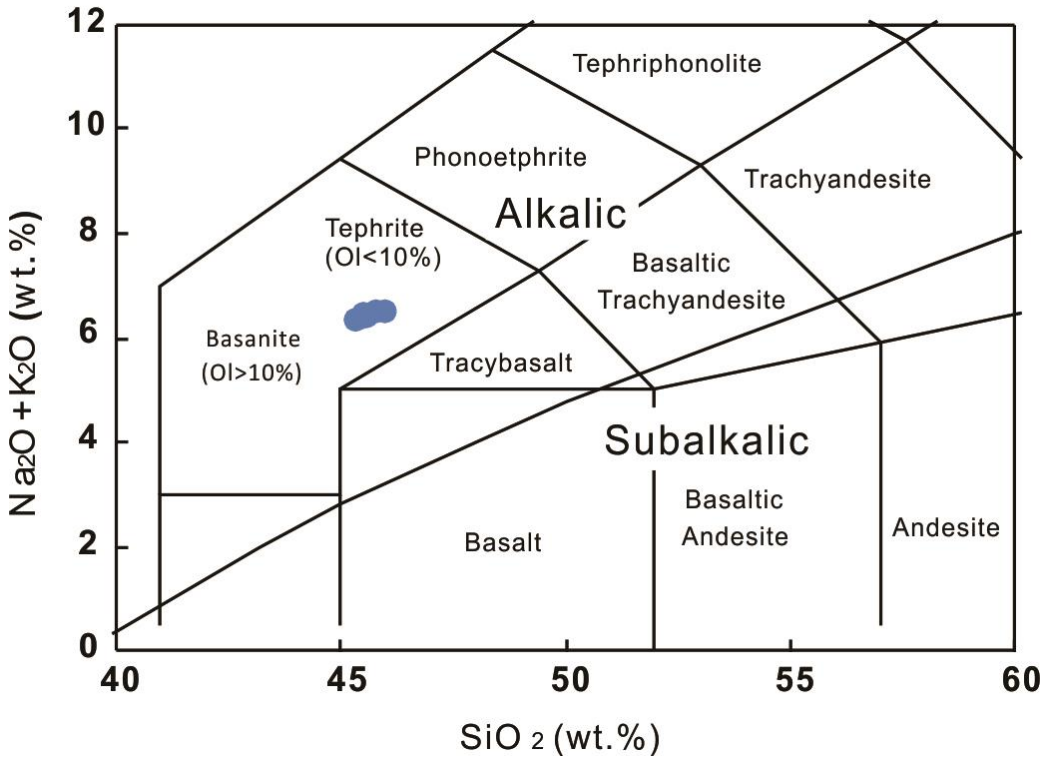

Figure 8-2. Total alkali compared with SiO_2 plots for the Allègre basalts. The classification of rock types is based on Le Bas et al. (1986).

Table 8-1. Major- and trace element compositions of Allègre basalts

sample	ALLE-1	ALLE-2	ALLE-3	ALLE-4	ALLE-5	ALLE-6
SiO_2 (wt.%)	45.34	45.52	45.44	45.80	45.59	46.00
TiO_2	2.54	2.61	2.60	2.64	2.57	2.64
Al_2O_3	13.87	13.99	14.11	14.10	13.93	14.20
$Fe_2O_3^T$	12.03	11.81	11.83	11.79	11.77	11.90
MnO	0.21	0.21	0.22	0.22	0.22	0.21
MgO	8.50	8.56	8.65	8.54	8.83	8.65
CaO	8.91	8.83	8.83	8.77	8.80	8.94
Na_2O	4.34	4.32	4.27	4.36	4.31	4.44
K_2O	2.00	2.13	2.10	2.14	2.09	2.06
P_2O_5	0.838	0.842	0.842	0.851	0.853	0.871
LOI	0.20	-0.04	0.16	-0.01	-0.10	-0.09
Total	98.78	98.78	99.05	99.20	98.86	99.82
Mg#[a]	62.44	63.04	63.24	63.02	63.84	63.10
Kˆ (ppm)	17400	18800	17700	18500	18300	18200
Tiˆ	15400	16350	15850	16050	16000	16500
Liˆ	9.6	10.6	11.0	10.1	10.2	10.4
Vˆ	202	212	202	206	207	211
Crˆ	202	217	205	207	206	203
Coˆ	43.1	44.5	44.1	41.9	44.3	44.7
Niˆ	190.5	197.5	192.5	191.5	204	201
Scˆ	19.5	20.3	20.2	19.3	19.9	20.3
Ga	20.1	19.1	19.9	19.2	19.4	18.5
Gaˆ	22.3	23.5	23.2	22.4	22.8	23.6
Rb	66.8	63.1	64.9	69.3	61.3	61.5
Rbˆ	63.9	64.1	65.7	66.0	63.4	66.8
Sr	850	849	847	868	830	845
Srˆ	950	1020	958	977	987	1010
Y	35.0	34.1	34.3	34.2	25.8	26.9
Yˆ	38.8	37.3	39.7	36.1	30.0	30.6
Nb	96.3	97.2	95.9	97.7	92.0	96.3
Nbˆ	104.0	109.0	107.5	103.0	106.0	108.5
Ba	599	596	610	621	572	623
Baˆ	660	700	690	680	690	700
La	63.9	62.5	62.7	63.6	61.3	62.9
Laˆ	66.3	69.1	68.6	64.7	67.1	69.4
Ce	116.0	112.5	116.5	114.0	112.0	113.0
Ceˆ	125.5	130.0	130.5	123.0	127.5	130.5
Pr	12.20	12.45	13.25	12.70	12.30	12.25
Nd	50.1	47.8	49.5	48.2	49.4	49.0
Sm	8.68	8.44	8.93	8.64	9.29	9.02
Eu	2.71	2.76	2.79	2.73	2.82	2.60
Gd	7.99	7.77	8.57	8.47	7.64	7.75
Tb	1.18	1.12	1.16	1.28	1.11	1.19
Dy	6.23	5.59	5.42	5.22	5.26	5.92
Ho	1.10	1.11	1.19	1.05	0.98	1.05
Er	2.56	2.79	2.42	2.98	2.53	2.75
Tm	0.40	0.37	0.35	0.34	0.34	0.32

Table 8-1. (continued)

sample	ALLE-1	ALLE-2	ALLE-3	ALLE-4	ALLE-5	ALLE-6
Yb	2.15	2.03	2.07	1.82	2.11	2.11
Lu	0.32	0.30	0.31	0.23	0.23	0.28
Ta	4.8	5.0	5.2	5.2	5.5	5.7
Taˆ	6.25	6.48	6.51	6.19	6.39	6.55
Th	8.54	8.24	8.29	8.15	8.31	8.52
Thˆ	9.6	9.9	10.1	9.4	9.6	10.0
U	2.41	2.41	2.59	2.38	2.26	2.35
Uˆ	2.6	2.7	2.9	2.7	2.7	2.8

[a] Mg#=$Mg^{2+}/(Mg^{2+}+Fe^{2+})$, assuming $Fe^{3+}/(Fe^{2+}/Fe^{3+})=0.15$

ˆ trace elements were analyzed by the method of HNO_3-HF-$HClO_4$ digestion, others were measured by the molten lithium metaborate method

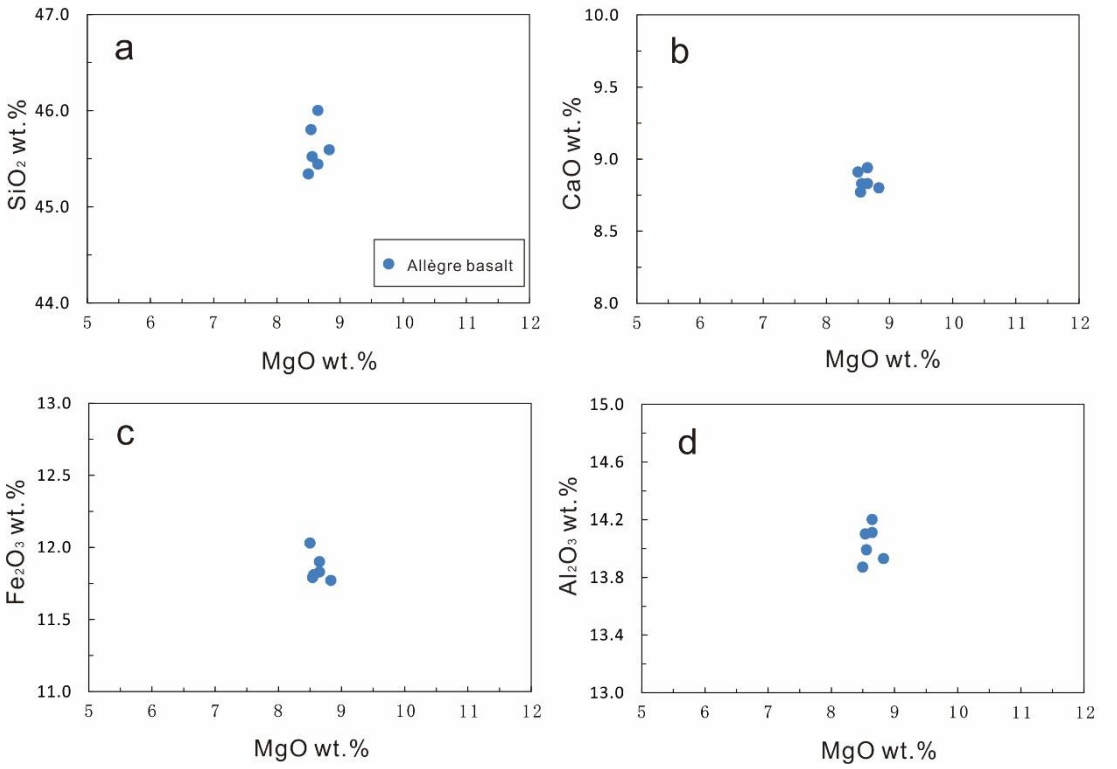

Figure 8-3. a) SiO_2 compared with MgO, b) CaO compared with MgO, c) Fe_2O_3 compared with MgO, d) Al_2O_3 compared with MgO for the Allègre basalts.

In Fig. 8-4, the primitive-mantle normalized trace elements and chondrite normalized rare earth element patterns of the Allègre basalts show typical OIB-like features, with high ratios of $(La/Yb)_N$ (20.8-25.1, N denotes normalization to chondrite), enriched in

Nb and Ta, relatively depleted in highly incompatible elements (Rb, Ba, Th, U). No Sr and Eu anomalies can be recognized in the Allègre basalts.

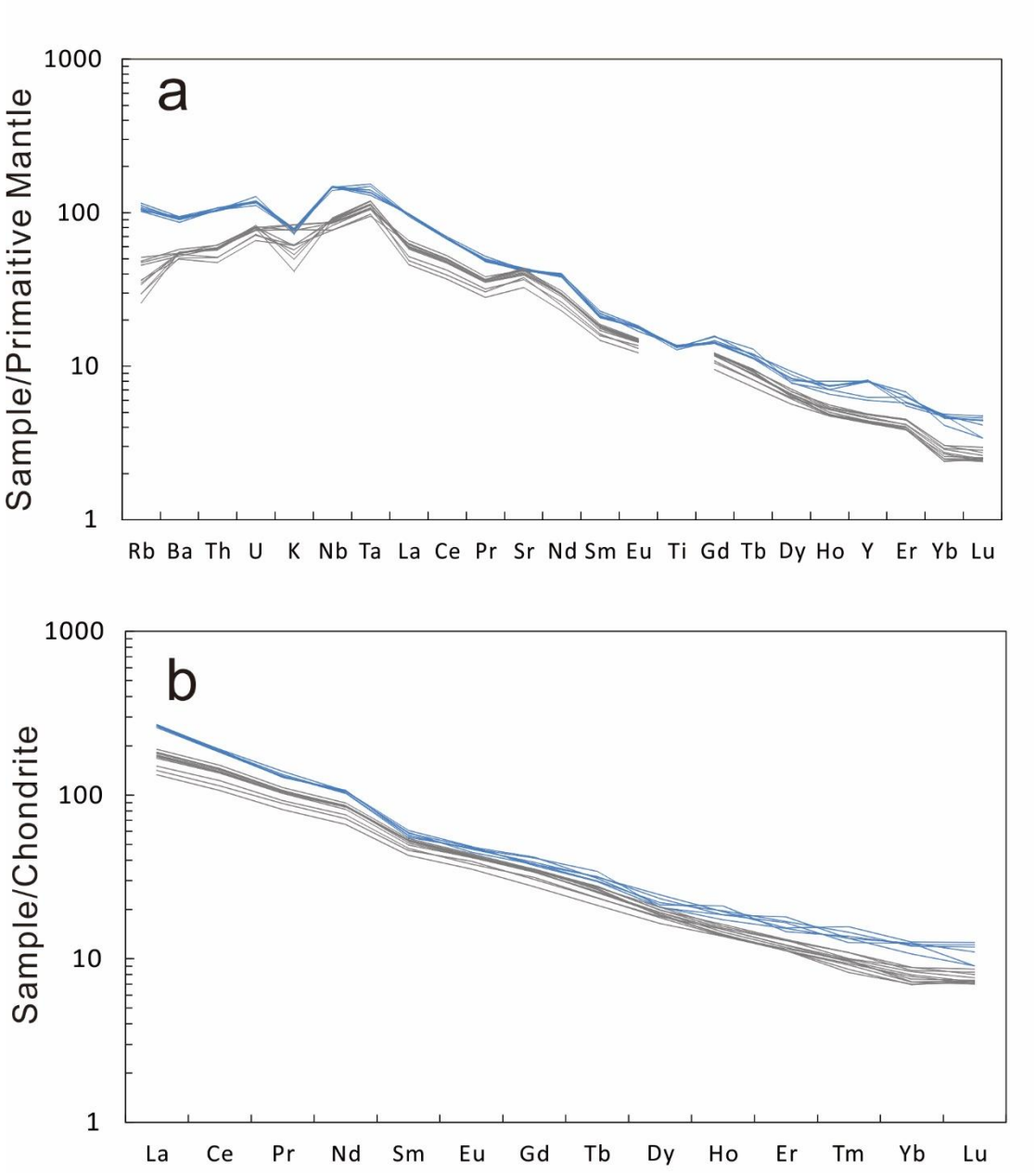

Figure 8-4. Primitive mantle-normalized trace elements concentration diagram for the Allègre basalts. Normalization values are after McDonough and Sun (1995). The basanite from the Shuangliao volcanic field are shown in the gray lines.

Chemical compositions of phenocrysts

Most of the cpx and ol phenocrysts in the Allègre basalts are euhedral. The BSE

images show that the compositions in the core of the cpx phenocrysts are homogeneous, with a narrow growth zone at the rim (Fig. 8-5a). The major element contents of cpx and olivine ol phenocrysts are listed in Tables 8-2 and 8-3. The cpx phenocrysts have relatively low Mg# (70.4-81.7) and Cr_2O_3 (<0.8 wt.%) and high TiO_2 (0.7-4 wt.%), compared to those of the cpx in the peridotite xenolith carried by the Allègre basalts (88.5-92.7 Mg#, 0.59-1.59 wt.% Cr_2O_3, 0.06-0.72 wt.% TiO_2) (Gu et al., 2016). For the ol phenocrysts, its Mg# (74.3-83.4) are lower than that of ol in the Allègre peridotite xenoliths (SiO_2, 40.36-41.90 wt.%; Mg#, 89.2-92.4) (Gu et al., 2016). The highest Mg# values of ol and cpx phenocrysts are generally similar, indicating that they are syn-crystallized.

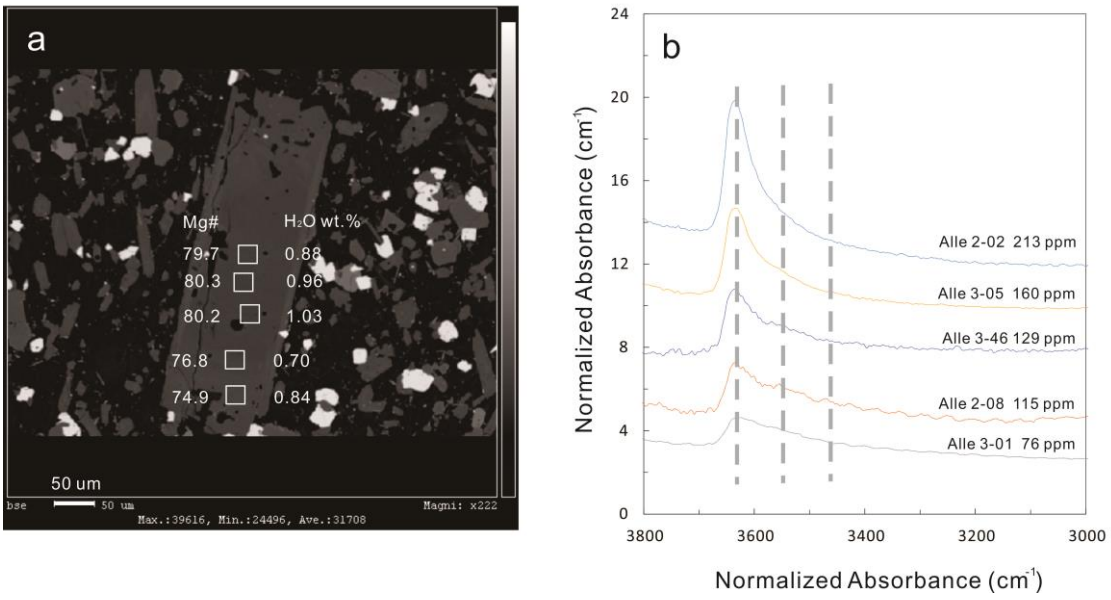

Figure 8-5. a) BSE image of a cpx phenocryst (alle 2-8~2-13 listed in Table 8-2) in the Allègre basalts. The red squares show the positions of the spots for profile analysis, from the core to the rim. b) Representative OH IR absorption spectrum of cpx phenocrysts, dashed lines mark the position of individual OH bands. The absorption intensity has been normalized to 1 cm.

Water content of clinopyroxene phenocrysts and associated melts

The representative IR spectrums are displayed in Fig. 8-5b. Similar to other cpx phenocrysts in Shuagliao, Wulanhada and Chaihe-aershan basalts from eastern China, the IR OH absorption bands of cpx phenocrysts in the Allègre can be subdivided into three groups (3630-3620 cm^{-1}, 3540-3520 cm^{-1}, and 3470-3450 cm^{-1}), and the band at

3620-3640 cm^{-1} is predominant. The calculated water concentration of cpx phenocrysts and corresponding melts are listed in Table 8-2 and plotted versus Mg# of cpx phenocrysts in Fig 8-6. Alle 2 and Alle 3 have almost the same H_2O content in cpx (50-300 ppm) and corresponding melt (0.3-2.5 wt.%). Considering the presence of the growth band at the rim of cpx phenocrysts, detailed profile IR analyses were conducted. The water content is homogenous in the core, and decrease at the narrow rim (Fig. 8-5a).

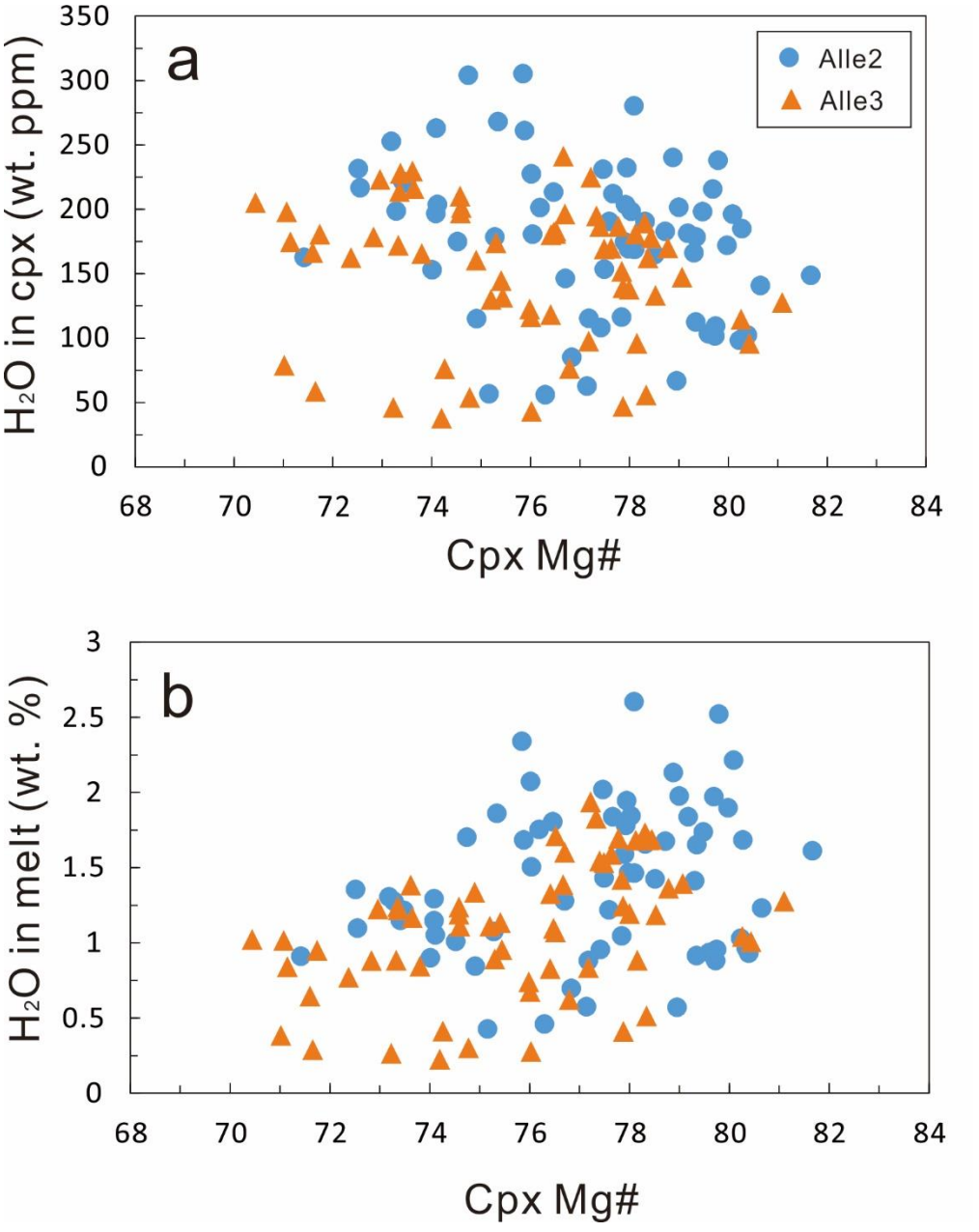

Figure 8-6. H_2O content of the cpx phenocrysts and corresponding melts compared with cpx Mg# for the Allègre basalts

Table 8-2. Major element composition of cpx phenocrysts and calculated water of cpx phenocrysts and corresponding melt in Allègre basalts

	SiO_2	Al_2O_3	TiO_2	Cr_2O_3	FeO	NiO	MnO	MgO	CaO	Na_2O	K_2O	Total	Mg#	$X(^{iv}Al)$	XCa	$D^{cpx/melt}$	$A(cm^{-2})$	t (mm)	H_2O in cpx (wt ppm)	H_2O in melt (wt %)
alle2-01	49.99	4.35	1.88	0.10	6.38	0.04	0.09	14.03	22.45	0.37	0.01	99.66	79.69	0.089	0.89	0.0109	5.8087	0.114	215.6	1.97
alle2-02	49.26	4.85	2.03	0.02	7.24	0.05	0.13	13.20	22.52	0.38	b.l.d.	99.89	76.47	0.102	0.90	0.0118	5.7427	0.114	213.2	1.80
alle2-03	49.26	4.62	1.99	0.02	6.97	b.l.d.	0.08	13.45	22.33	0.41	b.l.d.	98.78	77.47	0.096	0.90	0.0114	6.2258	0.114	231.1	2.02
alle2-04	49.91	4.41	1.96	0.04	6.82	b.l.d.	0.15	13.65	22.35	0.37	b.l.d.	99.75	78.10	0.086	0.89	0.0108	7.5514	0.114	280.3	2.60
alle2-05	45.58	8.01	3.67	0.13	7.84	b.l.d.	0.11	11.62	22.48	0.47	b.l.d.	99.12	72.56	0.182	0.91	0.0197	5.8325	0.114	216.5	1.10
alle2-08	48.34	5.46	2.05	0.09	6.78	b.l.d.	0.11	12.86	22.59	0.48	0.01	100.16	77.18	0.119	0.91	0.0131	2.6949	0.099	115.2	0.88
alle2-09	49.75	4.62	1.85	0.15	6.28	0.05	0.16	13.85	22.62	0.42	b.l.d.	100.44	79.73	0.098	0.90	0.0115	2.3747	0.099	101.5	0.88
alle2-10	49.87	3.88	1.75	0.11	6.20	b.l.d.	0.12	14.21	22.62	0.35	0.01	99.59	80.34	0.085	0.91	0.0106	2.377	0.099	101.6	0.96
alle2-11	51.26	3.62	1.45	0.07	6.32	0.03	0.12	14.38	22.51	0.40	b.l.d.	99.01	80.23	0.068	0.89	0.0096	2.3002	0.099	98.3	1.03
alle2-12	49.26	4.93	2.33	0.06	7.23	0.04	0.14	13.45	22.56	0.42	0.01	100.07	76.84	0.107	0.90	0.0122	1.9916	0.099	85.1	0.70
alle2-13	47.91	5.43	2.60	0.02	7.66	b.l.d.	0.13	12.82	22.59	0.42	0.01	100.39	74.91	0.125	0.91	0.0136	2.692	0.099	115.1	0.84
alle2-14	49.00	4.75	1.81	0.17	6.35	b.l.d.	0.10	13.68	22.66	0.48	0.01	99.51	79.34	0.110	0.91	0.0123	2.6304	0.099	112.4	0.91
alle2-15	50.02	4.53	1.75	0.20	6.32	0.06	0.11	13.95	22.77	0.37	b.l.d.	100.17	79.75	0.097	0.90	0.0114	2.5571	0.099	109.3	0.96
alle2-16	50.06	4.46	1.99	0.09	6.96	0.08	0.11	13.71	22.47	0.45	0.01	99.09	77.85	0.091	0.89	0.0111	2.7176	0.099	116.2	1.05
alle2-17	46.32	7.69	3.03	0.03	8.03	0.10	0.07	11.26	22.48	0.50	b.l.d.	100.01	71.42	0.167	0.91	0.0179	3.8054	0.099	162.6	0.91
alle2-18	47.01	7.21	2.99	0.02	7.60	0.01	0.09	12.14	22.62	0.47	0.01	99.95	74.01	0.159	0.91	0.0170	3.5777	0.099	152.9	0.90
alle2-19	49.57	4.49	1.99	0.07	6.88	b.l.d.	0.14	13.28	22.29	0.39	b.l.d.	99.46	77.49	0.086	0.90	0.0107	3.7688	0.104	153.3	1.43
alle2-20	49.71	4.60	1.95	0.12	6.84	0.02	0.14	13.69	22.52	0.42	0.01	98.45	78.10	0.098	0.90	0.0115	4.148	0.104	168.8	1.46
alle2-21	47.03	7.14	2.78	0.04	7.60	b.l.d.	0.08	12.19	22.61	0.49	b.l.d.	99.38	74.09	0.160	0.91	0.0172	4.8344	0.104	196.7	1.15
alle2-22	46.52	7.42	3.11	0.06	7.81	0.04	0.11	11.56	22.26	0.55	0.02	99.55	72.52	0.158	0.90	0.0171	6.0736	0.111	231.5	1.35
alle2-23	45.09	7.60	3.38	0.06	7.58	0.01	0.09	11.61	22.55	0.48	b.l.d.	98.92	73.18	0.181	0.92	0.0193	7.0432	0.118	252.6	1.31
alle2-25	48.80	5.17	2.15	0.03	7.09	0.03	0.12	12.81	22.72	0.45	0.02	99.13	76.30	0.109	0.91	0.0122	1.2853	0.097	56.1	0.46
alle2-26	46.59	6.52	3.40	0.16	7.76	0.07	0.12	11.94	22.56	0.42	0.02	99.28	73.28	0.146	0.91	0.0156	3.2389	0.069	198.6	1.28
alle2-27	49.46	4.19	1.68	0.19	6.46	0.03	0.13	14.03	22.39	0.38	b.l.d.	100.00	79.48	0.096	0.90	0.0114	3.2309	0.069	198.1	1.74
alle2-28	46.87	7.10	2.79	0.27	7.05	0.03	0.11	12.05	22.38	0.49	b.l.d.	99.77	75.28	0.155	0.90	0.0166	2.9512	0.07	178.4	1.07
alle2-29	46.73	6.94	2.63	0.26	7.42	b.l.d.	0.10	12.17	22.50	0.52	0.02	100.03	74.52	0.162	0.91	0.0174	2.8939	0.07	174.9	1.01
alle2-30	49.09	4.70	2.31	0.05	7.52	0.05	0.16	13.39	22.30	0.42	b.l.d.	99.44	76.04	0.103	0.89	0.0120	3.6254	0.085	180.5	1.50
alle2-31	49.31	4.52	2.16	0.02	7.47	b.l.d.	0.12	13.41	22.37	0.38	0.01	99.14	76.19	0.097	0.90	0.0115	3.9957	0.084	201.3	1.75
alle2-32	50.45	3.48	1.88	0.22	6.65	b.l.d.	0.15	14.19	22.68	0.33	b.l.d.	99.39	79.18	0.074	0.90	0.0099	3.5981	0.084	181.2	1.84
alle2-33	51.14	3.35	1.44	0.17	6.19	0.01	0.13	13.97	22.62	0.40	0.01	99.77	80.09	0.058	0.90	0.0089	3.8027	0.082	196.2	2.22
alle2-34	47.41	5.90	2.34	0.29	6.77	0.04	0.09	13.15	22.72	0.43	b.l.d.	99.98	77.59	0.147	0.92	0.0156	3.6904	0.082	190.4	1.22
alle2-35	49.82	4.37	1.63	0.44	6.00	b.l.d.	0.10	14.03	22.64	0.37	b.l.d.	98.73	80.65	0.097	0.90	0.0114	2.6934	0.081	140.7	1.23

Table 8-2. (continued)

	SiO_2	Al_2O_3	TiO_2	Cr_2O_3	FeO	NiO	MnO	MgO	CaO	Na_2O	K_2O	Total	Mg#	$X(^{iv}Al)$	XCa	$D^{cpx/melt}$	$A(cm^{-2})$	t (mm)	H_2O in cpx (wt ppm)	H_2O in melt (wt %)
alle2-36	49.47	4.34	2.11	0.05	7.02	0.03	0.13	13.28	22.98	0.35	0.01	99.96	77.14	0.093	0.92	0.0109	1.2001	0.081	62.7	0.57
alle2-37	49.65	4.32	1.83	0.15	6.66	0.02	0.13	14.01	22.77	0.42	0.02	99.26	78.96	0.102	0.91	0.0117	1.2769	0.081	66.7	0.57
alle2-38	47.65	4.94	2.37	0.06	7.61	0.01	0.14	12.92	22.64	0.39	b.l.d.	99.30	75.16	0.123	0.92	0.0133	1.085	0.081	56.7	0.43
alle2-39	49.37	4.28	2.23	0.05	7.43	0.05	0.11	13.71	22.28	0.43	0.02	99.36	76.70	0.095	0.89	0.0114	2.8325	0.082	146.2	1.28
alle2-40	49.37	4.37	1.91	0.08	7.04	0.05	0.08	13.54	22.45	0.37	b.l.d.	99.92	77.42	0.095	0.90	0.0113	2.0928	0.082	108.0	0.96
alle2-41	49.92	3.57	1.52	0.38	6.34	0.02	0.09	14.58	22.52	0.35	b.l.d.	99.82	80.39	0.091	0.90	0.0110	1.9836	0.082	102.4	0.93
alle2-42	49.69	3.85	1.68	0.17	6.49	b.l.d.	0.11	14.21	22.85	0.30	b.l.d.	99.02	79.60	0.094	0.92	0.0110	2.0002	0.082	103.2	0.93
alle2-43	49.43	4.38	1.91	0.07	7.03	b.l.d.	0.16	13.93	22.57	0.45	b.l.d.	99.43	77.95	0.104	0.90	0.0119	4.7749	0.087	232.2	1.94
alle2-44	49.80	4.43	1.74	0.05	6.82	0.01	0.12	13.97	22.50	0.39	b.l.d.	100.11	78.52	0.098	0.90	0.0116	3.6232	0.093	164.8	1.43
alle2-45	49.31	4.21	1.81	0.12	6.96	0.09	0.11	13.79	22.24	0.39	b.l.d.	99.75	77.93	0.096	0.90	0.0114	4.5186	0.094	203.4	1.78
alle2-46	46.14	7.53	2.86	0.04	7.80	0.01	0.06	12.08	22.40	0.51	b.l.d.	99.36	73.42	0.178	0.91	0.0193	4.9241	0.094	221.7	1.15
alle2-47	50.22	4.30	1.86	0.09	6.93	0.04	0.12	13.81	22.37	0.36	0.01	100.17	78.04	0.086	0.89	0.0108	4.5468	0.097	198.3	1.84
alle2-48	49.62	4.10	1.76	0.07	6.95	b.l.d.	0.13	14.07	22.69	0.36	0.01	99.04	78.32	0.099	0.91	0.0115	4.3649	0.097	190.4	1.66
alle2-49	46.18	7.16	2.94	0.35	7.61	0.01	0.07	11.83	22.74	0.47	b.l.d.	100.15	73.49	0.171	0.92	0.0181	5.0442	0.097	220.0	1.21
alle2-50	46.99	7.03	2.76	0.24	7.54	b.l.d.	0.08	12.52	22.51	0.48	0.02	100.12	74.75	0.166	0.90	0.0179	6.9689	0.097	304.0	1.70
alle2-51	45.23	7.50	3.29	0.14	7.57	b.l.d.	0.08	12.13	22.67	0.44	b.l.d.	99.16	74.09	0.189	0.92	0.0203	6.0256	0.097	262.8	1.29
alle2-53	50.05	4.13	1.88	0.18	6.71	b.l.d.	0.13	13.93	22.70	0.42	b.l.d.	99.59	78.72	0.090	0.90	0.0109	4.1026	0.095	182.7	1.68
alle2-54	49.33	4.42	1.72	0.11	6.91	b.l.d.	0.10	13.49	22.69	0.39	b.l.d.	99.19	77.67	0.100	0.91	0.0115	4.7602	0.095	212.0	1.84
alle2-55	49.67	3.95	1.59	0.22	6.20	b.l.d.	0.12	14.15	22.58	0.41	b.l.d.	100.22	80.27	0.092	0.91	0.0110	3.9322	0.09	184.9	1.68
alle2-56	50.41	3.80	1.50	0.19	6.61	0.04	0.16	13.94	22.66	0.29	b.l.d.	99.62	79.00	0.080	0.90	0.0102	4.2858	0.09	201.5	1.98
alle2-57	49.83	3.86	1.63	0.17	6.55	0.04	0.12	14.11	22.51	0.37	0.01	100.13	79.35	0.088	0.90	0.0108	3.6709	0.087	178.5	1.65
alle2-58	50.16	4.16	1.77	0.07	7.05	b.l.d.	0.12	13.95	22.55	0.39	0.01	98.52	77.90	0.090	0.90	0.0110	3.5879	0.087	174.5	1.59
alle2-59	49.62	4.06	1.66	0.19	6.68	0.03	0.10	14.37	22.57	0.34	b.l.d.	99.78	79.31	0.102	0.90	0.0118	3.4155	0.087	166.1	1.41
alle2-60	49.98	4.14	1.74	0.11	6.72	b.l.d.	0.13	14.08	22.82	0.40	0.01	100.26	78.88	0.096	0.91	0.0113	4.9381	0.087	240.2	2.13
alle2-61	47.46	5.30	2.23	0.01	7.63	0.04	0.13	13.07	22.21	0.45	b.l.d.	99.62	75.34	0.133	0.90	0.0144	5.5113	0.087	268.0	1.86
alle2-62	50.95	3.56	1.76	0.15	6.21	0.05	0.12	13.91	22.71	0.38	b.l.d.	99.63	79.98	0.061	0.90	0.0091	3.5332	0.087	171.8	1.90
alle2-63	46.15	7.78	3.31	0.04	7.51	0.02	0.09	12.07	22.79	0.48	0.02	100.09	74.12	0.180	0.91	0.0193	4.1845	0.087	203.5	1.05
alle2-64	47.48	6.43	2.50	0.10	7.07	b.l.d.	0.13	12.47	22.92	0.47	0.01	99.83	75.88	0.147	0.92	0.0155	5.6763	0.092	261.1	1.68
alle2-65	48.09	5.80	3.05	b.l.d.	7.09	0.03	0.10	12.49	22.62	0.72	b.l.d.	99.54	75.85	0.118	0.91	0.0130	6.634	0.092	305.1	2.34
alle2-66	50.01	4.63	2.04	b.l.d.	7.43	b.l.d.	0.11	13.21	22.55	0.47	b.l.d.	100.19	76.02	0.090	0.90	0.0110	4.5706	0.085	227.5	2.07
alle2-67	50.98	3.82	1.55	0.02	6.27	b.l.d.	0.16	13.88	22.70	0.43	0.02	99.72	79.79	0.067	0.90	0.0094	4.7808	0.085	238.0	2.52
alle2-68	49.57	4.69	1.84	0.01	6.84	b.l.d.	0.14	13.59	22.46	0.40	b.l.d.	99.73	77.98	0.098	0.90	0.0116	3.2024	0.08	169.4	1.47
alle2-69	51.62	3.24	1.30	0.35	5.89	b.l.d.	0.09	14.72	22.60	0.39	b.l.d.	100.19	81.67	0.062	0.89	0.0092	2.5657	0.073	148.7	1.61

Table 8-2. (continued)

	SiO_2	Al_2O_3	TiO_2	Cr_2O_3	FeO	NiO	MnO	MgO	CaO	Na_2O	K_2O	Total	Mg#	$X(^{iv}Al)$	XCa	$D^{cpx/melt}$	$A(cm^{-2})$	t (mm)	H_2O in cpx (wt ppm)	H_2O in melt (wt %)
alle3-01	46.42	7.27	2.83	0.11	7.60	0.02	0.13	12.30	22.27	0.58	b.l.d.	99.45	74.27	0.171	0.90	0.0186	1.859	0.104	75.6	0.41
alle3-02	45.77	8.07	3.33	0.02	8.41	0.03	0.13	11.56	22.39	0.67	b.l.d.	99.01	71.02	0.188	0.90	0.0207	1.927	0.104	78.4	0.38
alle3-03	45.33	8.17	3.65	0.12	7.90	b.l.d.	0.14	11.61	22.82	0.52	0.02	99.13	72.37	0.194	0.92	0.0211	3.9771	0.104	161.8	0.77
alle3-04	47.20	6.25	2.30	0.44	6.99	0.02	0.11	12.75	22.92	0.46	b.l.d.	100.39	76.48	0.158	0.92	0.0166	4.4644	0.104	181.6	1.09
alle3-05	48.54	5.14	2.31	0.03	7.53	0.02	0.12	12.61	22.38	0.32	b.l.d.	100.01	74.90	0.105	0.90	0.0120	4.0073	0.106	160.0	1.33
alle3-06	48.80	4.45	1.94	0.05	7.05	b.l.d.	0.09	13.55	22.85	0.34	0.01	100.18	77.40	0.108	0.92	0.0121	4.6627	0.106	186.1	1.54
alle3-07	50.45	4.12	1.73	0.17	7.05	0.03	0.12	13.90	22.47	0.33	b.l.d.	100.19	77.85	0.085	0.89	0.0107	3.788	0.106	151.2	1.42
alle3-08	47.06	7.04	2.81	0.18	7.06	b.l.d.	0.08	12.55	22.72	0.52	b.l.d.	99.92	76.01	0.162	0.91	0.0173	2.7965	0.102	116.0	0.67
alle3-09	48.40	5.84	2.19	0.02	7.11	0.03	0.12	12.91	23.13	0.44	0.01	99.35	76.41	0.134	0.92	0.0143	2.8337	0.102	117.6	0.82
alle3-10	50.38	4.29	1.74	0.01	7.09	0.02	0.08	13.80	22.35	0.42	b.l.d.	100.00	77.64	0.085	0.89	0.0107	4.0807	0.102	169.3	1.58
alle3-11	49.63	4.32	2.09	0.07	7.03	b.l.d.	0.09	13.58	22.76	0.35	b.l.d.	99.69	77.49	0.092	0.91	0.0110	4.0612	0.102	168.5	1.53
alle3-12	46.29	7.42	3.03	0.19	7.30	b.l.d.	0.06	12.03	22.54	0.48	b.l.d.	99.66	74.60	0.169	0.91	0.0182	4.8385	0.102	200.7	1.11
alle3-13	50.29	4.14	1.57	0.12	6.92	0.03	0.09	14.02	22.51	0.30	0.01	99.67	78.31	0.089	0.90	0.0109	4.7703	0.107	188.6	1.73
alle3-14	46.99	6.31	2.40	0.21	7.08	0.05	0.10	13.05	23.04	0.44	0.01	100.02	76.67	0.166	0.93	0.0174	6.086	0.107	240.7	1.38
alle3-15	46.46	6.88	3.33	0.01	7.67	0.05	0.12	12.00	22.51	0.63	0.01	100.10	73.62	0.155	0.91	0.0166	5.7919	0.107	229.0	1.38
alle3-16	50.21	3.93	1.76	0.05	6.92	0.03	0.14	14.13	22.10	0.39	b.l.d.	99.58	78.45	0.081	0.88	0.0105	4.4804	0.107	177.2	1.68
alle3-17	45.39	7.66	3.60	0.14	7.93	0.04	0.10	11.92	22.77	0.46	0.02	99.55	72.83	0.188	0.92	0.0203	4.4983	0.107	177.9	0.88
alle3-18	47.17	6.63	2.71	0.48	6.91	0.03	0.07	12.64	23.02	0.45	b.l.d.	100.22	76.52	0.160	0.92	0.0169	5.246	0.123	180.5	1.07
alle3-19	48.46	5.19	2.07	b.l.d.	7.36	b.l.d.	0.14	13.38	22.54	0.45	0.01	99.58	76.42	0.124	0.91	0.0136	5.223	0.123	179.7	1.32
alle3-20	50.04	3.93	1.69	0.05	6.60	0.05	0.09	13.97	22.75	0.38	b.l.d.	100.14	79.07	0.086	0.91	0.0106	4.266	0.123	146.8	1.39
alle3-21	49.19	4.42	2.00	0.06	7.39	0.04	0.07	13.71	22.97	0.37	b.l.d.	99.87	76.79	0.110	0.92	0.0123	1.8448	0.103	75.8	0.62
alle3-22	46.80	6.61	2.65	0.37	7.55	b.l.d.	0.15	12.18	22.78	0.49	b.l.d.	100.25	74.20	0.161	0.92	0.0170	0.8724	0.099	37.3	0.22
alle3-23	50.15	4.04	1.79	0.02	7.18	0.03	0.13	13.75	22.69	0.39	b.l.d.	99.91	77.34	0.086	0.90	0.0107	5.3264	0.116	194.3	1.82
alle3-24	44.13	9.12	3.81	0.23	8.03	b.l.d.	0.11	11.36	22.52	0.54	0.01	99.86	71.60	0.224	0.91	0.0259	4.2349	0.108	165.9	0.64
alle3-25	50.17	4.32	1.91	0.14	6.86	0.01	0.13	13.78	22.59	0.35	b.l.d.	100.13	78.16	0.088	0.90	0.0108	2.4358	0.108	95.4	0.88
alle3-26	47.28	6.70	2.64	0.35	7.52	b.l.d.	0.13	12.38	22.42	0.51	b.l.d.	99.31	74.59	0.154	0.90	0.0166	4.046	0.087	196.8	1.18
alle3-27	50.29	4.23	1.67	0.20	6.92	0.02	0.15	13.87	22.18	0.32	0.01	99.82	78.13	0.085	0.88	0.0108	3.7096	0.087	180.4	1.68
alle3-28	45.91	7.57	3.28	0.02	8.53	0.01	0.07	11.75	22.42	0.58	b.l.d.	99.93	71.07	0.180	0.90	0.0195	4.7605	0.102	197.5	1.01
alle3-29	46.83	7.19	2.60	0.07	7.71	0.02	0.11	11.90	22.34	0.57	b.l.d.	99.73	73.36	0.161	0.90	0.0173	5.1922	0.103	213.3	1.23
alle3-30	45.83	7.68	3.36	0.07	7.77	0.05	0.11	11.98	22.44	0.53	b.l.d.	99.73	73.33	0.180	0.90	0.0195	4.176	0.103	171.6	0.88
alle3-32	46.54	7.13	2.75	0.10	7.97	0.02	0.07	12.32	22.47	0.55	0.01	99.63	73.37	0.173	0.90	0.0187	5.1584	0.096	227.4	1.22
alle3-33	49.45	4.70	2.12	0.06	7.14	0.02	0.11	13.58	22.13	0.41	0.02	100.22	77.22	0.097	0.88	0.0116	5.0906	0.096	224.4	1.93
alle3-34	46.00	7.32	3.35	0.10	7.71	0.03	0.11	12.08	22.56	0.48	b.l.d.	100.41	73.65	0.173	0.91	0.0185	5.1934	0.102	215.4	1.16

Table 8-2. (continued)

	SiO_2	Al_2O_3	TiO_2	Cr_2O_3	FeO	NiO	MnO	MgO	CaO	Na_2O	K_2O	Total	Mg#	$X(^{iv}Al)$	XCa	$D^{cpx/melt}$	$A(cm^{-2})$	t (mm)	H_2O in cpx (wt ppm)	H_2O in melt (wt %)
alle3-35	46.03	7.61	3.37	0.07	7.70	b.l.d.	0.13	11.66	22.60	0.47	b.l.d.	99.56	72.96	0.170	0.91	0.0182	5.3647	0.102	222.5	1.22
alle3-36	49.29	5.06	2.16	0.05	7.20	0.02	0.12	13.30	22.63	0.39	0.01	100.17	76.70	0.108	0.90	0.0123	4.7204	0.102	195.8	1.60
alle3-37	47.59	6.68	2.43	0.23	7.70	0.02	0.11	12.67	22.49	0.49	b.l.d.	99.85	74.58	0.157	0.90	0.0170	5.0507	0.102	209.5	1.23
alle3-38	45.75	8.01	3.01	0.02	8.44	b.l.d.	0.10	11.28	22.37	0.57	0.02	100.05	70.44	0.185	0.91	0.0201	4.9339	0.102	204.7	1.02
alle3-39	50.80	3.71	1.70	0.15	6.79	0.07	0.06	13.81	22.73	0.36	b.l.d.	100.44	78.38	0.071	0.90	0.0096	3.898	0.102	161.7	1.68
alle3-40	49.73	4.36	2.05	b.l.d.	7.24	b.l.d.	0.11	13.23	22.72	0.43	b.l.d.	99.34	76.52	0.088	0.91	0.0107	4.3989	0.102	182.5	1.71
alle3-43	49.68	4.36	1.97	0.19	6.98	0.04	0.15	13.89	22.42	0.37	b.l.d.	99.75	78.00	0.097	0.89	0.0116	2.891	0.089	137.4	1.19
alle3-44	49.98	4.23	1.99	0.05	7.07	b.l.d.	0.10	13.96	22.62	0.43	b.l.d.	99.43	77.87	0.093	0.90	0.0112	3.0795	0.094	138.6	1.24
alle3-45	48.45	4.75	2.25	0.08	7.74	0.01	0.11	13.32	22.22	0.40	b.l.d.	99.36	75.41	0.113	0.90	0.0127	2.7914	0.082	144.0	1.13
alle3-46	49.13	4.60	2.15	0.03	7.74	b.l.d.	0.15	13.17	22.36	0.42	b.l.d.	98.61	75.20	0.100	0.90	0.0117	2.5088	0.082	129.5	1.11
alle3-47	47.62	6.19	3.06	0.04	7.13	0.10	0.16	12.28	22.15	0.68	0.02	99.68	75.44	0.125	0.89	0.0138	2.5416	0.082	131.2	0.95
alle3-48	49.49	4.18	1.97	0.13	6.81	0.05	0.14	13.96	22.25	0.40	b.l.d.	99.70	78.53	0.093	0.89	0.0112	2.5694	0.082	132.6	1.18
alle3-49	45.37	6.97	2.92	0.35	7.66	0.02	0.14	12.11	22.60	0.45	0.02	99.14	73.81	0.184	0.92	0.0196	3.196	0.082	164.9	0.84
alle3-50	50.05	4.04	1.61	0.17	6.24	0.01	0.14	14.23	22.71	0.42	0.02	99.29	80.26	0.091	0.91	0.0110	2.478	0.092	114.0	1.04
alle3-51	50.67	3.53	1.47	0.30	6.00	0.03	0.10	14.44	22.72	0.37	0.01	100.17	81.10	0.076	0.90	0.0100	2.7598	0.092	126.9	1.27
alle3-52	47.27	6.69	2.80	0.25	7.13	b.l.d.	0.09	12.65	22.70	0.50	0.01	99.21	75.98	0.155	0.91	0.0166	2.65	0.092	121.9	0.74
alle3-53	51.01	3.59	1.16	0.16	6.13	0.01	0.11	14.13	22.65	0.35	0.01	99.54	80.43	0.069	0.90	0.0095	2.0742	0.092	95.4	1.00
alle3-54	49.22	5.31	2.20	0.31	6.36	0.01	0.09	13.25	22.98	0.44	0.02	98.91	78.78	0.112	0.91	0.0125	3.9293	0.098	169.7	1.36
alle3-55	44.74	8.27	3.77	0.07	8.01	0.02	0.07	11.08	22.67	0.50	0.01	99.13	71.15	0.192	0.92	0.0208	4.0302	0.098	174.0	0.84
alle3-56	46.00	7.59	3.05	b.l.d.	8.21	0.05	0.15	11.69	22.30	0.50	b.l.d.	99.68	71.74	0.176	0.90	0.0191	4.1685	0.098	180.0	0.94
alle3-57	45.60	7.74	3.16	0.16	6.96	0.01	0.10	11.91	22.76	0.52	0.02	99.50	75.31	0.183	0.92	0.0195	3.7674	0.092	173.3	0.89
alle3-58	49.48	4.50	1.93	0.08	6.83	b.l.d.	0.13	13.41	22.42	0.35	b.l.d.	99.67	77.78	0.091	0.90	0.0110	4.0481	0.092	186.2	1.69
alle3-59	49.29	4.64	2.08	0.13	7.09	0.04	0.08	13.45	22.49	0.38	0.01	99.26	77.18	0.100	0.90	0.0117	2.1769	0.095	97.0	0.83
alle3-60	49.63	4.51	1.77	0.04	6.91	b.l.d.	0.16	13.64	22.40	0.43	b.l.d.	100.09	77.88	0.096	0.90	0.0114	0.9876	0.09	46.4	0.41
alle3-61	50.15	4.05	1.52	0.04	6.90	b.l.d.	0.13	14.01	22.41	0.44	0.01	100.24	78.34	0.089	0.89	0.0109	1.1767	0.09	55.3	0.51
alle3-63	46.71	6.90	2.50	0.12	7.92	b.l.d.	0.13	12.16	22.34	0.49	b.l.d.	99.71	73.23	0.164	0.90	0.0176	0.8974	0.083	45.7	0.26
alle3-64	45.38	7.98	3.68	0.17	8.16	0.06	0.11	11.57	22.49	0.51	b.l.d.	99.18	71.66	0.188	0.91	0.0205	1.1405	0.083	58.1	0.28
alle3-65	47.01	7.12	2.77	0.25	7.51	0.03	0.09	12.48	22.47	0.51	b.l.d.	99.57	74.78	0.166	0.90	0.0180	1.0445	0.083	53.2	0.30
alle3-66	47.53	6.26	2.62	0.10	7.25	b.l.d.	0.15	12.90	22.45	0.44	b.l.d.	99.98	76.03	0.145	0.90	0.0156	0.7518	0.075	42.4	0.27

Note: b.l.d., below the limit of detection

Table 8-3. Major element composition of ol phenocrysts in Allègre basalts

		SiO_2	MgO	Al_2O_3	CaO	FeO	Cr_2O_3	MnO	TiO_2	NiO	Total	Mg#
	2-01	39.49	42.39	0.04	0.21	17.23	0.01	0.20	0.05	0.14	99.77	81.43
	2-02	39.68	39.14	0.03	0.24	20.78	0.03	0.35	0.06	0.13	100.43	77.05
	2-03	41.01	45.20	b.l.d.	0.02	13.65	b.l.d.	0.13	0.01	0.24	100.26	85.51
	2-04	38.89	37.61	0.03	0.25	22.19	0.02	0.60	0.05	0.09	99.73	75.14
	2-05	38.99	38.31	0.02	0.10	22.33	0.01	0.53	0.01	0.14	100.44	75.36
	2-06	38.43	37.82	0.01	0.34	22.31	0.03	0.56	0.05	0.18	99.71	75.14
	2-07	39.30	37.34	0.01	0.31	22.26	b.l.d.	0.59	0.02	0.11	99.95	74.95
ALLE2	2-08	38.57	37.03	0.03	0.21	22.80	b.l.d.	0.51	0.04	0.11	99.30	74.33
	2-09	38.72	38.71	0.02	0.16	21.03	0.01	0.43	b.l.d.	0.11	99.18	76.64
	2-10	39.69	40.08	0.01	0.09	20.43	0.03	0.39	0.02	0.11	100.85	77.77
	2-11	39.77	41.68	0.01	0.04	17.62	b.l.d.	0.34	b.l.d.	0.22	99.67	80.84
	2-12	39.65	41.86	b.l.d.	0.04	17.77	0.02	0.41	0.01	0.23	99.99	80.77
	2-13	38.99	38.05	0.02	0.25	22.10	0.03	0.46	b.l.d.	0.12	100.01	75.42
	2-14	38.70	37.61	0.02	0.29	22.55	0.02	0.55	b.l.d.	0.09	99.84	74.83
	2-15	38.75	38.76	0.01	0.13	21.98	0.01	0.44	0.01	0.13	100.23	75.86
	3-01	38.70	38.17	0.03	0.25	21.86	0.01	0.52	0.01	0.13	99.67	75.68
	3-02	38.98	38.22	0.03	0.31	21.43	b.l.d.	0.53	0.03	0.15	99.68	76.08
	3-03	40.79	41.28	0.04	0.17	17.44	0.11	0.27	b.l.d.	0.17	100.27	80.84
	3-04	37.57	44.05	0.03	0.21	15.66	0.02	0.21	b.l.d.	0.29	98.03	83.37
	3-05	39.53	44.00	0.02	0.21	16.27	0.05	0.22	b.l.d.	0.19	100.49	82.82
	3-06	39.35	40.81	0.04	0.21	19.26	0.01	0.42	b.l.d.	0.21	100.33	79.07
	3-07	38.21	38.55	0.02	0.30	22.20	0.01	0.57	b.l.d.	0.11	99.96	75.59
ALLE3	3-08	38.63	38.98	0.03	0.20	22.01	0.03	0.52	0.01	0.13	100.55	75.94
	3-09	39.30	39.42	0.02	0.13	21.00	b.l.d.	0.45	b.l.d.	0.17	100.49	76.99
	3-10	38.34	39.43	0.01	0.15	20.37	b.l.d.	0.48	0.01	0.18	98.96	77.53
	3-11	39.30	39.72	0.02	0.21	19.60	0.03	0.47	b.l.d.	0.13	99.48	78.32
	3-12	39.05	39.18	0.11	0.26	20.18	0.09	0.40	0.01	0.08	99.35	77.58
	3-13	38.76	38.38	0.02	0.15	21.08	0.02	0.38	b.l.d.	0.12	98.91	76.45
	3-14	38.56	39.49	0.01	0.19	21.15	0.03	0.49	b.l.d.	0.12	100.03	76.90
	3-15	39.25	41.71	0.03	0.18	16.89	0.04	0.25	0.01	0.15	98.51	81.49

Note: b.l.d., below the limit of detection

Oxygen isotope compositions of clinopyroxene phenocrysts

The oxygen isotope compositions of the cpx phenocrysts in Allègre basalts are corrected by the standards (NSH2, NSH5, NSH8, NSH9, NSH10, NSH14) and plotted in Fig 8-7. The $\delta^{18}O$ values of cpx phenocrysts range from 5.52 to 6.65‰ (Table 8-4, Fig. 8-7) and are higher than the value of cpx in typical MORB and mantle peridotites (5.4‰-5.8‰) (Eiler et al., 1997; Mattey et al., 1994). The difference in $\delta^{18}O$ values within individual samples varies from 0.76‰ to 0.99‰.

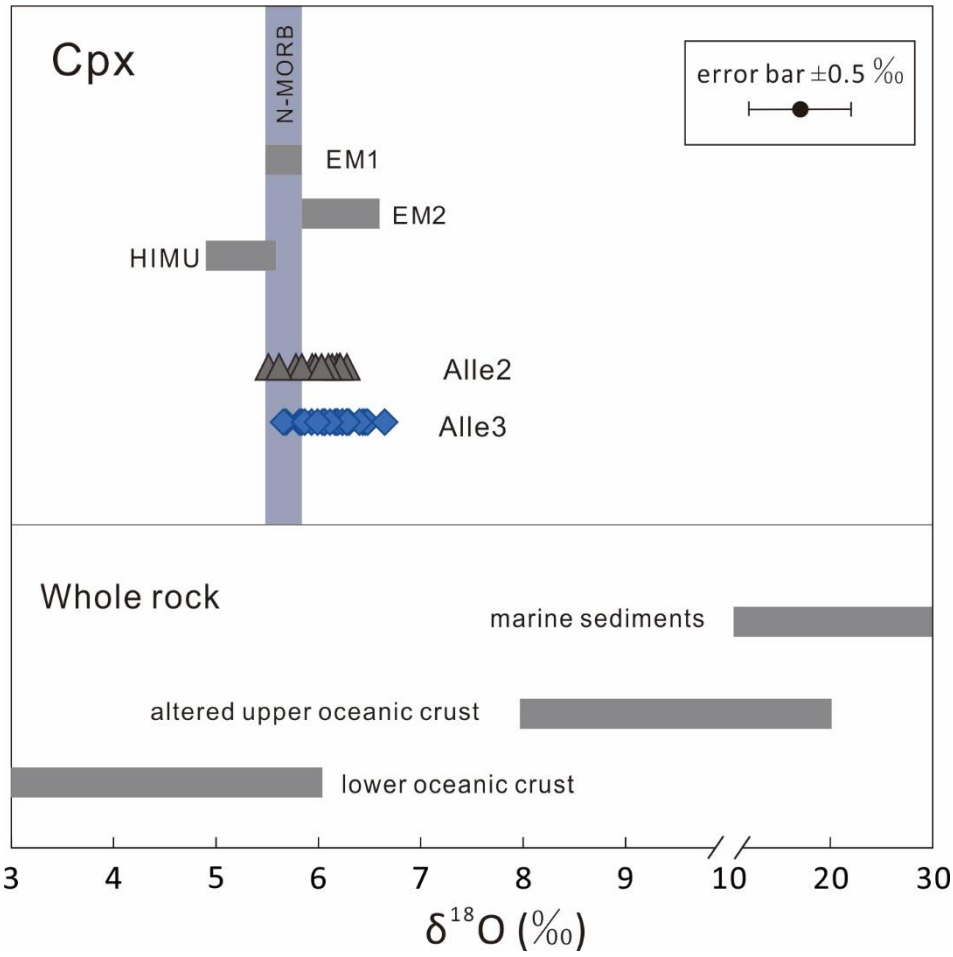

Figure 8-7. Oxygen isotope compositions of cpx phenocrysts in the Allègre basalts. The range of $\delta^{18}O$ values of cpx phenocrysts in N-MORB, EM1, EM2 and HIMU are calculated from the $\delta^{18}O$ values of ol phenocrysts (Eiler et al., 1997), assuming an equilibrium fractionation between cpx and ol of 0.4‰ (Mattey et al., 1994). The $\delta^{18}O$ values of bulk rock (marine sediments, altered upper oceanic crust and lower oceanic crust) are based on Eiler (2001).

Table 8-4. The oxygen isotope composition of cpx phenocrysts in Allègre basalts

	Mg#	$\delta^{18}O$ measured	IMF*	$\delta^{18}O$ corrected by IMF	1SE**
Alle3-50	80.2	8.02	1.58	6.44	0.19
Alle3-51	81.1	7.96	1.50	6.46	0.27
Alle3-52	76	7.99	1.95	6.04	0.17
Alle3-53	80.4	8.05	1.57	6.48	0.07
Alle2-69	81.7	8.11	1.45	6.65	0.21
Alle3-23	77.3	8.14	1.83	6.30	0.01
Alle3-33	77.2	7.78	1.84	5.94	0.33
Alle3-32	73.4	7.99	2.17	5.82	0.12
Alle3-22	74.2	8.28	2.10	6.18	0.18
Alle3-38	70.4	8.12	2.43	5.69	0.32
Alle3-37	74.6	7.91	2.07	5.84	0.11
Alle3-36	76.7	7.95	1.89	6.07	0.28
Alle3-40	78.4	7.98	1.74	6.24	0.14
Alle3-40	76.5	8.07	1.90	6.17	0.30
Alle3-24	71.6	7.99	2.33	5.66	0.08
Alle3-05	74.9	8.45	2.04	6.40	0.04
Alle3-06	77.4	8.02	1.82	6.19	0.08
Alle3-07	77.8	8.03	1.79	6.24	0.17
Alle3-21	76.8	8.16	1.88	6.28	0.23
Alle3-03	72.4	8.13	2.26	5.87	0.28
Alle3-04	76.5	8.19	1.90	6.28	0.05
Alle3-18	76.5	7.96	1.90	6.06	0.17
Alle3-28	71.1	8.49	2.37	6.12	0.17
Alle3-44	77.9	7.78	1.78	5.99	0.19
Alle2-36/37	78	7.96	1.77	6.19	0.25
Alle2-38	75.2	7.80	2.02	5.78	0.16
Alle3-35	80.7	7.68	1.54	6.14	0.30
Alle2-23	73.2	5.96	2.19	3.77	0.13
Alle2-25	76.3	8.13	1.92	6.21	0.10
Alle2-1	79.7	7.91	1.63	6.28	0.26
Alle2-2/2-3	77	7.82	1.87	5.94	0.18
Alle2-4	78.1	7.99	1.77	6.21	0.12
ALLe2-5	72.5	7.80	2.29	5.52	0.23
Alle2-44	78.5	7.96	1.74	6.22	0.19
Alle2-43	77.9	7.77	1.79	5.98	0.19
Alle2-39	76.7	7.75	1.90	5.84	0.04
Alle2-42	79.6	7.74	1.64	6.10	0.23
Alle2-19/20	77.8	7.84	1.80	6.03	0.12
Alle2-22	72.5	7.91	2.29	5.62	0.13

* IMF is the instrumental mass fractionation

** SE the standard error of the mean for the group of measurements in a single cpx grain

Discussion

Crustal contamination and crystal fractionation

The Allègre basalts carried abundant peridotite xenoliths, which suggest a rapid magma ascent process (generally within a maximum of 50 hours after xenolith entrainment, O'Reilly and Griffin (2010)). Thus, the time for the magma to be influenced by crustal contamination is limited. Moreover, the Allègre basalts have high Nb/U ratios (37.0-41.0, falling into the range of MORBs and OIBs, Hofmann et al., (1986)); while the Nb/U ratio of continental crust is quite low (Rudnick and Gao, 2014). In addition, the continental crust is characterized by high Ba/Nb and La/Nb ratios. Thus, the crustal contamination is insignificantly for the Allègre basalts.

The Allègre basalts have relatively high Mg# (62.4-63.8), high Ni (190.5-204 ppm) and Cr (202-217 ppm) and no Eu anomaly. The Mg# of the continental basalts in FMC and eastern China are generally around 65-70 (e.g., Chauvel and Jahn, 1984; Wilson and Downes, 1991; Zhou and Armstrong, 1982), suggesting a small proportion of crystal fractionation (ol and cpx) in Allègre basalts.

High oxygen isotope compositions

The Allègre cpx phenocrysts are characterized by high $\delta^{18}O$ values (5.52-6.65‰) compare to cpx in the normal mantle (Fig. 8-7) (Eiler et al., 1997; Mattey et al., 1994). Considering that 1) the selected cpx phenocrysts is fresh and without crack and inclusion; 2) the crustal contamination in the Allègre basalts is limited and 3) the fractionation of oxygen isotopes caused by fractional crystallization is less than 0.1‰ in basaltic melt (Eiler, 2001), the oxygen isotope compositions of the Allègre cpx phenocrysts mainly represent the information of the mantle source. The high oxygen isotopic composition in silicate rocks are primarily the result of low temperature water-rock interactions at the surface of the Earth and crust (Eiler, 2001; Eiler et al., 1997), which means that there is a $\delta^{18}O$-enriched crust component in the mantle source of the Allègre basalts.

Water content in the "primary" melts

The averaged H_2O contents of the Allègre basalts calculated by cpx with Mg#> 75

range from 1.21 to 1.48 wt.%. As discussed above, the variation of the H_2O content in the magma caused by crystallization process would be less than 30% (within the measurement uncertainties) when the Mg# of crystallized cpx phenocrysts is higher than 75 (Fig. 4-8). In addition, the crustal contamination is insignificant and the homogeneous H_2O content profile in the core of cpx phenocrysts suggest that H diffusion didn't affect the interior H_2O content of the cpx phenocrysts (Fig. 8-5a). Thus, the calculated H_2O content can reflect the original information of the mantle source.

The H_2O contents of the Allègre basalts are higher than the values of MORBs (0.1-0.3 wt%, Asimow et al., 2004; Danyushevsky et al., 1993, 2000; Dixon, 1988; Michael, 1988, 1995; Sobolev and Chaussidon, 1996; Saal et al., 2002; Simons et al., 2002) and OIBs (0.3-1.0 wt%, Dixon et al., 1997, 2002; Dixon and Clague, 2001; Nichols et al., 2002; Simons et al., 2002; Wallace, 1998), falling in the range of back-arc basin basalts (BABBs, 0.2-2.0 wt%, Danyushevsky et al., 1993; Hochstaedter et al., 1990; Stolper and Newmann, 1994) (Fig. 8-8a). The calculated H_2O/Ce ratios of the Allègre basalts (93-114) are similar to the EM-type OIBs (50-100, Kendrick et al., 2014, 2015; Workman et al., 2006) and lower than the normal mantle (150-210, Bizimis et al., 2015; Dixon et al. 2002) (Fig. 8-8b). Consisted with the basalts in eastern China, the estimated source water contents of the Allègre basalts (700-900 ppm) are also significantly higher than those of the peridotite xenoliths in FMC (4.7-117 ppm) (Denis et al., 2015; Grant et al., 2007; Gu, 2016).

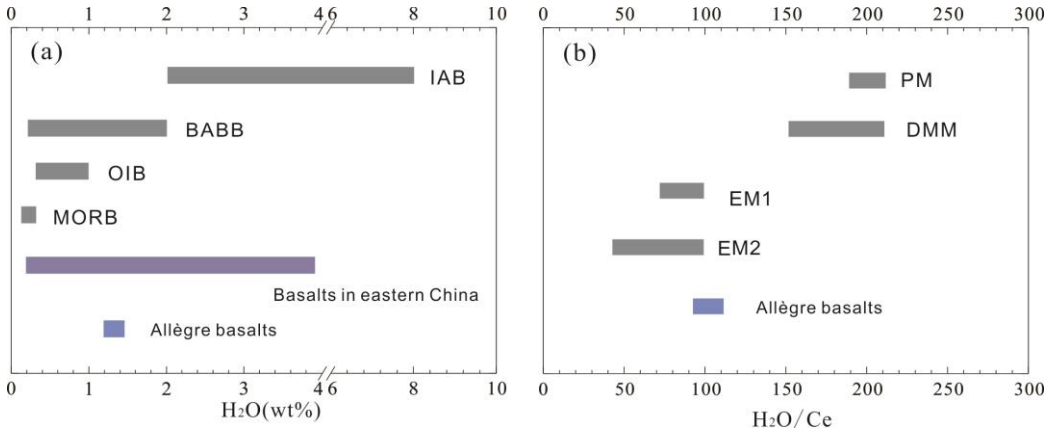

Figure 8-8. a) Calculated H_2O content of the Allègre basalts. The ranges of H_2O content for OIBs, MORBs, BABBs and IABs are from Dixon et al. (2004) and references therein. b) Comparison of the H_2O/Ce ratio of the Allègre basalts with that of PM, DMM, EM1 and EM2 (Bizimis et al., 2015; Dixon et al., 2002; Kendrick et al., 2014; 2015; Workman et al., 2006).

Compared with the basalts in eastern China

The enriched component in the mantle source of the Allègre basalts has low H_2O/Ce ratio, high oxygen isotope composition and Nb/La ratio (1.50-1.56), which are consistent with those of continental basalts in eastern China. As discussed before, the recycled marine sediments and oceanic crust have been identified in the mantle source of Shuangliao, Wulanhada and Chaihe-aershan basalts. The composition of recycled oceanic slab, particularly the upper crust and marine sediments with a $\delta^{18}O$ up to 20‰ (Eiler, 2001; Gregory and Taylor, 1981) and a H_2O/Ce down to 100 (Dixon et al., 2002) is consistent with the characteristics of enriched components in the Allègre basalts. In addition, the seismic tomography studies have identified a subducted African slab in the mantle transition zone beneath the Allègre basalts (Fichtner and Villaseñor, 2015), which is also similar to the situation in eastern China. Thus, a recycled oceanic slab is probably the most likely candidate for the enriched component in the mantle source of the Allègre basalts.

Hamelin et al. (2009) conducted Li isotope studies on basalts from the Chaîne des Puys in FMC, which also identified the recycled oceanic crust in the mantle source. Besides, the recycled oceanic crust can also account for the widespread HIMU-like signal in the basalts from FMC (e.g., Lustrino and Wilson, 2007; Négrel et al., 2015; Wilson and Downes, 1991).

Summary

(1) The H_2O contents of the Allègre "primary" magmas range from 1.21 to 1.48 wt.%. The H_2O/Ce ratios of the Allègre basalts are around 100, which are similar to those of the EM-type OIBs.

(2) The $\delta^{18}O$ values of cpx phenocrysts (5.52-6.65‰) are relatively higher than those of cpx in the normal mantle.

(3) Compared with the basalts in eastern China, a recycled oceanic slab is the most likely candidate for the enriched components in the mantle source of the Allègre basalts, which also can be a credible explication for the HIMU-like signal in the mantle source of basalts from FMC.

References

Asimow, P., Dixon, J., Langmuir, C., 2004. A hydrous melting and fractionation model for mid-ocean ridge basalts: Application to the Mid-Atlantic Ridge near the Azores. *Geochemistry, Geophysics, Geosystems 5*. doi: 10.1029/2003GC000568.

Bizimis, M., Peslier, A.H., 2015. Water in Hawaiian garnet pyroxenites: Implications for water heterogeneity in the mantle. *Chemical Geology 397*, 61-75.

Chauvel, C., Jahn, B. M., 1984. Nd-Sr isotope and REE geochemistry of alkali basalts from the Massif Central, France. *Geochimica et Cosmochimica Acta 48*, 93-110.

Danyushevsky, L., Falloon, T., Sobolev, A., Crawford, A., Carroll, M., Price, R., 1993. The H_2O content of basalt glasses from Southwest Pacific back-arc basins. *Earth and Planetary Science Letters 117*, 347-362.

Danyushevsky, L.V., Eggins, S.M., Falloon, T.J., Christie, D.M., 2000. H_2O abundance in depleted to moderately enriched mid-ocean ridge magmas; Part I: incompatible behaviour, implications for mantle storage, and origin of regional variations. *Journal of Petrology 41*, 1329-1364.

Denis, C. M., Alard, O., Demouchy, S., 2015. Water content and hydrogen behaviour during metasomatism in the uppermost mantle beneath Ray Pic volcano (Massif Central, France). *Lithos 236*, 256-274.

Dixon, J.E., Clague, D.A., 2001. Volatiles in basaltic glasses from Loihi Seamount, Hawaii: Evidence for a relatively dry plume component. *Journal of Petrology 42*, 627-654.

Dixon, J.E., Clague, D.A., Wallace, P., Poreda, R., 1997. Volatiles in alkalic basalts form the North Arch Volcanic Field, Hawaii: extensive degassing of deep submarine-erupted alkalic series lavas. *Journal of Petrology 38*, 911-939.

Dixon, J.E., Dixon,T.H., Bell,D.R., Malservisi,R., 2004. Lateral variation in upper mantle viscosity: role of water. *Earth and Planetary Science Letters 222*, 451–467.

Dixon, J.E., Leist, L., Langmuir, C., Schilling, J.-G., 2002. Recycled dehydrated lithosphere observed in plume-influenced mid-ocean-ridge basalt. *Nature 420*, 385-389.

Dixon, J.E., Stolper, E., Delaney, J.R., 1988. Infrared spectroscopic measurements of CO_2 and H_2O in Juan de Fuca Ridge basaltic glasses. *Earth and Planetary Science Letters 90*, 87-104.

Downes, H., 1987. Tertiary and quaternary volcanism in the Massif Central,

France. *Geological Society, London, Special Publications 30,* 517-530.

Downes, H., Reichow, M. K., Mason, P. R. D., Beard, A. D., Thirlwall, M. F., 2003. Mantle domains in the lithosphere beneath the French Massif Central: trace element and isotopic evidence from mantle clinopyroxenes. *Chemical Geology 200,* 71-87.

Eiler, J.M., 2001. Oxygen isotope variations of basaltic lavas and upper mantle rocks. *Reviews in Mineralogy and Geochemistry 43,* 319-364.

Eiler, J.M., Farley, K.A., Valley, J.W., Hauri, E., Craig, H., Hart, S.R., Stolper, E.M., 1997. Oxygen isotope variations in ocean island basalt phenocrysts. *Geochimica et Cosmochimica Acta 61,* 2281-2293.

Faure, M., Mézème, E.B., Duguet, M., Cartier, C., Talbot, J.Y., 2005. Paleozoic tectonic evolution of medio-Europa from the example of the French Massif Central and Massif Armoricain. *Journal of the virtual Explorer 19,* 1-25.

Faure, M., Lardeaux, J. M., Ledru, P., 2009. A review of the pre-Permian geology of the Variscan French Massif Central. *Comptes Rendus Geoscience 341,* 202-213.

Fichtner, A., Villaseñor, A., 2015. Crust and upper mantle of the western Mediterranean-Constraints from full-waveform inversion. *Earth and Planetary Science Letters 428,* 52-62.

Grant, K., Ingrin, J., Lorand, J. P., Dumas, P., 2007. Water partitioning between mantle minerals from peridotite xenoliths. *Contributions to Mineralogy and Petrology 154,* 15-34.

Granet, M., Wilson, M., Achauer, U., 1995. Imaging a mantle plume beneath the French Massif Central. *Earth and Planetary Science Letters 136,* 281-296.

Gregory R.T., Taylor H.P., 1981. An oxygen isotope profile in a section of Cretaceous oceanic crust, Samail ophiolite, Oman: evidence for $\delta^{18}O$ buffering of the oceans by deep (>5 km) seawater-hydrothermal circulation at mid-ocean ridges. *Journal of Geophysical Research: Solid Earth.* doi: 10.1029/86iB04p02737.

Gu, X., Deloule, E., France, L., Ingrin, J., 2016. Multi-stage metasomatism revealed by trace element and Li isotope distributions in minerals of peridotite xenoliths from Allègre volcano (French Massif Central). *Lithos 264,* 158-174.

Hamelin, C., Seitz, H. M., Barrat, J. A., Dosso, L., Maury, R. C., Chaussidon, M., 2009. A low $\delta^{7}Li$ lower crustal component: Evidence from an alkalic intraplate volcanic series (Chaîne des Puys, French Massif Central). *Chemical Geology 266,* 205-217.

Hochstaedter, A.G., Gill, J.B., Kusakabe, M., Newman, S., Pringle, M., Taylor, B.,

Fryer, P., 1990. Volcanism in the Sumisu Rift, I. Major element, volatile, and stable isotope geochemistry. *Earth and Planetary Science Letters 100,* 179-19

Hofmann, A.W., Jochum, K.P., Seufert, M., White, W.M., 1986. Nb and Pb in oceanic basalts: new constraints on mantle evolution. *Earth and Planetary Science Letters 79*, 33-45.

Juvigne, E., 1992. Studies on the age of 2 volcanic lacustrine craters of Auvergne (France). *Comptes Rendus de L'Acdemie des Sciences Serie II 314*, 401-404.

Kendrick, M.A., Jackson, M.G., Kent, A.J., Hauri, E.H., Wallace, P.J., Woodhead, J., 2014. Contrasting behaviours of CO_2, S, H_2O and halogens (F, Cl, Br, and I) in enriched-mantle melts from Pitcairn and Society seamounts. *Chemical Geology 370*, 69-81.

Kendrick, M.A., Jackson, M.G., Hauri, E.H., Phillips, D., 2015. The halogen (F, Cl, Br, I) and H_2O systematics of Samoan lavas: Assimilated-seawater, EM2 and high-$^3He/^4He$ components. *Earth and Planetary Science Letters 410,* 197-209.

Lardeaux, J. M., Ledru, P., Daniel, I., Duchene, S., 2001. The Variscan French Massif Central-a new addition to the ultra-high pressure metamorphic 'club': exhumation processes and geodynamic consequences. *Tectonophysics 332,* 143-167.

Le Bas, M., Le Maitre, R., Streckeisen, A., Zanettin, B., 1986. A chemical classification of volcanic rocks based on the total alkali-silica diagram. *Journal of Petrology 27,* 745-750.

Lenoir, X., Garrido, C. J., Bodinier, J. L., Dautria, J. M., 2000. Contrasting lithospheric mantle domains beneath the Massif Central (France) revealed by geochemistry of peridotite xenoliths. *Earth and Planetary Science Letters 181*, 359-375.

Lustrino, M., Wilson, M., 2007. The circum-Mediterranean anorogenic Cenozoic igneous province. *Earth-Science Reviews 81*, 1-65.

Mattey, D., Lowry, D., Macpherson, C., 1994. Oxygen isotope composition of mantle peridotite. *Earth and Planetary Science Letters 128*, 231-241.

McDonough, W.F., Sun, S.S., 1995. The composition of the Earth. *Chemical Geology 120*, 223-253.

Michael, P.J., 1988. The concentration, behavior and storage of H_2O in the suboceanic upper mantle: Implications for mantle metasomatism. *Geochimica et Cosmochimica Acta 52*, 555-566.

Michael, P., 1995. Regionally distinctive sources of depleted MORB: Evidence from trace elements and H_2O. *Earth and Planetary Science Letters 131*, 301-320.

Michon, L., Merle, O., 2001. The evolution of the Massif Central Rift; spatio-temporal distribution of the volcanism. *Bulletin de la Société géologique de France 172,* 201-211.

Négrel, P., Guerrot, C., Petelet-Giraud, E., Millot, R., 2015. Reinforcing the origin of volcanic rocks from the Massif Central through the isotopic composition of lead and strontium. *Journal of Geochemical Exploration 153,* 79-87.

Nichols, A., Carroll, M., Höskuldsson, A., 2002. Is the Iceland hot spot also wet? Evidence from the water contents of undegassed submarine and subglacial pillow basalts. *Earth and Planetary Science Letters 202,* 77-87.

O'Reilly, S.Y., Griffin, W.L., 2010. Rates of magma ascent, constraints from mantle-derived Xenoliths. In: Dosseto A., Turner S.P., Van Orman J.A., (Eds.), Timescales of magmatic processes, from core to atmosphere. John Wiley & Sons, Ltd, Chichester, UK, 116-124.

Rudnick, R., Gao, S., 2014. Composition of the continental crust. *Treatise on geochemistry (Second Edition) 4,* 1-51. doi:10.1016/B978-0-08-095975-7.00301-6.

Saal, A.E., Hauri, E.H., Langmuir, C.H., Perfit, M.R., 2002. Vapour undersaturation in primitive mid-ocean-ridge basalt and the volatile content of Earth's upper mantle. *Nature 419,* 451-455.

Simons, K., Dixon, J., Schilling, J.G., Kingsley, R., Poreda, R., 2002. Volatiles in basaltic glasses from the Easter-Salas y Gomez Seamount Chain and Easter Microplate: Implications for geochemical cycling of volatile elements. *Geochemistry, Geophysics, Geosystems 3,* 1-29.

Sobolev, A.V., Chaussidon, M., 1996. H_2O concentrations in primary melts from supra-subduction zones and mid-ocean ridges: implications for H_2O storage and recycling in the mantle. *Earth and Planetary Science Letters 137,* 45-55.

Stolper, E., Newman, S., 1994. The role of water in the petrogenesis of Mariana trough magmas. *Earth and Planetary Science Letters 121,* 293-325.

Wallace, P.J., 1998. Water and partial melting in mantle plumes: Inferences from the dissolved H_2O concentrations of Hawaiian basaltic magmas. *Geophysical Research Letters 25,* 3639-3642.

Wilson, M., Downes, H., 1991. Tertiary-Quaternary extension-related alkaline magmatism in western and central Europe. *Journal of Petrology 32,* 811-849.

Workman, R.K., Hauri, E., Hart, S.R., Wang, J., Blusztajn, J., 2006. Volatile and trace

elements in basaltic glasses from Samoa: implications for water distribution in the mantle. *Earth and Planetary Science Letters 241,* 932-951.